TECHNISCHE UNIVERSITÄT MÜNCHEN

Institut für Zellbiologie des Nervensystems

In vivo imaging of axonal degeneration and axonal transport in mouse models of multiple sclerosis

Catherine Diamante Sorbara

Vollständiger Abdruck der von der Fakultät für Medizin der Technischen Universität München zur Erlangung des akademischen Grades eines

Doctor of Philosophy (Ph.D.).

genehmigten Dissertation.

Vorsitzender: Univ.-Prof. Dr. Claus Zimmer

Betreuer: Univ.-Prof. Dr. Thomas Misgeld

Prüfer der Dissertation:

1. Univ.-Prof. Dr. Thomas Korn

2. Univ.-Prof. Dr. Martin Kerschensteiner, Ludwig-Maximilians-Universität München

3. Priv.-Doz. Dr. Naoto Kawakami, Ludwig-Maximilians-Universität München

Die Dissertation wurde am 16.06.2014 bei der Fakultät für Medizin der Technischen Universität München eingereicht und durch die Fakultät für Medizin am 16.09.2014 angenommen.

Acknowledgements

To begin, I would like to thank my supervisor Prof. Dr. Martin Kerschensteiner and Prof. Dr. Thomas Misgeld for their guidance, support and encouragement. Your ambition, hard-working attitude and genuine fascination of science was inspirational and helped me to strive to be a better scientist. Thank you to Prof. Dr. Thomas Korn for his support as a member of my thesis committee and to Dr. Leanne Godinho for being a wonderful mentor to me and always lending an empathetic ear.

As I was fortunate enough to spend my PhD working in two amazing labs, I am also lucky to have many colleagues and friends to extend special thanks to. Your visits with me in the dungeon, mid-afternoon outings for gelato and girls' night dinners lifted my spirits and helped make these past years more enjoyable.

Thank you to all my friends and family back in Canada. Your support and unwavering faith that I would complete my doctorate despite my continuous reply of "just one more year" was greatly appreciated. Special thanks to Mom, Dad, Lu, Peen, Sarah, Scott, Larissa and my precious nieces Sofia, Natalia and Alessia for all the skype dates, gmail chats and email updates that always brought a smile to my face.

Finally I have to thank my best friend and husband, Ryan. We survived two years in a long distance relationship, one year of living in an apartment the size of a closet and another two years living in a seniors' residence and despite all of this, I consider the past five (.. or so) years to be amazing. This journey towards my PhD is one we have taken and accomplished together and it would have not been possible without you by my side. I know no matter what our next steps are, if we do it together, we can accomplish anything. I love you!

Abstract

Immune-mediated axonal damage is associated with permanent neurological deficits in multiple sclerosis (MS), a common inflammatory disease of the central nervous system. In this thesis, *in vivo* imaging complemented with *in vivo* application of vital dyes were used to characterize axon dysfunction in mouse models of multiple sclerosis.

First, I helped describe a novel process entitled focal axonal degeneration (FAD) whereby axons form focal swellings which then progress to fragmentation in acute experimental autoimmune encephalitis (EAE), a commonly used mouse model of MS. This process can be recapitulated in healthy mice with application of reactive oxygen/nitrogen species (ROS/RNS) suggestive of their roles as mediators of neuroinflammatory axon damage. How the function of these axons are affected during this damage process, however, was not known.

Axonal transport of organelles between soma and synapses is fundamental to maintain neuronal viability and transport disturbances have been proposed to contribute to neurodegeneration although direct association with neuroinflammatory conditions such as MS has yet to be shown. To bridge these two concepts, I developed an *in vivo* imaging approach that allowed me to directly follow, for the first time, transport of single fluorescently labeled organelles in spinal axons. The results show that axonal transport deficits are pervasive in EAE axons affecting both anterograde and retrograde transport of mitochondria and peroxisomes. Significantly, transport is abolished in the majority of morphologically normal axons independent of demyelination, suggesting axon dysfunction is an early event that precedes overt axon damage. Single particle analysis revealed that organelles stop more persistently within axons of neuroinflammatory lesions compared to control axons. Furthermore, the orientation of microtubules are normal in early stages of axon dysfunction and only appear significantly altered in the more advanced stages of axon damage. Likewise altered microtubule dynamics and tyrosination, which are only increased in a subset of normal-appearing axons, are likely to represent a transition from reversible transport disturbance to permanent transport failure. Administration of a single injection of a corticosteroid (methyl-prednisolone), a

drug often employed to curb relapse symptoms in MS patients, accelerated the recovery of the transport deficit in acute EAE. While transport deficits spontaneously recover in acute EAE, they persist in a chronic EAE model. Finally, application of low concentrations of RNS abolished axonal transport in healthy mice. Conversely, treatment with ROS/RNS scavengers in EAE reversed the transport block, suggesting once again that these inflammatory mediators are important to initiate, and potentially reverse, axon dysfunction. Overall, abnormal axon transport characterizes a prevalent, potentially reversible, early stage of axon dysfunction previously undefined in MS, likely representing an important factor leading to functional deficits in MS and eventual axon loss if left unabated.

Table of Contents

1. Introduction

1.1 Multiple Sclerosis

Multiple sclerosis (MS) is an inflammatory and demyelinating disease of the central nervous system (CNS). It was first described as a distinct clinical entity, "sclérose en plaques," in 1868 by the renowned French neurologist Jean Marie Charcot who also contributed to the development of diagnostic criteria and gave the first complete histological account of MS lesions which included myelin loss and proliferation of nuclei (Charcot, 1868). Although it is considered the most common neurological disease to affect young adults, its pathological heterogeneity has subsequently led to only limited success in understanding its etiology and providing clinical treatment and therefore research into this disease remains essential.

1.1.1 Etiology

Genetic susceptibility as well as environmental factors are believed to play a role in the manifestation of the disease. This interplay, however established, unleashes a series of events including breakdown of the blood brain barrier, multifocal inflammation leading to demyelination, loss of oligodendrocytes, reactive gliosis and axon degeneration (Rejdak et al., 2010).

The genetic makeup of MS susceptibility is complex, showing the greatest prominence amongst individuals of northern European ancestry (Compston and Coles, 2002). The major histocompatibility complex (MHC) has been associated with MS for both class I and class II alleles but this is not unique to MS and is also associated with other inflammatory diseases (Barcellos et al., 2006; Yeo et al., 2007). Owing to the introduction of genome wide association studies (GWAS) the genetic structure of the disease is beginning to unfold and many non-MHC susceptibility alleles have been identified (Hafler et al., 2007; International Multiple Sclerosis Genetics et al., 2011). According to the most recent report, 110 MS risk variants have been identified at 103 discrete loci excluding the MHC complex (Beecham et al., 2013). Essential follow up studies are already underway to understand

whether these genes are causally linked and what is the functional consequence of the genetic variation (Gregory et al., 2012).

Both infectious and non-infectious environmental factors have also been linked to disease predisposition. Most notable among the list of proposed pathogens is the Epstein-Barr virus (EBV) where evidence suggests there is an association of infectious mononucleosis, obtained by individuals who contracted EBV, and MS occurrence (Levin et al., 2010; Warner and Carp, 1981). It is hypothesized that similarities in the pathogenesis of T-cell mediated inflammation within both diseases allows EBV-coded antigens to initiate or enhance the immune response seen in MS (Lunemann et al., 2008). Meanwhile, Vitamin D and smoking are the highest cited non-infectious environmental factors associated with MS susceptibility (Kakalacheva and Lunemann, 2011). Vitamin D is known to act as an immunomodulator, likely exerting its effects through the activity of regulatory T cells as well as other proinflammatory pathways (May et al., 2004). Fittingly, epidemiological studies have linked high vitamin D levels, either through nutrition or exposure to sunlight with lower prevalence of MS (Pierrot-Deseilligny and Souberbielle, 2013). While such studies are still lacking irrefutable results, they may provide insight for the development of prevention strategies or more effective treatment.

1.1.2 Classification

Clinically, MS can reveal itself in several forms. The most common is relapsing remitting disease, whereby episodes of neurological deficits alternate with periods of recovery. Within 25 years of onset, it is then likely that the patient proceeds to secondary progressive form of MS in which there is a gradual increase in permanent neurological disability. In less than 15% of cases, there is a steady decline of neurologic function beginning at the onset of disease without periods of recovery (primary progressive MS) and in an even smaller subset of cases, there arises a steady, progressive neurologic decline interrupted by well-defined acute attacks with or without recovery known as progressive

relapsing MS (Figure 1.1) (Compston and Coles, 2002; Rejdak et al., 2010). Relapse symptoms are thought to reflect the anatomical location of the lesion or plaque, the pathological hallmark of the disease although this correlation does not hold true in the progressive form of the disease. It may affect different sites within the brain or spinal cord, temporally or spatially separated (Lucchinetti et al., 2000). The lesions are classically divided into three pathological categories: active (acute), chronic active and chronic inactive although this classification has now been further divided to include inflammatory components and lesion morphology and it is speculative whether the appearance of the lesion is correlated to disease stage (Lucchinetti et al., 2000).

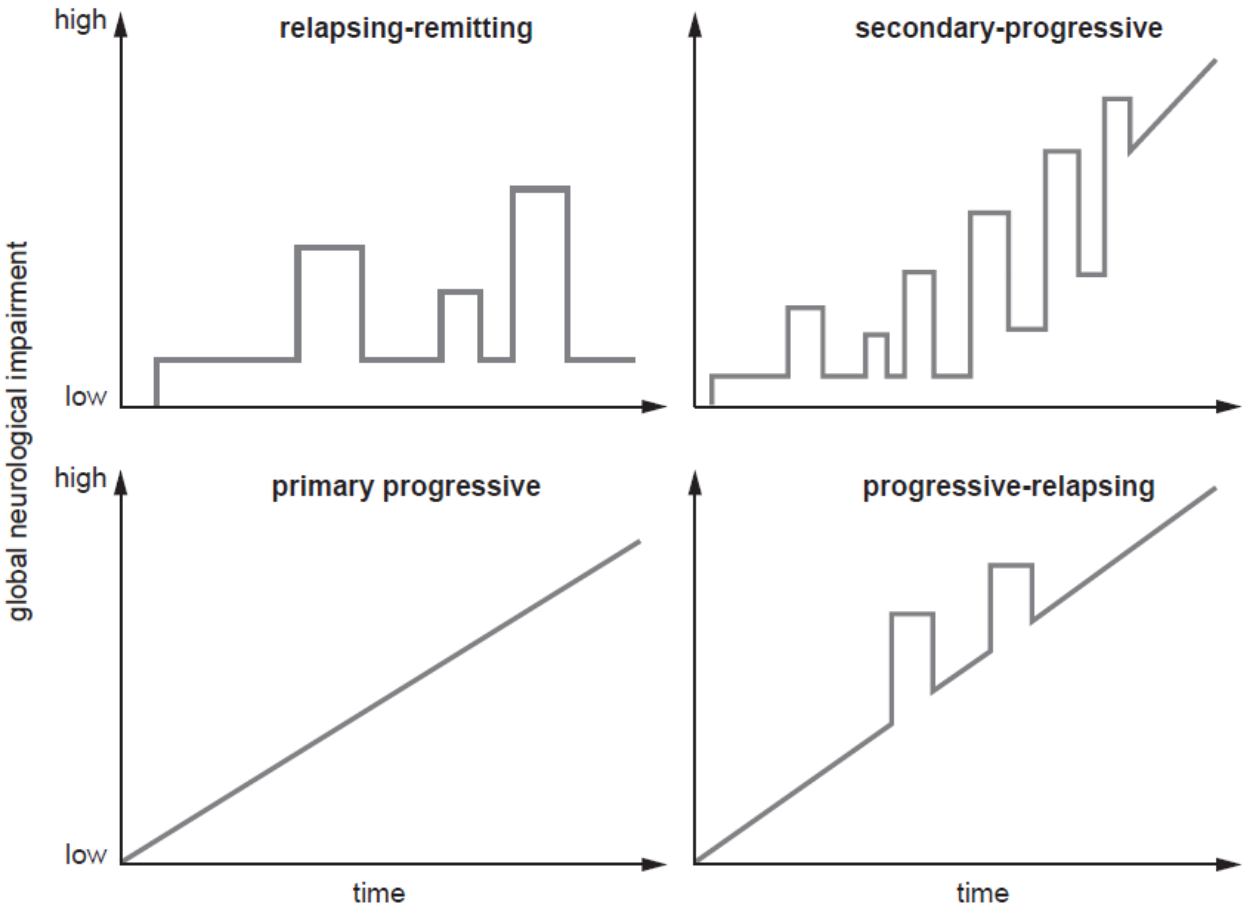

Figure 1.1. Classification of multiple sclerosis

1.1.3 Pathogenesis of MS: Inflammation

The CNS is considered an immune-privileged site with the blood brain barrier (BBB) acting as a barricade, restricting the passage of leuckocytes from the periphery. However, in MS BBB

dysfunction and leukocyte entry from the periphery is believed to be an early event in the disease pathogenesis resulting in demyelination and eventual axon degeneration (Minagar and Alexander, 2003). Thus, the pathogenesis of MS is complex with every immune cell of the innate and adaptive immune response playing a role in orchestrating its devastating effects. Adding to the complexity is the helpful but imperfect animal models including experimental autoimmune encephalomyelitis (EAE, discussed in more detail in section 1.2.6). In the following section, I will review some of the main immune cell contributors.

T cells

T cells have been at the forefront of MS research and have shown to be able to recapitulate the clinical and histological features of autoimmune disease with the EAE model (Zamvil et al., 1985). . Originally derived in the thymus, conventional T cells depart as naïve T cells and become committed to a certain lineage depending on the cytokine environment at the time of priming. Once activated, T cells can enter the bloodstream and the CNS after breakdown of the BBB. Here, they become reactivated by myelin antigens, release mediators and are involved in the recruitment of other immune cells from the blood (Fletcher et al., 2010). Initially, two distinct T helper cell subsets were ascribed as playing the main roles in EAE: Th1 cells which are induced by IFN-γ and IL-12 and Th2 cells which are induced by the presence of IL-4 (Mosmann et al., 1986). Th1 cells primarily target cell-mediated immunity through activation of macrophages and release IFN-γ while Th2 cells serve humoral immunity by targeting B cells and secreting IL-4, IL5, IL-13 and IL-25 (Fletcher et al., 2010). The general view stood that Th1 was responsible for the autoimmune response in MS as IFN-γ was identified in active MS lesions and in EAE at the peak of disease yet decreased during recovery and Th2 responses were found in mice that were resistant to EAE (Constantinescu et al., 2001; Issazadeh et al., 1995). However, a related cytokine, IL-23 caused a reevaluation of this concept. It was essential for EAE induction and yielded a unique subset of T helper cells producing IL-17, consequently named Th17 cells (Cua et al., 2003; Zhang et al., 2003). From these initial discoveries it is now known that IL-23 is required for growth and maturation of pathogenic Th17 cells while TGF-β

in addition to IL-6 or IL-21 were needed for differentiation (Korn et al., 2007a; McGeachy et al., 2007).

An additional class of CD4+ T cells, regulatory T cells (Treg) have shown involvement in MS. Naturally occurring, Treg cells are identified by the intramolecular marker FoxP3 can suppress effector T cell responses directly or through antigen presenting cells (Gavin et al., 2007; Marson et al., 2007). Reduction in their suppressive function or endogenous levels have been shown in MS (Haas et al., 2007; Viglietta et al., 2004). During periods of recovery in EAE the effector T cell response is diminished in favor of an increased presence of Treg cells and have been shown to protect against neuroinflammation (Korn et al., 2007b; Liu et al., 2006; McGeachy et al., 2005). Promotion of this population of cells is therefore an attractive strategy for MS treatment and recent evidence suggests a correlation between clinical symptoms and the decrease in Treg cell number (Carbone et al., 2014). The differentiation and classification of CD4+ T cells is summarized in Figure 1.2.

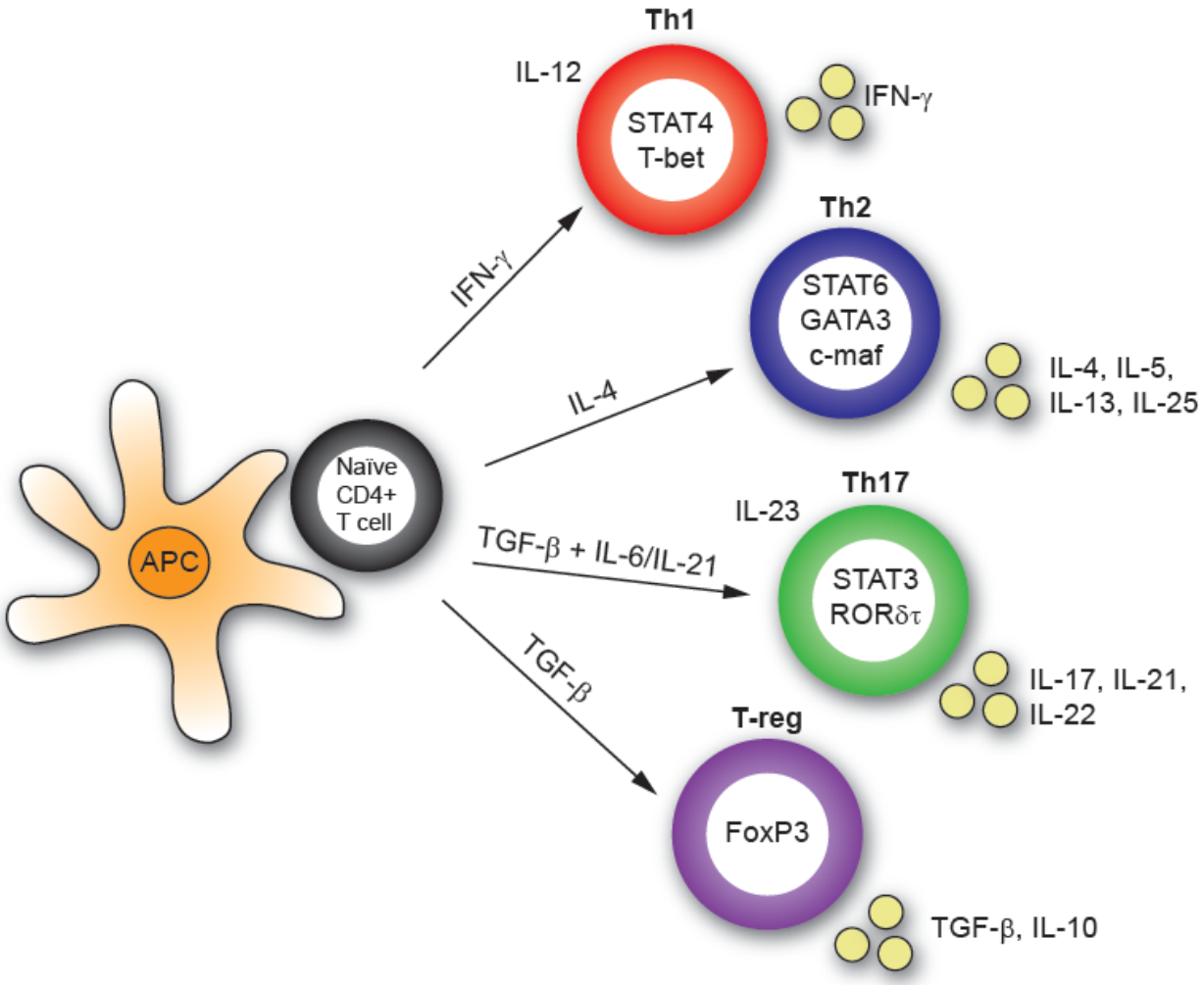

Figure 1.2. Differentiation of CD4+ T cell subsets. Naïve T cells become primed by antigen presenting cells (APC) and differentiate into T helper type 1 (Th1), Th2, Th17 or T regulatory (Treg) cells depending on the cytokine environment. Expression of transcription factors specify each distinct lineage. For example, STAT4 and T-bet expression signify differentiation of a Th1 cell lineage. The functions of the T cells are defined by the unique set of cytokines which they produce. For example, Th1 cells secrete IFN-γ. IL-12 and IL-23 are essential differentiation factors for Th1 and Th17 cells, respectively. Modified from (Korn, 2008)

While classically believed to be a CD4+ T cell mediated disease, CD8+ T cells cannot be overlooked. CD8+ T cells are activated by APCs expressing MHC class I, explaining their original snub as genetic association of MS with MHC class II alleles was significant. Meanwhile, CD8+ T cells outnumber their CD4+ counterparts in acute and chronic lesions, in the aCSF of relapsing-remitting patients and better correlate with axon damage and macrophage/microglia infiltration in lesions (Friese and Fugger,

2009). The molecular mechanisms underpinning the pathogenic role for CD8+ T cells in MS is still unclear. Upon antigen recognition, they release proinflammatory cytokines TNF-α and IFN-γ as well as perforin, granzymes A and B which can directly damage neurons (Huse et al., 2008). For example, TNF-α can bind to the p55 receptor on neurons, silencing survival signals and triggers cell death (Venters et al., 2000). In addition to their cytotoxic role, regulatory CD8+ T cells exist although whether abnormalities in this subset of cells are causes or effects of the disease course is still a debated issue (Hu et al., 2004; Jiang et al., 1992).

Finally, the last class of T cells worthy of discussion in MS pathogenesis are the $\gamma\delta$ T cells. As opposed to conventional T cells whose receptors (TCR) contain a α and β chain, these TCRs are composed of a γ and δ chain. They are believed to be the first line of defense in infection owing to their fast response dynamics and have the ability to influence the adaptive immune response. Early studies show the presence of clonally expanded $\gamma\delta$ T cells in acute MS brain lesions and in cerebrospinal fluid of MS patients with recent disease onset (Oksenberg et al., 1993; Wucherpfennig et al., 1992). However, attributing a protective or pathogenic role to these cells have been inconsistent in part due to methodology and the differences between animal strains (Fletcher et al., 2010). One of the more interesting studies to date on these cells showed that they were able to diminish Treg cell responses and stimulate antigen-specific T cell responses through IL-23, the receptor of which is constitutively expressed on $\gamma\delta$ T cells (Petermann et al., 2010).

Microglia and Macrophages

Microglia are the resident immune cells of the CNS and play an essential role in maintaining homeostasis during development, adulthood and aging. Macrophages, on the other hand, originate from hematopoietic stem cells in the bone marrow and differentiate into blood monocytes which circulate the peripheral vasculature (Ousman and Kubes, 2012). They only enter the CNS and differentiate into macrophages upon injury or inflammation. There is a range of evidence linking both beneficial and harmful effects of macrophages/microglia in MS and its animal models. Studies

have shown that they aide in the recruitment of T cells into the CNS through the increased expression of proteases such as matrix metalloproteinases (MMPs) which allow successful transmigration through the laminin-containing basement membrane of the CNS parenchyma (Dasilva and Yong, 2008; Toft-Hansen et al., 2004). Activated microglia also provide a major source of pro-inflammatory cytokines, chemokines and reactive oxygen/nitrogen species (Carson, 2002; Heppner et al., 2005). These cytokines mediate damage to CNS tissue through sensitization of axons to glutamate toxicity and can also activate and recruit other leukocytes into the CNS propagating the inflammatory response (Pitt et al., 2000). Upon activation, macrophages can be distinguished into two phenotypes which have opposing effects during the disease progression, defined as type 1 (M1) and type 2 (M2) (Figure 1.3) (Gordon, 2003; Martinez et al., 2008). M1 cells are classically activated and are present in the early stages of EAE (Liu et al., 2013; Mikita et al., 2011). M1 cells express high levels of CD86, CD40 and MHCII on their cell surface giving them the ability to prime and recruit T cells into the CNS (Edwards et al., 2006). In addition they also produce pro-inflammatory cytokines and reactive nitrogen species and thus can contribute to EAE development and tissue injury. Alternatively activated M2 macrophages/microglia, on the other hand, gradually increase their expression up until the peak of disease. This later expression profile is believed to contribute to decreased inflammatory infiltrates as a result of their expression of anti-inflammatory cytokines (Porcheray et al., 2005). In addition it has been shown that M2 cell polarization mediates oligodendrocyte differentiation and enhances remyelination *in vitro* and *in vivo* (Miron et al., 2013). Therefore, the balance between these populations represents an interesting aspect of disease progression with potential for therapeutic targeting.

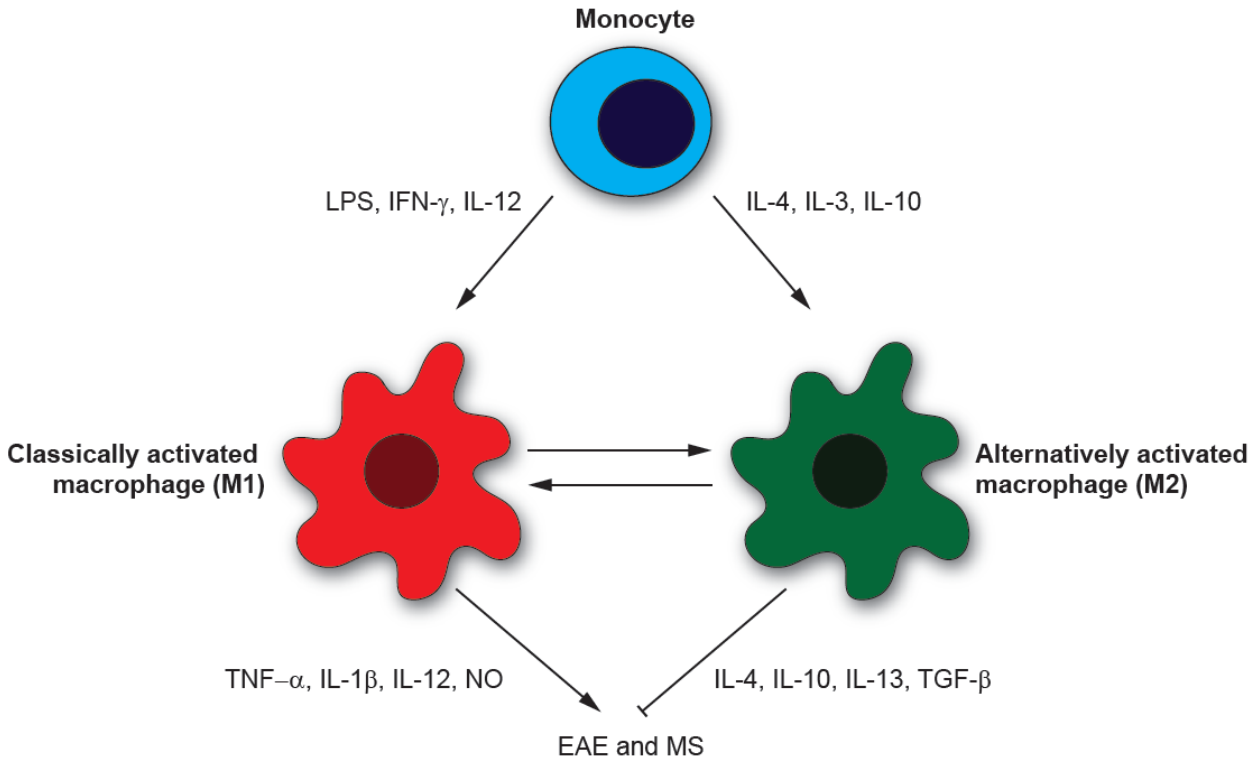

Figure 1.3. Opposing roles of M1 and M2 cells. M1 expression begins early in disease progression, is pro-inflammatory and can induce tissue damage. Meanwhile, M2 cells are involved in immune suppression and tissue repair. Indicated are the factors required for activation as well as the factors secreted following activation. For example, LPS, IFN-γ and IL-12 are required for M1 activation following which, M1 cells release pro-inflammatory cytokines TNF-α, IL-1β, IL-12 as well as nitric oxide (NO). Modified from (Jiang et al., 2014)

B cells

The contribution of B cells in neuroinflammation is often understated and yet many current immunomodulatory therapies in MS are targeted to or inadvertently affect the B cell compartment (Krumbholz et al., 2012). Moreover, histopathological studies have revealed a prominence of immunoglobulins and complement activation in acute, demyelinating lesions (Breij et al., 2008; Lucchinetti et al., 2000; Storch et al., 1998). B cells have both regulatory and proinflammatory effects. They can act as antigen presenting cells as well as a source of auto-antibodies against CNS targets (Molnarfi et al., 2013; Stefferl et al., 1999). They are able to secrete inflammatory cytokines that function to activate both T cells and macrophages as well as the converse, secreting cytokines

that inhibit T cell and macrophage activation although the latter is considerably less predominant in MS patients (Barr et al., 2012; Fillatreau et al., 2002). Identifying specific autoantibody responses in MS is currently the focus of much research, especially after the successful identification of the serum autoantibody against water channel aquaporin-4 (AQP4) distinguishing neuromyelitis optica as a distinct disease from MS (Roemer et al., 2007). Promising candidates thus far include, neurofascin, a protein found on myelinated axons at the nodes of Ranvier, which has been associated with axonal damage in EAE (Mathey et al., 2007) and an ATP-sensitive inward rectifying potassium channel KIR4.1 (Srivastava et al., 2012).

1.1.4 Pathogenesis of MS: Tissue/Neuronal damage

Although originally overlooked in importance, the best correlate for the severity of persisting neurological deficits and an early event in the progression of MS is axon loss and represents a new avenue for therapy based upon neuroprotective strategies (Bitsch et al., 2000; Bjartmar et al., 2000; Ferguson et al., 1997; Trapp et al., 1998). Technical limitations for the identification of axons in multiple sclerosis biopsies had long since dogged the proper characterization and extent of axon damage. It was not until the late 1990's and the use of a staining technique for amyloid precursor protein (APP) to label damaged axons that the first clues that axon damage occurs early within MS lesions began to emerge (Ferguson et al., 1997). This was followed a year later with a study that could also identify terminal axonal swellings or ovoids using an antibody against non-phosphorylated neurofilament, SMI-32 within both active and chronic lesions (Trapp et al., 1998). Abnormal accumulations of other proteins also emerged including the pore forming subunit of neuronal (N)-type voltage-gated calcium channels (Kornek et al., 2001) and metabotropic glutamate receptors (Geurts et al., 2003). In addition to improvements in visualization of fixed tissue samples, advances were also made in the 1990's using a different imaging modality than the commonly used T_2-weighted MRI brain lesion volume measurements to follow patients with MS and understand the correlation between clinical signs and pathological features of the disease. Proton magnetic

resonance spectroscopy demonstrated decreases in N-acetylaspartate (NAA) in the brains of patients with MS, a metabolite found almost exclusively in neurons and neuronal processes (Arnold et al., 1994; Matthews et al., 1996; Wolinsky et al., 1990). Axonal damage, as measured by this means, was positively correlated with disability in those suffering from relapsing remitting MS (De Stefano et al., 1998; Fu et al., 1998). In follow-up studies, the extent of axon of axon loss in spinal cord autopsies from 5 severely disabled, chronic MS patients could be quantified and correlated with reduced levels of NAA. Interestingly, it was found that the average axonal loss in these lesions was about 70% and affected both myelinated and demyelinated axons and both white and gray matter of the spinal cord (Bjartmar et al., 2000).

MS has traditionally been viewed as a disease affecting the white matter and, indeed, most of the above mentioned studies investigated this region alone. However, with the development of more advanced MRI techniques, grey matter atrophy can now be reliably measured and associates with physical disability and cognitive impairment (Jacobsen and Farbu, 2014). Post-mortem analyses have revealed axonal damage and neuronal loss also present in the cortical grey matter (Peterson et al., 2001; Wegner et al., 2006). Grey matter atrophy was also enhanced in patients with advance stages of MS (Fisher et al., 2008; Oreja-Guevara et al., 2005; Valsasina et al., 2005) although they can already be detected after a single isolated episode and may be predictive of patients who quickly fall to MS (Calabrese et al., 2011; Dalton et al., 2004; De Stefano et al., 2003). Importantly, studies show that grey matter atrophy was significantly correlated with disability (Fisher et al., 2008; Geurts et al., 2009) underlining its clinical relevance and suggesting that grey matter atrophy results directly from grey matter pathology and is not secondary to white matter damage. Whether the neuronal damaging mechanisms at play in white versus grey matter are similar have yet to be determined.

1.1.5 Mechanisms of Axon Dysfunction

It was not long after this paradigm shift in MS research that theories arose as to what mechanism causes axon degeneration in MS (summarized in Figure 1.4). Correlation of acute axonal damage and inflammatory cell infiltration suggest that either a direct immunological attack or indirect damage by release of soluble mediators by such cells could initiate the damage process leaving the axon vulnerable to breakdown (Bitsch et al., 2000; Kuhlmann et al., 2002). Isolating a sole culprit is clearly a challenging task in such a complex disease (Liblau et al., 2013; Siffrin et al., 2010b). With the advent of *in vivo* deep-tissue imaging, direct monitoring of immune-neuron interactions is being investigated in hopes of capturing this process as it happens. In acute mouse brain slice preparations, Nitsch *et al* were able to demonstrate direct contact of T cells specific to proteolipid protein (PLP) epitope or the non-murine protein ovalbumin (OVA) onto neurons causing a rise in neuronal calcium levels eventually reaching a lethal degree (Nitsch et al., 2004). Furthermore, *in vivo* observation of Th17 cells in the brainstem of EAE mice showed direct interaction onto neurons causing potentially reversible neuronal dysfunction once again including increased intracellular calcium levels (Siffrin et al., 2010a). Soluble factors and surface molecules that may play a role in mediating immune-neuron interaction have also been suggested, such as reactive oxygen species, which will be discussed in detail later, myelin breakdown products or apoptotic mediators. Tumor necrosis factor (TNF)-related apoptosis inducing ligand (TRAIL), as an example, is upregulated on the surface of T cells following antigen-specific stimulation and clinical severity in EAE mice can be significantly reduced after brain-specific inhibition (Aktas et al., 2005).

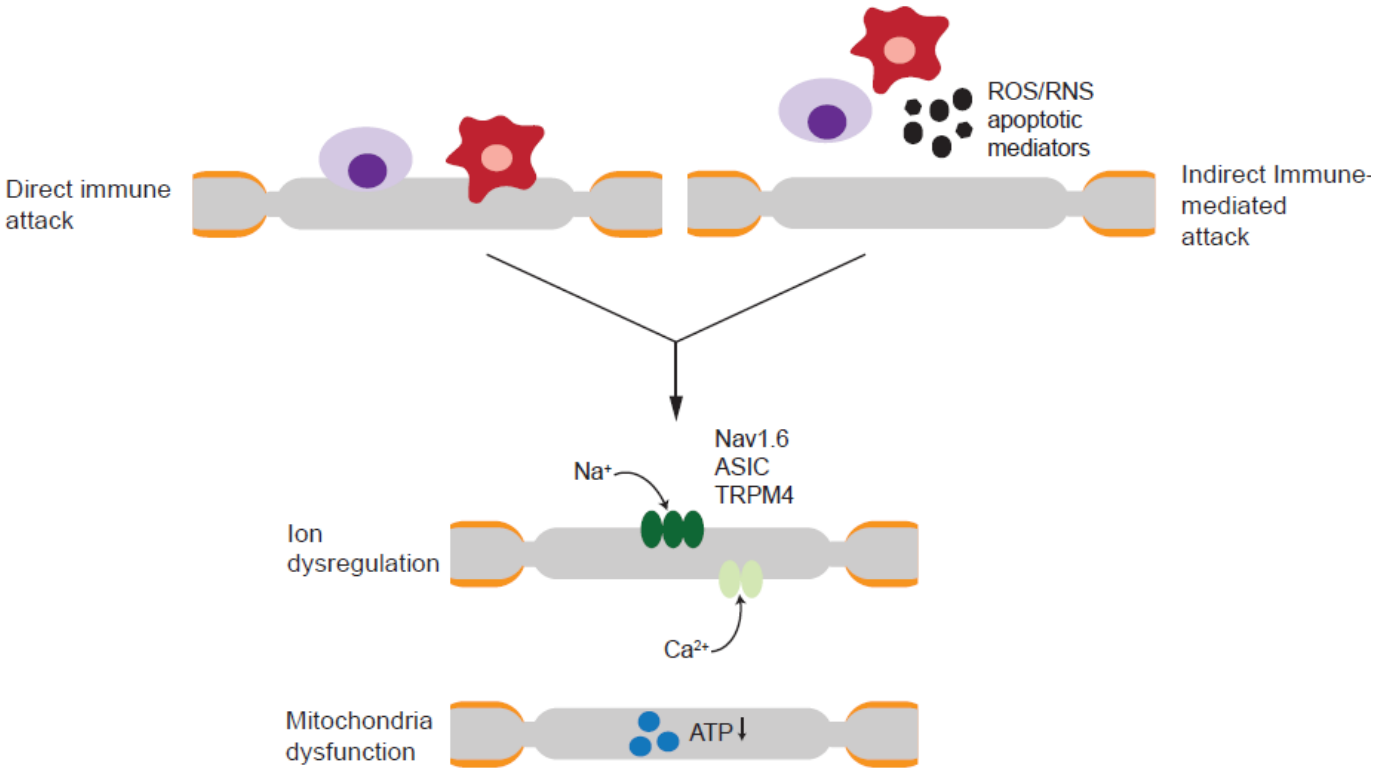

Figure 1.4. Mechanisms of axon damage in multiple sclerosis. Axon damage is believed to occur due to direct immune attack or an indirect immune attack mediated by the release of reactive oxygen/nitrogen species (ROS/RNS) as well as proteases and other apoptotic mediators by immune cells. This initial immune-mediated attack and demyelination leaves the axon susceptible to breakdown through ion dysregulation and mitochondrial dysfunction.

Ion dysregulation

Another potential contributor to axonal damage following immune attack is ion dysregulation as a compensatory mechanism to demyelination. Insulation of axons provided by myelin sheaths serve to prevent the loss of current through the axonal membrane as well as the aggregation of sodium channels at Nodes of Ranvier, areas devoid of myelin, thus enabling action potentials to jump from one node to another, known as salutatory nerve conduction, and allowing for the fast processing of information. Loss of myelin can lead to ectopic expression of sodium channels, believed to support the recovery of axon potential conduction (Black et al., 2007; Craner et al., 2004a; Craner et al., 2004b). This altered expression by, in particular, the Nav1.6 sodium channel, produces a persistent

sodium current which drives the sodium-calcium exchanger to operate in reverse, thus importing calcium and triggering detrimental secondary cascades including calcium release from internal stores, activation of nitric oxide (NO) synthase as well as proteases (Stys et al., 1992). Sodium channel blockers have hence proven successful in protecting axons in EAE (Bechtold et al., 2004; Lo et al., 2003). An additional immunomodulatory mechanism may also be at play, though, as recent evidence indicates that sodium channels are also present in microglia and macrophages and this expression is increased during EAE and is important for their function *in vitro* (Black et al., 2009; Craner et al., 2005). To this end, blocking sodium channels pharmacologically with phenytoin in wildtype mice or genetically in mice which lack Nav1.6 channels, also attenuated the inflammatory activity (Craner et al., 2005). Altered expression of other ion channels such as Na^+-Ca^+ antiporters (Craner et al., 2004a), acid-sensing ion channels (ASICS) (Friese et al., 2007) and transient receptor potential melastatin 4 (TRPM4) (Schattling et al., 2012) have also been shown to contribute to axonal degeneration in MS models.

Despite these advances, there is a glaring conflict – axonal damage can take place independent of demyelination (Aboul-Enein et al., 2006; Das Sarma et al., 2009; Rivera-Quinones et al., 1998) and evidence is lacking in the human disease that loss of axons is secondary to demyelination as axonal loss is also seen in normal appearing white matter (Arnold et al., 1994; De Stefano et al., 1998). It remains unclear whether this represents two independent forms of axon degeneration within an already heterogeneous disease.

Chronic CNS inflammation can affect the homeostasis of a host of other factors as well. Disturbance of the glutamate metabolism and subsequent excitotoxicity has also been shown in mouse models as well as MS lesions to contribute to or correlate with axonal damage (Pitt et al., 2000; Werner et al., 2001) with treatment by AMPA antagonists providing partial amelioration in the animal model (Smith et al., 2000).

Mitochondrial dysfunction and oxidative damage

Finally, axonal injury can be caused by an energy failure, a lack of ATP produced by mitochondria and ultimately mitochondrial dysfunction. This can present itself in many forms. It can be downstream of the aforementioned ion dysregulation, impairing the ability of the axon to maintain resting membrane potential and therefore the mitochondria's ability to maintain proper calcium balance. It can also be caused by exposure of the mitochondria to increased levels reactive oxygen species (ROS) and nitric oxide (NO), termed oxidative stress (Brorson et al., 1999; Smith et al., 2001).

ROS are produced intracellularly e.g. during ATP production and have important physiological roles in cell signaling and homeostasis. However, if present in excessive amounts (e.g. during an immune-mediated attack when they are exogenously released by immune cells) they can become pathogenic. NO, similarly, is normally produced in nanomolar quantities in a calcium-dependent manner by nitric oxide synthase (NOS), either endothelial or neuronal, for activities such as regulation of blood flow and synaptic transmission. During inflammation, concentrations of NO greatly increase due to its production by an inducible form of the enzyme, iNOS, in a calcium independent manner. It can be released by activated macrophages and is increased in MS lesions as well as EAE animal models (Bo et al., 1994; Lin et al., 1993). Emerging evidence is underlining the significance of oxidative damage and MS, and suggests that oxidative bursts through ROS production by NADPH oxidase can be important for the progression of demyelination and neurodegeneration in MS lesions (Fischer et al., 2012; Haider et al., 2011).

Oxidative stress can also lead to mitochondria dysfunction in several ways. Free radicals can abolish mitochondrial enzyme function, modify mitochondrial proteins and induce their degradation as well as induce damage to mitochondrial DNA (Bolanos et al., 1997; Federico et al., 2012). Indeed, oxidative damage to mitochondrial DNA and enzymes has been seen in chronic active plaques from MS patients (Lu et al., 2000). Analysis within acute and chronic active lesions of progressive MS patients showed a decrease in activity of the mitochondrial respiratory chain complex IV, mostly due

to mitochondria depletion, in demyelinated and APP positive axons which was inversely related to immune infiltration (Mahad et al., 2008; Mahad et al., 2009).

1.1.6 Treatment

The current aims for treatment of MS are extensive: reduce the number of relapses, the severity of attacks, and the accumulation of lesions, slow the progression of disability as well as manage neurological deficits (Conway and Cohen, 2010). The number of approved drugs has increased over the last 20 years and, while encouraging, presents many challenges to the physician in choosing the correct treatment and balancing efficacy, safety, and compliance to the treatment regime by the patient. The current guidelines for therapy published by German Society for Neurology appears below in Table 1.

Immunomodulating therapies have shown the greatest success in modifying the disease course. The most commonly prescribed of these are the self-injectable interferons and glatiramer acetate followed by natalizumab (multiple sclerosis international federation, www.msif.org). Other available treatments in Germany include alemtuzumab, fingolimod, dimethyl fumarate, mitoxantrone, and teriflunomide, each of which will be described briefly below.

Classification	CIS[1]		RRMS[1]			SPMS[1]	
Disease-modifying Therapy	(High) extensively active form		*Option 1* - Alemtuzumab - Fingolimod - Natalizumab	*Option 2* - Mitoxantrone (-Cyclophosphamide)[4]	*Option 3* - Experimental Methods	*with relapses*	*without relapses*
	Mild / moderate progressive form	- Glatiramer acetate - Interferon-β 1a i.m. - Interferon-β 1a s.c. - Interferon-β 1b s.c. - Teriflunomide *(-Azathioprine)[2]* *(-Mg)[3]*	- Dimethyl fumarate - Glatiramer acetate - Interferon-β 1a i.m. - Interferon-β 1a s.c. - Interferon-β 1b s.c. - Terifluonomide *(-Azathioprine)[2]* *(-Mg)[3]*			- Interferon-β 1a s.c. - Interferon-β 1b s.c. - Mitoxantrone *(-Cyclophosphamide)[4]*	-Mitoxantrone *(- Cyclophosphamide)[4]*
Relapsing Therapy	*Option 2*	- Plasma exchange					
	Option 1	- Methylprednisolone					

Upon failure of a disease modifying therapy in mild / moderate progressive form of MS, these patients are treated as an active MS case

[1] Substances in alphabetical order; the representation chosen here implies NO superiority of one substance to another within an indication group (shown inside a box)

[2] Approval achieved when interferon-ß is not possible and the clinical course with Azathioprine therapy is stable

[3] Use after childbirth only justified in individual cases, especially in the context of lacking treatment alternatives

[4] Provide only for severe cases as an alternative therapy, ideally at designated MS centers

Table 1. Stepwise therapy for Multiple Sclerosis. Translated into English from the "Leitlinien für Diagnostik und Therapie in der Neurologie", published by the Kommission "Leitlinien" der Deutschen Gesellschaft für Neurologie, Stuttgart, September 2012

CIS = clinically isolated syndrome, RRMS = relapsing remitting multiple sclerosis, SPMS = secondary progressive multiple sclerosis, s.c = subcutaneously, i.m = intramuscularly

For the treatment of relapsing MS, Interferon beta 1-b and glatiramer acetate are still considered to be the first line of response and have been found to reduce the frequency of relapse and may delay the progression of disability (Kappos et al., 2007; Kappos et al., 2006; Khan et al., 2013). Their safety profiles are very favorable and require minimal monitoring requirements which allows them to remain at the forefront of treatment. However, compliance to the treatment regimen is low due to frequency and route of administration (intramuscular or subcutaneously) and in light of new drugs with infrequent dosing and oral administration (Wingerchuk and Carter, 2014). The specific mechanism of action of these drugs are still not fully known although they are certain to intervene in immune activities. In short, the interferons decrease T cell proliferation, production of tumor necrosis factor α (TNF α), reduce antigen presentation, modify cytokine production, and lessen the passage of immune cells across the blood brain barrier through modification of adhesion molecules, chemokines and proteases (Compston and Coles, 2002; Noseworthy et al., 2000). Glatiramer acetate

is a mixture of synthetic polypeptides of glutamic acid, lysine, alanine and tyrosine. It mimics a peptide fragment of myelin basic protein (an auto-antigen) thereby blocking T cell activation or possibly acting as an altered peptide ligand (Noseworthy et al., 2000). There is also evidence in EAE that it can promote the development of anti-inflammatory M2 macrophages, inducing regulatory T cell and improving disease outcome (Weber et al., 2007).

Alemtuzumab is a monoclonal antibody which is directed against CD52 receptors, found on monocytes and lymphocytes. Intravenous treatment depletes T, B and natural killer cells, in particular though, CD4+ T cells. Treatment with alemtuzumab is typically repeated at 1 year when T cells are believed to have repopulated with the potential to extend annually after that (Wingerchuk and Carter, 2014). The largest safety concern for this drug, and one reason it has not yet been given approval for use in America is novel autoimmunity, occurring in 20-30% of people up to five years after treatment (Jones and Coles, 2014). It remains a viable treatment option especially as the dosing is infrequent, for those who dislike injections, and it is the only treatment that provides disease control safely during gestation for women who wish to become pregnant (Jones and Coles, 2014).

Mitoxantrone is a general immunosuppressive drug delivered intravenously and is generally used for aggressive relapsing-remitting MS as well as secondary progressive MS. While it had been shown to mildly reduce the rate of attacks, cumulative dose-related cardiac toxicity and leukemia limits its administration to two years (Marriott et al., 2010).

Natalizumab, also administered intravenously, is designated for patients with aggressive MS, classified as two or more disabling relapses in one year and subsequent increase in lesion size as shown by an MRI. It was the first recombinant, humanized monoclonal antibody developed for MS against the α4 chain of α4β1 integrin, an adhesion molecule whose antigen is expressed on the majority of leukocytes thereby preventing these cells from leaving the periphery and reducing inflammation (Compston and Coles, 2002).

Oral Treatments

Fingolimod is a first-line orally administered drug that structurally mimics the sphingosine 1-phosphate receptor (S1PR), present on the surface of lymphocytes providing selective and reversible retention of lymphocytes in lymph nodes (Pelletier and Hafler, 2012). Treatment resulted in a decrease in the number of new or growing lesions based on MRI data and reductions of brain volume were smaller with fingolimod-treated patients compared to controls (FREEDOMS II, NCT00355134, clinicaltrals.gov).

Terifunomide, a once-daily oral drug is the active metabolite of the rheumatoid arthritis drug leflunomide. It is a high affinity inhibitor of the enzyme dihydroorotate dehydrogenase, essential for pyrimidine synthesis. Fast proliferating cells such as activated lymphocytes require this reaction for sustainability of DNA, lipid and sugar metabolism (Claussen and Korn, 2012; O'Connor et al., 2011; Wolinsky et al., 2013).

Dimethyl fumarate is also a first-line oral medication for treatment of relapsing remitting MS as has been proven more effective than its non-oral counterparts (Bitsch et al., 2000; Fox et al., 2012; Gold et al., 2012a). It has been shown to activate the nuclear factor erythroid-derived 2-related factor 2 (NRF2) pathway, which protects against oxidative stress-related neuronal death and damage to myelin although whether this occurs *in vivo* and modifies the pathogenesis of MS is debated (Gold et al., 2012b; Linker et al., 2011). New evidence suggests that dimethyl fumarate or more specifically its active metabolite, monomethyl fumarate, exerts its protective effect by acting as an agonist of the G protein coupled membrane receptor, hydroxycarboxylic acid receptor 2 (HCA_2), expressed by immune cells such as neutrophils (Chen et al., 2014).

Treating exacerbations

Clinical treatment during relapses to speed recovery can be accomplished by repeated, high dose intravenous injections of glucocorticosteroids, namely methylprednisolone (Miller et al., 2000). This

potent anti-inflammatory drug is believed to exert its affects in part by inducing T-cell and microglial apoptosis, stimulating regulatory T cells, and constriction of the blood brain barrier (Reichardt et al., 2006).

Future strategies

Despite the disease modifying treatments which are available, advancement into secondary progressive MS is at present difficult as is a convincing therapy to repair or regenerate neurons, oligodendrocytes or supporting glia. Recently, there is positive evidence for the use of 3-hydroxy-3-methylglutaryl-CoA (HMG-CoA) reductase inhibitors, statins, to treat secondary progressive MS (Chataway et al., 2014). Normally beneficial for their cholesterol lowering effect, new studies show they also have immunomodulatory function. These include inhibition of MHC class II antigen presentation, decrease in T-cell activation and proliferation as well as a switch towards a Th2 pro-inflammatory response (Greenwood et al., 2006). High-dose simvastatin is now in phase 3 testing after a significantly lower atrophy rate was seen in treated patients (Chataway et al., 2014).

1.1.7 EAE for the study of MS

The classical model for the study of MS in animals has been experimental autoimmune encephalomyelitis (EAE) first developed in the 1930s at Rockefeller University through experiments proposed to understand acute neurologic episodes that accompanied viral infections such as smallpox or vaccinations such as those against rabies (Rivers et al., 1933). Although not without its share of critics (Sriram and Steiner, 2005), it can be credited for the development of at least three currently available disease modifying therapies: glatiramer acetate, (Teitelbaum et al., 1971; Teitelbaum et al., 1972) natalizumab (Yednock et al., 1992) and most recently fingolimod (Brinkmann et al., 2002).

In active EAE, as is used in this thesis, induction occurs by immunization with myelin agents, complete Freund's adjuvant (CFA) and pertussis toxin. This causes activation of antigen presenting

dendritic cells by the Toll-like receptor (TLR) agonists within the mycobacterium tuberculosis component of CFA, which then present the myelin antigen to naïve T cells (Su et al., 2005). Following this, activated myelin-specific T cells enter the bloodstream and ultimately pass into the CNS. Subsequent breakdown of the blood brain barrier recruits other inflammatory cells into the CNS. T cells, upon entering the CNS, meet similar myelin antigens and are in turn reactivated by local antigen presenting cells. As a result they multiply, release inflammatory mediators and recruit other immune cells (Stromnes and Goverman, 2006). As is the case in MS, this immune infiltration promotes myelin breakdown, axonal damage and neurological deficits.

There are, however, other methods of inducing EAE. In adoptive transfer of EAE, activated myelin specific Th1 or Th17 cells from immunized donors are transferred into naïve, genetically-identical recipients (Raine et al., 1984; Zamvil et al., 1985). It is considered a more direct way of characterizing T cell effector function in CNS and can be used to track T cells *in vivo*, to study CNS immune infiltration and to easily pharmacologically manipulate T cell function. The clinical features of the disease, nevertheless, are identical to those in active EAE (Rangachari and Kuchroo, 2013).

The artificial mode of induction of EAE was a commonly described disadvantage of the model as it could not simulate the spontaneous onset of MS and therefore was considered significantly less complex than its human counterpart. Recently, however, two spontaneous EAE models have been discovered. The OSE (opticospinal encephalomyelitis) mouse in a C57BL/6 background (Bettelli et al., 2006; Krishnamoorthy et al., 2006) and the RR (relapsing-remitting) mouse in a SJL/J background (Pollinger et al., 2009). In these mice models B cells play a larger role in modulating the disease and are being used to further understand their function in EAE and MS (Berer et al., 2011).

Despite the caveats of animal models, EAE is a powerful tool for studying the mechanisms behind autoimmune mediated inflammation and axonal damage in the CNS and ultimately to discover and test potential therapeutic targets for MS although, as with any animal model, caution is warranted before using results as a predictor for efficacy in patients (Friese et al., 2006; Steinman and Zamvil, 2006)

1.2 Axonal Transport

1.2.1 Significance

As neurons are inherently polar with three unique components, namely the cell body, the axon and dendrites, the trafficking of organelles, especially mitochondria, is essential for their function and survival. The metabolic requirements within these neuronal parts differ, so then must the distribution of organelles. The most well studied organelle which undergoes axonal transport is the mitochondrion, whose function is essential for energy production and calcium buffering within axons. Therefore, axonal transport as is known for mitochondria will be the main focus of this section. Areas which require large amounts of energy in the form of adenosine triphosphate (ATP) such as pre- and post-synaptic terminals, and nodes of Ranvier, will subsequently require more mitochondria than other areas (Li et al., 2004; Morris and Hollenbeck, 1993; Sun et al., 2013; Zhang et al., 2010). This signifies the requirement for specialized, efficient transport machinery for both organelle delivery and regulation of docking when necessary.

1.2.2 Mitochondrial movement behavior

The movement of mitochondria is bidirectional and they have the ability to quickly switch between outward (anterograde) and inward (retrograde) transport directions although in most experimental settings the majority of their movement is in the anterograde direction (Hollenbeck, 1996). Mitochondria can, as well, switch from moving to stationary states depending on intracellular signals and axonal growth (Morris and Hollenbeck, 1993). Long distance fast axonal transport of these organelles requires microtubules (MTs). MTs are uniformly oriented within axons with plus ends pointing to the synapse and minus ends to the cell soma lending itself to unidirectional and organized transport when coupled to the correct MT-binding motor protein (Black and Baas, 1989).

1.2.3 Mitochondrial transport machinery

Great strides have been recently made in understanding the mitochondrial motor/adaptor complex (Brickley and Stephenson, 2011; Fransson et al., 2003; Fransson et al., 2006; Glater et al., 2006; Guo et al., 2005; Stowers et al., 2002). The core contains kinesin-1, the anterograde motor protein that can carry many cellular cargos along the microtubule track and is bound to mitochondria by two organelle-specific adaptor proteins: Milton and Miro. Dynein, the retrograde motor protein, can also interact with Milton and Miro and will be discussed below (summarized in Figure 1.5).

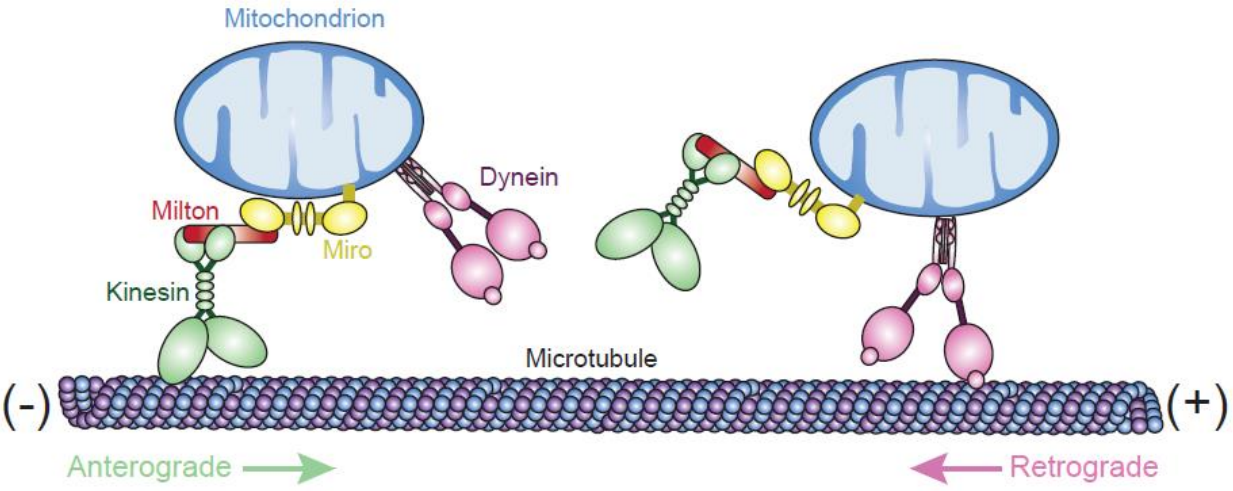

Figure 1.5. Mitochondrial transport machinery (modified from (Sheng and Cai, 2012))

Kinesin-1, which is made up of a kinesin heavy-chain (KHC) and kinesin light chain (KLC) subunit, was first discovered in squid axoplasm as a MT-dependent organelle transporter (Figure 1.6) (Brady, 1985; Vale et al., 1985). The mammalian genome encodes three different KHC isoforms, KIF5A, KIF5B and KIF5C (Nakagawa et al., 1997) and at least three KLC subunits named KLC1, KLC2 and KLC3 (Rahman et al., 1998). KIF5B is ubiquitously expressed while KIF5A and 5C are expressed solely in neurons. Meanwhile, KLC1 expression is increased in neurons while KLC2 is uniformly expressed amongst different tissues. All KHC isoforms have an amino-terminal motor domain that travels toward the plus-end of the MT, a large coiled-coil tail that facilitates dimerization and a carboxyl

terminal region that binds cargo with the help of the KLC, although the necessity of KLC is currently debatable, as discussed later. The KHC is indispensable for mitochondrial movement as shown following generation of mutations in both mice (Tanaka et al., 1998) and *Drosophilia* (Hurd and Saxton, 1996) and from its association with other proteins of the motor/adaptor complex (Glater et al., 2006).

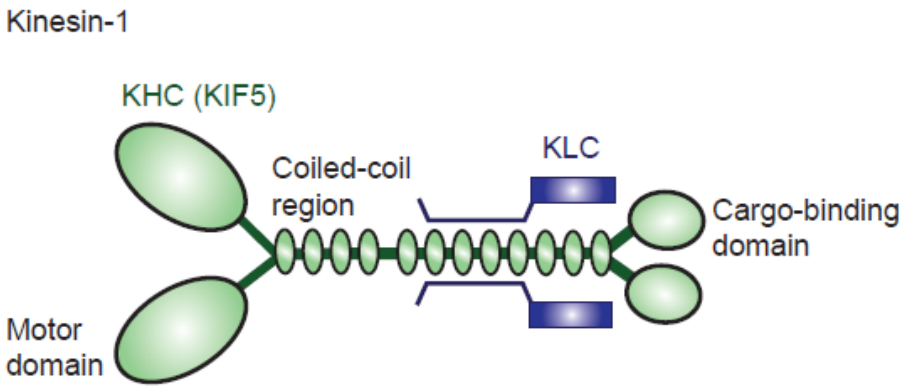

Figure 1.6. Structure of anterograde motor protein, kinesin-1. Kinesin is composed of two heavy chains (KHC) and two light chains (KLC). The KHC contains three domains: the N-terminal motor domain which interacts with the microtubules, a coiled-coil region which facilitates dimerization and the carboxyl terminal cargo-binding domain which interacts with adaptor and cargo molecules. (modified from (Sheng and Cai, 2012))

Milton, an adaptor protein, was first identified in a mutant screen for blind *Drosophilia* and thus named after the blind seventeenth century poet, John Milton (Stowers et al., 2002). The mutant flies had impaired synaptic transmission and photoreceptor axons were devoid of mitochondria although their distribution and functionality in the soma were unchanged. The protein itself was found to co-localize with mitochondria *in vitro* and *in vivo* within axons and synaptic regions and associate with the KHC (Stowers et al., 2002). There exists two mammalian homologs, TRAK (trafficking kinesin protein) 1 and TRAK2 also known as O-linked N-acetylglucosamine-interacting protein 106 (OIP6) and γ–aminobutyric acid A receptor-interacting factor-1 (GRIF-1) which display the same characteristics as the fly ortholog (Beck et al., 2002; Brickley and Stephenson, 2011; Iyer et al., 2003). This includes, most importantly, its direct association with the KHC, which surprisingly is independent of the KLC

(Glater et al., 2006). The KLC actually competes with Milton for binding to the KHC begging the question of what the role of KLC is, if any, in mitochondrial trafficking.

The association of the motor/adaptor complex with mitochondria is mediated by interactions with Miro, a Mitochondrial Rho GTPase (Figure 1.7). It was first discovered in the yeast model, *Saccharomyces cerevisiae,* and displayed an abnormal growth phenotype following gene disruption only when grown in medium supplemented with high concentrations of calcium, foreshadowing the forthcoming calcium-sensing role (Wolff et al., 1999). It was later re-identified in a human genomic screen in an effort to uncover other families of Rho GTPases. Miro-1 and Miro-2, atypical when compared to other classical Rho GTPases, were found to interact with mitochondria and contained two potential calcium-binding sites, termed EF hands in the linker region between the two GTPase domains (Fransson et al., 2003). Here, a mutation causing a constitutively active Miro-1 caused aggregation of mitochondria which was later attributed to its role in mitochondrial trafficking by showing an interaction of Miro-1 and Milton homologs (Fransson et al., 2003; Fransson et al., 2006). Soon thereafter, the *Drosophilia* Miro (dMiro) was discovered in a genetic screen that produced changes in synaptic structure and function and could link dMiro with an essential role in anterograde axonal transport of mitochondria and its correct subcellular distribution (Guo et al., 2005).

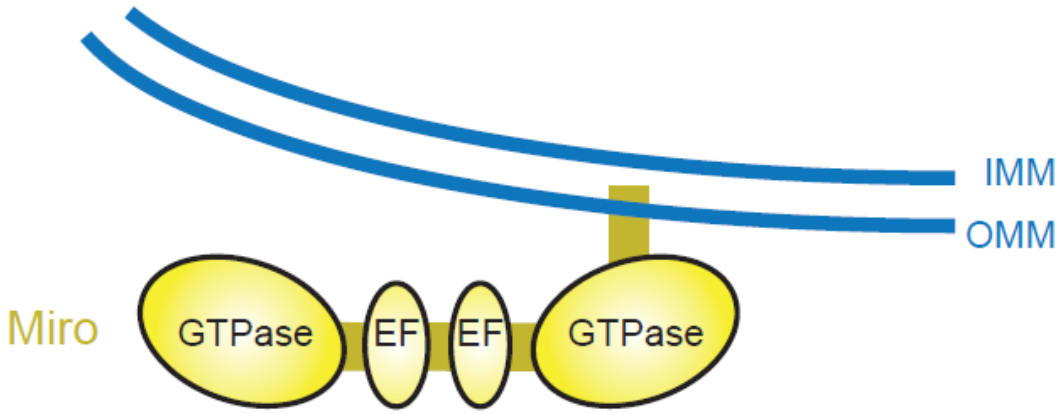

Figure 1.7. Structure of mitochondrion-specific adaptor protein, Miro. It contains two calcium binding EF hands which are flanked by GTPase domains. The protein is anchored to the outer mitochondrial membrane (OMM) via a trans-membrane domain at its carboxyl terminus (IMM, inner mitochondrial membrane) (modified from (Schwarz, 2013)).

The establishment of the retrograde motor, dynein, came in the same experimental model as that of kinesin, the squid axon (Schnapp and Reese, 1989; Waterman-Storer et al., 1997). It is involved in the retrograde transport of mitochondria in axons, some synaptic vesicle components and neurotrophic signals back to the cell soma. It is composed of two dynein heavy chains (DHCs) which fold to function as motors, and many dynein intermediate chains, dynein light intermediate chains and dynein light chains (Figure 1.8) (Karki and Holzbaur, 1999). Dynactin, consisting of at least 7 polypeptides including $p150^{Glued}$, is required for most, perhaps all of dynein-mediated transport (Holleran et al., 1998). In contrast to the many kinesin isoforms, only a few cytoplasmic dynein isoforms have been so far described (Vaisberg et al., 1996). They are believed to selectively direct cargo into dendrites which, in contrast to axons, contain a mixed microtubule array and drive bidirectional transport (Kapitein et al., 2010). An interdependence of kinesin-1 and dynein has been shown suggesting a direct physical or regulatory connection that is essential for controlling transport and distribution of mitochondria (LaMonte et al., 2002; Martin et al., 1999; Waterman-Storer et al., 1997). Most recently, it was shown that TRAK1 and TRAK2 can differentially regulate sorting of mitochondria between axons and dendrites by alternative binding with kinesin or dynein motors (van Spronsen et al., 2013). TRAK1 is able to bind both motors, is chiefly expressed in axons and is essential for axon outgrowth while TRAK2 preferentially binds to dynein/dynactin, present mostly in dendrites and is required for their development.

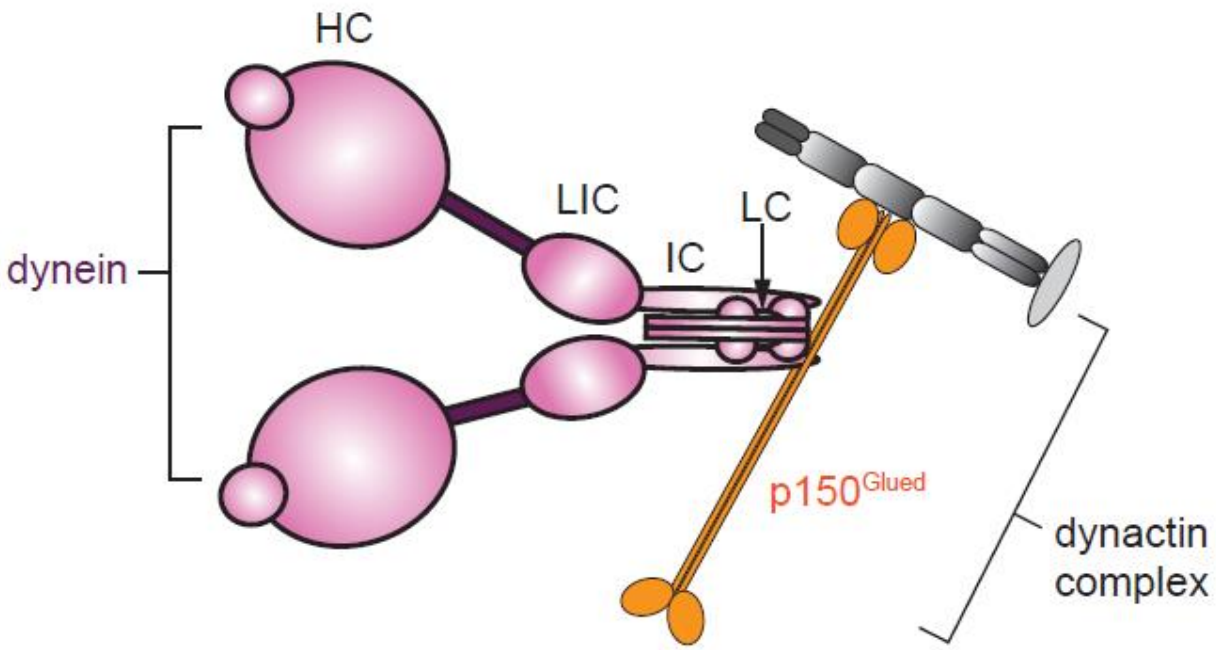

Figure 1.8. Structure of retrograde motor protein, dynein and the dynactin complex. Dynein consists of heavy chains (HC), light intermediate chains (LIC), intermediate chains (IC) and light chains (LC). In order to transport cargoes, dynein binds to the dynein binds to the dynactin complex (modified from (Sheng and Cai, 2012)).

1.2.4 Regulation of Transport: Calcium-mediated

One important factor determining the distribution of mitochondria are cytoplasmic calcium levels (Figure 1.9). In response to changes in calcium, mitochondria can buffer access or increase ATP production depending on the needs of the cell. (Rintoul et al., 2003; Yi et al., 2004). Increases in calcium can originate from various sources – ionotropic glutamate receptors in dendrites, action potentials within axons and neuromodulators triggering release from intracellular stores (Ohno et al., 2011; Rintoul et al., 2003; Yi et al., 2004). The calcium signal is then transferred to mitochondria by means of their adaptor molecule, Miro (Fransson et al., 2003). Indeed, in primary neuronal cultures through various mutant expression analysis, Miro was found to aid mitochondrial trafficking and, following an increase in intracellular calcium, which binds to Miro by means of its EF hands, relays a signal to the motors to arrest transport (Saotome et al., 2008). The exact mechanism by which this arrest occurs is under some scrutiny. One hypothesis by MacAskill *et al.*, based on dendritic

mitochondria, is that following binding of calcium to Miro, KIF5 motors are detached from mitochondria leaving behind a complex composed of the mitochondrion, Miro and Milton (Macaskill et al., 2009). The authors further show that after glutamate application, there was a 45% decrease in KIF5 motors bound to mitochondria. The second hypothesis by Wang and Schwarz based upon axonal mitochondria states that the binding of calcium to Miro EF hands causes a detachment of the kinesin motor from the microtubules and the direct binding of the motor domain of KHC with Miro (Wang and Schwarz, 2009). Evidence here indicates that irrespective of whether mitochondria are moving or stationary and irrespective of calcium levels, the KHC remains bound to mitochondria. This study also revealed that Miro is able to mediate the arrest of retrograde as well as anterograde transport, again supporting the interplay between the two motor systems (Wang and Schwarz, 2009).

1.2.5 Regulation of Transport: Docking of Mitochondria

Syntaphilin, a specific docking molecule for axonal mitochondria has recently been described to aid the recruitment of mitochondria to the stationary pool (Chen and Sheng, 2013; Kang et al., 2008). It was first discovered in a genetic screen for synaptic vesicle regulatory components and was found to reduce neurotransmitter release when exogenously overexpressed in culture (Lao et al., 2000). Creation of a mouse mutant carrying a homozygous deletion for the syntaphilin gene then led to the discovery of its role as a docking molecule for axonal mitochondria (Kang et al., 2008). Here, it was shown that exogenously expressed GFP-tagged syntaphilin immobilized mitochondria while the mutant mice had significantly increased mitochondrial motility thereby reducing the density in axons and impeding proper synaptic functioning. The authors also suggest a reconciliation in the discrepancies of how calcium-induced mitochondrial arrest is established based upon axon versus dendrite-specific expression of syntaphilin. In their model, arrest is mediated by switching KIF5 binding from the Miro/Miltion complex to syntaphilin in a calcium-dependent manner and inhibiting the motor ATPase activity. However, syntaphilin also directly interacts with the mitochondrion

creating a complex with KIF5, Miro and Milton (Chen and Sheng, 2013). As syntaphilin is not found within dendrites, the MacAskill *et al.* model is still plausible for dendrite-specific mitochondrial transport while the Wang and Schwarz model is likely more accurate for axon-specific transport arrest.

1.2.6 Regulation of Transport: PINK/Parkin

Well-known for their link to hereditary forms of early onset recessive Parkinson's Disease, PINK1 (Valente et al., 2004), a serine/threonine kinase, and Parkin (Kitada et al., 1998), an E3 ubiquitin ligase, have also been implicated as a means of irreversibly arresting mitochondria, independent of calcium (Wang et al., 2011). Together they thought to make up a quality control pathway whereby impaired mitochondria may be cleared by mitophagy (Ashrafi and Schwarz, 2013; Narendra and Youle, 2011). Briefly, this pathway is triggered after PINK1 stabilization on the outer membrane of damaged mitochondria. Typically it is inactivated by import into mitochondria and proteolytic cleavage. Upon loss of membrane potential, PINK1 moves to the mitochondrial surface and recruits Parkin (Narendra et al., 2010). From here, ubiquitination of proteins on the mitochondrial surface by Parkin begins the process of mitophagy.

The first evidence of its role in regulating mitochondrial movement came from a mass spectrometry screen of PINK1 interacting proteins that revealed a complex of PINK1, Miro and Milton (Weihofen et al., 2009). In addition, Miro was shown to be downregulated by Parkin overexpression (Chan et al., 2011). Based on these results, it was subsequently shown that PINK1 and Parkin can halt mitochondrial motility (Wang et al., 2011). More specifically, PINK1 was shown to phosphorylate Miro leading to its rapid degradation through a Parkin-dependent pathway. This released kinesin from mitochondria sequestering it from the healthy pool for degradation. Further coordination of the pathway is most likely aided by Mitofusin (Mfn) 2, a mitochondrial outer-membrane fusion protein and a substrate for Parkin ubiquitination (Gegg et al., 2010; Rakovic et al., 2011). It was also

recently shown in mouse cardiac myocytes that Mfn2 can also act upstream of Parkin, becoming phosphorylated by PINK1 and in so doing acting as a receptor for Parkin binding and enhancing mitophagy (Chen and Dorn, 2013). Mfn2 can interact with Miro and Milton proteins and cause selective transport deficits in knockout mouse models and after downregulation by si-RNA. In these experiments axonal mitochondria spend more time paused and have decreased movements in both the anterograde and retrograde direction independent of any alteration in their fusion dynamics (Misko et al., 2010).

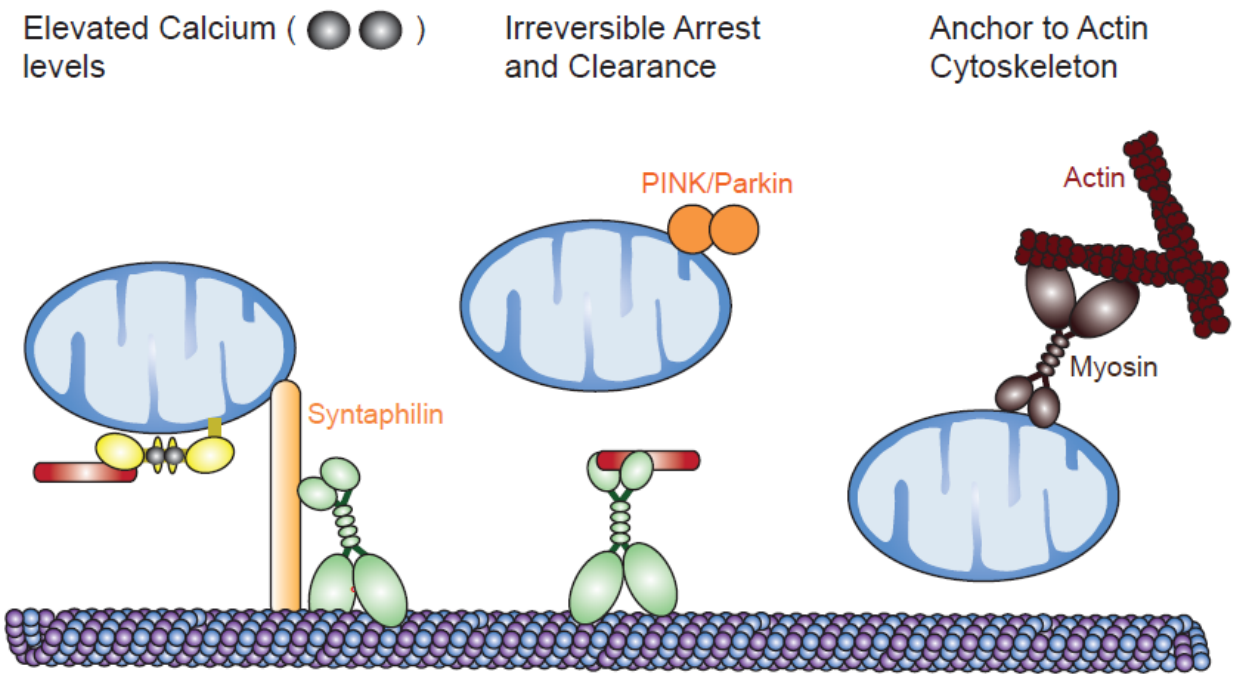

Figure 1.9. Three types of regulation of axonal transport of mitochondria (modified from (Schwarz, 2013; Sheng and Cai, 2012))

1.2.7 Regulation of Transport: Other modulatory factors

There are many other proteins which can influence the movement behavior of mitochondria. One such protein named syntabulin has been shown to link syntaxin-containing vesicles to KHC (Su et al., 2004) and, more recently, to link mitochondria to KHC *in vivo* (Cai et al., 2005). It was described as a peripheral membrane-associated protein of mitochondria bound by its C-terminal tail which, following knockdown in cultured hippocampal neurons, caused the reduction of mitochondrial density in processes. Furthermore, its effects on mitochondria transport were solely in the

anterograde direction. The exact function of syntabulin within the transport complex is currently speculative but, as with other adaptor molecules, it has been shown to preserve pre-synaptic function and, when knocked out, impairs synaptic transmission and transport of mitochondria to pre-synaptic terminals (Ma et al., 2009).

Mitochondrial transport is also important during axonal outgrowth and one particular signaling molecule which affects this process, nerve growth factor, is also influential in modulating the anterograde mitochondria-specific movement (Chada and Hollenbeck, 2003, 2004; Morris and Hollenbeck, 1993). Mitochondria increase their movement towards the area of NGF stimulation while their movement out is inhibited by docking with the actin cytoskeleton. Enhancement of motor activity towards the stimulation and their subsequent arrest is believed to be caused by downstream signaling molecules of NGF, that are known to modify kinesin motor activity by post-translational modification such as mitogen activated protein (MAP) kinase (De Vos et al., 2000) and phosphatidyl (4,5) bisphosphate (De Vos et al., 2003). In addition, fasciculation and elongation protein zeta-1 (FEZ1), an axonal guidance protein activated by NGF has been shown to associate with tubulin and kinesin to promote transport in neurites (Fujita et al., 2007; Ikuta et al., 2007).

There is also a broad range of factors that have been shown to alter transport through modification of motor-cargo interactions but are non-specific for mitochondria. This includes glycogen synthase kinase (GSK) 3β and cyclin dependent kinase (cdk) 5. GSK 3β activation leads to phosphorylation of the KLC, already shown to be dispensable for axonal mitochondrial transport. Regardless, activation of both proteins leads to a decrease in total anterograde transport in *in vitro* studies (Fu and Holzbaur, 2013; Morel et al., 2010; Morfini et al., 2002). Finally, fast axonal transport of amyloid precursor protein (APP) as well as other vesicles has been shown to be mediated through JNK-interacting protein 1 (JIP1) and its binding of both anterograde and retrograde motor proteins (Fu and Holzbaur, 2013; Horiuchi et al., 2007).

1.2.8 Microtubules

Microtubules are dynamic structures which can be assembled and disassembled with the addition or removal of α- and β-tubulin dimers (Figure 1.10) (Purves et al., 2001). Microtubule associated proteins (MAPs) as well as post-translational modifications of microtubules affect not only the stability of the microtubules but also their affinity for cargo molecules. Novel and highly dynamic microtubules are enriched in tyrosinated tubulin while long-lived and stable microtubules are enriched in detyrosinated and acetylated tubulin (Westermann and Weber, 2003). Microtubule acetylation (Reed et al., 2006) and detyrosination (Liao and Gundersen, 1998) positively regulates the binding and motility of kinesin-1 although the exact mechanism is as of yet unknown. MAPs help to stabilize microtubules but can also compete with motors for microtubule binding (Hagiwara et al., 1994). One such MAP, tau, implicated in Alzheimer's disease, has been shown to inhibit organelle flux by both kinesin and dynein although kinesin is affected to a greater extent (Ebneth et al., 1998; Seitz et al., 2002). Recently, fluorescently tagged purified tau, kinesin and dynein proteins were used to directly visualize tau-mediated effect on single motor molecules using total internal reflectance (TIRF) microscopy (Dixit et al., 2008). Tau accumulations caused dynein to change directions whereas kinesin molecules became completely separated from microtubules. Overall it decreased the binding rate, motile fraction and run length of both motor protein but interestingly, its effect on kinesin occurred at one tenth the concentration necessary to see effects with dynein (Dixit et al., 2008).

Phosphorylation of MAPs by kinases, however, can remove them from the microtubules, as has been shown for the microtubule affinity regulation kinase (MARK)/Par1 kinase, which can phosphorylate tau and other MAPs at a KXGS motif (Drewes et al., 1997). Indeed, MARK has been used *in vitro* to rescue tau-mediated inhibition of axonal transport by detaching it from the microtubule tracks (Mandelkow et al., 2004) and continuing development in this field has therapeutic potential for neurodegenerative diseases as will be discussed below.

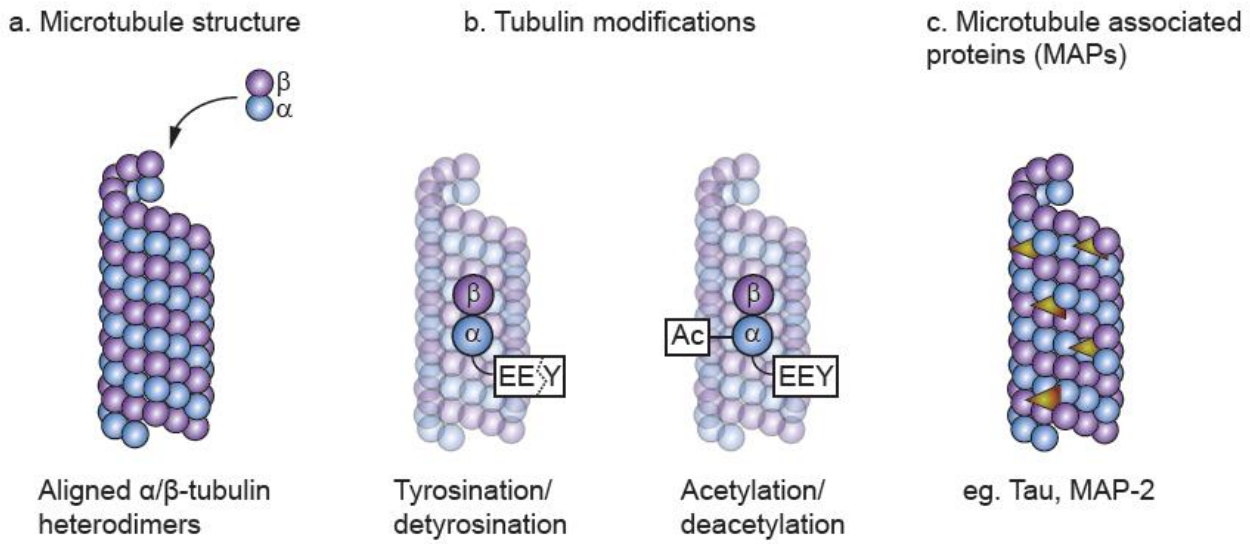

Figure 1.10. Microtubule structure and modifications a. Microtubules consist of stable a/b-tubulin heterodimers that align in a defined polarity to form a helical structure that is dynamic, with the ability to polymerize and depolymerize. b. The tubulin heterodimer may be modified in several ways, with two examples depicted here, that can affect their function and stability. The amino acid tyrosine within the C-terminal consensus motif EEY can be reversibly cleaved on α-tubulin, generating a more stable structure. In addition, acetylation at position 40 in the amino-terminal is also believed to stabilize microtubules. c. Microtubule-associated proteins (MAP) provide stability to the microtubules but in access can competitively inhibit binding of motor molecules. (modified from (Akhmanova and Steinmetz, 2008))

1.2.9 Other methods of Transport

Beside microtubule-based transport, actin-based movement may also play a role, albeit to a lesser extent, in mitochondria trafficking. Actin, a globular protein, can form linear microfilaments termed filamentous (F)-actin. It is polar with the (+)-end or barbed end having its ATP-binding site exposed and the opposing side being the (-)-end or pointed end (naming was based on their appearance with the transmission electron microscope) (Purves et al., 2001). Myosin motors move along actin filaments, generating force by hydrolyzing ATP, with myosin V moving toward the barbed end (Cheney et al., 1993) and myosin VI moving in the reverse direction, toward the pointed end (Wells et al., 1999). Original studies suggested that myosin was involved in short-range movements along actin filaments at slower velocities than microtubule-based transport (Morris and Hollenbeck, 1995). This led to the hypothesis that actin-based transport complements that of microtubules, moving them through small areas lacking microtubules or returning them to their microtubule tracks after becoming separated (Langford, 1995). A recent study however, argues that actin opposes microtubule-based movement and serves primarily as a docking mechanism (Pathak et al., 2010). In

Drosophilia primary neurons, it was observed that following myosin V depletion, movement of axonal mitochondria were increased in both directions and following myosin VI depletion, there was a retrograde-specific increase in trafficking (Pathak et al., 2010). This idea is consistent with studies demonstrating that in the absence of actin, axonally transported mitochondrial show higher velocities and longer times spent moving (Ligon and Steward, 2000; Morris and Hollenbeck, 1995) and that actin was required for docking following NGF stimulation (Chada and Hollenbeck, 2004). Additional interactions with neurofilaments which have also been shown to interact with mitochondria *in vitro* (Wagner et al., 2003), may also contribute to the docking process. However this could not be addressed in this study as *Drosophilia* lack neurofilaments.

1.2.10 Transport Deficiencies and Neurodegeneration

Transport defects have been implicated in multiple neurodegenerative diseases (Millecamps and Julien, 2013) and thus have propelled the study of this topic over the past years in hopes of uncovering potential therapeutic treatments. Here, I will discuss some of the most recent research which link common neurodegenerative diseases to axonal transport (summarized in Figure 1.11).

Alzheimer's disease (AD) leads to progressive cognitive decline caused by synaptic and neuronal loss. The two main pathological hallmarks of AD are amyloid plaques and neurofibrillary tangles. The amyloid cascade hypothesis purports that β-amyloid precursor protein (APP) is processed into amyloid β peptides or oligomers which accumulate inside neuronal cells and extracellulary where they can aggregate into plaques leading to synaptic dysfunction and neuronal death (Ballard et al., 2011). In Familial AD, mutations are found within APP and presenilin genes, which play a pivotal role in processing of the APP and thus contribute to the altered production of amyloid-β peptides. Meanwhile, neurofibrillary tangles are composed of insoluble hyperphosphorylated aggregates of the microtubule associated protein tau. It remains controversial what the relationship between these two pathologies is and how they contribute to the degenerative process (Armstrong, 2006).

Regardless, there have been several studies showing that mutant presenilin (Lazarov et al., 2007; Pigino et al., 2003), overexpression of mutant tau (Ebneth et al., 1998; Kanaan et al., 2011; Zhang et al., 2004) and APP and its cleavage products (Decker et al., 2010; Hiruma et al., 2003; Rui et al., 2006; Stokin et al., 2005), lead to a defect in axonal transport. There has been some insight into the mechanism of this transport breakdown although much is still unknown.

One study which focused on oligomers of amyloid-β in hippocampal cultures indicated that the transport deficit was independent of changes to microtubule stability but may instead be initiated by NMDA receptor activation perhaps coupled to activation of GSK-3β, already shown to be activated by fibrillar forms of amyloid-β (Giese, 2009) and disruptive to anterograde transport of organelles (Morfini et al., 2002). This was corroborated by another similar study focusing on active amyloid β peptide 25-35 and showing that the manipulation of GSK-3β could alleviate the amyloid β peptide induced transport deficit (Rui et al., 2006). Indeed, even presenilin mutations have been shown to interact with GSK-3β and increase their activity when mutated leading to increased kinesin-1 phosphorylation and impaired transport and targeting of membrane bound organelles (Pigino et al., 2003).

The role of tau in axonal transport impairment is more contentious. Independently of tau's ability to impede axonal transport through binding to microtubules, it has also been suggested that filamentous, hyperphosphorylated tau can activate axonal protein phosphatase 1 (PP1), which can dephosphorylate and thus activate GSK-3β leading to the phosphorylation of KLC and release of cargo from motors (Kanaan et al., 2011). As previously discussed, monomeric tau has also been shown to inhibit transport by blocking the attachment of kinesin motors to microtubules thus inhibiting their motility (Seitz et al., 2002; Stamer et al., 2002). However, axonal transport rates in retinal ganglion cells analyzed in mice that either overexpress a tau transgene derived from a human PAC (P1-derviced artificial chromosome) known as 8c mice, or have a targeted disruption in exon one of tau, showed an opposite effect. Here, there was no significant difference in axonal transport using either mouse model (Yuan et al., 2008). This diverging result suggests the need for better methods

for measuring axonal transport and more verification of causal relationships between axonal transport defects and degeneration.

Parkinson's disease is caused by the degeneration of dopaminergic neurons in the substantia nigra causing rigidity, shaking and gait disturbance and has idiopathic, familial and neurotoxic forms. It is pathologically characterized by accumulation of Lewy bodies, lesions containing hyperphosphorylated α-synuclein and deficient formation and activity of dopamine (Lees et al., 2009). Direct evidence for defective axonal transport in Parkinson's disease neurons has not yet been shown although many studies suggest there is a relation between it and early events leading to neurodegeneration or Lewy body formation.

For example, mutations in α-synuclein mimicking the hyperphosphorylated form and causing familial autosomal dominant Parkinson's have shown defects in axonal transport *in vitro* (Saha et al., 2004). Disruption of transport resulted in accumulation of the pre-synaptic protein proximal to the cell body which may also lead to accumulation in the soma and eventual formation of Lewy bodies in the diseased CNS. Conversely, it has also been suggested that the propagation of Lewy bodies occurs by means of axonal transport of α-synuclein fibrils rather than by the spread of conditions favorable to its aggregation (Desplats et al., 2009; Freundt et al., 2012).

Mutations in other genes known to cause recessive early onset Parkinson's target proteins involved in maintenance of mitochondria function and regulation of axonal transport (Lees et al., 2009). These include Parkin (Kitada et al., 1998) and PINK1 (Valente et al., 2004), previously discussed for their roles in mitophagy and their connection with the motor/adaptor complex and DJ-1 (Bonifati et al., 2003). DJ-1 localizes to mitochondria where it can reduce oxidative stress caused by inhibitors of the respiratory chain. A decrease in DJ-1 expression changes mitochondria dynamics leading to altered mitochondrial morphology and an increase in the production of reactive oxygen species (ROS) (Canet-Aviles et al., 2004; Irrcher et al., 2010).

Neurotoxin 1-methyl-4-phenyl-1,2,3,6-tetrahydropyridine and its metabolite 1-methyl-4-phenylpyridium (MPP+) can induce Parkinson's symptoms as well as the pathological hallmarks seen in human and mouse models (Speciale, 2002). In isolated squid axoplasm experiments, it was shown that MPP+ significantly alters axonal transport, inverting the normal net movement of organelles, increasing dynein-driven retrograde transport and decreasing kinesin-driven anterograde transport (Morfini et al., 2007). This led to a depletion of synaptic vesicles at pre-synaptic sites and was mediated by endogenous axonal caspases and protein kinase C isoform, PKCδ by a currently unknown mechanism. It has also been shown that microtubule dysfunction may be an early event in MPP+ induced neurodegeneration, preceding and perhaps leading to transport defects and mitochondrial damage (Cartelli et al., 2010). Interestingly, similar microtubule dysfunction has also been described in patients with idiopathic and familial forms of the disease (Cartelli et al., 2012).

Huntington's disease is caused by an autosomal dominate single mutant *Huntingtin* (Htt) gene. The mutation is characterized by an expansion of a CAG trinucleotide repeat encoding a polyglutamine (polyQ) tract (Orr and Zoghbi, 2007). It was discovered that a decrease in *Drosophila huntingtin* and expression of proteins having pathogenic polyQ repeats abrogated axonal transport eventually leading to neuronal apoptosis (Gunawardena et al., 2003). Suggestions for this transport deficit were proposed including physical blockade by polyQ-Htt aggregates (Gunawardena et al., 2003; Lee et al., 2004) and sequestering of motor molecules by polyQ-Htt (Trushina et al., 2004). New compelling molecular evidence indicates that inhibition of axonal transport occurs through activation of neuron-specific c-Jun N-terminal kinase 3 (JNK3) by polyQ-Htt, which in turn phosphorylates the kinesin-1 motor domain impeding its binding to microtubules (Morfini et al., 2009). The same mechanism is thought to affect another polyQ disease, a lower motor neuron neurodegenerative disease, spinal and bulbar muscular atrophy (SBMA), where the polyQ stretch is found within the androgen receptor protein (Morfini et al., 2006). Further studies are needed to ascertain exactly how JNK3 is activated by polyQ-Htt.

Charcot-Marie-Tooth disease (CMT) is the name of a group of commonly occurring, genetically heterogeneous peripheral neuropathies that can be classified into two main forms: demyelinating CMT type 1 characterized by decreased nerve conduction velocities and an axonal, non-demyelinating form, CMT type 2 (Barisic et al., 2008). Of the over 40 causative genes known to be associated with CMT, a number of them with autosomal dominant inheritance for CMT type 2 are found within genes encoding proteins physiologically or pathologically involved in axonal transport including kinesin subunit KIF1Bβ (Zhao et al., 2001), mitofusion2 (MFN2) (Zuchner et al., 2004) and heat-shock protein (HSPB1) (Evgrafov et al., 2004). The mechanisms of the mutated genes are only beginning to be understood.

The link between Mfn2 and axonal transport independent from its role in mitochondrial fusion, discussed above (Misko et al., 2010), corroborated previous evidence that Mfn2 mutation disrupted axonal transport (Baloh et al., 2007). New evidence suggests that mutations in Mfn2 induce axon degeneration through incorrect distribution of mitochondria leading to an energy crisis rather than a net decrease in bulk transport or mitochondria dysfunction suggesting a new role of Mfn2 and mitochondria docking that may be rescued by its homolog Mfn1 (Misko et al., 2012).

Recent development of a transgenic mouse model for HSPB1-induced CMT type 2 also describes an axonal transport link to this degenerative disease (d'Ydewalle et al., 2011). Mice expressing a HSPB1 genetic mutation show clear axonal transport deficits in isolated dorsal root ganglion (DRG) neurons that are caused by a decrease in acetylated tubulin in peripheral nerves. This could be rescued by inhibiting histone deacetylase (HDAC) 6, an enzyme with α-tubulin deacetylating activity previously shown *in vitro* to regulate axonal transport of hippocampal neurons (Chen et al., 2010).

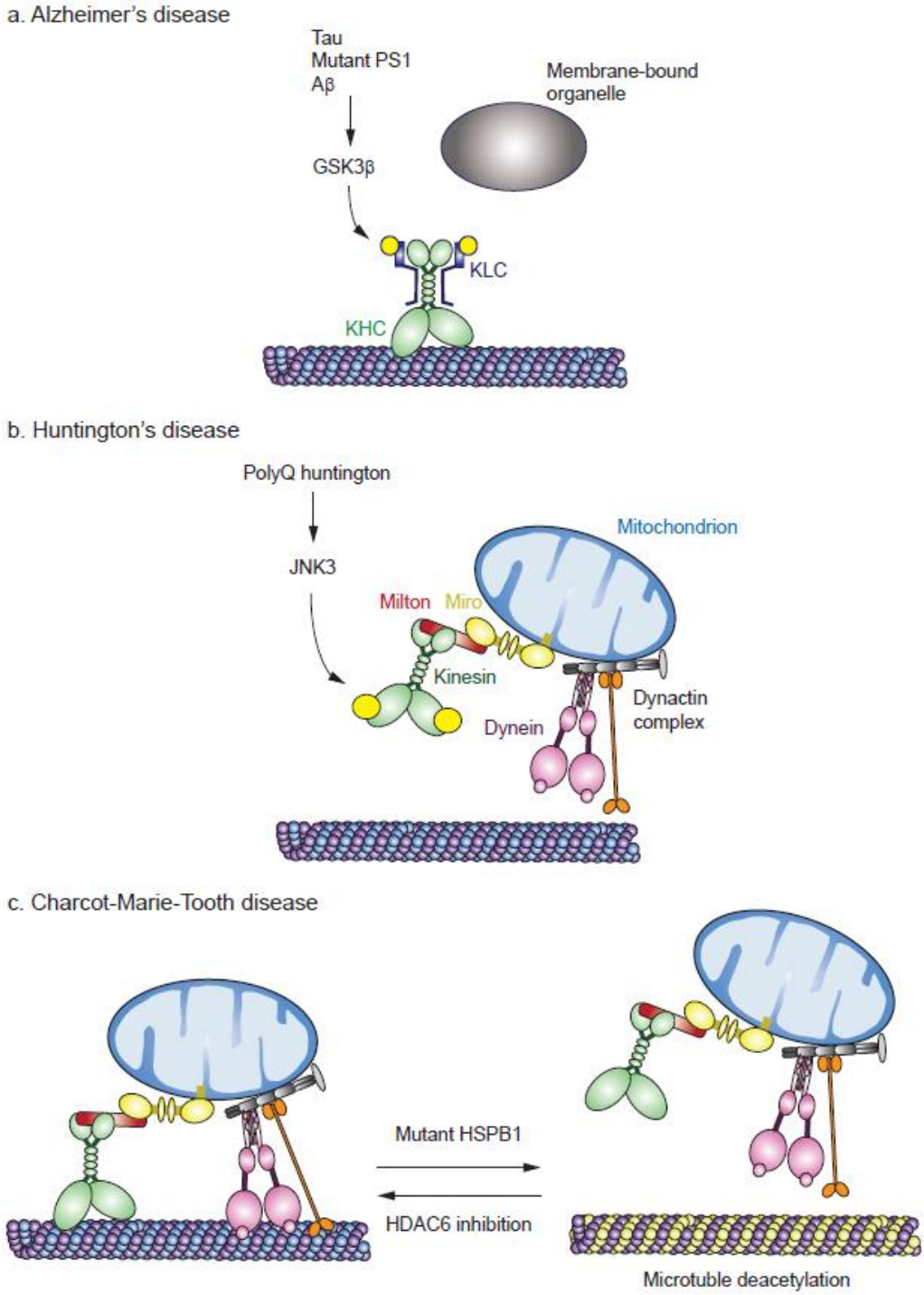

Figure 1.11. Axonal transport disturbances and neurodegenerative disease. a. In Alzheimer's disease, glycogen synthase kinase 3β (GSK3β), upon activation by forms of amyloid-β, mutations in presenilin 1 (PS1) or hyperphosphorylated tau, has been shown to phosphorylate (represented by yellow circle) the kinesin light chain (KLC) causing it to dissociate from membrane-bound organelles thus arresting transport. b. In Huntingtin's disease, pathogenic polyglutamine (polyQ) repeats were shown to activate c-Jun N-terminal kinase 3 (JNK3) which in turn phosphorylated the motor domain of kinesin-1, inhibiting its ability to bind to microtubules. c. In Charcot-Marie-Tooth disease, mice generated with mutant heat shock protein, HSPB1 genes showed transport disturbances linked to an increase in microtubule deacetylation which could be reversed upon inhibition of the histone deacetlyase, HDAC6. (modified from (Millecamps and Julien, 2013))

1.3 Experimental Aims

The overall aim of the work presented in this thesis was to use advanced two-photon microscopy techniques to directly observe and characterize axonal processes that occur within neuroinflammatory lesions in mouse models of multiple sclerosis. Firstly, I studied the process of axonal degeneration followed by, and more extensively, axonal transport. To enhance these findings and complement our already-established genetic tools, I, in parallel, established a fast and reliable way to visualize cellular behavior and function *in vivo* using vital dye labeling techniques. The work addressed in this thesis has therefore been divided into three projects, discussed below, as well as a fourth, concluding chapter which summarizes the importance of using *in vivo* imaging techniques to study neurodegenerative conditions.

Project I: A reversible form of axon damage in experimental autoimmune encephalomyelitis and multiple sclerosis

The novel process of neuroinflammatory-induced axon breakdown, termed FAD, was described in spinal axons of acute EAE mice immunized with myelin oligodendrocyte glycoprotein (MOG) (Nikic et al., 2011). Lesions found here contained three types of axon morphologies: Stage 0 axons which were normal appearing, stage 1 axons that contained focal swellings and stage 2 axons which were fragmented (Figure 1.11). These alterations appeared to progress sequentially over time and, of particular interest, stage 1 axons had the potential to progress to fragmentation but also to recover to a morphologically normal axon. In addition, toxic mediators (reactive oxygen/nitrogen species, ROS/RNS) secreted by activated macrophages/microglia negatively influenced this process.

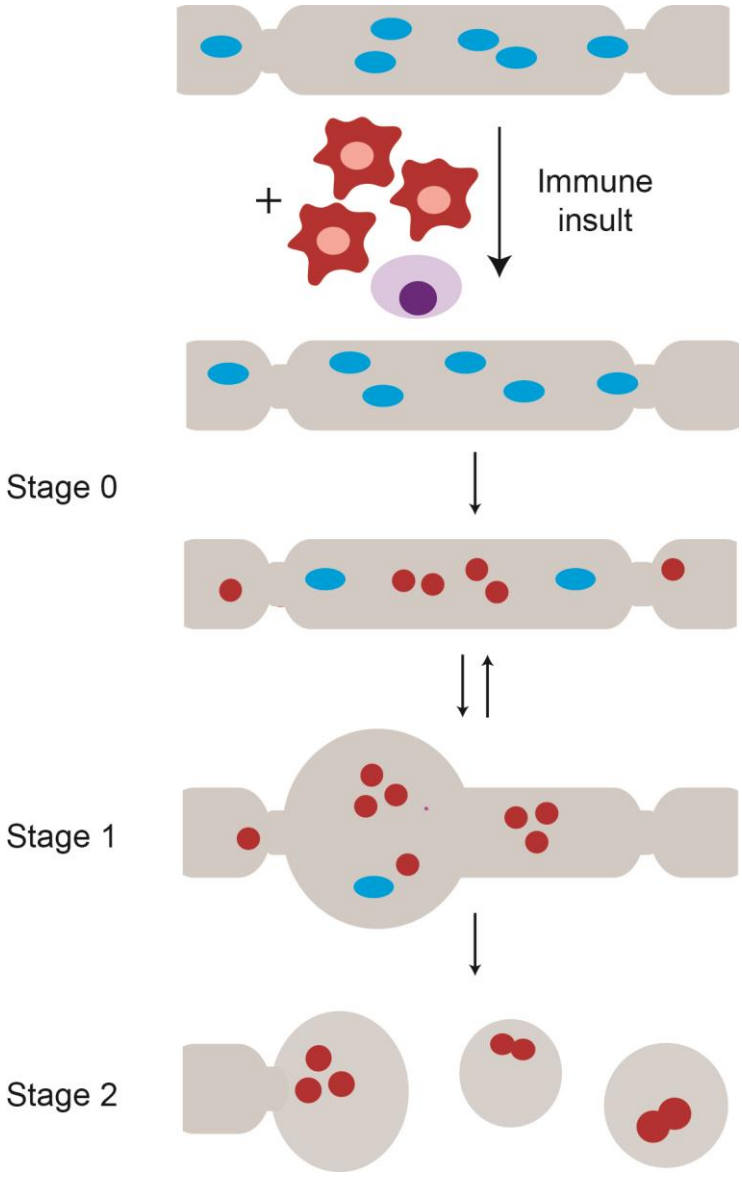

Figure 1.12. Focal Axonal Degeneration

To expand upon these findings, the aim of my first project was to follow a populations of spinal axons *in vivo* over many hours to better understand their behavior and stability within EAE lesions and following exposure to ROS/RNS. Specifically the aims were to:

- Measure the conversion rates between the various stages of FAD
- Determine the influence of intrinsic and extrinsic axonal properties on the progression of, or recovery from, FAD (eg. axon diameter, inflammatory activity)

- Determine whether FAD be induced in a healthy mouse upon exposure to reactive oxygen/nitrogen species

Project II: Cellular, subcellular and functional *in vivo* labeling of the spinal cord using vital dyes

To complement the transgenic mouse lines that were used for *in vivo* imaging, vital dye application would allow for the rapid visualization of cellular, subcellular and functional entities thus enhancing the information gained in each experiment. For example, with the application of the appropriate vital dye one could examine the extent of cellular infiltration in a given lesion, assess the myelination status of axons, or measure the extracellular levels of reactive oxygen specie such as hydrogen peroxide (H_20_2). In addition to saving time and money otherwise spent on producing new transgenic mouse lines, some dyes were commercially available across a broad spectral range allowing for flexibility when choosing an appropriate dye on per experiment basis and could potentially be fixed and additionally studied in situ. The aim of this project was therefore as follows:

- Establish a protocol for vital dye application which provides the optimal imaging quality and tissue penetration
- Determine which vital dye of a given class is most suitable for the desired application
- Determine the appropriate dye concentration
- Determine whether the vital dye is also suitable for post mortem analysis and, if so, under which fixation conditions is this possible.

Project III: Pervasive axonal transport deficits in multiple sclerosis models

As previously mentioned, axonal transport is essential for neuronal viability and deficits are significant contributors to axon loss in many neurodegenerative conditions. Axon degeneration in

multiple sclerosis has become an important hallmark in the progression towards permanent disability. Whether axonal transport is also involved in neuroinflammatory axon damage, however, has never been directly investigated. Moving forward from project I's assessment of axon breakdown, we next chose to assess the functionality of these axons in the context of axonal transport. The following aims were thus proposed:

- Establish an *in vivo* imaging approach to directly visualize axonal transport of organelles
- Determine whether axonal transport is affected in spinal lesions of both acute and chronic mouse model of multiple sclerosis:
    - At what stage of axon morphology is the transport altered?
    - Is one transport direction (anterograde vs retrograde) primarily affected?
    - Using single particle analyses, do speed or stopping parameters of organelles differ?

Based on initial findings showing a widespread and pervasive transport deficit, this project was then extended to investigate what factors are involved in eliciting this deficit and to determine whether the deficit is reversible by answering the following questions:

- Is the transport deficit dependent on axon demyelination?
- What is the role of microtubules in axonal transport disturbances?
- What role do reactive oxygen/nitrogen species play in axonal transport disturbances?
- Is transport deficit reversible either spontaneously during the clinical course and/or following pharmacological intervention?

The results of Project I and Project II have been published in peer-reviewed journals (Nikic et al., 2011; Romanelli et al., 2013) while the results of Project III is currently under consideration in Nature Neuroscience (Manuscript no. NN-BC48910). Project IV was written as an invited review (Sorbara et al., 2012).

2. Project I: A reversible form of axon damage in experimental autoimmune encephalomyelitis and multiple sclerosis

Nikic, I., Merkler, D., **Sorbara, C**. **D.**, Brinkoetter, M., Kreutzfeldt, M., Bareyre, F. M., Bruck, W., Bishop, D., Misgeld, T. & Kerschensteiner, M.

Published in **Nature Medicine**, 2011 Apr:17(4):495-9

In this paper, we characterized immune-mediated axon damage using *in vivo* imaging in a mouse model of multiple sclerosis. While axon injury was known to exist in MS, how the axons become permanently damaged was unknown and had never been shown *in vivo.* We discovered a process entitled Focal Axonal Degeneration (FAD) that underlies axon loss whereby mitochondrial pathology precedes changes to axon morphology. Axons then progressed to form focal swellings which have the ability to spontaneously recover or eventually fragment. This sequence of events can be elicited by exposure to ROS and RNS and rescued by scavenging these reactive species.

In the initial phase of my PhD research, I contributed to this effort by performing *in vivo* two-photon imaging experiments and subsequent image analysis. I continuously monitored spinal axons over a period of about 6 hours in neuroinflammatory lesions and globally assessed the proportion of axons undergoing FAD and the potential of axons for recovery. In addition, I performed time-lapse experiments of spinal axons and their mitochondria after hydrogen peroxide (H_20_2), and nitric oxide (NO) application to show that exposure to these reactive species was sufficient to induce mitochondrial and axonal changes similar to FAD.

3. Project II: Cellular, subcellular and functional *in vivo* labeling of the spinal cord using vital dyes

Sorbara, C. D.*, Romanelli, E.*, Nikic, I.*, Dagkalis, A., Misgeld, T. & Kerschensteiner, M.

*authors contributed equally

Published in **Nature Protocols**, 2013 Mar; 8(3):481-90.

During the course of experimentation for the Nature Medicine paper, I helped establish an approach for using synthetic vital dyes to efficiently label *in vivo* different cell types, subcellular components and to monitor the release of toxic mediators in the spinal cord of mice. This, combined with transgenic labeling methods, greatly aided in visualizing the pathogenesis of immune-mediated axon damage. Therefore, a protocol was assembled to describe the procedure and provide a comprehensive list of dyes and application conditions that are suitable for *in vivo* imaging and potentially for subsequent fixation and in situ tissue analyses.

I helped to conceive the experiments for this publication as well as perform imaging experiments, image analysis and helped to write the protocol.

4. Project III: Pervasive axonal transport deficits in multiple sclerosis models

Sorbara, C. D., Wagner, N.E., Ladwig, A., Nikic, I., Merkler, D., Marinkovic, P., Godinho, L., Bareyre, F., Bishop, D., Misgeld, T. & Kerschensteiner, M.

Submitted to Nature Neuroscience, Manuscript No. NN-BC48910

Axonal transport deficits have been shown to contribute to neurodegenerative diseases but their role in immune-mediated axon damage, as seen in multiple sclerosis, has never been directly investigated. Here I used *in vivo* two photon imaging to visualize for the first time organelle transport in individual axons in the adult mammalian CNS. These results identify pervasive axonal transport deficits in neuroinflammatory lesions that precede changes in axon morphology, demyelination or cytoskeletal alteration and thus represent an early stage of axon dysfunction. For this study, I executed all the EAE experiments including all the *in vivo* imaging experiments and image analysis. I also performed histology, molecular biology and anatomical analysis for this study. I helped to conceive the experiments, interpret the results and write the paper.

5. Project IV: *In vivo* imaging of the diseased nervous system: An update

Sorbara, C.D, Misgeld, T. & Kerschensteiner, M.

Published in **Current Pharmaceutical Design**, 2012; 18(29) 4465-70

This article was written as an update to the previously published review in Nature Review Neuroscience (Misgeld and Kerschensteiner, 2006). The aim was to demonstrate how the understanding of neurological conditions such as trauma, degeneration, ischemia and inflammation is continuing to improve due to the advancement optical microscopy and therefore the capabilities of *in vivo* imaging.

For this publication, I collected the literature and wrote a draft of the manuscript.

6. Discussion

In vivo two-photon imaging of the lumbar spinal cord enabled us to observe and characterize axonal processes in mouse models of multiple sclerosis. This was further developed with the application of vital dyes to assess cellular, subcellular and functional properties in parallel with fluorescent transgenic mice.

6.1 Key Findings

Project I: A reversible form of axon damage in experimental autoimmune encephalomyelitis and multiple sclerosis

In this project, using time-lapse *in vivo* imaging, the aim was to better understand the behavior of spinal axons within inflamed areas during the process of focal axonal degeneration. The following conclusions could be drawn:

- Population analyses confirm that the conversion of axons between stages occurs in a step-wise fashion with stage 1 (swelling) always preceded stage 2 (fragmentation)
- Instances of progression to advanced stages of axon damage as well as recovery of swellings to normal appearing stage 0 axons could be observed although stages were relatively stable over time
- Axon diameter impacts the susceptibility of axons to degenerate with small-diameter axons being more susceptible than large-diameter axons
- After the peak of clinical symptoms and likely a decrease in inflammatory activity, the probability of FAD progression is decreased
- FAD progression can be induced in healthy axons following exposure to ROS or RNS indicating that they are likely mediators of the process

Project II: Cellular, subcellular and functional *in vivo* labeling of the spinal cord using vital dyes

This project served to enhance the repertoire of tools available for *in vivo* two-photon imaging. Through thorough testing of commercially available vital dyes, a protocol was produced that optimized tissue penetration and imaging quality. Exact dye concentrations and whether the dye was fixable was could also established. Now, vital dyes could be applied to the dorsal spinal cord of mice in order to reliably observe various cell types, subcellular components, and functional entities such as mitochondria potential in combination with genetic tools.

Project III: Pervasive axonal transport deficits in multiple sclerosis models

The overall goal of this project was to directly assess the role of axonal transport during neuroinflammatory axon damage. Using *in vivo* imaging, organelle as well as microtubule dynamics were visualized in single axons of the lumbar spinal cord. Using this as well as ultrastructure analysis, and pharmacological manipulations, the following conclusion were made:

- Axonal transport disturbances are widespread and pervasive in acute EAE models within neuroinflammatory lesions. They occur prior to changes in axon or organelle morphology. In addition, they affect both anterograde and retrograde transport and show no organelle-specificity as both mitochondria and peroxisomes showed abnormal transport rates.
- Single particle analyses showed that stop duration of mitochondria within EAE axons are significantly increased and many mitochondria appear to stop permanently, suggesting that organelles become immovable within sites of inflammation.
- Demyelination was not a prerequisite for transport deficits in morphologically normal axons.
- Microtubule orientation, tyrosination and dynamics became significantly altered *only* in late stages of axon damage suggesting they are not the cause of the transport disturbance but may initiate events leading to an irreversible transport failure.

- Transport deficits are reversible and spontaneously recover when inflammation subsides in acute EAE and this can be enhanced with a single injection of corticosteroids, commonly used for MS patients to reduce relapses. However, in a chronic EAE model, transport deficits persist causing the distal organelle supply to decrease.
- ROS/RNS species are a leading candidate to initiate the transport deficit for two reasons: transport disturbances could be recapitulated in healthy mice upon application of low-dose RNS and treatment of acute EAE mice with scavengers to both ROS/RNS rescued transport.

6.2 *In vivo* imaging for studying of focal axonal degeneration

In vivo two-photon imaging has provided a way to directly observe events and interactions as opposed to evaluating static snap shots from fixed tissue of the diseased nervous system (Misgeld and Kerschensteiner, 2006; Sorbara et al., 2012). As such, we could conclude that FAD was a novel form of axon loss due to its spatial restriction, speed and, interestingly, its reversibility (Nikic et al., 2011).

This imaging modality could now be extended to see how pharmacological manipulations, disease time course and/or EAE disease model could affect FAD progression. For example, using the same *in vivo* population analysis one could look at a chronic EAE model and ask what occurs during the remission and relapse phases of the disease and test neuroprotective strategies for their ability to increase the probability of stage 1 to stage 0 recovery. Infiltrating cells, labeled using vital dyes or the appropriate transgenic mouse crossed with *Thy1-XFP* could also be used to monitor whether the direct interaction of axons with inflammatory cells are necessary or sufficient for these changes to occur as a 'likely' decrease in inflammatory activity slowed progression of FAD (imaged one day after the peak of clinical symptoms). In point of fact, a recent study performing *in vivo* imaging in the brainstem showed that direct interaction of myelin oligodendrocyte glycoprotein (MOG) specific Th17 cells onto axons elicited intra-axonal calcium rises and subsequent axon damage (Siffrin et al., 2010a).

In vivo application of the vital dye MitoTracker Red (at high concentrations in order to label myelin rather than mitochondria (Romanelli et al., 2013)) could also show that these processes can occur independently of demyelination, shown only in fixed tissue in (Nikic et al., 2011). This raises an interesting question as to how mediators such as ROS and RNS, believed to elicit FAD progression, can penetrate the myelin barrier. Current studies are underway in our laboratory investigating the potential that small membrane pores would allow for passage of molecules into the axon eliciting an increase in intra-axonal calcium and subsequently the occurrence of FAD.

Certainly, there are many avenues in which to further explore the process of axonal degeneration in MS and EAE using *in vivo* imaging as a tool. The chosen one, as studied in this thesis, was axonal transport and how it may serve as an early marker of ensuing axon damage. The remainder of the discussion henceforth will address this function, how *in vivo* imaging served as a model for studying it and what can be learned.

6.3 *In vitro* versus *in vivo* imaging of axonal transport

Many tools have already been developed for studying axonal transport and it is therefore necessary to ask what advantages our imaging approach serves compared with these other methods. One classical approach employed pulse-labeling techniques with amino acids that are subsequently incorporated into newly formed proteins and transported along axons. These could be monitored by immunoprecipitation at various time intervals. The advent of superior imaging systems combined with fluorescent organelle markers or transgenically labeled fluorescent organelles brought about more sophisticated methods to visualize transport in real-time. *In vitro* neuronal cell cultures, for example, are readily used to study mitochondrial movement by transfection of fluorescently labeled mitochondria-targeted protein or loading with mitochondria-specific dyes such as MitoTracker. Here, axons extend a few mm in length, allowing for long-range monitoring of movement and a relatively simple means in which to manipulate transport by modulating the cellular environment or

the application of agonists or antagonists. However, there are some glaring limitations. Firstly, these cultures are mostly prepared from embryos or early post-natal mice and while their morphology is ideal for imaging purposes, it can vastly differ from neurons *in vivo*. Similarly, much of what we know about mitochondrial adaptor proteins came from monitoring axonal transport in Drosophila, a model system where genetic analysis is unsurpassed compared to most other model systems. The *in vivo* and cross-species relevance of these proteins, however, must be corroborated. Direct monitoring of axonal transport in the PNS has been recently accomplished using transgenically labeled mitochondria and triangularis sterni nerve-muscle explants allowing for the study of PNS neurodegenerative diseases (Misgeld et al., 2007). Studying axonal transport in this more physiological setting, lead to surprising results in animal models of ALS where for the first time deficits in organelle transport were shown to be independent of motor neuron degeneration highlighting the importance of an appropriate setting for monitoring axon transport in relation to disease (Marinkovic et al., 2012). Therefore, to truly understand how axonal transport is affected under neuroinflammatory conditions such as the EAE model of multiple sclerosis, it was imperative to develop a method to study this *in vivo* as mimicking this complex environment in a dish would be an insurmountable task.

6.4 Pitfalls of experimental design

Although the advantages of *in vivo* imaging are many, there are some drawbacks which warrant discussion. One question that arose in our model was if there was an increase in the density of mitochondria within the lesion area then one may expect a focal axonal transport block where mitochondria travel from the cell soma or from the periphery and then become "trapped" inside the inflammatory lesion. As I only image a small portion of the axon within or adjacent to a neuroinflammatory lesion, I initially proposed to follow single axons entering the dorsal column from the dorsal root, traversing a lesion and then exiting using *Thy1-GFPs x Thy1-MitoP* mice where only a subset of axons are labeled (Feng et al., 2000), facilitating tracking single axons. Unfortunately, it

was extremely rare that an axon would remain at a depth that was superficial enough to allow for imaging. While two-photon microscopy does tout a greater imaging depth than other traditional microscopy techniques, I can still only manage to observe transport in a depth of at most around 30 microns in the spinal cord due to the heavily myelinated axons. This is consistent even for our EAE model in which there are signs of demyelination but this does not appear to change the maximum imaging depth. The confined imaging window in both x,y and z also means that I cannot comment on the morphology/myelination status/mitochondrial status of the axon outside this region. Therefore if, for example, rostral to the laminectomy area or below the imaging depth, the axon runs through a lesion which causes a focal swelling to form initiating a block in transport, I would not be able to see this. This may be circumvented by post-imaging analyses where one could potentially trace the axon that was imaged *in vivo*, in *situ*. Recent methods developed for transforming biological tissue into an optically transparent form could facilitate correlated analyses by allowing for imaging without sectioning of the spinal cord and increasing the accessible imaging depth (Chung et al., 2013; Erturk and Bradke, 2013).

Another source of problems during this study was testing pharmacological inhibitors or enhancers of transport and being able to definitely exclude their role in an EAE-mediated axonal transport deficit. Most pilot experiments involved bath application of the molecule of interest onto the spinal cord of an EAE mouse and imaging prior to and after treatment the same group of axons for a potential recovery of transport. Some obvious problems arose from this: first being that I could not say for certain whether the factor was entering the axons, especially as the transport block is independent of demyelination, the factor of interest must have been able to pass through myelinated axons. Second, it was not obvious how long of a treatment was necessary to elicit an effect. If it was known that the molecule could pass the blood brain barrier than it may have been possible to try an intraperitoneal injection treatment but this is a less direct method than bath application and there is a strong possibility of also affecting pathways not directly involved in axon transport but perhaps lessening the neuroinflammatory insult and causing a secondary transport recovery.

Finally, an important factor is the heterogeneity of the population of axons within the dorsal column. When entering the spinal cord from the dorsal root, some lumbar afferent fibers bifurcate, with one collateral descending caudally in the spinal cord and the other ascending rostrally along the dorsal column eventually reaching the level of the medulla and synapsing in the nucleus gracilis. It is therefore plausible that in some axons the anterograde direction is caudal while in other cases it is rostral. This was accounted for in two ways. First, I examined the axons from healthy mice and noticed that more mitochondria were moving rostral rather than caudal in a given axon, consistent with the notion that the number of mitochondria travelling in the anterograde direction exceeds those traveling in the retrograde direction and designated the direction of transport as such. Second, I assessed microtubule direction in the *Thy1-EB3-YFP* transgenic mouse line where the fluorescently labeled plus-end tracking protein associates with the microtubule plus-end. Therefore it is visualized moving anterogradely within axons and rostrally within the spinal cord. This does not exclude that in a small proportion of axons this designation is incorrect although the same holds true in both the control and EAE axons substantially decreasing the likelihood of this adversely altering the results.

6.5 Mitochondria versus Peroxisome Transport

Mitochondria aside, one distinguishing feature of my study is that the transport deficit was not specific to mitochondria but was also observed with peroxisomes. In accordance with mitochondria transport, peroxisome transport is also microtubule based and is known to involve both dynein and kinesin-1 (Kif5) motor proteins, shown *in vitro* in both mammalian and *Drosophilia* cell culture (Kural et al., 2005; Rapp et al., 1996; Wiemer et al., 1997). Mechanisms which regulate their transport, however, have not been thoroughly investigated. Peroxisome distribution is important to carry out their many, diverse functions such as protection of ROS damage as well as to meet specific metabolic conditions such as peroxisomal lipid metabolism (Smith and Aitchison, 2013). The movement of peroxisomes interestingly exhibit qualities that differ from mitochondria. Previous *in vitro* studies (Kural et al., 2005; Wiemer et al., 1997) as well as my *in vivo* analysis has shown that two types of

movement are clearly visible: a random, vibrational movement with little net displacement and fast, directional movement. It is believed that the vibrational movement is microtubule independent while the directional movement is microtubule dependent (Wiemer et al., 1997). Given the similarities in the transport machinery and the observed transport deficits in both peroxisomes and mitochondria, the underlining cause is likely not cargo-based but rather related to motors, or other components that are shared between the two organelles, which will be further discussed in the following section.

6.6 Insight into potential mechanisms of transport deficit

There are various mechanisms by which transport could be disturbed by inflammatory mediators such as reactive species so although the cascade of events which underlies the transport block in EAE were not fully resolved, discussion of potential candidates is warranted.

6.6.1 Histone deacetlyases

In 2010, Kim *et al* reported that nuclear export of the class I Histone deacetylase (HDAC) 1 instigated axonal damage in the cuprizone-induced demyelinaton mouse model (Kim et al., 2010). Here, they stated that following export HDAC1 formed complexes with kinesin motors inhibiting transport and leading to axon degeneration. HDAC1 accumulation were also shown in biopsy samples from MS patients. However upon immuno-labeling with the same antibody against HDAC1 in our acute EAE model a similar number of HDAC1 positive axons in spinal cord tissue derived from healthy animals as well as from mice perfused at the peak of EAE was detected. This finding makes it unlikely that HDAC1 accumulation mediates transport deficits in our MS models.

Class II HDACs, on the other hand, are able to shuttle between the nucleus and the cytoplasm in the absence of a pathological trigger and HDAC6 has been found to localize solely in the cytoplasm, associate with and subsequently deacetylate microtubules (Hubbert et al., 2002). The acetylation

status of tubulin is a key factor in regulating axonal transport. High levels of acetylated tubulin enhances binding of the kinesin motor protein thereby promoting transport of cargo molecules. Inhibition of HDAC6 has been shown to rescue transport deficits in models of Huntington's disease (Dompierre et al., 2007) and HSPB1-induced Charcot-Marie-Tooth disease (d'Ydewalle et al., 2011). It has also been suggested that the Akt-GSK3β pathway is responsible for increasing the activity of HDAC6 (Chen et al., 2010). This addition, however, makes this proposition less attractive for explaining the results because, as previously mentioned, the only interaction of GSK3β with the kinesin motor complex found thus far is through its' light chain which is not essential for mitochondria transport, probably due to the role of Milton as the linkage between kinesin and Miro. Nonetheless, initial experiments were performed where tubastatin A, a selective HDAC6 inhibitor, was bath applied onto the exposed spinal cord of acute EAE mice at the peak of disease and axon transport of mitochondria was measured before and after application. No clear effect was seen although further testing is needed to conclusively rule out HDAC6 as a contributor of the transport deficit.

6.6.2 Tau

Another interesting, unexplored area regarding microtubule stabilization involves the microtubule binding protein, tau, which rose to fame in Alzheimer's disease, as discussed in the Introduction, where accumulations in neurons disrupts its microtubule-binding ability causing neurodegeneration. In addition, elevated tau was found to impede kinesin-dependent transport of organelles, both mitochondria and peroxisomes, consistent with our findings, by competitive inhibition of kinesin to microtubules first in cultured fibroblasts (Ebneth et al., 1998) and more recently in primary neuronal cultures (Stamer et al., 2002). This concomitantly increased axonal levels of reactive oxygen species probably due to the lack of buffering capabilities by means of mitochondria and peroxisomes. The same group also described tau pathology within brainstem lesions of EAE rats creating a potential link of axonal transport deficits and hyperphosphorylated or aggregated tau (Schneider et al., 2004).

Furthermore, abnormally phosphorylated tau is present in chronic EAE mice within the dorsal white matter tract of the spinal cord and in both primary progressive and secondary progressive MS biopsies (Anderson et al., 2008; Anderson et al., 2010). Interestingly, it has been proposed, using an *in vitro* motility assay, that tau, depending on the isoform and concentration, can decrease the number of engaged motors on a given cargo molecule whereby an increase in the number of motors on a cargo molecule works in an additive fashion, steadily increasing the transport rate and total distance travelled (Vershinin et al., 2007). Moreover, it was found that kinesin inhibition by tau could occur at a concentration of tau that was substantially less than what was needed to elicit inhibition of dynein (Dixit et al., 2008). This is important as my results show that while both anterograde and retrograde transport is affected, the reduction anterogradely is more significant (in EAE, normal appearing axons have transport rates which are 89% lower than controls versus 50% retrogradely). As these deficits were also seen "early" in the process of focal axonal degeneration, one could propose that at this stage tau concentrations are only beginning to climb to pathological levels hence effecting first anterograde transport in these axons and eventually both kinesin and dynein at the later stages of axon damage. One final note is that some studies suggest that levels of phosphorylated tau are altered as a result of oxidative stress (Giraldo et al., 2014; Melov et al., 2007; Mondragon-Rodriguez et al., 2013) again coinciding with my results that ROS/RNS are like mediators of axon transport disturbances. To test the role of tau directly in our EAE model, compounds which pharmacologically inhibit tau aggregation and/or hyperphosphorylation can be tested to see if they exert effects on axonal transport in EAE *in vivo* (Bulic et al., 2010; Le Corre et al., 2006).

6.6.3 Calcium

Another possible candidate mechanism for the axon transport deficit would be one that is calcium-mediated. As previously mentioned, axon calcium levels are linked to the mitochondria adaptor protein, Miro, which contains two calcium-sensing motifs and will arrest anterograde transport upon calcium binding in a high calcium environment. In our laboratory, a study is underway looking at the

role of axonal calcium influx in EAE. Here, transgenic mice containing a neuron-specific calcium indicator, Thy1-CerTN were used to measure axonal calcium in various stages of axonal damage in acute EAE. Results indicate that 16% of axons in neuroinflammatory lesions with normal morphology, stage 0, exhibited high calcium levels when normalized to controls (Schumacher, A.M., Mahler, C., Bewersdorf, J., Misgeld, T., and Kerschensteiner, M., unpublished observations). In contrast, my study shows that 72% of stage 0 axons within neuroinflammatory lesions have no observed anterograde transport compared to 16% of axons in healthy mice. This indicates that axonal transport is already perturbed in a large proportion of axons in which an elevated cytoplasmic calcium levels are not detectable. In principle these findings argue against calcium as a main driver of axonal transport deficits in EAE. However, this also begs the question of how much calcium would be sufficient to elicit an effect on the transport. To add another level of complexity, a study by Chang *et al* suggested mitochondrial calcium levels also play an active role in transport (Chang et al., 2011). Using a GFP-based fluorescent calcium indicator, Case12, targeted to mitochondria, they showed that mitochondrial calcium content is inversely related to the speed of mitochondrial movement *in vitro* with no correlation observed in terms of the direction of movement (Chang et al., 2011). In addition, they suggested that Miro may act as a regulator for calcium entry into the mitochondria.

One approach that could be used address this and that I have begun performing, is to create an AAV virus expressing the previously described Miro-KK mutation in which the EF-hands are mutated creating a constitutively active, calcium-independent, Miro protein. This virus is then injected into the lumbar dorsal root ganglia of mice and subsequently expressed in dorsal lumbar axons in EAE mice, the accessible population for spinal imaging. Transport rates *in vivo* of axons expressing the mutated Miro virus could then be quantified and compared to those injected with a control virus to determine whether transport had recovered in EAE in lieu of a calcium hindrance. Of course, Miro is an anterograde-specific adaptor molecule and it has not yet been shown that the retrograde transport machinery also contains calcium-sensing ability while our transport effects were seen in both the anterograde and retrograde direction, potentially confounding these results.

It is evident, however, that mitochondria transport is closely linked to mitochondrial function. Changes in its calcium retention capacity as well as its membrane potential and ROS production that precede detectable morphological abnormalities may effect changes in its transport rate. Correlation between membrane potential and direction of mitochondria movement under non-pathological conditions has been studied although with contradictory conclusions. Using mitochondrial potential sensing dye, JC-1, Miller and Sheetz, observed that the majority of high potential mitochondria moved anterogradely while the majority of mitochondria with low potential moved retrogradely toward the cell body (Miller and Sheetz, 2004). Meanwhile, using the dye tetramethylrhodamine methylester (TMRM), Verburg and Hollenbeck found that the direction of mitochondria was independent of their potential (Verburg and Hollenbeck, 2008). In pathological conditions, blockade of cyclophilin D, a component of the mitochondrial permeability transition pore (mPTP), has been linked to enhanced mitochondrial transport (Guo et al., 2013). Release of cylophilin D from the mitochondrial matrix initiates a series of events which opens the mPTP creating a non-selective, high conductance channel that has the ability to alter the mitochondria membrane potential, decrease its calcium buffering capacity as well as increase production of ROS. In a study by Guo *et al*, loss of cyclophilin D was able to restore mitochondria transport in Aβ-treated neurons and decrease subsequent changes to intra-axonal calcium and ROS levels associated with Aβ-toxicity (Guo et al., 2013). In our laboratory, transgenic mice containing neuronal-specific mitochondrial redox sensors have been described and could be used to address the question of a possible correlation of mitochondria function and their transport under neuroinflammatory conditions (Breckwoldt et al., 2014).

6.6.4 S-nitrosylation by nitric oxide

Another avenue which must be considered when trying to piece together the mechanism comes from my finding that application of nitric oxide (NO) can reversibly inhibit axonal transport of mitochondria. NO is an important signaling molecule that exerts its effect by *S*-nitrosylation, the

covalent attachment of NO to cysteine residues. This post-translation modification is reversible, can regulate a wide variety of cellular functions and, analogous to phosphorylation, is precisely controlled in time and space (Broillet, 1999). NO levels are greatly increased in MS lesions, from studies in both patients and animal models (Bo et al., 1994; Lin et al., 1993; Lu et al., 2000) due to the presence of the inducible form of the enzyme, nitric oxide synthase at sites of inflammation. Its pathological expression has already been linked to impairment of the axon conduction, synaptic transmission and ultimately axon degeneration (Smith and Lassmann, 2002). In one such study, *S*-nitrosylation of microtubule-associated protein 1B (MAP1B) elicited a signal cascade which resulted in axon retraction and growth-cone collapse by impeding the interaction of dynein with microtubules *in vitro* (Stroissnigg et al., 2007). It is therefore conceivable that NO may modify cargo molecules, adaptors or microtubules obstructing their coordination of axonal transport during neuroinflammation. Various sophisticated methods now exist in order to detect *S*-nitrosylated proteins although it becomes considerable more challenging when the goal is to detect a direct, *in vivo* interaction as the bond is considered unstable, rare and can be easily degraded by chemicals needed for the detection process (Uehara and Nishiya, 2011). Still, Wang *et al*, were able to overcome these hindrances and directly visualize interactions using quadropole time-of-flight mass spectrometry (Wang et al., 2008) opening the door for future studies in EAE models.

6.7 Axonal transport deficits and Inflammation

The findings corroborate previous indirect evidence for transport deficits in MS as well as evidence that under inflammatory insult, intra-axonal organelle accumulations arise and may contribute to subsequent tissue damage.

Accumulations of amyloid precursor protein, APP, has been historically described in MS and its models as an indicator of axon damage (Schirmer et al., 2011; Vergo et al., 2011). Biopsy analysis examining the density of mitochondria and molecules which aide in their transport also consistently show they have increased in MS lesions and could potentially contribute to subsequent axon damage

(Mahad et al., 2009; Witte et al., 2009). In a viral model of MS, spinal cords from Theiler's murine encephalomyelitis virus (TMEV)-infected mice showed axon accumulations of non-phosphorylated neurofilament and axonal swellings believed to arise from axon transport dysfunction as microarray analysis showed down regulation of components of the motor complex, tau and tubulin (Kreutzer et al., 2012). This is all consistent with a transport deficit phenotype although difficult to ascertain until now whether these accumulations represented axon dysfunction or the final stages of irreversible, permanent axon loss.

Neuroinflammation in other mouse models have been associated with axon transport impairment. Retrograde transport was evaluated using fluorogold stereotactically injected into the colliculus superior in mice overexpressing proteolipid protein (PLP) in oligodendrocytes (Ip et al., 2012). Here, a reduction of retrograde transport and an accumulation of mitochondria was seen dependent on the infiltration of cytotoxic CD8+ T cells (Ip et al., 2012). In addition, using the same technique to study retrograde transport, lymphocyte infiltration in the neurodegenerative disorder, infantile neuronal ceroid lipofuscinosis (CLN1), significantly perturbed axonal transport and ultimately neuronal survival which could be attenuated by crossbreeding with Rag1-deficient mice that lack mature T- and B- lymphocytes (Groh et al., 2013). Lastly, Inflammatory cytokine tumor necrosis factor-α (TNF-α) is released by activated glia cells and treatment has been shown, *in vitro*, to dissociate kinesin from tubulin in axons thus halting transport of mitochondria and synaptophysin (Stagi et al., 2006).

Noticeably, some studies report that an increase in organelle content and arrest in inflammatory conditions is associated with demyelination (Edgar et al., 2004; Kim et al., 2010; Kiryu-Seo et al., 2010). Meanwhile, the transport disturbance I report likely occurs independently of demyelination suggesting that demyelination is not a prerequisite for a transport deficit but may perpetuate it.

6.8 Axon transport: Cause or Consequence of Axon Degeneration

Like many processes believed to be linked to neurodegeneration, the question always arises whether it is a cause or simply a consequence of a degenerative process already underway. If causal, transport deficits in neurodegenerative diseases are able to lead to very distinct disease phenotypes. Delineating the exact timeline of events will be challenging and due to the heterogeneity in a disease like MS, it is more likely that many processes acts concertedly rather than there being a single, independent pathway that ultimately leads to axon loss. Nonetheless mutations in genes encoding proteins involved in transport have been shown to cause neurodegenerative diseases giving credence to a more direct role for transport defects and disease. Even more importantly, finding an early event in the degenerative process regardless of whether it stands alone, if amenable to therapeutic manipulation has the potential to slow disease progression, a desirable outcome of current MS therapies. As it happens, the transport deficit precedes morphological changes to the axon making highly probable to be an early disturbance and not a result of axon degeneration.

I am now pursuing further studies to explore the sequel of a chronic transport deficit by following dorsal axons as they pass through spinal lesions and eventually synapse in the medulla and evaluating their synaptic viability. A recent study looked at the effect of motile mitochondria on presynaptic strength using syntaphilin expression to manipulate the number mitochondria maintained at a given synapse (Sun et al., 2013). Here, they described the importance of mitochondria docking at synapses for influencing synaptic vesicle release through alteration of ATP homeostasis. Decreasing the density of mitochondria at presynaptic sites negatively regulates the strength of the synapse (Sun et al., 2013). Transport deficits where mitochondria were not anterogradely shuttled to synapses could depress the strength of the synapse short-term and chronically this could lead to synaptic loss and therefore a persistent neurological deficit.

6.9 Axon Transport as a Therapeutic Target for Neuroprotection

Remarkably, it does seem that axonal transport deficits are a common thread amongst several, diverse neurodegenerative diseases. This may open the door for therapies where benefits are achieved by interfering with a common target or pathway helping multiple CNS/PNS diseases. The challenge, as with many potential therapeutic targets is designing something with high specificity that can directly target the axon transport system. While this is still an untapped source of therapies, success has already been described in the previously mentioned report describing the role of HDAC6 in a mouse model of Charcot-Marie tooth disease (d'Ydewalle et al., 2011). Here, a specific inhibitor for HDAC6 not only rescued the transport deficit but also reversed the clinical phenotype. One could imagine that such drugs that modify the transport machinery would be an ideal target. For example, proteins that directly phosphorylate motor proteins leading to their detachment from microtubules/cargoes or microtubule associated proteins which can decrease the affinity of motors for microtubules. One final consideration for therapeutics is that they must take into account that some links to transport failure are, when at non-pathological concentrations, absolutely necessary for the normal functioning of axon transport. In this sense, targeting said process must be done in such a way that it can still occur at physiological levels while hindering its pathological consequences. Consider the case of calcium-mediated axon transport deficits. Calcium is an essential regulator for axon transport, monitoring when mitochondria are needed to pause and aid in its buffering or ATP production but when at pathological levels mitochondria can permanently pause causing energy failures elsewhere along its trajectory. Overall, much information of the machinery and operation of the transport system needs to be deciphered before proper therapy targets can be made. This includes the exact stoichiometry of the motor/adaptor complex, a hotly debated concept and a detailed mechanistic understanding of the modulatory pathways, especially the *in vivo* relevance as most of these experiments have been performed in cell culture-based setting.

6.10 General Conclusions

The aim of this study was to further understand the pathogenesis of immune-mediated axon damage in multiple sclerosis and its mouse models. Axonal transport plays a fundamental role in maintaining the proper functioning of a neuron and abrogation has been shown to play a role in other neurodegenerative diseases but has never been directly measured in neuroinflammatory conditions such as MS although previously reported histological analyses suggests its' involvement. Therefore, it seemed fitting to investigate this in an *in vivo* setting where single axons could be directly analyzed within the inflammatory milieu present in the spinal cord of EAE mice, something which could not be achieved with tradition methods of measuring axonal transport *in vitro*. After establishing this imaging method, I discovered and characterized pervasive axonal transport deficits in neuroinflammatory lesions of EAE models which interestingly preceded morphological changes within axons, identifying a novel stage of axonal dysfunction with the potential for reversibility. Reversible axon dysfunction in MS may hold the key to explaining relapsing-remitting disease characteristics where there exists little structural damage but functional deficits are widespread. Pharmacological targeting of axon transport either directly or through upstream effectors such as reactive oxygen/nitrogen species may hold the key to alleviating relapses acutely or improving the persistent neurological damage associated with long term, progressive phase of the disease.

7. References

Aboul-Enein, F., Weiser, P., Hoftberger, R., Lassmann, H., and Bradl, M. (2006). Transient axonal injury in the absence of demyelination: a correlate of clinical disease in acute experimental autoimmune encephalomyelitis. Acta neuropathologica *111*, 539-547.

Akhmanova, A., and Steinmetz, M.O. (2008). Tracking the ends: a dynamic protein network controls the fate of microtubule tips. Nature reviews Molecular cell biology *9*, 309-322.

Aktas, O., Smorodchenko, A., Brocke, S., Infante-Duarte, C., Schulze Topphoff, U., Vogt, J., Prozorovski, T., Meier, S., Osmanova, V., Pohl, E.*, et al.* (2005). Neuronal damage in autoimmune neuroinflammation mediated by the death ligand TRAIL. Neuron *46*, 421-432.

Anderson, J.M., Hampton, D.W., Patani, R., Pryce, G., Crowther, R.A., Reynolds, R., Franklin, R.J., Giovannoni, G., Compston, D.A., Baker, D.*, et al.* (2008). Abnormally phosphorylated tau is associated with neuronal and axonal loss in experimental autoimmune encephalomyelitis and multiple sclerosis. Brain : a journal of neurology *131*, 1736-1748.

Anderson, J.M., Patani, R., Reynolds, R., Nicholas, R., Compston, A., Spillantini, M.G., and Chandran, S. (2010). Abnormal tau phosphorylation in primary progressive multiple sclerosis. Acta neuropathologica *119*, 591-600.

Armstrong, R.A. (2006). Plaques and tangles and the pathogenesis of Alzheimer's disease. Folia neuropathologica / Association of Polish Neuropathologists and Medical Research Centre, Polish Academy of Sciences *44*, 1-11.

Arnold, D.L., Riess, G.T., Matthews, P.M., Francis, G.S., Collins, D.L., Wolfson, C., and Antel, J.P. (1994). Use of proton magnetic resonance spectroscopy for monitoring disease progression in multiple sclerosis. Annals of neurology *36*, 76-82.

Ashrafi, G., and Schwarz, T.L. (2013). The pathways of mitophagy for quality control and clearance of mitochondria. Cell death and differentiation *20*, 31-42.

Ballard, C., Gauthier, S., Corbett, A., Brayne, C., Aarsland, D., and Jones, E. (2011). Alzheimer's disease. Lancet *377*, 1019-1031.

Baloh, R.H., Schmidt, R.E., Pestronk, A., and Milbrandt, J. (2007). Altered axonal mitochondrial transport in the pathogenesis of Charcot-Marie-Tooth disease from mitofusin 2 mutations. The Journal of neuroscience : the official journal of the Society for Neuroscience *27*, 422-430.

Barcellos, L.F., Sawcer, S., Ramsay, P.P., Baranzini, S.E., Thomson, G., Briggs, F., Cree, B.C., Begovich, A.B., Villoslada, P., Montalban, X.*, et al.* (2006). Heterogeneity at the HLA-DRB1 locus and risk for multiple sclerosis. Human molecular genetics *15*, 2813-2824.

Barisic, N., Claeys, K.G., Sirotkovic-Skerlev, M., Lofgren, A., Nelis, E., De Jonghe, P., and Timmerman, V. (2008). Charcot-Marie-Tooth disease: a clinico-genetic confrontation. Annals of human genetics *72*, 416-441.

Barr, T.A., Shen, P., Brown, S., Lampropoulou, V., Roch, T., Lawrie, S., Fan, B., O'Connor, R.A., Anderton, S.M., Bar-Or, A.*, et al.* (2012). B cell depletion therapy ameliorates autoimmune disease through ablation of IL-6-producing B cells. The Journal of experimental medicine *209*, 1001-1010.

Bechtold, D.A., Kapoor, R., and Smith, K.J. (2004). Axonal protection using flecainide in experimental autoimmune encephalomyelitis. Annals of neurology *55*, 607-616.

Beck, M., Brickley, K., Wilkinson, H.L., Sharma, S., Smith, M., Chazot, P.L., Pollard, S., and Stephenson, F.A. (2002). Identification, molecular cloning, and characterization of a novel GABAA receptor-associated protein, GRIF-1. The Journal of biological chemistry *277*, 30079-30090.

Beecham, A.H., Patsopoulos, N.A., Xifara, D.K., Davis, M.F., Kemppinen, A., Cotsapas, C., Shah, T.S., Spencer, C., Booth, D., Goris, A.*, et al.* (2013). Analysis of immune-related loci identifies 48 new susceptibility variants for multiple sclerosis. Nature genetics *45*, 1353-1360.

Berer, K., Wekerle, H., and Krishnamoorthy, G. (2011). B cells in spontaneous autoimmune diseases of the central nervous system. Mol Immunol *48*, 1332-1337.

Bettelli, E., Baeten, D., Jager, A., Sobel, R.A., and Kuchroo, V.K. (2006). Myelin oligodendrocyte glycoprotein-specific T and B cells cooperate to induce a Devic-like disease in mice. J Clin Invest *116*, 2393-2402.

Bitsch, A., Schuchardt, J., Bunkowski, S., Kuhlmann, T., and Bruck, W. (2000). Acute axonal injury in multiple sclerosis. Correlation with demyelination and inflammation. Brain : a journal of neurology *123 (Pt 6)*, 1174-1183.

Bjartmar, C., Kidd, G., Mork, S., Rudick, R., and Trapp, B.D. (2000). Neurological disability correlates with spinal cord axonal loss and reduced N-acetyl aspartate in chronic multiple sclerosis patients. Annals of neurology *48*, 893-901.

Black, J.A., Liu, S., and Waxman, S.G. (2009). Sodium channel activity modulates multiple functions in microglia. Glia *57*, 1072-1081.

Black, J.A., Newcombe, J., Trapp, B.D., and Waxman, S.G. (2007). Sodium channel expression within chronic multiple sclerosis plaques. Journal of neuropathology and experimental neurology *66*, 828-837.

Black, M.M., and Baas, P.W. (1989). The basis of polarity in neurons. Trends in neurosciences *12*, 211-214.

Bo, L., Dawson, T.M., Wesselingh, S., Mork, S., Choi, S., Kong, P.A., Hanley, D., and Trapp, B.D. (1994). Induction of nitric oxide synthase in demyelinating regions of multiple sclerosis brains. Annals of neurology *36*, 778-786.

Bolanos, J.P., Almeida, A., Stewart, V., Peuchen, S., Land, J.M., Clark, J.B., and Heales, S.J. (1997). Nitric oxide-mediated mitochondrial damage in the brain: mechanisms and implications for neurodegenerative diseases. Journal of neurochemistry *68*, 2227-2240.

Bonifati, V., Rizzu, P., van Baren, M.J., Schaap, O., Breedveld, G.J., Krieger, E., Dekker, M.C., Squitieri, F., Ibanez, P., Joosse, M.*, et al.* (2003). Mutations in the DJ-1 gene associated with autosomal recessive early-onset parkinsonism. Science *299*, 256-259.

Brady, S.T. (1985). A novel brain ATPase with properties expected for the fast axonal transport motor. Nature *317*, 73-75.

Breckwoldt, M.O., Pfister, F.M., Bradley, P.M., Marinkovic, P., Williams, P.R., Brill, M.S., Plomer, B., Schmalz, A., St Clair, D.K., Naumann, R.*, et al.* (2014). Multiparametric optical analysis of mitochondrial redox signals during neuronal physiology and pathology in vivo. Nature medicine *20*, 555-560.

Breij, E.C., Brink, B.P., Veerhuis, R., van den Berg, C., Vloet, R., Yan, R., Dijkstra, C.D., van der Valk, P., and Bo, L. (2008). Homogeneity of active demyelinating lesions in established multiple sclerosis. Annals of neurology *63*, 16-25.

Brickley, K., and Stephenson, F.A. (2011). Trafficking kinesin protein (TRAK)-mediated transport of mitochondria in axons of hippocampal neurons. The Journal of biological chemistry *286*, 18079-18092.

Brinkmann, V., Davis, M.D., Heise, C.E., Albert, R., Cottens, S., Hof, R., Bruns, C., Prieschl, E., Baumruker, T., Hiestand, P*., et al.* (2002). The immune modulator FTY720 targets sphingosine 1-phosphate receptors. The Journal of biological chemistry *277*, 21453-21457.

Broillet, M.C. (1999). S-nitrosylation of proteins. Cellular and molecular life sciences : CMLS *55*, 1036-1042.

Brorson, J.R., Schumacker, P.T., and Zhang, H. (1999). Nitric oxide acutely inhibits neuronal energy production. The Committees on Neurobiology and Cell Physiology. The Journal of neuroscience : the official journal of the Society for Neuroscience *19*, 147-158.

Bulic, B., Pickhardt, M., Mandelkow, E.M., and Mandelkow, E. (2010). Tau protein and tau aggregation inhibitors. Neuropharmacology *59*, 276-289.

Cai, Q., Gerwin, C., and Sheng, Z.H. (2005). Syntabulin-mediated anterograde transport of mitochondria along neuronal processes. The Journal of cell biology *170*, 959-969.

Calabrese, M., Rinaldi, F., Mattisi, I., Bernardi, V., Favaretto, A., Perini, P., and Gallo, P. (2011). The predictive value of gray matter atrophy in clinically isolated syndromes. Neurology *77*, 257-263.

Canet-Aviles, R.M., Wilson, M.A., Miller, D.W., Ahmad, R., McLendon, C., Bandyopadhyay, S., Baptista, M.J., Ringe, D., Petsko, G.A., and Cookson, M.R. (2004). The Parkinson's disease protein DJ-1 is neuroprotective due to cysteine-sulfinic acid-driven mitochondrial localization. Proceedings of the National Academy of Sciences of the United States of America *101*, 9103-9108.

Carbone, F., De Rosa, V., Carrieri, P.B., Montella, S., Bruzzese, D., Porcellini, A., Procaccini, C., La Cava, A., and Matarese, G. (2014). Regulatory T cell proliferative potential is impaired in human autoimmune disease. Nature medicine *20*, 69-74.

Carson, M.J. (2002). Microglia as liaisons between the immune and central nervous systems: functional implications for multiple sclerosis. Glia *40*, 218-231.

Cartelli, D., Goldwurm, S., Casagrande, F., Pezzoli, G., and Cappelletti, G. (2012). Microtubule destabilization is shared by genetic and idiopathic Parkinson's disease patient fibroblasts. PloS one *7*, e37467.

Cartelli, D., Ronchi, C., Maggioni, M.G., Rodighiero, S., Giavini, E., and Cappelletti, G. (2010). Microtubule dysfunction precedes transport impairment and mitochondria damage in MPP+ - induced neurodegeneration. Journal of neurochemistry *115*, 247-258.

Chada, S.R., and Hollenbeck, P.J. (2003). Mitochondrial movement and positioning in axons: the role of growth factor signaling. The Journal of experimental biology *206*, 1985-1992.

Chada, S.R., and Hollenbeck, P.J. (2004). Nerve growth factor signaling regulates motility and docking of axonal mitochondria. Current biology : CB *14*, 1272-1276.

Chan, N.C., Salazar, A.M., Pham, A.H., Sweredoski, M.J., Kolawa, N.J., Graham, R.L., Hess, S., and Chan, D.C. (2011). Broad activation of the ubiquitin-proteasome system by Parkin is critical for mitophagy. Human molecular genetics *20*, 1726-1737.

Chang, K.T., Niescier, R.F., and Min, K.T. (2011). Mitochondrial matrix Ca2+ as an intrinsic signal regulating mitochondrial motility in axons. Proceedings of the National Academy of Sciences of the United States of America *108*, 15456-15461.

Charcot, J. (1868). Histologie de la sclerose en plaques. Gazette des hopitaux, Paris *41*, 554-555.

Chataway, J., Schuerer, N., Alsanousi, A., Chan, D., Macmanus, D., Hunter, K., Anderson, V., Bangham, C.R., Clegg, S., Nielsen, C.*, et al.* (2014). Effect of high-dose simvastatin on brain atrophy and disability in secondary progressive multiple sclerosis (MS-STAT): a randomised, placebo-controlled, phase 2 trial. Lancet.

Chen, H., Assmann, J.C., Krenz, A., Rahman, M., Grimm, M., Karsten, C.M., Kohl, J., Offermanns, S., Wettschureck, N., and Schwaninger, M. (2014). Hydroxycarboxylic acid receptor 2 mediates dimethyl fumarate's protective effect in EAE. J Clin Invest.

Chen, S., Owens, G.C., Makarenkova, H., and Edelman, D.B. (2010). HDAC6 regulates mitochondrial transport in hippocampal neurons. PloS one *5*, e10848.

Chen, Y., and Dorn, G.W., 2nd (2013). PINK1-phosphorylated mitofusin 2 is a Parkin receptor for culling damaged mitochondria. Science *340*, 471-475.

Chen, Y., and Sheng, Z.H. (2013). Kinesin-1-syntaphilin coupling mediates activity-dependent regulation of axonal mitochondrial transport. The Journal of cell biology *202*, 351-364.

Cheney, R.E., O'Shea, M.K., Heuser, J.E., Coelho, M.V., Wolenski, J.S., Espreafico, E.M., Forscher, P., Larson, R.E., and Mooseker, M.S. (1993). Brain myosin-V is a two-headed unconventional myosin with motor activity. Cell *75*, 13-23.

Chung, K., Wallace, J., Kim, S.Y., Kalyanasundaram, S., Andalman, A.S., Davidson, T.J., Mirzabekov, J.J., Zalocusky, K.A., Mattis, J., Denisin, A.K.*, et al.* (2013). Structural and molecular interrogation of intact biological systems. Nature *497*, 332-337.

Claussen, M.C., and Korn, T. (2012). Immune mechanisms of new therapeutic strategies in MS: teriflunomide. Clinical immunology *142*, 49-56.

Compston, A., and Coles, A. (2002). Multiple sclerosis. Lancet *359*, 1221-1231.

Constantinescu, C.S., Hilliard, B., Ventura, E., Wysocka, M., Showe, L., Lavi, E., Fujioka, T., Scott, P., Trinchieri, G., and Rostami, A. (2001). Modulation of susceptibility and resistance to an autoimmune model of multiple sclerosis in prototypically susceptible and resistant strains by neutralization of interleukin-12 and interleukin-4, respectively. Clinical immunology *98*, 23-30.

Conway, D., and Cohen, J.A. (2010). Emerging oral therapies in multiple sclerosis. Current neurology and neuroscience reports *10*, 381-388.

Craner, M.J., Damarjian, T.G., Liu, S., Hains, B.C., Lo, A.C., Black, J.A., Newcombe, J., Cuzner, M.L., and Waxman, S.G. (2005). Sodium channels contribute to microglia/macrophage activation and function in EAE and MS. Glia *49*, 220-229.

Craner, M.J., Hains, B.C., Lo, A.C., Black, J.A., and Waxman, S.G. (2004a). Co-localization of sodium channel Nav1.6 and the sodium-calcium exchanger at sites of axonal injury in the spinal cord in EAE. Brain : a journal of neurology *127*, 294-303.

Craner, M.J., Newcombe, J., Black, J.A., Hartle, C., Cuzner, M.L., and Waxman, S.G. (2004b). Molecular changes in neurons in multiple sclerosis: altered axonal expression of Nav1.2 and Nav1.6 sodium channels and Na+/Ca2+ exchanger. Proceedings of the National Academy of Sciences of the United States of America *101*, 8168-8173.

Cua, D.J., Sherlock, J., Chen, Y., Murphy, C.A., Joyce, B., Seymour, B., Lucian, L., To, W., Kwan, S., Churakova, T.*, et al.* (2003). Interleukin-23 rather than interleukin-12 is the critical cytokine for autoimmune inflammation of the brain. Nature *421*, 744-748.

d'Ydewalle, C., Krishnan, J., Chiheb, D.M., Van Damme, P., Irobi, J., Kozikowski, A.P., Vanden Berghe, P., Timmerman, V., Robberecht, W., and Van Den Bosch, L. (2011). HDAC6 inhibitors reverse axonal

loss in a mouse model of mutant HSPB1-induced Charcot-Marie-Tooth disease. Nature medicine *17*, 968-974.

Dalton, C.M., Chard, D.T., Davies, G.R., Miszkiel, K.A., Altmann, D.R., Fernando, K., Plant, G.T., Thompson, A.J., and Miller, D.H. (2004). Early development of multiple sclerosis is associated with progressive grey matter atrophy in patients presenting with clinically isolated syndromes. Brain : a journal of neurology *127*, 1101-1107.

Das Sarma, J., Kenyon, L.C., Hingley, S.T., and Shindler, K.S. (2009). Mechanisms of primary axonal damage in a viral model of multiple sclerosis. The Journal of neuroscience : the official journal of the Society for Neuroscience *29*, 10272-10280.

Dasilva, A.G., and Yong, V.W. (2008). Expression and regulation of matrix metalloproteinase-12 in experimental autoimmune encephalomyelitis and by bone marrow derived macrophages in vitro. Journal of neuroimmunology *199*, 24-34.

De Stefano, N., Matthews, P.M., Filippi, M., Agosta, F., De Luca, M., Bartolozzi, M.L., Guidi, L., Ghezzi, A., Montanari, E., Cifelli, A.*, et al.* (2003). Evidence of early cortical atrophy in MS: relevance to white matter changes and disability. Neurology *60*, 1157-1162.

De Stefano, N., Matthews, P.M., Fu, L., Narayanan, S., Stanley, J., Francis, G.S., Antel, J.P., and Arnold, D.L. (1998). Axonal damage correlates with disability in patients with relapsing-remitting multiple sclerosis. Results of a longitudinal magnetic resonance spectroscopy study. Brain : a journal of neurology *121 (Pt 8)*, 1469-1477.

De Vos, K., Severin, F., Van Herreweghe, F., Vancompernolle, K., Goossens, V., Hyman, A., and Grooten, J. (2000). Tumor necrosis factor induces hyperphosphorylation of kinesin light chain and inhibits kinesin-mediated transport of mitochondria. The Journal of cell biology *149*, 1207-1214.

De Vos, K.J., Sable, J., Miller, K.E., and Sheetz, M.P. (2003). Expression of phosphatidylinositol (4,5) bisphosphate-specific pleckstrin homology domains alters direction but not the level of axonal transport of mitochondria. Molecular biology of the cell *14*, 3636-3649.

Decker, H., Lo, K.Y., Unger, S.M., Ferreira, S.T., and Silverman, M.A. (2010). Amyloid-beta peptide oligomers disrupt axonal transport through an NMDA receptor-dependent mechanism that is mediated by glycogen synthase kinase 3beta in primary cultured hippocampal neurons. The Journal of neuroscience : the official journal of the Society for Neuroscience *30*, 9166-9171.

Desplats, P., Lee, H.J., Bae, E.J., Patrick, C., Rockenstein, E., Crews, L., Spencer, B., Masliah, E., and Lee, S.J. (2009). Inclusion formation and neuronal cell death through neuron-to-neuron transmission of alpha-synuclein. Proceedings of the National Academy of Sciences of the United States of America *106*, 13010-13015.

Dixit, R., Ross, J.L., Goldman, Y.E., and Holzbaur, E.L. (2008). Differential regulation of dynein and kinesin motor proteins by tau. Science *319*, 1086-1089.

Dompierre, J.P., Godin, J.D., Charrin, B.C., Cordelieres, F.P., King, S.J., Humbert, S., and Saudou, F. (2007). Histone deacetylase 6 inhibition compensates for the transport deficit in Huntington's disease by increasing tubulin acetylation. The Journal of neuroscience : the official journal of the Society for Neuroscience *27*, 3571-3583.

Drewes, G., Ebneth, A., Preuss, U., Mandelkow, E.M., and Mandelkow, E. (1997). MARK, a novel family of protein kinases that phosphorylate microtubule-associated proteins and trigger microtubule disruption. Cell *89*, 297-308.

Ebneth, A., Godemann, R., Stamer, K., Illenberger, S., Trinczek, B., and Mandelkow, E. (1998). Overexpression of tau protein inhibits kinesin-dependent trafficking of vesicles, mitochondria, and endoplasmic reticulum: implications for Alzheimer's disease. The Journal of cell biology *143*, 777-794.

Edgar, J.M., McLaughlin, M., Yool, D., Zhang, S.C., Fowler, J.H., Montague, P., Barrie, J.A., McCulloch, M.C., Duncan, I.D., Garbern, J.*, et al.* (2004). Oligodendroglial modulation of fast axonal transport in a mouse model of hereditary spastic paraplegia. The Journal of cell biology *166*, 121-131.

Edwards, J.P., Zhang, X., Frauwirth, K.A., and Mosser, D.M. (2006). Biochemical and functional characterization of three activated macrophage populations. J Leukoc Biol *80*, 1298-1307.

Erturk, A., and Bradke, F. (2013). High-resolution imaging of entire organs by 3-dimensional imaging of solvent cleared organs (3DISCO). Exp Neurol *242*, 57-64.

Evgrafov, O.V., Mersiyanova, I., Irobi, J., Van Den Bosch, L., Dierick, I., Leung, C.L., Schagina, O., Verpoorten, N., Van Impe, K., Fedotov, V.*, et al.* (2004). Mutant small heat-shock protein 27 causes axonal Charcot-Marie-Tooth disease and distal hereditary motor neuropathy. Nature genetics *36*, 602-606.

Federico, A., Cardaioli, E., Da Pozzo, P., Formichi, P., Gallus, G.N., and Radi, E. (2012). Mitochondria, oxidative stress and neurodegeneration. Journal of the neurological sciences *322*, 254-262.

Feng, G., Mellor, R.H., Bernstein, M., Keller-Peck, C., Nguyen, Q.T., Wallace, M., Nerbonne, J.M., Lichtman, J.W., and Sanes, J.R. (2000). Imaging neuronal subsets in transgenic mice expressing multiple spectral variants of GFP. Neuron *28*, 41-51.

Ferguson, B., Matyszak, M.K., Esiri, M.M., and Perry, V.H. (1997). Axonal damage in acute multiple sclerosis lesions. Brain : a journal of neurology *120 (Pt 3)*, 393-399.

Fillatreau, S., Sweenie, C.H., McGeachy, M.J., Gray, D., and Anderton, S.M. (2002). B cells regulate autoimmunity by provision of IL-10. Nat Immunol *3*, 944-950.

Fischer, M.T., Sharma, R., Lim, J.L., Haider, L., Frischer, J.M., Drexhage, J., Mahad, D., Bradl, M., van Horssen, J., and Lassmann, H. (2012). NADPH oxidase expression in active multiple sclerosis lesions in relation to oxidative tissue damage and mitochondrial injury. Brain : a journal of neurology *135*, 886-899.

Fisher, E., Lee, J.C., Nakamura, K., and Rudick, R.A. (2008). Gray matter atrophy in multiple sclerosis: a longitudinal study. Annals of neurology *64*, 255-265.

Fletcher, J.M., Lalor, S.J., Sweeney, C.M., Tubridy, N., and Mills, K.H. (2010). T cells in multiple sclerosis and experimental autoimmune encephalomyelitis. Clinical and experimental immunology *162*, 1-11.

Fox, R.J., Miller, D.H., Phillips, J.T., Hutchinson, M., Havrdova, E., Kita, M., Yang, M., Raghupathi, K., Novas, M., Sweetser, M.T.*, et al.* (2012). Placebo-controlled phase 3 study of oral BG-12 or glatiramer in multiple sclerosis. The New England journal of medicine *367*, 1087-1097.

Fransson, A., Ruusala, A., and Aspenstrom, P. (2003). Atypical Rho GTPases have roles in mitochondrial homeostasis and apoptosis. The Journal of biological chemistry *278*, 6495-6502.

Fransson, S., Ruusala, A., and Aspenstrom, P. (2006). The atypical Rho GTPases Miro-1 and Miro-2 have essential roles in mitochondrial trafficking. Biochemical and biophysical research communications *344*, 500-510.

Freundt, E.C., Maynard, N., Clancy, E.K., Roy, S., Bousset, L., Sourigues, Y., Covert, M., Melki, R., Kirkegaard, K., and Brahic, M. (2012). Neuron-to-neuron transmission of alpha-synuclein fibrils through axonal transport. Annals of neurology *72*, 517-524.

Friese, M.A., Craner, M.J., Etzensperger, R., Vergo, S., Wemmie, J.A., Welsh, M.J., Vincent, A., and Fugger, L. (2007). Acid-sensing ion channel-1 contributes to axonal degeneration in autoimmune inflammation of the central nervous system. Nature medicine *13*, 1483-1489.

Friese, M.A., and Fugger, L. (2009). Pathogenic CD8(+) T cells in multiple sclerosis. Annals of neurology *66*, 132-141.

Friese, M.A., Montalban, X., Willcox, N., Bell, J.I., Martin, R., and Fugger, L. (2006). The value of animal models for drug development in multiple sclerosis. Brain : a journal of neurology *129*, 1940-1952.

Fu, L., Matthews, P.M., De Stefano, N., Worsley, K.J., Narayanan, S., Francis, G.S., Antel, J.P., Wolfson, C., and Arnold, D.L. (1998). Imaging axonal damage of normal-appearing white matter in multiple sclerosis. Brain : a journal of neurology *121 (Pt 1)*, 103-113.

Fu, M.M., and Holzbaur, E.L. (2013). JIP1 regulates the directionality of APP axonal transport by coordinating kinesin and dynein motors. The Journal of cell biology.

Fujita, T., Maturana, A.D., Ikuta, J., Hamada, J., Walchli, S., Suzuki, T., Sawa, H., Wooten, M.W., Okajima, T., Tatematsu, K.*, et al.* (2007). Axonal guidance protein FEZ1 associates with tubulin and kinesin motor protein to transport mitochondria in neurites of NGF-stimulated PC12 cells. Biochemical and biophysical research communications *361*, 605-610.

Gavin, M.A., Rasmussen, J.P., Fontenot, J.D., Vasta, V., Manganiello, V.C., Beavo, J.A., and Rudensky, A.Y. (2007). Foxp3-dependent programme of regulatory T-cell differentiation. Nature *445*, 771-775.

Gegg, M.E., Cooper, J.M., Chau, K.Y., Rojo, M., Schapira, A.H., and Taanman, J.W. (2010). Mitofusin 1 and mitofusin 2 are ubiquitinated in a PINK1/parkin-dependent manner upon induction of mitophagy. Human molecular genetics *19*, 4861-4870.

Geurts, J.J., Stys, P.K., Minagar, A., Amor, S., and Zivadinov, R. (2009). Gray matter pathology in (chronic) MS: modern views on an early observation. Journal of the neurological sciences *282*, 12-20.

Geurts, J.J., Wolswijk, G., Bo, L., van der Valk, P., Polman, C.H., Troost, D., and Aronica, E. (2003). Altered expression patterns of group I and II metabotropic glutamate receptors in multiple sclerosis. Brain : a journal of neurology *126*, 1755-1766.

Giese, K.P. (2009). GSK-3: a key player in neurodegeneration and memory. IUBMB life *61*, 516-521.

Giraldo, E., Lloret, A., Fuchsberger, T., and Viña, J. (2014). Aβ and tau toxicities in Alzheimer's are linked via oxidative stress-induced p38 activation. Protective role of vitamin E. Redox Biology.

Glater, E.E., Megeath, L.J., Stowers, R.S., and Schwarz, T.L. (2006). Axonal transport of mitochondria requires milton to recruit kinesin heavy chain and is light chain independent. The Journal of cell biology *173*, 545-557.

Gold, R., Kappos, L., Arnold, D.L., Bar-Or, A., Giovannoni, G., Selmaj, K., Tornatore, C., Sweetser, M.T., Yang, M., Sheikh, S.I.*, et al.* (2012a). Placebo-controlled phase 3 study of oral BG-12 for relapsing multiple sclerosis. The New England journal of medicine *367*, 1098-1107.

Gold, R., Linker, R.A., and Stangel, M. (2012b). Fumaric acid and its esters: an emerging treatment for multiple sclerosis with antioxidative mechanism of action. Clinical immunology *142*, 44-48.

Gordon, S. (2003). Alternative activation of macrophages. Nat Rev Immunol *3*, 23-35.

Greenwood, J., Steinman, L., and Zamvil, S.S. (2006). Statin therapy and autoimmune disease: from protein prenylation to immunomodulation. Nat Rev Immunol *6*, 358-370.

Gregory, A.P., Dendrou, C.A., Attfield, K.E., Haghikia, A., Xifara, D.K., Butter, F., Poschmann, G., Kaur, G., Lambert, L., Leach, O.A.*, et al.* (2012). TNF receptor 1 genetic risk mirrors outcome of anti-TNF therapy in multiple sclerosis. Nature *488*, 508-511.

Groh, J., Kuhl, T.G., Ip, C.W., Nelvagal, H.R., Sri, S., Duckett, S., Mirza, M., Langmann, T., Cooper, J.D., and Martini, R. (2013). Immune cells perturb axons and impair neuronal survival in a mouse model of infantile neuronal ceroid lipofuscinosis. Brain : a journal of neurology *136*, 1083-1101.

Gunawardena, S., Her, L.S., Brusch, R.G., Laymon, R.A., Niesman, I.R., Gordesky-Gold, B., Sintasath, L., Bonini, N.M., and Goldstein, L.S. (2003). Disruption of axonal transport by loss of huntingtin or expression of pathogenic polyQ proteins in Drosophila. Neuron *40*, 25-40.

Guo, L., Du, H., Yan, S., Wu, X., McKhann, G.M., Chen, J.X., and Yan, S.S. (2013). Cyclophilin D deficiency rescues axonal mitochondrial transport in Alzheimer's neurons. PloS one *8*, e54914.

Guo, X., Macleod, G.T., Wellington, A., Hu, F., Panchumarthi, S., Schoenfield, M., Marin, L., Charlton, M.P., Atwood, H.L., and Zinsmaier, K.E. (2005). The GTPase dMiro is required for axonal transport of mitochondria to Drosophila synapses. Neuron *47*, 379-393.

Haas, J., Fritzsching, B., Trubswetter, P., Korporal, M., Milkova, L., Fritz, B., Vobis, D., Krammer, P.H., Suri-Payer, E., and Wildemann, B. (2007). Prevalence of newly generated naive regulatory T cells (Treg) is critical for Treg suppressive function and determines Treg dysfunction in multiple sclerosis. Journal of immunology *179*, 1322-1330.

Hafler, D.A., Compston, A., Sawcer, S., Lander, E.S., Daly, M.J., De Jager, P.L., de Bakker, P.I., Gabriel, S.B., Mirel, D.B., Ivinson, A.J.*, et al.* (2007). Risk alleles for multiple sclerosis identified by a genomewide study. The New England journal of medicine *357*, 851-862.

Hagiwara, H., Yorifuji, H., Sato-Yoshitake, R., and Hirokawa, N. (1994). Competition between motor molecules (kinesin and cytoplasmic dynein) and fibrous microtubule-associated proteins in binding to microtubules. The Journal of biological chemistry *269*, 3581-3589.

Haider, L., Fischer, M.T., Frischer, J.M., Bauer, J., Hoftberger, R., Botond, G., Esterbauer, H., Binder, C.J., Witztum, J.L., and Lassmann, H. (2011). Oxidative damage in multiple sclerosis lesions. Brain : a journal of neurology *134*, 1914-1924.

Heppner, F.L., Greter, M., Marino, D., Falsig, J., Raivich, G., Hovelmeyer, N., Waisman, A., Rulicke, T., Prinz, M., Priller, J.*, et al.* (2005). Experimental autoimmune encephalomyelitis repressed by microglial paralysis. Nature medicine *11*, 146-152.

Hiruma, H., Katakura, T., Takahashi, S., Ichikawa, T., and Kawakami, T. (2003). Glutamate and amyloid beta-protein rapidly inhibit fast axonal transport in cultured rat hippocampal neurons by different mechanisms. The Journal of neuroscience : the official journal of the Society for Neuroscience *23*, 8967-8977.

Hollenbeck, P.J. (1996). The pattern and mechanism of mitochondrial transport in axons. Frontiers in bioscience : a journal and virtual library *1*, d91-102.

Holleran, E.A., Karki, S., and Holzbaur, E.L. (1998). The role of the dynactin complex in intracellular motility. International review of cytology *182*, 69-109.

Horiuchi, D., Collins, C.A., Bhat, P., Barkus, R.V., Diantonio, A., and Saxton, W.M. (2007). Control of a kinesin-cargo linkage mechanism by JNK pathway kinases. Current biology : CB *17*, 1313-1317.

Hu, D., Ikizawa, K., Lu, L., Sanchirico, M.E., Shinohara, M.L., and Cantor, H. (2004). Analysis of regulatory CD8 T cells in Qa-1-deficient mice. Nat Immunol *5*, 516-523.

Hubbert, C., Guardiola, A., Shao, R., Kawaguchi, Y., Ito, A., Nixon, A., Yoshida, M., Wang, X.F., and Yao, T.P. (2002). HDAC6 is a microtubule-associated deacetylase. Nature *417*, 455-458.

Hurd, D.D., and Saxton, W.M. (1996). Kinesin mutations cause motor neuron disease phenotypes by disrupting fast axonal transport in Drosophila. Genetics *144*, 1075-1085.

Huse, M., Quann, E.J., and Davis, M.M. (2008). Shouts, whispers and the kiss of death: directional secretion in T cells. Nat Immunol *9*, 1105-1111.

Ikuta, J., Maturana, A., Fujita, T., Okajima, T., Tatematsu, K., Tanizawa, K., and Kuroda, S. (2007). Fasciculation and elongation protein zeta-1 (FEZ1) participates in the polarization of hippocampal neuron by controlling the mitochondrial motility. Biochemical and biophysical research communications *353*, 127-132.

International Multiple Sclerosis Genetics, C., Wellcome Trust Case Control, C., Sawcer, S., Hellenthal, G., Pirinen, M., Spencer, C.C., Patsopoulos, N.A., Moutsianas, L., Dilthey, A., Su, Z*., et al.* (2011). Genetic risk and a primary role for cell-mediated immune mechanisms in multiple sclerosis. Nature *476*, 214-219.

Ip, C.W., Kroner, A., Groh, J., Huber, M., Klein, D., Spahn, I., Diem, R., Williams, S.K., Nave, K.A., Edgar, J.M*., et al.* (2012). Neuroinflammation by cytotoxic T-lymphocytes impairs retrograde axonal transport in an oligodendrocyte mutant mouse. PloS one *7*, e42554.

Irrcher, I., Aleyasin, H., Seifert, E.L., Hewitt, S.J., Chhabra, S., Phillips, M., Lutz, A.K., Rousseaux, M.W., Bevilacqua, L., Jahani-Asl, A*., et al.* (2010). Loss of the Parkinson's disease-linked gene DJ-1 perturbs mitochondrial dynamics. Human molecular genetics *19*, 3734-3746.

Issazadeh, S., Mustafa, M., Ljungdahl, A., Hojeberg, B., Dagerlind, A., Elde, R., and Olsson, T. (1995). Interferon gamma, interleukin 4 and transforming growth factor beta in experimental autoimmune encephalomyelitis in Lewis rats: dynamics of cellular mRNA expression in the central nervous system and lymphoid cells. Journal of neuroscience research *40*, 579-590.

Iyer, S.P., Akimoto, Y., and Hart, G.W. (2003). Identification and cloning of a novel family of coiled-coil domain proteins that interact with O-GlcNAc transferase. The Journal of biological chemistry *278*, 5399-5409.

Jacobsen, C.O., and Farbu, E. (2014). MRI evaluation of grey matter atrophy and disease course in multiple sclerosis: an overview of current knowledge. Acta Neurol Scand Suppl, 32-36.

Jiang, H., Zhang, S.I., and Pernis, B. (1992). Role of CD8+ T cells in murine experimental allergic encephalomyelitis. Science *256*, 1213-1215.

Jiang, Z., Jiang, J.X., and Zhang, G.X. (2014). Macrophages: A double-edged sword in experimental autoimmune encephalomyelitis. Immunol Lett *160*, 17-22.

Jones, J.L., and Coles, A.J. (2014). Mode of action and clinical studies with alemtuzumab. Exp Neurol.

Kakalacheva, K., and Lunemann, J.D. (2011). Environmental triggers of multiple sclerosis. FEBS letters *585*, 3724-3729.

Kanaan, N.M., Morfini, G.A., LaPointe, N.E., Pigino, G.F., Patterson, K.R., Song, Y., Andreadis, A., Fu, Y., Brady, S.T., and Binder, L.I. (2011). Pathogenic forms of tau inhibit kinesin-dependent axonal transport through a mechanism involving activation of axonal phosphotransferases. The Journal of neuroscience : the official journal of the Society for Neuroscience *31*, 9858-9868.

Kang, J.S., Tian, J.H., Pan, P.Y., Zald, P., Li, C., Deng, C., and Sheng, Z.H. (2008). Docking of axonal mitochondria by syntaphilin controls their mobility and affects short-term facilitation. Cell *132*, 137-148.

Kapitein, L.C., Schlager, M.A., Kuijpers, M., Wulf, P.S., van Spronsen, M., MacKintosh, F.C., and Hoogenraad, C.C. (2010). Mixed microtubules steer dynein-driven cargo transport into dendrites. Current biology : CB *20*, 290-299.

Kappos, L., Freedman, M.S., Polman, C.H., Edan, G., Hartung, H.P., Miller, D.H., Montalban, X., Barkhof, F., Radu, E.W., Bauer, L.*, et al.* (2007). Effect of early versus delayed interferon beta-1b treatment on disability after a first clinical event suggestive of multiple sclerosis: a 3-year follow-up analysis of the BENEFIT study. Lancet *370*, 389-397.

Kappos, L., Traboulsee, A., Constantinescu, C., Eralinna, J.P., Forrestal, F., Jongen, P., Pollard, J., Sandberg-Wollheim, M., Sindic, C., Stubinski, B.*, et al.* (2006). Long-term subcutaneous interferon beta-1a therapy in patients with relapsing-remitting MS. Neurology *67*, 944-953.

Karki, S., and Holzbaur, E.L. (1999). Cytoplasmic dynein and dynactin in cell division and intracellular transport. Current opinion in cell biology *11*, 45-53.

Khan, O., Rieckmann, P., Boyko, A., Selmaj, K., and Zivadinov, R. (2013). Three times weekly glatiramer acetate in relapsing-remitting multiple sclerosis. Annals of neurology *73*, 705-713.

Kim, J.Y., Shen, S., Dietz, K., He, Y., Howell, O., Reynolds, R., and Casaccia, P. (2010). HDAC1 nuclear export induced by pathological conditions is essential for the onset of axonal damage. Nature neuroscience *13*, 180-189.

Kiryu-Seo, S., Ohno, N., Kidd, G.J., Komuro, H., and Trapp, B.D. (2010). Demyelination increases axonal stationary mitochondrial size and the speed of axonal mitochondrial transport. The Journal of neuroscience : the official journal of the Society for Neuroscience *30*, 6658-6666.

Kitada, T., Asakawa, S., Hattori, N., Matsumine, H., Yamamura, Y., Minoshima, S., Yokochi, M., Mizuno, Y., and Shimizu, N. (1998). Mutations in the parkin gene cause autosomal recessive juvenile parkinsonism. Nature *392*, 605-608.

Korn, T. (2008). Pathophysiology of multiple sclerosis. Journal of neurology *255 Suppl 6*, 2-6.

Korn, T., Bettelli, E., Gao, W., Awasthi, A., Jager, A., Strom, T.B., Oukka, M., and Kuchroo, V.K. (2007a). IL-21 initiates an alternative pathway to induce proinflammatory T(H)17 cells. Nature *448*, 484-487.

Korn, T., Reddy, J., Gao, W., Bettelli, E., Awasthi, A., Petersen, T.R., Backstrom, B.T., Sobel, R.A., Wucherpfennig, K.W., Strom, T.B.*, et al.* (2007b). Myelin-specific regulatory T cells accumulate in the CNS but fail to control autoimmune inflammation. Nature medicine *13*, 423-431.

Kornek, B., Storch, M.K., Bauer, J., Djamshidian, A., Weissert, R., Wallstroem, E., Stefferl, A., Zimprich, F., Olsson, T., Linington, C.*, et al.* (2001). Distribution of a calcium channel subunit in dystrophic axons in multiple sclerosis and experimental autoimmune encephalomyelitis. Brain : a journal of neurology *124*, 1114-1124.

Kreutzer, M., Seehusen, F., Kreutzer, R., Pringproa, K., Kummerfeld, M., Claus, P., Deschl, U., Kalkul, A., Beineke, A., Baumgartner, W.*, et al.* (2012). Axonopathy is associated with complex axonal transport defects in a model of multiple sclerosis. Brain Pathol *22*, 454-471.

Krishnamoorthy, G., Lassmann, H., Wekerle, H., and Holz, A. (2006). Spontaneous opticospinal encephalomyelitis in a double-transgenic mouse model of autoimmune T cell/B cell cooperation. J Clin Invest *116*, 2385-2392.

Krumbholz, M., Derfuss, T., Hohlfeld, R., and Meinl, E. (2012). B cells and antibodies in multiple sclerosis pathogenesis and therapy. Nature reviews Neurology *8*, 613-623.

Kuhlmann, T., Lingfeld, G., Bitsch, A., Schuchardt, J., and Bruck, W. (2002). Acute axonal damage in multiple sclerosis is most extensive in early disease stages and decreases over time. Brain : a journal of neurology *125*, 2202-2212.

Kural, C., Kim, H., Syed, S., Goshima, G., Gelfand, V.I., and Selvin, P.R. (2005). Kinesin and dynein move a peroxisome in vivo: a tug-of-war or coordinated movement? Science *308*, 1469-1472.

LaMonte, B.H., Wallace, K.E., Holloway, B.A., Shelly, S.S., Ascano, J., Tokito, M., Van Winkle, T., Howland, D.S., and Holzbaur, E.L. (2002). Disruption of dynein/dynactin inhibits axonal transport in motor neurons causing late-onset progressive degeneration. Neuron *34*, 715-727.

Langford, G.M. (1995). Actin- and microtubule-dependent organelle motors: interrelationships between the two motility systems. Current opinion in cell biology *7*, 82-88.

Lao, G., Scheuss, V., Gerwin, C.M., Su, Q., Mochida, S., Rettig, J., and Sheng, Z.H. (2000). Syntaphilin: a syntaxin-1 clamp that controls SNARE assembly. Neuron *25*, 191-201.

Lazarov, O., Morfini, G.A., Pigino, G., Gadadhar, A., Chen, X., Robinson, J., Ho, H., Brady, S.T., and Sisodia, S.S. (2007). Impairments in fast axonal transport and motor neuron deficits in transgenic mice expressing familial Alzheimer's disease-linked mutant presenilin 1. The Journal of neuroscience : the official journal of the Society for Neuroscience *27*, 7011-7020.

Le Corre, S., Klafki, H.W., Plesnila, N., Hubinger, G., Obermeier, A., Sahagun, H., Monse, B., Seneci, P., Lewis, J., Eriksen, J*., et al.* (2006). An inhibitor of tau hyperphosphorylation prevents severe motor impairments in tau transgenic mice. Proceedings of the National Academy of Sciences of the United States of America *103*, 9673-9678.

Lee, W.C., Yoshihara, M., and Littleton, J.T. (2004). Cytoplasmic aggregates trap polyglutamine-containing proteins and block axonal transport in a Drosophila model of Huntington's disease. Proceedings of the National Academy of Sciences of the United States of America *101*, 3224-3229.

Lees, A.J., Hardy, J., and Revesz, T. (2009). Parkinson's disease. Lancet *373*, 2055-2066.

Levin, L.I., Munger, K.L., O'Reilly, E.J., Falk, K.I., and Ascherio, A. (2010). Primary infection with the Epstein-Barr virus and risk of multiple sclerosis. Annals of neurology *67*, 824-830.

Li, Z., Okamoto, K., Hayashi, Y., and Sheng, M. (2004). The importance of dendritic mitochondria in the morphogenesis and plasticity of spines and synapses. Cell *119*, 873-887.

Liao, G., and Gundersen, G.G. (1998). Kinesin is a candidate for cross-bridging microtubules and intermediate filaments. Selective binding of kinesin to detyrosinated tubulin and vimentin. The Journal of biological chemistry *273*, 9797-9803.

Liblau, R.S., Gonzalez-Dunia, D., Wiendl, H., and Zipp, F. (2013). Neurons as targets for T cells in the nervous system. Trends in neurosciences *36*, 315-324.

Ligon, L.A., and Steward, O. (2000). Role of microtubules and actin filaments in the movement of mitochondria in the axons and dendrites of cultured hippocampal neurons. The Journal of comparative neurology *427*, 351-361.

Lin, R.F., Lin, T.S., Tilton, R.G., and Cross, A.H. (1993). Nitric oxide localized to spinal cords of mice with experimental allergic encephalomyelitis: an electron paramagnetic resonance study. The Journal of experimental medicine *178*, 643-648.

Linker, R.A., Lee, D.H., Ryan, S., van Dam, A.M., Conrad, R., Bista, P., Zeng, W., Hronowsky, X., Buko, A., Chollate, S*., et al.* (2011). Fumaric acid esters exert neuroprotective effects in neuroinflammation via activation of the Nrf2 antioxidant pathway. Brain : a journal of neurology *134*, 678-692.

Liu, C., Li, Y., Yu, J., Feng, L., Hou, S., Liu, Y., Guo, M., Xie, Y., Meng, J., Zhang, H*., et al.* (2013). Targeting the shift from M1 to M2 macrophages in experimental autoimmune encephalomyelitis mice treated with fasudil. PloS one *8*, e54841.

Liu, Y., Teige, I., Birnir, B., and Issazadeh-Navikas, S. (2006). Neuron-mediated generation of regulatory T cells from encephalitogenic T cells suppresses EAE. Nature medicine *12*, 518-525.

Lo, A.C., Saab, C.Y., Black, J.A., and Waxman, S.G. (2003). Phenytoin protects spinal cord axons and preserves axonal conduction and neurological function in a model of neuroinflammation in vivo. Journal of neurophysiology *90*, 3566-3571.

Lu, F., Selak, M., O'Connor, J., Croul, S., Lorenzana, C., Butunoi, C., and Kalman, B. (2000). Oxidative damage to mitochondrial DNA and activity of mitochondrial enzymes in chronic active lesions of multiple sclerosis. Journal of the neurological sciences *177*, 95-103.

Lucchinetti, C., Bruck, W., Parisi, J., Scheithauer, B., Rodriguez, M., and Lassmann, H. (2000). Heterogeneity of multiple sclerosis lesions: implications for the pathogenesis of demyelination. Annals of neurology *47*, 707-717.

Lunemann, J.D., Jelcic, I., Roberts, S., Lutterotti, A., Tackenberg, B., Martin, R., and Munz, C. (2008). EBNA1-specific T cells from patients with multiple sclerosis cross react with myelin antigens and co-produce IFN-gamma and IL-2. The Journal of experimental medicine *205*, 1763-1773.

Ma, H., Cai, Q., Lu, W., Sheng, Z.H., and Mochida, S. (2009). KIF5B motor adaptor syntabulin maintains synaptic transmission in sympathetic neurons. The Journal of neuroscience : the official journal of the Society for Neuroscience *29*, 13019-13029.

Macaskill, A.F., Rinholm, J.E., Twelvetrees, A.E., Arancibia-Carcamo, I.L., Muir, J., Fransson, A., Aspenstrom, P., Attwell, D., and Kittler, J.T. (2009). Miro1 is a calcium sensor for glutamate receptor-dependent localization of mitochondria at synapses. Neuron *61*, 541-555.

Mahad, D., Ziabreva, I., Lassmann, H., and Turnbull, D. (2008). Mitochondrial defects in acute multiple sclerosis lesions. Brain : a journal of neurology *131*, 1722-1735.

Mahad, D.J., Ziabreva, I., Campbell, G., Lax, N., White, K., Hanson, P.S., Lassmann, H., and Turnbull, D.M. (2009). Mitochondrial changes within axons in multiple sclerosis. Brain : a journal of neurology *132*, 1161-1174.

Mandelkow, E.M., Thies, E., Trinczek, B., Biernat, J., and Mandelkow, E. (2004). MARK/PAR1 kinase is a regulator of microtubule-dependent transport in axons. The Journal of cell biology *167*, 99-110.

Marinkovic, P., Reuter, M.S., Brill, M.S., Godinho, L., Kerschensteiner, M., and Misgeld, T. (2012). Axonal transport deficits and degeneration can evolve independently in mouse models of amyotrophic lateral sclerosis. Proceedings of the National Academy of Sciences of the United States of America *109*, 4296-4301.

Marriott, J.J., Miyasaki, J.M., Gronseth, G., and O'Connor, P.W. (2010). Evidence Report: The efficacy and safety of mitoxantrone (Novantrone) in the treatment of multiple sclerosis: Report of the Therapeutics and Technology Assessment Subcommittee of the American Academy of Neurology. Neurology *74*, 1463-1470.

Marson, A., Kretschmer, K., Frampton, G.M., Jacobsen, E.S., Polansky, J.K., MacIsaac, K.D., Levine, S.S., Fraenkel, E., von Boehmer, H., and Young, R.A. (2007). Foxp3 occupancy and regulation of key target genes during T-cell stimulation. Nature *445*, 931-935.

Martin, M., Iyadurai, S.J., Gassman, A., Gindhart, J.G., Jr., Hays, T.S., and Saxton, W.M. (1999). Cytoplasmic dynein, the dynactin complex, and kinesin are interdependent and essential for fast axonal transport. Molecular biology of the cell *10*, 3717-3728.

Martinez, F.O., Sica, A., Mantovani, A., and Locati, M. (2008). Macrophage activation and polarization. Frontiers in bioscience : a journal and virtual library *13*, 453-461.

Mathey, E.K., Derfuss, T., Storch, M.K., Williams, K.R., Hales, K., Woolley, D.R., Al-Hayani, A., Davies, S.N., Rasband, M.N., Olsson, T.*, et al.* (2007). Neurofascin as a novel target for autoantibody-mediated axonal injury. The Journal of experimental medicine *204*, 2363-2372.

Matthews, P.M., Pioro, E., Narayanan, S., De Stefano, N., Fu, L., Francis, G., Antel, J., Wolfson, C., and Arnold, D.L. (1996). Assessment of lesion pathology in multiple sclerosis using quantitative MRI morphometry and magnetic resonance spectroscopy. Brain : a journal of neurology *119 (Pt 3)*, 715-722.

May, E., Asadullah, K., and Zugel, U. (2004). Immunoregulation through 1,25-dihydroxyvitamin D3 and its analogs. Current drug targets Inflammation and allergy *3*, 377-393.

McGeachy, M.J., Bak-Jensen, K.S., Chen, Y., Tato, C.M., Blumenschein, W., McClanahan, T., and Cua, D.J. (2007). TGF-beta and IL-6 drive the production of IL-17 and IL-10 by T cells and restrain T(H)-17 cell-mediated pathology. Nat Immunol *8*, 1390-1397.

McGeachy, M.J., Stephens, L.A., and Anderton, S.M. (2005). Natural recovery and protection from autoimmune encephalomyelitis: contribution of CD4+CD25+ regulatory cells within the central nervous system. Journal of immunology *175*, 3025-3032.

Melov, S., Adlard, P.A., Morten, K., Johnson, F., Golden, T.R., Hinerfeld, D., Schilling, B., Mavros, C., Masters, C.L., Volitakis, I.*, et al.* (2007). Mitochondrial oxidative stress causes hyperphosphorylation of tau. PloS one *2*, e536.

Mikita, J., Dubourdieu-Cassagno, N., Deloire, M.S., Vekris, A., Biran, M., Raffard, G., Brochet, B., Canron, M.H., Franconi, J.M., Boiziau, C.*, et al.* (2011). Altered M1/M2 activation patterns of monocytes in severe relapsing experimental rat model of multiple sclerosis. Amelioration of clinical status by M2 activated monocyte administration. Multiple sclerosis *17*, 2-15.

Millecamps, S., and Julien, J.P. (2013). Axonal transport deficits and neurodegenerative diseases. Nature reviews Neuroscience *14*, 161-176.

Miller, D.M., Weinstock-Guttman, B., Bethoux, F., Lee, J.C., Beck, G., Block, V., Durelli, L., LaMantia, L., Barnes, D., Sellebjerg, F.*, et al.* (2000). A meta-analysis of methylprednisolone in recovery from multiple sclerosis exacerbations. Multiple sclerosis *6*, 267-273.

Miller, K.E., and Sheetz, M.P. (2004). Axonal mitochondrial transport and potential are correlated. Journal of cell science *117*, 2791-2804.

Minagar, A., and Alexander, J.S. (2003). Blood-brain barrier disruption in multiple sclerosis. Multiple sclerosis *9*, 540-549.

Miron, V.E., Boyd, A., Zhao, J.W., Yuen, T.J., Ruckh, J.M., Shadrach, J.L., van Wijngaarden, P., Wagers, A.J., Williams, A., Franklin, R.J.*, et al.* (2013). M2 microglia and macrophages drive oligodendrocyte differentiation during CNS remyelination. Nature neuroscience *16*, 1211-1218.

Misgeld, T., and Kerschensteiner, M. (2006). In vivo imaging of the diseased nervous system. Nature reviews Neuroscience *7*, 449-463.

Misgeld, T., Kerschensteiner, M., Bareyre, F.M., Burgess, R.W., and Lichtman, J.W. (2007). Imaging axonal transport of mitochondria in vivo. Nature methods *4*, 559-561.

Misko, A., Jiang, S., Wegorzewska, I., Milbrandt, J., and Baloh, R.H. (2010). Mitofusin 2 is necessary for transport of axonal mitochondria and interacts with the Miro/Milton complex. The Journal of neuroscience : the official journal of the Society for Neuroscience *30*, 4232-4240.

Misko, A.L., Sasaki, Y., Tuck, E., Milbrandt, J., and Baloh, R.H. (2012). Mitofusin2 mutations disrupt axonal mitochondrial positioning and promote axon degeneration. The Journal of neuroscience : the official journal of the Society for Neuroscience *32*, 4145-4155.

Molnarfi, N., Schulze-Topphoff, U., Weber, M.S., Patarroyo, J.C., Prod'homme, T., Varrin-Doyer, M., Shetty, A., Linington, C., Slavin, A.J., Hidalgo, J*., et al.* (2013). MHC class II-dependent B cell APC function is required for induction of CNS autoimmunity independent of myelin-specific antibodies. The Journal of experimental medicine *210*, 2921-2937.

Mondragon-Rodriguez, S., Perry, G., Zhu, X., Moreira, P.I., Acevedo-Aquino, M.C., and Williams, S. (2013). Phosphorylation of tau protein as the link between oxidative stress, mitochondrial dysfunction, and connectivity failure: implications for Alzheimer's disease. Oxid Med Cell Longev *2013*, 940603.

Morel, M., Authelet, M., Dedecker, R., and Brion, J.P. (2010). Glycogen synthase kinase-3beta and the p25 activator of cyclin dependent kinase 5 increase pausing of mitochondria in neurons. Neuroscience *167*, 1044-1056.

Morfini, G., Pigino, G., Opalach, K., Serulle, Y., Moreira, J.E., Sugimori, M., Llinas, R.R., and Brady, S.T. (2007). 1-Methyl-4-phenylpyridinium affects fast axonal transport by activation of caspase and protein kinase C. Proceedings of the National Academy of Sciences of the United States of America *104*, 2442-2447.

Morfini, G., Pigino, G., Szebenyi, G., You, Y., Pollema, S., and Brady, S.T. (2006). JNK mediates pathogenic effects of polyglutamine-expanded androgen receptor on fast axonal transport. Nature neuroscience *9*, 907-916.

Morfini, G., Szebenyi, G., Elluru, R., Ratner, N., and Brady, S.T. (2002). Glycogen synthase kinase 3 phosphorylates kinesin light chains and negatively regulates kinesin-based motility. The EMBO journal *21*, 281-293.

Morfini, G.A., You, Y.M., Pollema, S.L., Kaminska, A., Liu, K., Yoshioka, K., Bjorkblom, B., Coffey, E.T., Bagnato, C., Han, D*., et al.* (2009). Pathogenic huntingtin inhibits fast axonal transport by activating JNK3 and phosphorylating kinesin. Nature neuroscience *12*, 864-871.

Morris, R.L., and Hollenbeck, P.J. (1993). The regulation of bidirectional mitochondrial transport is coordinated with axonal outgrowth. Journal of cell science *104 (Pt 3)*, 917-927.

Morris, R.L., and Hollenbeck, P.J. (1995). Axonal transport of mitochondria along microtubules and F-actin in living vertebrate neurons. The Journal of cell biology *131*, 1315-1326.

Mosmann, T.R., Cherwinski, H., Bond, M.W., Giedlin, M.A., and Coffman, R.L. (1986). Two types of murine helper T cell clone. I. Definition according to profiles of lymphokine activities and secreted proteins. Journal of immunology *136*, 2348-2357.

Nakagawa, T., Tanaka, Y., Matsuoka, E., Kondo, S., Okada, Y., Noda, Y., Kanai, Y., and Hirokawa, N. (1997). Identification and classification of 16 new kinesin superfamily (KIF) proteins in mouse genome. Proceedings of the National Academy of Sciences of the United States of America *94*, 9654-9659.

Narendra, D.P., Jin, S.M., Tanaka, A., Suen, D.F., Gautier, C.A., Shen, J., Cookson, M.R., and Youle, R.J. (2010). PINK1 is selectively stabilized on impaired mitochondria to activate Parkin. PLoS biology *8*, e1000298.

Narendra, D.P., and Youle, R.J. (2011). Targeting mitochondrial dysfunction: role for PINK1 and Parkin in mitochondrial quality control. Antioxidants & redox signaling *14*, 1929-1938.

Nikic, I., Merkler, D., Sorbara, C., Brinkoetter, M., Kreutzfeldt, M., Bareyre, F.M., Bruck, W., Bishop, D., Misgeld, T., and Kerschensteiner, M. (2011). A reversible form of axon damage in experimental autoimmune encephalomyelitis and multiple sclerosis. Nature medicine *17*, 495-499.

Nitsch, R., Pohl, E.E., Smorodchenko, A., Infante-Duarte, C., Aktas, O., and Zipp, F. (2004). Direct impact of T cells on neurons revealed by two-photon microscopy in living brain tissue. The Journal of neuroscience : the official journal of the Society for Neuroscience *24*, 2458-2464.

Noseworthy, J.H., Lucchinetti, C., Rodriguez, M., and Weinshenker, B.G. (2000). Multiple sclerosis. The New England journal of medicine *343*, 938-952.

O'Connor, P., Wolinsky, J.S., Confavreux, C., Comi, G., Kappos, L., Olsson, T.P., Benzerdjeb, H., Truffinet, P., Wang, L., Miller, A.*, et al.* (2011). Randomized trial of oral teriflunomide for relapsing multiple sclerosis. The New England journal of medicine *365*, 1293-1303.

Ohno, N., Kidd, G.J., Mahad, D., Kiryu-Seo, S., Avishai, A., Komuro, H., and Trapp, B.D. (2011). Myelination and axonal electrical activity modulate the distribution and motility of mitochondria at CNS nodes of Ranvier. The Journal of neuroscience : the official journal of the Society for Neuroscience *31*, 7249-7258.

Oksenberg, J.R., Panzara, M.A., Begovich, A.B., Mitchell, D., Erlich, H.A., Murray, R.S., Shimonkevitz, R., Sherritt, M., Rothbard, J., Bernard, C.C.*, et al.* (1993). Selection for T-cell receptor V beta-D beta-J beta gene rearrangements with specificity for a myelin basic protein peptide in brain lesions of multiple sclerosis. Nature *362*, 68-70.

Oreja-Guevara, C., Rovaris, M., Iannucci, G., Valsasina, P., Caputo, D., Cavarretta, R., Sormani, M.P., Ferrante, P., Comi, G., and Filippi, M. (2005). Progressive gray matter damage in patients with relapsing-remitting multiple sclerosis: a longitudinal diffusion tensor magnetic resonance imaging study. Archives of neurology *62*, 578-584.

Orr, H.T., and Zoghbi, H.Y. (2007). Trinucleotide repeat disorders. Annual review of neuroscience *30*, 575-621.

Ousman, S.S., and Kubes, P. (2012). Immune surveillance in the central nervous system. Nature neuroscience *15*, 1096-1101.

Pathak, D., Sepp, K.J., and Hollenbeck, P.J. (2010). Evidence that myosin activity opposes microtubule-based axonal transport of mitochondria. The Journal of neuroscience : the official journal of the Society for Neuroscience *30*, 8984-8992.

Pelletier, D., and Hafler, D.A. (2012). Fingolimod for multiple sclerosis. The New England journal of medicine *366*, 339-347.

Petermann, F., Rothhammer, V., Claussen, M.C., Haas, J.D., Blanco, L.R., Heink, S., Prinz, I., Hemmer, B., Kuchroo, V.K., Oukka, M.*, et al.* (2010). gammadelta T cells enhance autoimmunity by restraining regulatory T cell responses via an interleukin-23-dependent mechanism. Immunity *33*, 351-363.

Peterson, J.W., Bo, L., Mork, S., Chang, A., and Trapp, B.D. (2001). Transected neurites, apoptotic neurons, and reduced inflammation in cortical multiple sclerosis lesions. Annals of neurology *50*, 389-400.

Pierrot-Deseilligny, C., and Souberbielle, J.C. (2013). Contribution of vitamin D insufficiency to the pathogenesis of multiple sclerosis. Therapeutic advances in neurological disorders *6*, 81-116.

Pigino, G., Morfini, G., Pelsman, A., Mattson, M.P., Brady, S.T., and Busciglio, J. (2003). Alzheimer's presenilin 1 mutations impair kinesin-based axonal transport. The Journal of neuroscience : the official journal of the Society for Neuroscience *23*, 4499-4508.

Pitt, D., Werner, P., and Raine, C.S. (2000). Glutamate excitotoxicity in a model of multiple sclerosis. Nature medicine *6*, 67-70.

Pollinger, B., Krishnamoorthy, G., Berer, K., Lassmann, H., Bosl, M.R., Dunn, R., Domingues, H.S., Holz, A., Kurschus, F.C., and Wekerle, H. (2009). Spontaneous relapsing-remitting EAE in the SJL/J mouse: MOG-reactive transgenic T cells recruit endogenous MOG-specific B cells. The Journal of experimental medicine *206*, 1303-1316.

Porcheray, F., Viaud, S., Rimaniol, A.C., Leone, C., Samah, B., Dereuddre-Bosquet, N., Dormont, D., and Gras, G. (2005). Macrophage activation switching: an asset for the resolution of inflammation. Clinical and experimental immunology *142*, 481-489.

Purves, D., Augustine, G., Fitzpatrick, D., Katz, L.C., LaMantia, A.-S., and Williams, S.M., eds. (2001). Neuroscience, Second Edition, Second edn (Sunderland, Massachusetts, Sinauer Associates, Inc.).

Rahman, A., Friedman, D.S., and Goldstein, L.S. (1998). Two kinesin light chain genes in mice. Identification and characterization of the encoded proteins. The Journal of biological chemistry *273*, 15395-15403.

Raine, C.S., Mokhtarian, F., and McFarlin, D.E. (1984). Adoptively transferred chronic relapsing experimental autoimmune encephalomyelitis in the mouse. Neuropathologic analysis. Lab Invest *51*, 534-546.

Rakovic, A., Grunewald, A., Kottwitz, J., Bruggemann, N., Pramstaller, P.P., Lohmann, K., and Klein, C. (2011). Mutations in PINK1 and Parkin impair ubiquitination of Mitofusins in human fibroblasts. PloS one *6*, e16746.

Rangachari, M., and Kuchroo, V.K. (2013). Using EAE to better understand principles of immune function and autoimmune pathology. J Autoimmun *45*, 31-39.

Rapp, S., Saffrich, R., Anton, M., Jakle, U., Ansorge, W., Gorgas, K., and Just, W.W. (1996). Microtubule-based peroxisome movement. Journal of cell science *109 (Pt 4)*, 837-849.

Reed, N.A., Cai, D., Blasius, T.L., Jih, G.T., Meyhofer, E., Gaertig, J., and Verhey, K.J. (2006). Microtubule acetylation promotes kinesin-1 binding and transport. Current biology : CB *16*, 2166-2172.

Reichardt, H.M., Gold, R., and Luhder, F. (2006). Glucocorticoids in multiple sclerosis and experimental autoimmune encephalomyelitis. Expert review of neurotherapeutics *6*, 1657-1670.

Rejdak, K., Jackson, S., and Giovannoni, G. (2010). Multiple sclerosis: a practical overview for clinicians. British medical bulletin *95*, 79-104.

Rintoul, G.L., Filiano, A.J., Brocard, J.B., Kress, G.J., and Reynolds, I.J. (2003). Glutamate decreases mitochondrial size and movement in primary forebrain neurons. The Journal of neuroscience : the official journal of the Society for Neuroscience *23*, 7881-7888.

Rivera-Quinones, C., McGavern, D., Schmelzer, J.D., Hunter, S.F., Low, P.A., and Rodriguez, M. (1998). Absence of neurological deficits following extensive demyelination in a class I-deficient murine model of multiple sclerosis. Nature medicine *4*, 187-193.

Rivers, T.M., Sprunt, D.H., and Berry, G.P. (1933). Observations on Attempts to Produce Acute Disseminated Encephalomyelitis in Monkeys. The Journal of experimental medicine *58*, 39-53.

Roemer, S.F., Parisi, J.E., Lennon, V.A., Benarroch, E.E., Lassmann, H., Bruck, W., Mandler, R.N., Weinshenker, B.G., Pittock, S.J., Wingerchuk, D.M*., et al.* (2007). Pattern-specific loss of aquaporin-4 immunoreactivity distinguishes neuromyelitis optica from multiple sclerosis. Brain : a journal of neurology *130*, 1194-1205.

Romanelli, E., Sorbara, C.D., Nikic, I., Dagkalis, A., Misgeld, T., and Kerschensteiner, M. (2013). Cellular, subcellular and functional in vivo labeling of the spinal cord using vital dyes. Nature protocols *8*, 481-490.

Rui, Y., Tiwari, P., Xie, Z., and Zheng, J.Q. (2006). Acute impairment of mitochondrial trafficking by beta-amyloid peptides in hippocampal neurons. The Journal of neuroscience : the official journal of the Society for Neuroscience *26*, 10480-10487.

Saha, A.R., Hill, J., Utton, M.A., Asuni, A.A., Ackerley, S., Grierson, A.J., Miller, C.C., Davies, A.M., Buchman, V.L., Anderton, B.H.*, et al.* (2004). Parkinson's disease alpha-synuclein mutations exhibit defective axonal transport in cultured neurons. Journal of cell science *117*, 1017-1024.

Saotome, M., Safiulina, D., Szabadkai, G., Das, S., Fransson, A., Aspenstrom, P., Rizzuto, R., and Hajnoczky, G. (2008). Bidirectional Ca2+-dependent control of mitochondrial dynamics by the Miro GTPase. Proceedings of the National Academy of Sciences of the United States of America *105*, 20728-20733.

Schattling, B., Steinbach, K., Thies, E., Kruse, M., Menigoz, A., Ufer, F., Flockerzi, V., Bruck, W., Pongs, O., Vennekens, R.*, et al.* (2012). TRPM4 cation channel mediates axonal and neuronal degeneration in experimental autoimmune encephalomyelitis and multiple sclerosis. Nature medicine *18*, 1805-1811.

Schirmer, L., Antel, J.P., Bruck, W., and Stadelmann, C. (2011). Axonal loss and neurofilament phosphorylation changes accompany lesion development and clinical progression in multiple sclerosis. Brain Pathol *21*, 428-440.

Schnapp, B.J., and Reese, T.S. (1989). Dynein is the motor for retrograde axonal transport of organelles. Proceedings of the National Academy of Sciences of the United States of America *86*, 1548-1552.

Schneider, A., Araujo, G.W., Trajkovic, K., Herrmann, M.M., Merkler, D., Mandelkow, E.M., Weissert, R., and Simons, M. (2004). Hyperphosphorylation and aggregation of tau in experimental autoimmune encephalomyelitis. The Journal of biological chemistry *279*, 55833-55839.

Schwarz, T.L. (2013). Mitochondrial trafficking in neurons. Cold Spring Harbor perspectives in biology *5*.

Seitz, A., Kojima, H., Oiwa, K., Mandelkow, E.M., Song, Y.H., and Mandelkow, E. (2002). Single-molecule investigation of the interference between kinesin, tau and MAP2c. The EMBO journal *21*, 4896-4905.

Sheng, Z.H., and Cai, Q. (2012). Mitochondrial transport in neurons: impact on synaptic homeostasis and neurodegeneration. Nature reviews Neuroscience *13*, 77-93.

Siffrin, V., Radbruch, H., Glumm, R., Niesner, R., Paterka, M., Herz, J., Leuenberger, T., Lehmann, S.M., Luenstedt, S., Rinnenthal, J.L.*, et al.* (2010a). In vivo imaging of partially reversible th17 cell-induced neuronal dysfunction in the course of encephalomyelitis. Immunity *33*, 424-436.

Siffrin, V., Vogt, J., Radbruch, H., Nitsch, R., and Zipp, F. (2010b). Multiple sclerosis - candidate mechanisms underlying CNS atrophy. Trends in neurosciences *33*, 202-210.

Smith, J.J., and Aitchison, J.D. (2013). Peroxisomes take shape. Nature reviews Molecular cell biology *14*, 803-817.

Smith, K.J., Kapoor, R., Hall, S.M., and Davies, M. (2001). Electrically active axons degenerate when exposed to nitric oxide. Annals of neurology *49*, 470-476.

Smith, K.J., and Lassmann, H. (2002). The role of nitric oxide in multiple sclerosis. Lancet neurology *1*, 232-241.

Smith, T., Groom, A., Zhu, B., and Turski, L. (2000). Autoimmune encephalomyelitis ameliorated by AMPA antagonists. Nature medicine *6*, 62-66.

Sorbara, C., Misgeld, T., and Kerschensteiner, M. (2012). In vivo imaging of the diseased nervous system: an update. Current pharmaceutical design *18*, 4465-4470.

Speciale, S.G. (2002). MPTP: insights into parkinsonian neurodegeneration. Neurotoxicology and teratology *24*, 607-620.

Sriram, S., and Steiner, I. (2005). Experimental allergic encephalomyelitis: a misleading model of multiple sclerosis. Annals of neurology *58*, 939-945.

Srivastava, R., Aslam, M., Kalluri, S.R., Schirmer, L., Buck, D., Tackenberg, B., Rothhammer, V., Chan, A., Gold, R., Berthele, A.*, et al.* (2012). Potassium channel KIR4.1 as an immune target in multiple sclerosis. The New England journal of medicine *367*, 115-123.

Stagi, M., Gorlovoy, P., Larionov, S., Takahashi, K., and Neumann, H. (2006). Unloading kinesin transported cargoes from the tubulin track via the inflammatory c-Jun N-terminal kinase pathway. FASEB journal : official publication of the Federation of American Societies for Experimental Biology *20*, 2573-2575.

Stamer, K., Vogel, R., Thies, E., Mandelkow, E., and Mandelkow, E.M. (2002). Tau blocks traffic of organelles, neurofilaments, and APP vesicles in neurons and enhances oxidative stress. The Journal of cell biology *156*, 1051-1063.

Stefferl, A., Brehm, U., Storch, M., Lambracht-Washington, D., Bourquin, C., Wonigeit, K., Lassmann, H., and Linington, C. (1999). Myelin oligodendrocyte glycoprotein induces experimental autoimmune encephalomyelitis in the "resistant" Brown Norway rat: disease susceptibility is determined by MHC and MHC-linked effects on the B cell response. Journal of immunology *163*, 40-49.

Steinman, L., and Zamvil, S.S. (2006). How to successfully apply animal studies in experimental allergic encephalomyelitis to research on multiple sclerosis. Annals of neurology *60*, 12-21.

Stokin, G.B., Lillo, C., Falzone, T.L., Brusch, R.G., Rockenstein, E., Mount, S.L., Raman, R., Davies, P., Masliah, E., Williams, D.S.*, et al.* (2005). Axonopathy and transport deficits early in the pathogenesis of Alzheimer's disease. Science *307*, 1282-1288.

Storch, M.K., Piddlesden, S., Haltia, M., Iivanainen, M., Morgan, P., and Lassmann, H. (1998). Multiple sclerosis: in situ evidence for antibody- and complement-mediated demyelination. Annals of neurology *43*, 465-471.

Stowers, R.S., Megeath, L.J., Gorska-Andrzejak, J., Meinertzhagen, I.A., and Schwarz, T.L. (2002). Axonal transport of mitochondria to synapses depends on milton, a novel Drosophila protein. Neuron *36*, 1063-1077.

Stroissnigg, H., Trancikova, A., Descovich, L., Fuhrmann, J., Kutschera, W., Kostan, J., Meixner, A., Nothias, F., and Propst, F. (2007). S-nitrosylation of microtubule-associated protein 1B mediates nitric-oxide-induced axon retraction. Nature cell biology *9*, 1035-1045.

Stromnes, I.M., and Goverman, J.M. (2006). Active induction of experimental allergic encephalomyelitis. Nature protocols *1*, 1810-1819.

Stys, P.K., Waxman, S.G., and Ransom, B.R. (1992). Ionic mechanisms of anoxic injury in mammalian CNS white matter: role of Na+ channels and Na(+)-Ca2+ exchanger. The Journal of neuroscience : the official journal of the Society for Neuroscience *12*, 430-439.

Su, Q., Cai, Q., Gerwin, C., Smith, C.L., and Sheng, Z.H. (2004). Syntabulin is a microtubule-associated protein implicated in syntaxin transport in neurons. Nature cell biology *6*, 941-953.

Su, S.B., Silver, P.B., Grajewski, R.S., Agarwal, R.K., Tang, J., Chan, C.C., and Caspi, R.R. (2005). Essential role of the MyD88 pathway, but nonessential roles of TLRs 2, 4, and 9, in the adjuvant effect promoting Th1-mediated autoimmunity. Journal of immunology *175*, 6303-6310.

Sun, T., Qiao, H., Pan, P.Y., Chen, Y., and Sheng, Z.H. (2013). Motile Axonal Mitochondria Contribute to the Variability of Presynaptic Strength. Cell reports.

Tanaka, Y., Kanai, Y., Okada, Y., Nonaka, S., Takeda, S., Harada, A., and Hirokawa, N. (1998). Targeted disruption of mouse conventional kinesin heavy chain, kif5B, results in abnormal perinuclear clustering of mitochondria. Cell *93*, 1147-1158.

Teitelbaum, D., Meshorer, A., Hirshfeld, T., Arnon, R., and Sela, M. (1971). Suppression of experimental allergic encephalomyelitis by a synthetic polypeptide. European journal of immunology *1*, 242-248.

Teitelbaum, D., Webb, C., Meshorer, A., Arnon, R., and Sela, M. (1972). Protection against experimental allergic encephalomyelitis. Nature *240*, 564-566.

Toft-Hansen, H., Nuttall, R.K., Edwards, D.R., and Owens, T. (2004). Key metalloproteinases are expressed by specific cell types in experimental autoimmune encephalomyelitis. Journal of immunology *173*, 5209-5218.

Trapp, B.D., Peterson, J., Ransohoff, R.M., Rudick, R., Mork, S., and Bo, L. (1998). Axonal transection in the lesions of multiple sclerosis. The New England journal of medicine *338*, 278-285.

Trushina, E., Dyer, R.B., Badger, J.D., 2nd, Ure, D., Eide, L., Tran, D.D., Vrieze, B.T., Legendre-Guillemin, V., McPherson, P.S., Mandavilli, B.S.*, et al.* (2004). Mutant huntingtin impairs axonal trafficking in mammalian neurons in vivo and in vitro. Molecular and cellular biology *24*, 8195-8209.

Uehara, T., and Nishiya, T. (2011). Screening systems for the identification of S-nitrosylated proteins. Nitric oxide : biology and chemistry / official journal of the Nitric Oxide Society *25*, 108-111.

Vaisberg, E.A., Grissom, P.M., and McIntosh, J.R. (1996). Mammalian cells express three distinct dynein heavy chains that are localized to different cytoplasmic organelles. The Journal of cell biology *133*, 831-842.

Vale, R.D., Reese, T.S., and Sheetz, M.P. (1985). Identification of a novel force-generating protein, kinesin, involved in microtubule-based motility. Cell *42*, 39-50.

Valente, E.M., Abou-Sleiman, P.M., Caputo, V., Muqit, M.M., Harvey, K., Gispert, S., Ali, Z., Del Turco, D., Bentivoglio, A.R., Healy, D.G.*, et al.* (2004). Hereditary early-onset Parkinson's disease caused by mutations in PINK1. Science *304*, 1158-1160.

Valsasina, P., Benedetti, B., Rovaris, M., Sormani, M.P., Comi, G., and Filippi, M. (2005). Evidence for progressive gray matter loss in patients with relapsing-remitting MS. Neurology *65*, 1126-1128.

van Spronsen, M., Mikhaylova, M., Lipka, J., Schlager, M.A., van den Heuvel, D.J., Kuijpers, M., Wulf, P.S., Keijzer, N., Demmers, J., Kapitein, L.C.*, et al.* (2013). TRAK/Milton motor-adaptor proteins steer mitochondrial trafficking to axons and dendrites. Neuron *77*, 485-502.

Venters, H.D., Dantzer, R., and Kelley, K.W. (2000). A new concept in neurodegeneration: TNFalpha is a silencer of survival signals. Trends in neurosciences *23*, 175-180.

Verburg, J., and Hollenbeck, P.J. (2008). Mitochondrial membrane potential in axons increases with local nerve growth factor or semaphorin signaling. The Journal of neuroscience : the official journal of the Society for Neuroscience *28*, 8306-8315.

Vergo, S., Craner, M.J., Etzensperger, R., Attfield, K., Friese, M.A., Newcombe, J., Esiri, M., and Fugger, L. (2011). Acid-sensing ion channel 1 is involved in both axonal injury and demyelination in multiple sclerosis and its animal model. Brain : a journal of neurology *134*, 571-584.

Vershinin, M., Carter, B.C., Razafsky, D.S., King, S.J., and Gross, S.P. (2007). Multiple-motor based transport and its regulation by Tau. Proceedings of the National Academy of Sciences of the United States of America *104*, 87-92.

Viglietta, V., Baecher-Allan, C., Weiner, H.L., and Hafler, D.A. (2004). Loss of functional suppression by CD4+CD25+ regulatory T cells in patients with multiple sclerosis. The Journal of experimental medicine *199*, 971-979.

Wagner, O.I., Lifshitz, J., Janmey, P.A., Linden, M., McIntosh, T.K., and Leterrier, J.F. (2003). Mechanisms of mitochondria-neurofilament interactions. The Journal of neuroscience : the official journal of the Society for Neuroscience *23*, 9046-9058.

Wang, X., and Schwarz, T.L. (2009). The mechanism of Ca2+ -dependent regulation of kinesin-mediated mitochondrial motility. Cell *136*, 163-174.

Wang, X., Winter, D., Ashrafi, G., Schlehe, J., Wong, Y.L., Selkoe, D., Rice, S., Steen, J., LaVoie, M.J., and Schwarz, T.L. (2011). PINK1 and Parkin target Miro for phosphorylation and degradation to arrest mitochondrial motility. Cell *147*, 893-906.

Wang, Y., Liu, T., Wu, C., and Li, H. (2008). A strategy for direct identification of protein S-nitrosylation sites by quadrupole time-of-flight mass spectrometry. Journal of the American Society for Mass Spectrometry *19*, 1353-1360.

Warner, H.B., and Carp, R.I. (1981). Multiple sclerosis and Epstein-Barr virus. Lancet *2*, 1290.

Waterman-Storer, C.M., Karki, S.B., Kuznetsov, S.A., Tabb, J.S., Weiss, D.G., Langford, G.M., and Holzbaur, E.L. (1997). The interaction between cytoplasmic dynein and dynactin is required for fast axonal transport. Proceedings of the National Academy of Sciences of the United States of America *94*, 12180-12185.

Weber, M.S., Prod'homme, T., Youssef, S., Dunn, S.E., Rundle, C.D., Lee, L., Patarroyo, J.C., Stuve, O., Sobel, R.A., Steinman, L*., et al.* (2007). Type II monocytes modulate T cell-mediated central nervous system autoimmune disease. Nature medicine *13*, 935-943.

Wegner, C., Esiri, M.M., Chance, S.A., Palace, J., and Matthews, P.M. (2006). Neocortical neuronal, synaptic, and glial loss in multiple sclerosis. Neurology *67*, 960-967.

Weihofen, A., Thomas, K.J., Ostaszewski, B.L., Cookson, M.R., and Selkoe, D.J. (2009). Pink1 forms a multiprotein complex with Miro and Milton, linking Pink1 function to mitochondrial trafficking. Biochemistry *48*, 2045-2052.

Wells, A.L., Lin, A.W., Chen, L.Q., Safer, D., Cain, S.M., Hasson, T., Carragher, B.O., Milligan, R.A., and Sweeney, H.L. (1999). Myosin VI is an actin-based motor that moves backwards. Nature *401*, 505-508.

Werner, P., Pitt, D., and Raine, C.S. (2001). Multiple sclerosis: altered glutamate homeostasis in lesions correlates with oligodendrocyte and axonal damage. Annals of neurology *50*, 169-180.

Westermann, S., and Weber, K. (2003). Post-translational modifications regulate microtubule function. Nature reviews Molecular cell biology *4*, 938-947.

Wiemer, E.A., Wenzel, T., Deerinck, T.J., Ellisman, M.H., and Subramani, S. (1997). Visualization of the peroxisomal compartment in living mammalian cells: dynamic behavior and association with microtubules. The Journal of cell biology *136*, 71-80.

Wingerchuk, D.M., and Carter, J.L. (2014). Multiple sclerosis: current and emerging disease-modifying therapies and treatment strategies. Mayo Clin Proc *89*, 225-240.

Witte, M.E., Bo, L., Rodenburg, R.J., Belien, J.A., Musters, R., Hazes, T., Wintjes, L.T., Smeitink, J.A., Geurts, J.J., De Vries, H.E.*, et al.* (2009). Enhanced number and activity of mitochondria in multiple sclerosis lesions. J Pathol *219*, 193-204.

Wolff, A.M., Petersen, J.G., Nilsson-Tillgren, T., and Din, N. (1999). The open reading frame YAL048c affects the secretion of proteinase A in S. cerevisiae. Yeast *15*, 427-434.

Wolinsky, J.S., Narayana, P.A., and Fenstermacher, M.J. (1990). Proton magnetic resonance spectroscopy in multiple sclerosis. Neurology *40*, 1764-1769.

Wolinsky, J.S., Narayana, P.A., Nelson, F., Datta, S., O'Connor, P., Confavreux, C., Comi, G., Kappos, L., Olsson, T.P., Truffinet, P.*, et al.* (2013). Magnetic resonance imaging outcomes from a phase III trial of teriflunomide. Multiple sclerosis *19*, 1310-1319.

Wucherpfennig, K.W., Newcombe, J., Li, H., Keddy, C., Cuzner, M.L., and Hafler, D.A. (1992). Gamma delta T-cell receptor repertoire in acute multiple sclerosis lesions. Proceedings of the National Academy of Sciences of the United States of America *89*, 4588-4592.

Yednock, T.A., Cannon, C., Fritz, L.C., Sanchez-Madrid, F., Steinman, L., and Karin, N. (1992). Prevention of experimental autoimmune encephalomyelitis by antibodies against alpha 4 beta 1 integrin. Nature *356*, 63-66.

Yeo, T.W., De Jager, P.L., Gregory, S.G., Barcellos, L.F., Walton, A., Goris, A., Fenoglio, C., Ban, M., Taylor, C.J., Goodman, R.S.*, et al.* (2007). A second major histocompatibility complex susceptibility locus for multiple sclerosis. Annals of neurology *61*, 228-236.

Yi, M., Weaver, D., and Hajnoczky, G. (2004). Control of mitochondrial motility and distribution by the calcium signal: a homeostatic circuit. The Journal of cell biology *167*, 661-672.

Yuan, A., Kumar, A., Peterhoff, C., Duff, K., and Nixon, R.A. (2008). Axonal transport rates in vivo are unaffected by tau deletion or overexpression in mice. The Journal of neuroscience : the official journal of the Society for Neuroscience *28*, 1682-1687.

Zamvil, S., Nelson, P., Trotter, J., Mitchell, D., Knobler, R., Fritz, R., and Steinman, L. (1985). T-cell clones specific for myelin basic protein induce chronic relapsing paralysis and demyelination. Nature *317*, 355-358.

Zhang, B., Higuchi, M., Yoshiyama, Y., Ishihara, T., Forman, M.S., Martinez, D., Joyce, S., Trojanowski, J.Q., and Lee, V.M. (2004). Retarded axonal transport of R406W mutant tau in transgenic mice with a neurodegenerative tauopathy. The Journal of neuroscience : the official journal of the Society for Neuroscience *24*, 4657-4667.

Zhang, C.L., Ho, P.L., Kintner, D.B., Sun, D., and Chiu, S.Y. (2010). Activity-dependent regulation of mitochondrial motility by calcium and Na/K-ATPase at nodes of Ranvier of myelinated nerves. The Journal of neuroscience : the official journal of the Society for Neuroscience *30*, 3555-3566.

Zhang, G.X., Gran, B., Yu, S., Li, J., Siglienti, I., Chen, X., Kamoun, M., and Rostami, A. (2003). Induction of experimental autoimmune encephalomyelitis in IL-12 receptor-beta 2-deficient mice: IL-12 responsiveness is not required in the pathogenesis of inflammatory demyelination in the central nervous system. Journal of immunology *170*, 2153-2160.

Zhao, C., Takita, J., Tanaka, Y., Setou, M., Nakagawa, T., Takeda, S., Yang, H.W., Terada, S., Nakata, T., Takei, Y.*, et al.* (2001). Charcot-Marie-Tooth disease type 2A caused by mutation in a microtubule motor KIF1Bbeta. Cell *105*, 587-597.

Zuchner, S., Mersiyanova, I.V., Muglia, M., Bissar-Tadmouri, N., Rochelle, J., Dadali, E.L., Zappia, M., Nelis, E., Patitucci, A., Senderek, J.*, et al.* (2004). Mutations in the mitochondrial GTPase mitofusin 2 cause Charcot-Marie-Tooth neuropathy type 2A. Nature genetics *36*, 449-451.

8. List of Publications

Sorbara, C. D., Wagner, N.E., Ladwig, A., Nikic, I., Merkler, D., Kleele, T., Marinkovic, P., Godinho, L., Bareyre, F., Bishop, D., Misgeld, T. & Kerschensteiner, M. 2014. Pervasive axonal transport deficits in multiple sclerosis models. *Nat Neurosci,* Submitted, Manuscript no. NN-BC48910.

Williams, P. R., **Sorbara, C. D.,** Mahler, C. F., Schumacher, A., Griesbeck, O., Kerschensteiner, M. & Misgeld, T. 2014. A recoverable state of axon injury persists for several hours after spinal cord contusion *in vivo. Nat Commun,* In Revision, Manuscript no. NCOMMS-14-04240A.

Sorbara, C. D., Romanelli, E., Nikic, I., Dagkalis, A., Misgeld, T. & Kerschensteiner, M. 2013. Cellular, subcellular and functional in vivo labeling of the spinal cord using vital dyes. *Nat Protoc,* 8**,** 481-90.

Nikic, I., Merkler, D., **Sorbara, C**. **D.**, Brinkoetter, M., Kreutzfeldt, M., Bareyre, F. M., Bruck, W., Bishop, D., Misgeld, T. & Kerschensteiner, M. 2011. A reversible form of axon damage in experimental autoimmune encephalomyelitis and multiple sclerosis. *Nat Med,* 17**,** 495-9.

Sorbara, C., Misgeld, T. & Kerschensteiner, M. 2012. In vivo imaging of the diseased nervous system: an update. Curr Pharm Des, 18, 4465-70.

nature medicine

LETTERS

A reversible form of axon damage in experimental autoimmune encephalomyelitis and multiple sclerosis

Ivana Nikić[1], Doron Merkler[2,3], Catherine Sorbara[1], Mary Brinkoetter[4], Mario Kreutzfeldt[2,3], Florence M Bareyre[1], Wolfgang Brück[2], Derron Bishop[4], Thomas Misgeld[5–7] & Martin Kerschensteiner[1,7]

In multiple sclerosis, a common inflammatory disease of the central nervous system, immune-mediated axon damage is responsible for permanent neurological deficits[1,2]. How axon damage is initiated is not known. Here we use *in vivo* imaging to identify a previously undescribed variant of axon damage in a mouse model of multiple sclerosis. This process, termed 'focal axonal degeneration' (FAD), is characterized by sequential stages, beginning with focal swellings and progressing to axon fragmentation. Notably, most swollen axons persist unchanged for several days, and some recover spontaneously. Early stages of FAD can be observed in axons with intact myelin sheaths. Thus, contrary to the classical view[2–6], demyelination—a hallmark of multiple sclerosis—is not a prerequisite for axon damage. Instead, focal intra-axonal mitochondrial pathology is the earliest ultrastructural sign of damage, and it precedes changes in axon morphology. Molecular imaging and pharmacological experiments show that macrophage-derived reactive oxygen and nitrogen species (ROS and RNS) can trigger mitochondrial pathology and initiate FAD. Indeed, neutralization of ROS and RNS rescues axons that have already entered the degenerative process. Finally, axonal changes consistent with FAD can be detected in acute human multiple sclerosis lesions. In summary, our data suggest that inflammatory axon damage might be spontaneously reversible and thus a potential target for therapy.

In multiple sclerosis, axons are damaged after the invasion of immune cells. Many different mechanisms for immune-mediated axon injury have been proposed on the basis of *in vitro* and post-mortem observations[2–13], but how axons are permanently damaged *in vivo* remains unknown.

To address this question, we used *in vivo* imaging[14–17] to study axonal pathology in spinal experimental autoimmune encephalomyelitis (EAE) lesions, induced by immunizing mice with myelin oligodendrocyte glycoprotein (MOG). These lesions showed the pathological hallmarks of multiple sclerosis, including inflammation and demyelination (**Supplementary Fig. 1**). Axons in these lesions showed a spectrum of morphologies: normal appearance (stage 0), focal swellings (stage 1) or fragmentation (stage 2; **Fig. 1a–c**). To determine whether these morphological alterations represent sequential stages of axon damage, we continuously monitored single axons in *Thy1-GFP-S* and *Thy1-CFP-S* (GFP and cyan fluorescent protein (CFP) under control of the *Thy1* promoter, respectively) transgenic mice in which a subset of medium-to-large caliber axons is fluorescently labeled[14,18]. When imaged on the second or third day after EAE onset, the majority of stage 1 axons did not change over imaging periods of several hours (45 of 50 axons imaged over 1.5–8 h). In five instances, however, we could directly visualize changes associated with axon damage and identified the following characteristics (**Fig. 1d** and **Supplementary Video 1**). First, prior to disruption, swellings occur along the axon at one or more discrete sites. Second, the initial disruption of the axon often (three of five cases) occurs at putative nodes of Ranvier. Axonal disruption can start almost synchronously at several sites along the axon (four of five cases). Last, from the sites of disruption, axon fragmentation spreads slowly ($3.5 \pm 0.9\ \mu m\ min^{-1}$) in both directions. Once fragmentation halts, terminal bulbs form on the proximal and distal axon stumps (average extent of axon loss: $248.9 \pm 80.5\ \mu m$, $n = 8$ axon ends). Taken together, these characteristics define FAD, a new variant of axon loss that is initiated at spatially restricted axonal swellings inside inflammatory foci.

FAD is characterized by the existence of relatively stable focal swellings of axons (stage 1). We investigated whether swollen axons invariably progress to fragmentation by repetitively imaging individual stage 1 axons every 24 h over 3 d starting 2 d after EAE onset. Our results show that during this time period, stage 1 axons can degenerate, persist or even recover (**Fig. 1e**). We determined the conversion rates between the FAD stages by imaging a large population of axons in *Thy1-YFP-16* (yellow fluorescent protein (YFP) under control of the *Thy1* promoter) transgenic mice, with a dense labeling pattern (**Supplementary Methods**; **Supplementary Videos 2** and **3**). In 13 mice, during 1,084 'axon hours' ($n = 230$ axons, imaged on average for ~4.7 h), we observed 15 instances of progression (five stage 0→1 and ten stage 1→2 conversions), as well as three instances of recovery (stage 1→0 conversions; **Fig. 1f** and **Supplementary Video 4**). All progressive events followed the characteristic sequence of FAD,

[1]Research Unit Therapy Development, Institute of Clinical Neuroimmunology, Ludwig-Maximilians-Universität München, Munich, Germany. [2]Institute of Neuropathology, Georg-August University, Göttingen, Germany. [3]Division of Clinical Pathology, Geneva University Hospital and Department of Pathology and Immunology, University of Geneva, Switzerland. [4]Department of Physiology, Indiana University School of Medicine-Muncie, Muncie, Indiana, USA. [5]Chair for Biomolecular Sensors, Center for Integrated Protein Sciences (Munich) at the Institute of Neuroscience, Technische Universität München, Munich, Germany. [6]Institute for Advanced Study, Technische Universität München, Munich, Germany. [7]These authors contributed equally to this work. Correspondence should be addressed to M. Kerschensteiner (martin.kerschensteiner@med.uni-muenchen.de) or T.M. (thomas.misgeld@lrz.tu-muenchen.de).

Received 27 July 2010; accepted 7 February 2011; published online 27 March 2011; doi:10.1038/nm.2324

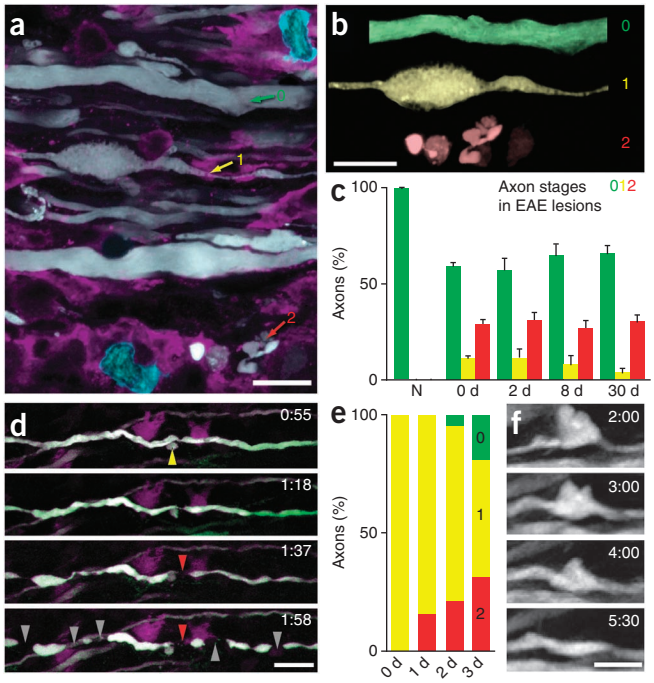

Figure 1 *In vivo* imaging of FAD. (**a**) Confocal projection showing axons (white), activated macrophages/microglia (magenta) and T cells (cyan) in an acute spinal EAE lesion. Some axons appear normal (stage 0), whereas others are swollen (1) or fragmented (2). (**b**) Pseudocolored axons isolated from those shown in **a**: normal appearing (0, green), swollen (1, yellow), and fragmented (2, red). (**c**) Frequency (in % ± s.e.m.) of axon stages in normal spinal cord (N) and in EAE lesions (0–30 d after EAE onset; differences at all EAE time points compared to control are significant, $P < 0.001$ to 0.05, one-tailed *t* test). (**d**) Multiphoton time-lapse images of a stage 1 axon (white) in EAE and activated macrophages/microglia (magenta). Time is shown as h:min; meningeal second harmonics (a scattering process) signal is green). The axon first breaks (red arrowhead) near a small swelling (yellow arrowhead) at a putative node of Ranvier before fragmenting (gray arrowheads). (**e**) Fate of stage 1 axons imaged 1–3 d after the peak of EAE (significant progression from 1–3 d, $P < 0.05$, chi-square test for trend). (**f**) Time-lapse images of recovering stage 1 axon (time is as shown in **d**). Scale bar in **a**,**b**, 10 µm; scale bar in **d**, 25 µm; scale bar in **f**, 10 µm.

with local swellings preceding fragmentation. The susceptibility of an axon to FAD depends both on intrinsic axonal properties and the extrinsic milieu. For example, axon diameter influences susceptibility. Large-caliber axons (diameter > 1.5 µm) show FAD progression as well as recovery (transition probability: 0.4% per h, stage 0→1; 2.6% per h, stage 1→2; 1.3% per h stage 1→0). In contrast, thin axons (<1.5 µm) showed higher rates of progression (2.4% per h, stage 0→1; 7.4% per h, stage 1→2). In addition, the age of lesions, and hence likely inflammatory activity, matters. Degeneration outweighs recovery at the peak of clinical symptoms (onset + 2 d; 8.1% per h, stage 1→2; 0% per h, stage 1→0), whereas this relation is reversed 1 d later (onset + 3 d; 0.6% per h, stage 1→2; 1.8% per h, stage 1→ 0; data not shown).

To identify subcellular changes that underlie axonal degeneration and recovery, we reconstructed stage 1 axons by serial-section transmission electron microscopy (ssTEM) after *in vivo* imaging

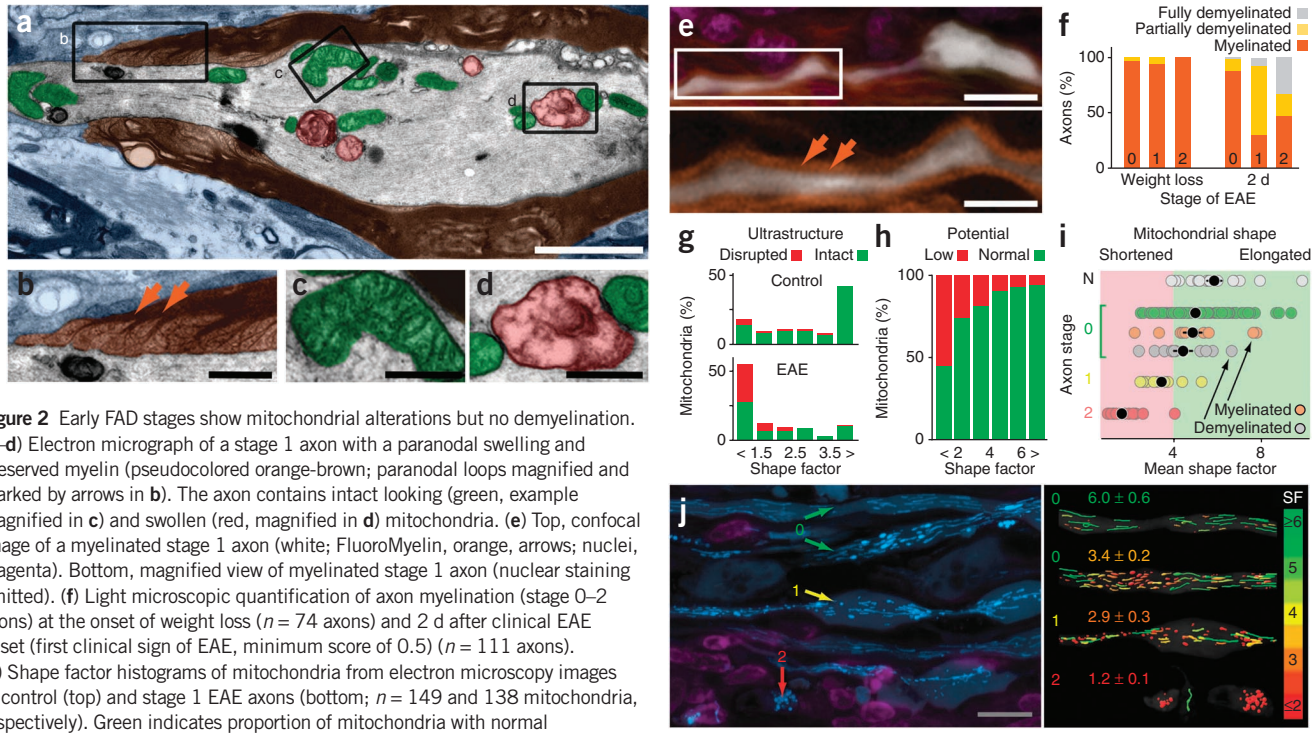

Figure 2 Early FAD stages show mitochondrial alterations but no demyelination. (**a**–**d**) Electron micrograph of a stage 1 axon with a paranodal swelling and preserved myelin (pseudocolored orange-brown; paranodal loops magnified and marked by arrows in **b**). The axon contains intact looking (green, example magnified in **c**) and swollen (red, magnified in **d**) mitochondria. (**e**) Top, confocal image of a myelinated stage 1 axon (white; FluoroMyelin, orange, arrows; nuclei, magenta). Bottom, magnified view of myelinated stage 1 axon (nuclear staining omitted). (**f**) Light microscopic quantification of axon myelination (stage 0–2 axons) at the onset of weight loss ($n = 74$ axons) and 2 d after clinical EAE onset (first clinical sign of EAE, minimum score of 0.5) ($n = 111$ axons). (**g**) Shape factor histograms of mitochondria from electron microscopy images of control (top) and stage 1 EAE axons (bottom; $n = 149$ and 138 mitochondria, respectively). Green indicates proportion of mitochondria with normal ultrastructure; red represents disrupted mitochondria. (**h**) Mitochondrial shape versus mitochondrial membrane potential in EAE lesions (green, normal; red, low (< mean – 2 s.d. of control), $n = 235$ mitochondria in four mice). (**i**) Confocal quantification of mean mitochondrial shape factor in axons from EAE and normal control (N) mice ($n = 23$–138 mitochondria per axon in stage 0 (green; myelination status was scored in additional stage 0 axons) and 1 (yellow); in stage 2 (red) all mitochondria were scored). (**j**) Left, confocal image of axons (gray) and their mitochondria (cyan) in EAE (nuclei, magenta). Right, shape of mitochondria (color coded, see scale at right) in axons at different stages of FAD selected from left panel. Stage and mean mitochondrial shape factor (SF ± s.e.m.) of the axon segment are indicated above each axon. Scale bar in **a**, 2 µm; scale bars in **b**–**d**, 0.5 µm; scale bar in **e** (top), 10 µm; scale bar in **e** (bottom), 5 µm; scale bar in **j** (left and right images), 10 µm.

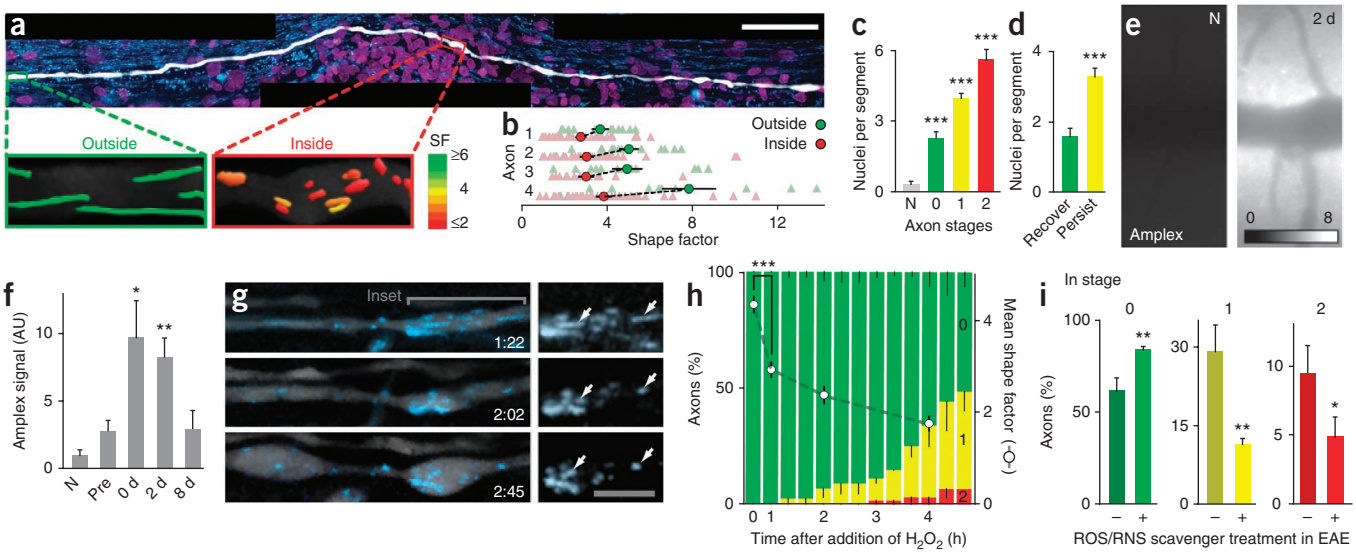

Figure 3 Activated macrophage/microglia-derived reactive species induce FAD. (**a**) Confocal reconstruction of an axon that courses through an EAE lesion (nuclei, magenta) in a mouse with sparse axon labeling (white) and dense labeling of axonal mitochondria (cyan). Enlarged areas below show color-coded (scale on right) shape of mitochondria in the labeled axon outside (left) and inside (right) the lesion. (**b**) Quantification of mitochondrial shape in different segments of longitudinally reconstructed axons (segments of each axon connected with dashed line, $n = 4$ axons) outside (green) and inside (red) of EAE lesions. Each triangle represents a mitochondrion, and circles indicate mean mitochondrial shape factor for the axon segment (± s.e.m.; mitochondria are significantly shorter inside versus outside; $P < 0.05$, paired t test). (**c**) Infiltration density (± s.e.m.) around control (N, gray) and EAE stage 0 (green), 1 (yellow) and 2 (red) axon segments ($n = 13$–83 segments; infiltration density is significantly increased in stage 0 vs. control axons, stage 1 vs. stage 0 axons and stage 2 vs. stage 1 axons; t test). (**d**) Cell density (± s.e.m.) around stage 1 axon segments that either recovered (green) or persisted in a swollen state (yellow) during *in vivo* imaging and were fixed afterward for analysis of cellular infiltration ($n = 60$ segments; density is significantly lower around recovered axons; t test). (**e**) *In vivo* measurement of H_2O_2 concentration (detected with Amplex) in the dorsal spinal cord of healthy (N, left) and EAE (2 d after onset) mice. (**f**) Quantification of H_2O_2 concentration (± s.e.m; $n = 3$–5 mice per time point; levels are significantly increased at 0 d and 2 d after EAE onset; t test). N, control; Pre, preclinical mice; d, days after EAE onset. (**g**) *In vivo* two-photon time-lapse of spinal axons (gray) and their mitochondria (cyan) after H_2O_2 application (330 mM) (time, h:min). Right, magnification of small cluster of mitochondria that swell over time (arrows). (**h**) Frequency of stage 0 (green), 1 (yellow) and 2 (red) axons before and up to 5 h after *in vivo* H_2O_2 application (100 mM; $n = 53$ axons). Superimposed is the change over time in mean mitochondrial shape (± s.e.m., $n = 15$ axons; t test). (**i**) Percentage (± s.e.m.) of EAE axons in different stages of FAD after ROS and RNS scavenger or vehicle treatment (starting at weight loss, analyzed by t test). (**j**) Fate of stage 1 axons after 2 d of ROS and RNS scavenger or vehicle treatment (started 2–3 d after EAE onset, $n = 22$–26 axons; chi-square test). Scale bar in **a**, 50 µm; scale bar in **e**, 250 µm (calibration bar); scale bar in **g**, 10 µm. $^*P < 0.05$; $^{**}P < 0.01$; $^{***}P < 0.001$.

(**Fig. 2a–d** and **Supplementary Video 5**). Unexpectedly, we found that stage 1 axons were still ensheathed by myelin (**Fig. 2b**). Confocal microscopy confirmed that a substantial proportion of axons in all stages of FAD retain myelin in acute lesions (**Fig. 2e,f**). Further, at the earliest stage of EAE (at the onset of weight loss; about 10–13 days post-immunization), before demyelination starts, axons in all stages of FAD are present (**Fig. 2f**).

A key ultrastructural characteristic of FAD stage 1 axons was the presence of dysmorphic, swollen mitochondria (**Fig. 2a,d,g**), which were absent in control axons (**Fig. 2g** and **Supplementary Fig. 2**). To relate the onset of mitochondrial alterations to axonal morphology, we induced EAE in double-transgenic mice with CFP-labeled axonal mitochondria[19] and YFP-labeled axoplasm (*Thy1-MitoCFP* × *Thy1-YFP-16*). We first confirmed that mitochondrial swelling is indeed a sign of mitochondrial dysfunction by simultaneous *in vivo* imaging of mitochondrial shape and mitochondrial membrane potential (**Fig. 2h**). Further analysis in fixed samples showed that mitochondrial swellings were absent in spinal axons from healthy control mice (mean shape factor or length/width ratio of ≥ 4; **Fig. 2i**), mice immunized with pertussis toxin alone and preclinical (6 days after immunization) EAE mice (data not shown). In contrast, in inflammatory lesions, already a proportion of normally shaped (stage 0) axons with intact myelin showed mitochondrial swelling (**Fig. 2i,j**).

To determine the spatial distribution of damaged mitochondria within individual axons, we reconstructed long segments of fluorescently labeled axons that traversed EAE lesions. Mitochondrial pathology was restricted to areas of immune infiltration (**Fig. 3a,b**). The notion that immune cells promote FAD was further supported by a correlation between FAD progression and local infiltration density (**Fig. 3c,d**). To investigate which immune cells might be responsible for inducing FAD, we followed the behavior of T cells and activated macrophages/microglia (labeled with GFP in *Cd2-GFP*[20] and *Cx3cr1*$^{GFP/+}$ mice[21], respectively) in apposition to axons (sparsely labeled with CFP in *Thy1-CFP-S* mice). In acute EAE lesions, primarily macrophages/microglia show prolonged periods of apposition to axons (**Supplementary Fig. 3** and **Supplementary Videos 6** and **7**).

Axon segments in EAE lesions can thus be exposed continuously to harmful mediators secreted by activated macrophages/microglia. To induce FAD, such mediators need to be able to diffuse through the myelin sheath and damage mitochondria. ROS and RNS fulfill these requirements and have been implicated in axon degeneration[9,22–24].

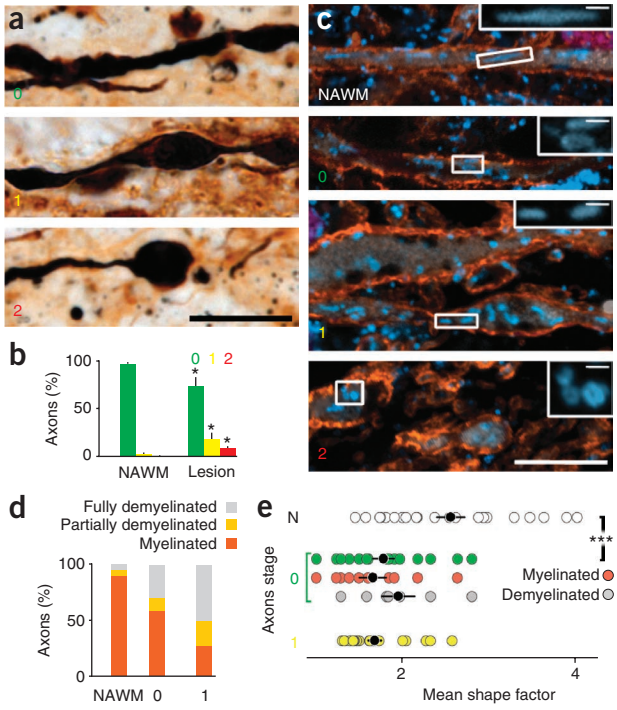

Figure 4 Axonal changes consistent with FAD are present in acute human multiple sclerosis lesions. (**a**) Representative axons in stages 0, 1 and 2 of FAD in an acute human multiple sclerosis lesion (Bielschowsky silver impregnation). (**b**) Prevalence of FAD stages in normal-appearing white matter (NAWM) and in acute multiple sclerosis lesions ($n = 3$ biopsies, > 450 axons per group; all stages are significantly different in lesion versus NAWM; one-tailed t test). (**c**) Confocal projections of an axon (top) that was located in NAWM around an active multiple sclerosis lesion, and examples of stage 0, 1 and 2 axons located inside the same lesion (quadruple immunostaining: axons, stained for neurofilament, white; myelin, stained for myelin basic protein, orange; nuclei, stained for NeuroTrace, magenta; mitochondria, stained for porin, cyan; mitochondria magnified in insets). (**d**) Myelination status of axons in NAWM and FAD stage 0 and 1 axons in multiple sclerosis lesions ($n = 17$–22 axons per group, from two to six biopsies). (**e**) Comparison of mean mitochondrial shape factors of axons in NAWM (N), and stage 0 and 1 multiple sclerosis axons (analyzed by t test). Scale bars in **a**,**c**, 10 μm; scale bars in **c** (insets), 1 μm. $^{*}P < 0.05$; $^{***}P < 0.001$.

In vivo imaging of hydrogen peroxide (H_2O_2) and nitric oxide (NO) indicators revealed increased ROS and RNS concentrations in acute EAE lesions (**Fig. 3e**,**f** and **Supplementary Fig. 4**). We then applied H_2O_2 (10–330 mM) or the NO donor spermine NONOate (10 mM) to the lumbar spinal cord of healthy *Thy1-MitoCFP* × *Thy1-YFP-16* mice (some of which were counterstained with a lipophilic dye, BODIPY). *In vivo* imaging revealed that application of either H_2O_2 (> 10 mM) or the NO donor is sufficient to induce the characteristic mitochondrial and axonal changes of FAD (**Fig. 3g**,**h**, **Supplementary Fig. 4** and **Supplementary Video 8**) in the absence of demyelination (data not shown). We then treated EAE mice with scavengers that reduced spinal ROS and RNS levels by 75% (± 6%) *in vivo* (data not shown). This treatment limited FAD progression (**Fig. 3i**) but did not affect the density of T cells or macrophages/microglia in acute EAE lesions (data not shown). To explore whether these scavengers promote recovery of axons in stage 1 of FAD, we imaged mice at the peak of EAE *in vivo* and identified axons with focal swellings (stage 1)(**Fig. 3j**). Repetitive *in vivo* imaging revealed that neutralization of ROS and RNS induced recovery in nearly 80% of treated axons (**Fig. 3j**).

To investigate the relevance of FAD to human multiple sclerosis, we analyzed biopsies of actively demyelinating multiple sclerosis lesions ($n = 6$; **Fig. 4** and **Supplementary Fig. 5**). Silver impregnation, as well as quadruple immunostaining of axons, myelin, mitochondria and cell infiltration, revealed morphological changes suggestive of axons undergoing FAD in multiple sclerosis (**Fig. 4a**–**c**). Notably, in human multiple sclerosis, as in EAE, a sizable proportion of swollen or fragmented axons are still wrapped in myelin (**Fig. 4c**,**d**). Further, as in mice, mitochondrial damage in human multiple sclerosis is restricted to the lesion area and is even observed in the absence of demyelination or changes in axon morphology (**Fig. 4c**,**e**).

Taken together, our findings provide a number of conclusions. First, we identify a new variant of axon loss, FAD, in inflammatory CNS lesions; it is characterized by a sequence of morphologically distinct stages. Reversibility, spatial restriction and speed distinguish FAD from other forms of axon loss in development and disease[25].

Second, demyelination does not seem to be a prerequisite for immune-mediated axon degeneration. Thus, inflammatory mediators (such as ROS or RNS) must be able to circumvent any protective barrier that myelin might represent[26], for example, by diffusing through membranes or by acting at the nodes of Ranvier[12,27]. This is in line with previous studies in animal models reporting transient axon injury[28] and virally induced axon loss[29] in the absence of primary demyelination.

Third, damage to mitochondria seems to be an early event in FAD that can contribute to axon degeneration, for example, by causing respiratory chain dysfunction[24], elevated intra-axonal calcium[5,6] and the release of proapoptotic mediators[30]. Indeed, induction of mitochondrial damage with the uncoupling agent CCCP is sufficient to cause the characteristic axonal and mitochondrial pathology of FAD in healthy mice (**Supplementary Fig. 4**). Our findings provide a mechanistic framework for recent histopathological studies that showed damage to neuronal mitochondria in acute and chronic stages of multiple sclerosis[31–33], and they suggest that neuroprotective strategies that target mitochondrial pathology might be effective not only in classical neurodegenerative disease but also in multiple sclerosis[34,35].

Fourth, ROS and RNS, primarily secreted by activated macrophages/microglia, can initiate the FAD process. Thus, ROS and RNS scavenging is a promising strategy to promote axonal recovery. However, given the pleiotropic actions of reactive species[23,36–38], strategies that neutralize specific ROS and/or RNS with high spatial and temporal precision seem necessary[39]. The results and techniques presented here may aid in the design of therapeutic strategies to limit axon damage in neuroinflammatory conditions.

METHODS

Methods and any associated references are available in the online version of the paper at http://www.nature.com/naturemedicine/.

Note: Supplementary information is available on the Nature Medicine website.

ACKNOWLEDGMENTS

We would like to thank B. Fiedler, G. Heitmann, M. Schedensack, A. Schmalz and S. Knecht for excellent technical assistance; D. Matzek for animal husbandry; A. Dagkalis for help with immunizations; M. Krumbholz for advice on statistical analysis; and R. Hohlfeld, H. Wekerle, J. Sanes, J. Lichtman, L. Godinho, D. Kerschensteiner, P. Williams, T. Dick, E. Meinl and K. Dornmair for discussions or critical reading of the manuscript. Work in M. Kerschensteiner's laboratory is financed through grants from the Deutsche Forschungsgemeinschaft (DFG; Emmy Noether Program and

Sonderforschungsbereich 571) and the 'Verein Therapieforschung für MS-Kranke e.V'. M. Kerschensteiner and W.B. are supported by a grant from the German Federal Ministry of Education and Research (Competence Network Multiple Sclerosis). T.M. is supported by the Institute for Advanced Study, Technische Universität München, by the Alexander von Humboldt Foundation and by the Center for Integrated Protein Science (Munich). D.M. and W.B. are supported by grants from the DFG (Sonderforschungsbereich Transregio 43). D.M. is supported by the Swiss National Science Foundation (PP00P3 128372). D.B. is supported by the US National Institutes of Health. This project was further financed by grants to M. Kerschensteiner and T.M. from the Dana Foundation and the Hertie Foundation, and by a grant from the Christopher and Dana Reeve Foundation to T.M. and D.B.

AUTHOR CONTRIBUTIONS

M. Kerschensteiner, T.M., D.B., D.M. and I.N. conceived the experiments. I.N. and C.S. did the imaging experiments. I.N., C.S., T.M. and M. Kerschensteiner did image analysis. M.B. and D.B. did and evaluated serial electron microscopy. I.N. and F.M.B. did therapy experiments. D.M., M. Kreutzfeldt and W.B. did histopathological evaluations of EAE and multiple sclerosis tissue. I.N., M. Kerschensteiner and T.M. wrote the paper.

COMPETING FINANCIAL INTERESTS

The authors declare no competing financial interests.

Published online at http://www.nature.com/naturemedicine/.
Reprints and permissions information is available online at http://npg.nature.com/reprintsandpermissions/.

1. Hauser, S.L. & Oksenberg, J.R. The neurobiology of multiple sclerosis: genes, inflammation, and neurodegeneration. *Neuron* **52**, 61–76 (2006).
2. Trapp, B.D. & Nave, K.A. Multiple sclerosis: an immune or neurodegenerative disorder? *Annu. Rev. Neurosci.* **31**, 247–269 (2008).
3. Trapp, B.D. *et al.* Axonal transection in the lesions of multiple sclerosis. *N. Engl. J. Med.* **338**, 278–285 (1998).
4. Lucchinetti, C. *et al.* Heterogeneity of multiple sclerosis lesions: implications for the pathogenesis of demyelination. *Ann. Neurol.* **47**, 707–17 (2000).
5. Trapp, B.D. & Stys, P.K. Virtual hypoxia and chronic necrosis of demyelinated axons in multiple sclerosis. *Lancet Neurol.* **8**, 280–291 (2009).
6. Waxman, S.G. Axonal conduction and injury in multiple sclerosis: the role of sodium channels. *Nat. Rev. Neurosci.* **7**, 932–941 (2006).
7. Pitt, D., Werner, P. & Raine, C.S. Glutamate excitotoxicity in a model of multiple sclerosis. *Nat. Med.* **6**, 67–70 (2000).
8. Medana, I., Martinic, M.A., Wekerle, H. & Neumann, H. Transection of major histocompatibility complex class I-induced neurites by cytotoxic T lymphocytes. *Am. J. Pathol.* **159**, 809–815 (2001).
9. Smith, K.J., Kapoor, R., Hall, S.M. & Davies, M. Electrically active axons degenerate when exposed to nitric oxide. *Ann. Neurol.* **49**, 470–476 (2001).
10. Lo, A.C., Saab, C.J., Black, J.A. & Waxman, S.G. Phenytoin protects spinal cord axons and preserves axonal conduction and neurological function in a model of neuroinflammation in vivo. *J. Neurophysiol.* **90**, 3566–3571 (2003).
11. Friese, M.A. *et al.* Acid-sensing ion channel-1 contributes to axonal degeneration in autoimmune inflammation of the central nervous system. *Nat. Med.* **13**, 1483–1489 (2007).
12. Mathey, E.K. *et al.* Neurofascin as a novel target for autoantibody-mediated axonal injury. *J. Exp. Med.* **204**, 2363–2372 (2007).
13. Bittner, S. *et al.* TASK1 modulates inflammation and neurodegeneration in autoimmune inflammation of the central nervous system. *Brain* **132**, 2501–2516 (2009).
14. Kerschensteiner, M., Schwab, M.E., Lichtman, J.W. & Misgeld, T. *In vivo* imaging of axonal degeneration and regeneration in the injured spinal cord. *Nat. Med.* **11**, 572–577 (2005).
15. Misgeld, T. & Kerschensteiner, M. *In vivo* imaging of the diseased nervous system. *Nat. Rev. Neurosci.* **7**, 449–463 (2006).
16. Bartholomäus, I. *et al.* Effector T cell interactions with meningeal vascular structure in nascent autoimmune CNS lesions. *Nature* **462**, 94–98 (2009).
17. Siffrin, V. *et al. In vivo* imaging of partially reversible T_H17 cell–induced neuronal dysfunction in the course of encephalomyelitis. *Immunity* **33**, 424–436 (2010).
18. Feng, G. *et al.* Imaging neuronal subsets in transgenic mice expressing multiple spectral variants of GFP. *Neuron* **28**, 41–51 (2000).
19. Misgeld, T., Kerschensteiner, M., Bareyre, F.M., Burgess, R.W. & Lichtman, J.W. Imaging axonal transport of mitochondria *in vivo*. *Nat. Methods* **4**, 559–561 (2007).
20. Singbartl, K. *et al.* A CD2-green fluorescence protein–transgenic mouse reveals very late antigen-4–dependent $CD8^+$ lymphocyte rolling in inflamed venules. *J. Immunol.* **166**, 7520–7526 (2001).
21. Jung, S. *et al.* Analysis of fractalkine receptor CX_3CR1 function by targeted deletion and green fluorescent protein reporter gene insertion. *Mol. Cell. Biol.* **20**, 4106–4114 (2000).
22. Kapoor, R., Davies, M., Blaker, P.A., Hall, S.M. & Smith, K.J. Blockers of sodium and calcium entry protect axons from nitric oxide-mediated degeneration. *Ann. Neurol.* **53**, 174–180 (2003).
23. Smith, K.J. & Lassmann, H. The role of nitric oxide in multiple sclerosis. *Lancet Neurol.* **1**, 232–241 (2002).
24. Lin, M.T. & Beal, M.F. Mitochondrial dysfunction and oxidative stress in neurodegenerative diseases. *Nature* **443**, 787–795 (2006).
25. Coleman, M. Axon degeneration mechanisms: commonality amid diversity. *Nat. Rev. Neurosci.* **6**, 889–898 (2005).
26. Franklin, R.J. & Ffrench-Constant, C. Remyelination in the CNS: from biology to therapy. *Nat. Rev. Neurosci.* **9**, 839–855 (2008).
27. Coman, I. *et al.* Nodal, paranodal and juxtaparanodal axonal proteins during demyelination and remyelination in multiple sclerosis. *Brain* **129**, 3186–3195 (2006).
28. Aboul-Enein, F., Weiser, P., Höftberger, R., Lassmann, H. & Bradl, M. Transient axonal injury in the absence of demyelination: a correlate of clinical disease in acute experimental autoimmune encephalomyelitis. *Acta Neuropathol.* **111**, 539–547 (2006).
29. Das Sarma, J., Kenyon, L.C., Hingley, S.T. & Shindler, K.S. Mechanisms of primary axonal damage in a viral model of multiple sclerosis. *J. Neurosci.* **29**, 10272–10280 (2009).
30. Kroemer, G., Galluzzi, L. & Brenner, C. Mitochondrial membrane permeabilization in cell death. *Physiol. Rev.* **87**, 99–163 (2007).
31. Dutta, R. *et al.* Mitochondrial dysfunction as a cause of axonal degeneration in multiple sclerosis patients. *Ann. Neurol.* **59**, 478–489 (2006).
32. Mahad, D., Ziabreva, I., Lassmann, H. & Turnbull, D. Mitochondrial defects in acute multiple sclerosis lesions. *Brain* **131**, 1722–1735 (2008).
33. Mahad, D.J. *et al.* Mitochondrial changes within axons in multiple sclerosis. *Brain* **132**, 1161–1174 (2009).
34. Forte, M. *et al.* Cyclophilin D inactivation protects axons in experimental autoimmune encephalomyelitis, an animal model of multiple sclerosis. *Proc. Natl. Acad. Sci. USA* **104**, 7558–7563 (2007).
35. Du, H. *et al.* Cyclophilin D deficiency attenuates mitochondrial and neuronal perturbation and ameliorates learning and memory in Alzheimer's disease. *Nat. Med.* **14**, 1097–1105 (2008).
36. D'Autréaux, B. & Toledano, M.B. ROS as signalling molecules: mechanisms that generate specificity in ROS homeostasis. *Nat. Rev. Mol. Cell Biol.* **8**, 813–824 (2007).
37. Hooper, D.C. *et al.* Uric acid, a peroxynitrite scavenger, inhibits CNS inflammation, blood-CNS barrier permeability changes and tissue damage in a mouse model of multiple sclerosis. *FASEB J.* **14**, 691–698 (2000).
38. Kizelsztein, P., Ovadia, H., Garbuzenko, O., Sigal, A. & Barenholz, Y. Pegylated nanoliposomes remote-loaded with the antioxidant tempamibe ameliorate experimental autoimmune encephalomyelitis. *J. Neuroimmunol.* **213**, 20–25 (2009).
39. Lipton, S.A. Pathologically activated therapeutics for neuroprotection. *Nat. Rev. Neurosci.* **8**, 803–808 (2007).

ONLINE METHODS

Mice. We used transgenic and knock-in male and female mice to label cellular interaction partners with distinct spectral variants of GFP. For a detailed description of the mouse strains, see the **Supplementary Methods**.

Induction of experimental autoimmune encephalomyelitis. We induced EAE in adult mice (about 6 –12 weeks old) according to a standard protocol[40]. Briefly, we immunized mice with 200–250 µl of an emulsion containing 100–375 µg of purified recombinant myelin oligodendrocyte glycoprotein (MOG, N1-125, expressed in *E. coli*) in complete Freund's adjuvant (Sigma) with 500–625 µg of mycobacterium tuberculosis H37 Ra (Difco). At day 0 and day 2 after immunization, we injected 250–400 ng of pertussis toxin (Sigma) intraperitoneally. We weighed mice daily and scored their neurological deficits according to a standard EAE scoring scale as follows: 0, no detectable clinical signs; 0.5, partial tail weakness; 1, tail paralysis; 1.5, gait instability or impaired righting ability; 2, hind limb paresis; 2.5, hind limb paresis with partial dragging; 3, hind limb paralysis; 3.5, hind limb paralysis and forelimb paresis; 4, hind limb and forelimb paralysis; 5, moribund. All animal work conformed to institutional guidelines and was approved by the Animal Study Committee of the Regierung von Oberbayern.

Immunohistochemistry. After transcardial perfusion of mice with 4% (wt/vol) paraformaldehyde in PBS, we post-fixed spinal cords for 12–24 h. We isolated the lumbar spinal cord and cut sections (50–150 µm) with a vibratome, or we cryoprotected the tissue by incubation in 30% (wt/vol) sucrose (Sigma) in PBS and cut cryosections (30–50 µm) in a cryostat. For immunohistochemistry, we first blocked the sections with 10% (vol/vol) goat serum in 0.5% (vol/vol) Triton X-100 (Sigma) in PBS and then incubated them with primary antibodies against ionized calcium binding adaptor 1 (Iba1) (rabbit IgG, 1 in 250, Wako Pure Chemical Industries, cat. no. 016-20001) or myelin basic protein (rabbit Ig fraction, 1 in 100, DAKO, cat. no. A0623) and counterstained them with the Nissl-like nucleic acid stain, NeuroTrace 640/660 (1 in 500, Invitrogen) and/or FluoroMyelin red fluorescent myelin stain (1 in 150–250, Invitrogen) in 0.5% Triton X-100 in PBS. For Iba1 immunohistochemistry, we used microwave treatment in citrate buffer (0.1 M, pH 6.0, Merck) for antigen retrieval. Sections were mounted in Vectashield (Vector Laboratories) and imaged by confocal microscopy.

Histopathological analysis. For histopathological analysis of EAE tissue, we embedded paraformaldehyde-fixed spinal cord or brain tissue in paraffin and cut either longitudinal sections or cross-sections of lumbar and thoracic spinal cord. For histopathological analysis of multiple sclerosis tissue, we obtained human brain biopsies of male and female individuals with multiple sclerosis from the collection of the Department of Neuropathology at the Georg August University, Göttingen, Germany. The people gave informed consent and the use of the brain biopsies for scientific purposes was in accordance with the guidelines of the Ethics Committee of the Georg-August-University of Göttingen, Germany. For further details, see the **Supplementary Methods**.

***In vivo* imaging.** To image cellular interactions in the lumbar spinal cord, we adapted our previously established *in vivo* imaging approach for visualizing axons in the cervical spinal cord[14]. We performed *in vivo* time-lapse imaging on two imaging setups: a wide-field setup on an Olympus BX51 microscope, and multiphoton microscopes using Olympus FV300 and FV1000 scanners equipped with femtosecond-pulsed Ti:Sapphire lasers (Mai Tai HP, Newport/Spectra-Physics). To measure the release of ROS, we used the Amplex UltraRed reagent (Invitrogen), which is a fluorogenic substrate that indicates H_2O_2 concentrations. We visualized nitric oxide with DAF-FM diacetate sensor dye (Invitrogen). Further details of image acquisition, processing and quantitative analysis are described in the **Supplementary Methods**.

Confocal microscopy. We obtained confocal images of fixed tissue on a FV1000 confocal system mounted on an upright BX61 microscope (Olympus) equipped with ×20/0.85 and ×60/1.42 oil-immersion objectives. To quantify axonal and mitochondrial morphology in EAE lesions, we recorded stacks of 12-bit images (spatial sampling approximately 100 nm in *x*–*y* and 300 nm in *z*). For large-scale longitudinal reconstructions, we documented individual fluorescently labeled axons by scanning overlapping stacks with an automated stage (Prior). Further details of image processing and quantitative analysis are described in the **Supplementary Methods**.

Correlated serial electron microscopy reconstruction. We identified swollen (stage 1) axons *in vivo* in EAE mice (or control axons in healthy mice) with multiphoton imaging (as described above) of fluorescently labeled axons in *Thy1-GFP-S* (× *Thy1-MitoCFP-P*) mice. We then fixed the tissue for ultrastructural analysis and obtained correlated serial electron microscopy reconstruction of the imaged axons as described in the **Supplementary Methods**.

ROS and RNS application and scavenging. To investigate the effects of ROS and RNS application on axonal and mitochondrial morphology *in vivo*, we applied either H_2O_2 (10, 100 and 330 mM, Sigma) or the NO donor spermine NONOate (10 mM, Alexis Biochemicals), to the exposed spinal cords of healthy *Thy1-YFP-16* × *Thy1-MitoCFP-P* mice and imaged axonal and mitochondrial changes over time. To scavenge ROS and/or RNS in EAE lesions, we used a cocktail containing FeTTPS (5,10,15,20-Tetrakis(4-sulfonatophenyl)porphyrinato Iron (III), Chloride; Calbiochem), PBN (*N-tert*-butyl-α-phenylnitrone; Sigma) and EUK134 (Cayman Chemicals). Details of the experiments are provided in the **Supplementary Methods**.

Statistical analyses. Results are given as mean ± s.e.m. unless indicated otherwise. Statistical significance was determined with GraphPad Prism (GraphPad Software), Excel (Microsoft) and SPSS Statistics 17 (SPSS). Unpaired *t* tests (one-tailed for treatment experiment, two-tailed otherwise) were used unless stated otherwise.

Additional methods. Detailed methodology is described in the **Supplementary Methods**.

40. Abdul-Majid, K.B. *et al.* Screening of several H-2 congenic mouse strains identified H-2(q) mice as highly susceptible to MOG-induced EAE with minimal adjuvant requirement. *J. Neuroimmunol.* **111**, 23–33 (2000).

doi:10.1038/nm.2324

SUPPLEMENTARY FIGURES AND VIDEOS

A reversible form of axon damage in experimental autoimmune encephalomyelitis and multiple sclerosis

Ivana Nikić[1], Doron Merkler[2, 3], Catherine Sorbara[1], Mary Brinkoetter[4], Mario Kreutzfeldt[2], Florence M. Bareyre[1], Wolfgang Brück[2], Derron Bishop[4], Thomas Misgeld[5,6*] and Martin Kerschensteiner[1*]

[1] Research Unit Therapy Development, Institute of Clinical Neuroimmunology, Ludwig-Maximilians-Universität München, Munich, Germany
[2] Institute of Neuropathology, Georg-August University, Göttingen, Germany
[3] Division of Clinical Pathology, Geneva University Hospital and Department of Pathology and Immunology, University of Geneva, Switzerland
[4] Department of Physiology, Indiana University School of Medicine-Muncie, Muncie, Indiana, USA
[5] Chair for Biomolecular Sensors, Center for Integrated Protein Sciences (Munich) at the Institute of Neuroscience, Technische Universität München, Munich, Germany
[6] TUM Institute for Advanced Study, Technische Universität München, Munich, Germany

* Authors contributed equally.

SUPPLEMENTARY FIGURES

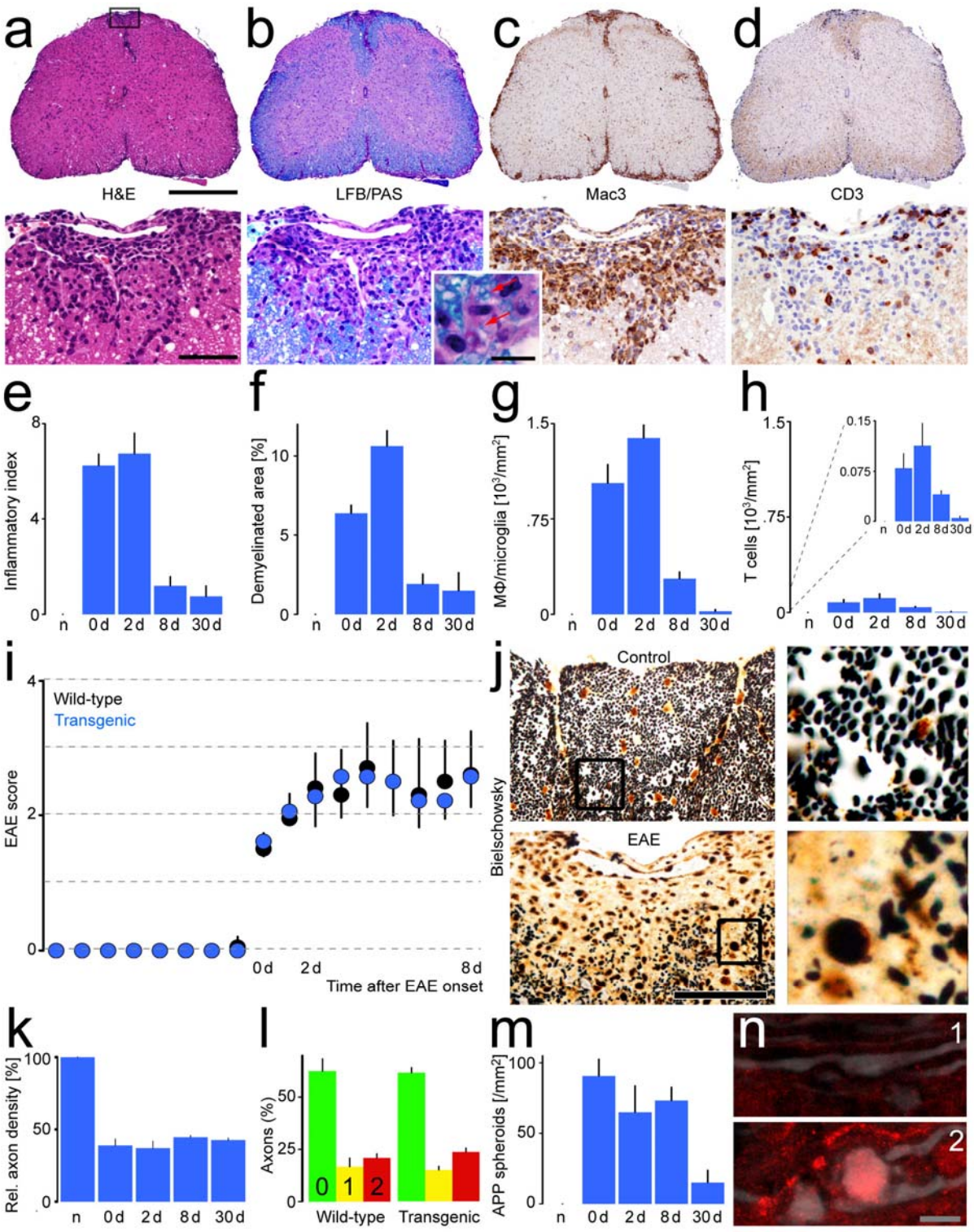

Supplementary Figure 1 – Histopathology of EAE lesions in *Thy1-XFP* transgenic mice.

(**a–d**) Histopathological characterization (top, overview; bottom, magnified view of dorsal column) of lumbar spinal sections of a double transgenic *Thy1-MitoCFP-S* x *Thy1-YFP-16* mouse perfused 2 d after EAE onset (**a**, cellular infiltrate – hematoxylin and eosin staining, H&E; **b**, myelin – luxol fast blue/periodic acid Schiff staining, LFB/PAS; **c**,

Nature Medicine doi:10.1038/nm.2324

macrophages/microglia – anti-Mac3 immunohistochemistry, Mac3; **d**, T cells – anti-CD3, CD3). Inset in **b** (lower panel) shows myelin debris (red arrows) in macrophages. (**e–h**) Quantification of inflammatory index (**e**), demyelination (**f**), macrophage/microglia (**g**) and T cell infiltration (**h**) per white matter area (control animals, "n", and different days after EAE onset; *n* = 3–5 animals per time-point). (**i**) Clinical EAE course in transgenic *Thy1-MitoCFP-S* x *Thy1-YFP-16* (blue) and wild-type C57BL/6 mice (black, *n* = 9–10 animals). Clinical courses were centered on disease onset (12 ± 1.7 d post immunization in transgenic and 15.4 ± 2.3 in wild-type mice). (**j**) Axons (Bielschowsky silver impregnation) in spinal cord cross-sections of *Thy1-MitoCFP-S* x *Thy1-YFP-16* control (top, overview on the left and boxed detail, right) and EAE (2 d after onset, bottom) mice. A swollen axon is visible in the lower magnified view of the EAE lesion. (**k**) Axon density measured in Bielschowsky-stained cross-sections (corrected for tissue edema, see **Supplementary Methods** online; *n* = 2–4 animals per time-point). (**l**) FAD stages in longitudinal, Bielschowsky-stained sections in C57BL/6 wild-type and *Thy1-MitoCFP-S* x *Thy1-YFP-16* transgenic mice (*n* = 3–5 animals per group). (**m**) Density of APP-immunoreactive structures (*n* = 3–5 animals per time-point). (**n**) APP-immuno-staining (red) in spinal cord sections of *Thy1-CFP*^{23} mice (axons, white) is mostly restricted to stage 2 axons (bottom).

Scale bars, 500 μm in **a**, top, 50 μm in **a**, bottom; 10 μm in inset in **b**; 50 μm in **j**; 25 μm in **n**.

Nature Medicine doi:10.1038/nm.2324

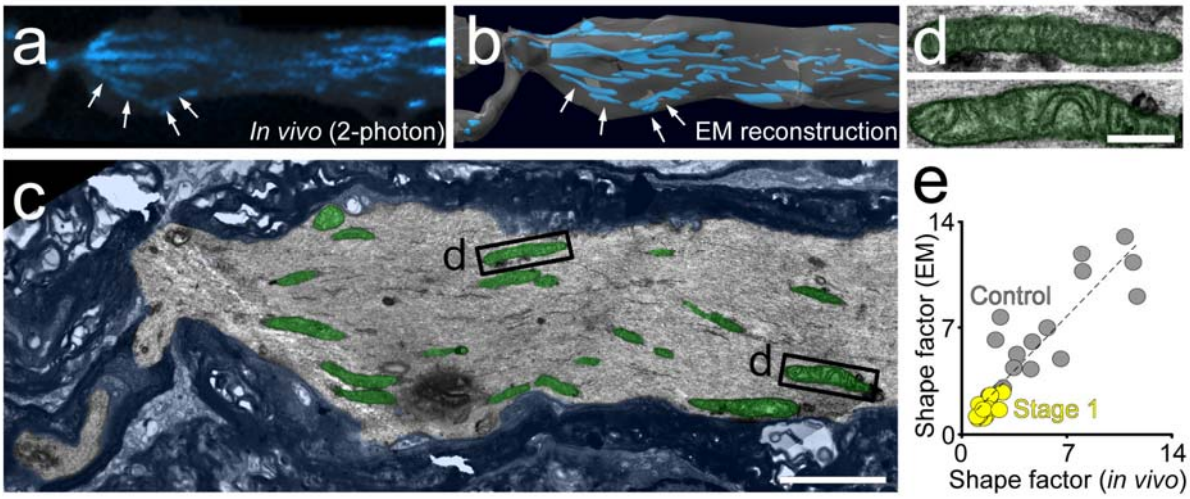

Supplementary Figure 2 – Mitochondrial ultrastructure in healthy control axons.

(**a–d**) Correlated serial-section transmission electron microscopy (ssTEM) reconstruction of a lumbar spinal axon of a healthy *Thy1-GFP-S* x *Thy1-MitoCFP-P* mouse. (**a**) *In vivo* image of the control axon with transgenically labeled healthy appearing mitochondria (cyan). (**b**) ssTEM reconstruction of the same axon. The same mitochondria can be detected *in vivo* (arrows in **a**) and in correlated ssTEM (arrows in **b**). (**c**) Single EM section illustrating that mitochondria (green) in control axons have an elongated shape and a regular ultrastructure (see mitochondrial membranes and cristae in the boxed mitochondria magnified in **d**). (**e**) Correlation of mitochondrial shape factors as measured for the same mitochondria, first *in vivo* and then in the three-dimensionally rendered correlated ssTEMs.

Scale bars, 2.5 µm in **c**; 0.5 µm in **d**.

Nature Medicine doi:10.1038/nm.2324

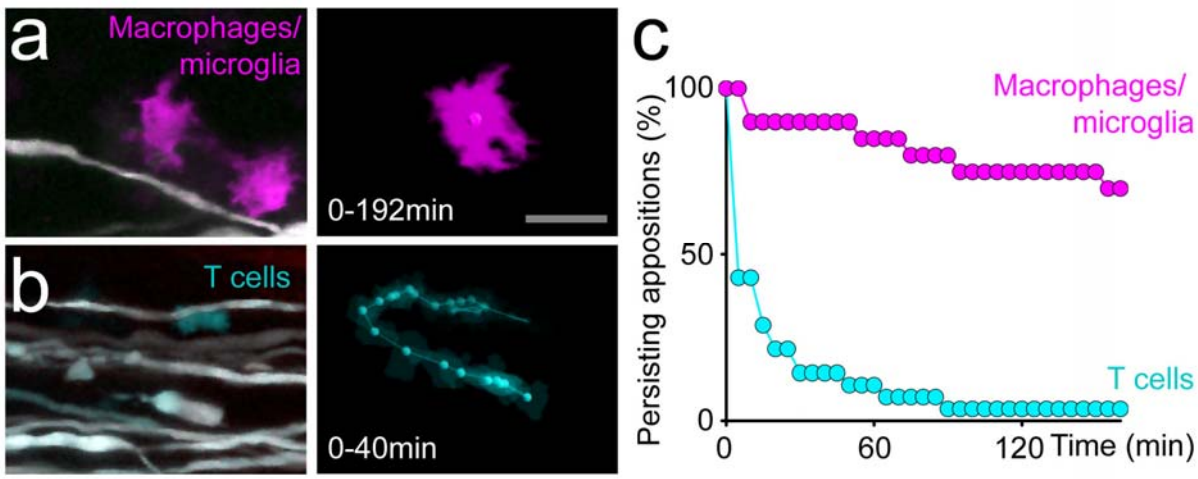

Supplementary Figure 3 – Activated macrophages/microglia appose axons in EAE.

(**a,b**) Two-photon images from time-lapse recordings showing appositions between immune cells (activated macrophage/microglia, magenta, in **a**; T cell, cyan, in **b**) and axons (white) imaged in double-transgenic mice (*Thy1-CFP-S* x *Cx3cr1*$^{GFP/+}$, *Thy1-CFP-S* x *Cd2-GFP*, respectively). The right panels show movement of immune cells starting at the immune cell-axon apposition superimposed onto the pseudo-colored cell outline (dot marks approximate center of cell; compare **Supplementary Videos 6, 7**). Note different time scales for macrophages/microglia and T cell. (**c**) Persistence plot for immune cell-axon appositions over time (n = 20–28 contacts, 3 animals per cell type).

Scale bar, 25 μm in **a** (also for **b**).

Nature Medicine doi:10.1038/nm.2324

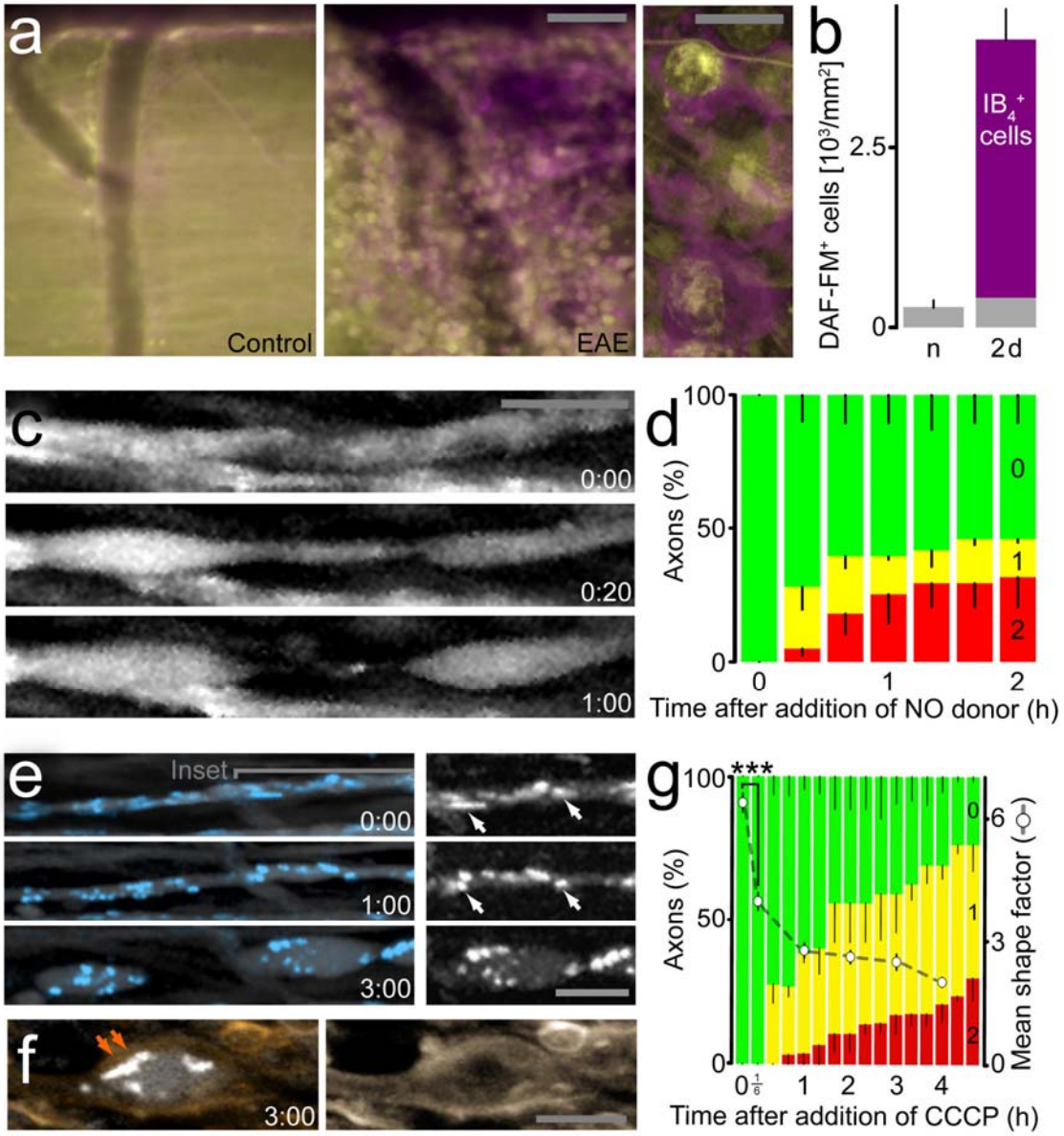

Supplementary Figure 4 – Oxidative stress and mitochondrial damage can induce FAD.

(**a**) *In vivo* images of the lumbar spinal cord of a healthy (left) and an EAE-induced C57BL/6 mouse (middle) after application of the NO sensor dye, DAF-FM diacetate (yellow) and isolectin GS-IB_4 (magenta) that stains activated macrophages/microglia. Right image shows larger confocal magnification after fixation. (**b**) Number of cells with NO sensor signals *in vivo* (for details see **Supplementary Methods** online) in the superficial spinal cord of healthy ("n") or EAE mice (2 d after the onset). The magenta-colored part of the bar indicates the proportion of the NO sensor-positive cells that were also isolectin GS-IB_4 (IB_4) positive. (**c**) *In vivo* multi-photon time-lapse of degenerating spinal axons (gray) after application of the NO donor, spermine NONOate (10 mM; *Thy1-YFP-16* mouse; time in h:min). (**d**) Frequency of stage 0 (green), stage 1 (yellow) and stage 2 (red) axons detected *in vivo* before and up to 2 h after the application of NO donor (n = 3 animals, 35 axons). (**e**) *In vivo* multi-photon time-lapse of spinal axons (gray) and their mitochondria (cyan) after application of CCCP (100 µM; *Thy1-MitoCFP-P* x *Thy1-YFP-16* mouse; time in h:min). Mitochondria that change

Nature Medicine doi:10.1038/nm.2324

shape (arrows) are magnified on the right. (**f**) *In vivo* view of the myelin sheath (arrows, orange) labeled by BODIPY TR methyl ester dye, 3 h after application of CCCP (100 μM). (**g**) Frequency of stage 0 (green), stage 1 (yellow) and stage 2 (red) axons followed *in vivo* for over 4 h after the application of CCCP (100 μM; n = 3 animals, 30 axons; the mean mitochondrial shape factor is displayed (circles) superimposed on the FAD stage histogram).

Scale bars, 50 μm in **a** (middle, also for left); 10 μm in **a** (right),**c**,**e**,**f**.

Nature Medicine doi:10.1038/nm.2324

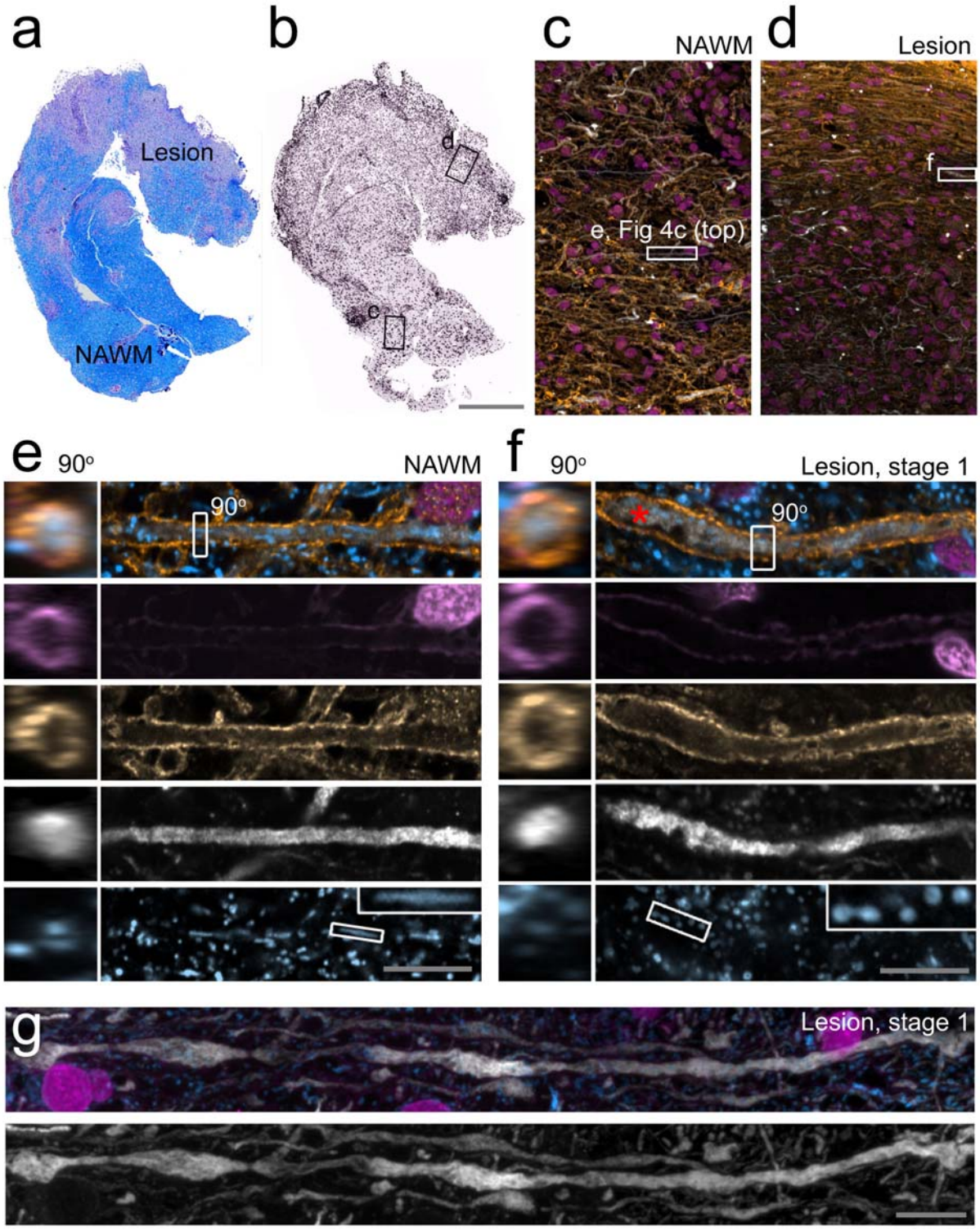

Supplementary Figure 5 – Axonal morphology in acute multiple sclerosis lesions and normal appearing white matter.

(**a**) Overview of a brain biopsy section from an individual with multiple sclerosis. LFB/PAS staining of myelin (blue) reveals a demyelinated multiple sclerosis lesion surrounded by normal-appearing white matter (NAWM). (**b**) Confocal overview of another section of the same biopsy stained with NeuroTrace (magenta, contrast-inverted) to indicate immune cell infiltration. (**c**,**d**) Magnified images of boxed areas in **b** (**c**, NAWM; **d**, lesion area; axons,

Nature Medicine doi:10.1038/nm.2324

white; myelin, orange; nuclei, magenta). (**e**) High resolution image of the axon boxed in **c** (and also shown in **Fig. 4c**) that illustrates normal morphology of the axon, its myelin sheath and mitochondria (upper panel, color combine; 2nd panel from top, nuclei, magenta; 3rd panel from top, myelin, orange; 4th panel from top, axon, white; bottom panel, mitochondria, cyan and magnified in inset). Left panels show a 90°-rotation of the axon (top to bottom panels as above, NeuroTrace dye stains myelin sheath in addition to nuclei). (**f**) High resolution image of a stage 1 axon at the active lesion edge (boxed in **d**) showing a focal swelling (asterisk), damaged mitochondria, and an intact myelin sheath. Left panels show a 90°-rotation of the axon. (**g**) Longitudinal reconstruction of a stage 1 axon with multiple swellings in an acute multiple sclerosis lesion (axons, white; mitochondria, cyan; nuclei, magenta).

Scale bars, 500 μm in **b**; 10 μm in **e**,**f**,**g**.

Nature Medicine doi:10.1038/nm.2324

SUPPLEMENTARY VIDEOS

Supplementary Video 1: *In vivo* multi-photon time-lapse that illustrates the degeneration of a transgenically labeled stage 1 axon (white) in an acute EAE lesion in a *Thy1-CFP-S* x *Cx3cr1*$^{GFP/+}$ mouse. Axonal degeneration is initiated near a putative node of Ranvier in close proximity to activated macrophages/microglia (magenta).

Supplementary Video 2: *In vivo* overview multi-photon time-lapse of the healthy lumbar spinal cord of a *Thy1-YFP-16* (x *Thy1-MitoCFP-P*) mouse in which axons are labeled with YFP (gray). The video illustrates that no obvious morphological changes are induced by our imaging approach. 300 min, 11 frames.

Supplementary Video 3: *In vivo* overview multi-photon time-lapse of the lumbar spinal cord of a *Thy1-YFP-16* (x *Thy1-MitoCFP-P*) mouse, in which axons are labeled with YFP (gray; in some axons, CFP-labeled mitochondria are visible due to spectral cross-talk) 2 d after the EAE onset. The video illustrates stage 1 to stage 2 transitions in three axons during the observation period. 300 min, 11 frames.

Supplementary Video 4: *In vivo* multi-photon time-lapse of the lumbar spinal cord of a *Thy1-YFP-16* (x *Thy1-MitoCFP-P*) mouse in which the axons are labeled with YFP (gray) 3 d after the EAE onset. This video illustrates the recovery of a stage 1 axon during the observation period. 330 min, 11 frames.

Supplementary Video 5: Video sequence of a stage 1 EAE axon (shown in **Fig. 2a-d**) that illustrates the correlation between *in vivo* multi-photon imaging and ssTEM.

Supplementary Video 6: *In vivo* multi-photon microscopy time-lapse of an activated macrophage/microglia (one cell was manually pseudo-colored in magenta based on GFP expression) in apposition to an axon (white) in an acute EAE lesion in a *Cx3cr1*$^{GFP/+}$ x *Thy1-CFP-S* mouse. The video illustrates how immune cells tracts were generated from time-lapse sequences. Note transition of the apposed axon from stage 0 to stage 1 during the time-lapse. Asterisk in first frame marks additional macrophage/microglia. 192 min, 20 frames.

Supplementary Video 7: *In vivo* multi-photon time-lapse of a T cell (one cell was manually pseudo-colored in cyan based on GFP expression) in apposition to an axon (white) in an acute EAE lesion in a *Thy1-CFP-S* x *Cd2-GFP* mouse. The video illustrates how immune cells tracts were generated from time-lapse sequences. Green asterisk in first frame marks additional T cell, gray asterisk marks axon fragment. 40 min, 27 frames.

Supplementary Video 8: *In vivo* multi-photon time-lapse of axonal (white) and mitochondrial (cyan) changes induced after application of H_2O_2 (330 mM) to the spinal cord of a *Thy1-YFP-16* x *Thy1-MitoCFP-P* mouse. Note that axonal mitochondria change before the transition of the axons from stage 0 to stage 1.

Nature Medicine doi:10.1038/nm.2324

SUPPLEMENTARY METHODS

A reversible form of axon damage in experimental autoimmune encephalomyelitis and multiple sclerosis

Ivana Nikić[1], Doron Merkler[2,3], Catherine Sorbara[1], Mary Brinkoetter[4], Mario Kreutzfeldt[2], Florence M. Bareyre[1], Wolfgang Brück[2], Derron Bishop[4], Thomas Misgeld[5,6*] and Martin Kerschensteiner[1*]

[1] Research Unit Therapy Development, Institute of Clinical Neuroimmunology, Ludwig-Maximilians-Universität München, Munich, Germany
[2] Institute of Neuropathology, Georg-August University, Göttingen, Germany
[3] Division of Clinical Pathology, Geneva University Hospital and Department of Pathology and Immunology, University of Geneva, Switzerland
[4] Department of Physiology, Indiana University School of Medicine-Muncie, Muncie, Indiana, USA
[5] Chair for Biomolecular Sensors, Center for Integrated Protein Sciences (Munich) at the Institute of Neuroscience, Technische Universität München, Munich, Germany
[6] TUM Institute for Advanced Study, Technische Universität München, Munich, Germany

* equal contribution

SUPPLEMENTARY METHODS

Animals

We used the following mouse strains: *Thy1-YFP-16* (Jackson Laboratory strain designation: *Tg(Thy1-YFP)16Jrs/J*), *Thy1-GFP-S*, *Thy1-CFP-23* and *Thy1-CFP-S* mice to label axons[1] (mice were gifts from Joshua Sanes and Jeff Lichtman, Harvard University). In *Thy1-GFP-S* and *Thy1-CFP-S* mice only a small subset of neurons is labeled, while in *Thy1-YFP-16* mice, 93.7 ± 0.9% (n = 6 sections, 2 animals) of all myelinated spinal axons express the transgene. In *Thy1-MitoCFP-S* mice (Jackson Laboratory strain designation: *Tg(Thy1-CFP/COX8A)S2Lich/J*) and *Thy1-MitoCFP-P* mice a mitochondrial import sequence directs CFP selectively to neuronal mitochondria[2]. In *Cd2-GFP* mice, all T cells are labeled with GFP[3] (gift from Klaus Ley, La Jolla Institute for Allergy and Immunology). *Cx3cr1*$^{GFP/+}$ mice (Jackson Laboratory strain designation: *Cx3cr1*^{tm1Litt}*/J)* harbor GFP-labeled macrophages and microglial cells[4] (gift from Dan Littman, New York University). *Cd2-GFP* and *Cx3cr1*$^{GFP/+}$ were maintained on a pure C57BL/6 background, the *Thy1*-mouse lines are on a mixed background. We used C57BL/6 (Elevage Janvier) for treatment experiments unless stated otherwise and as a wild-type control group for the histopathological evaluation.

Histopathological analysis

Histopathological analysis of EAE tissue was performed on PFA-fixed longitudinal or cross-sections of lumbar and thoracic spinal cords. Images of tissue sections were recorded using an Olympus light microscope with a CCD camera (DP71; Soft Imaging System) using the Analysis Software Color View II (Soft Imaging System). Bielschowsky silver impregnation was performed on longitudinal serial sections (thickness, 6 μm) to assess the frequency of different FAD stages in demyelinated areas (stage 0: unaltered axon, stage 1: axonal swelling, stage 2: axon fragments, expressed as % of total axons within a given

lesion). Cross-sections (thickness, 3 μm) were obtained from lumbar and thoracic spinal cords to assess inflammation, demyelination and axonal densities. Numbers of inflammatory foci per spinal cord cross-sections were expressed as inflammatory index. The extent of demyelination was quantified by measuring the demyelinated area on overview photographs (40x magnification) of LFB/PAS-stained sections. The area of demyelination was calculated as % of total analyzed area of white matter within a given section. Immunostaining for amyloid precursor protein (APP, clone 22C11, Chemicon) was used as a marker of acute axonal damage. Further immunostaining was performed in adjacent sections to assess numbers of activated macrophages/microglia (MAC3, Clone M3/84, BP Pharmingen) and T-cells (CD3, Clone CD3-12, AbD Serotec), astrocytes (glial fibrillary acidic protein, GFAP, DakoCytomation, Hamburg, Germany) and oligodendrocytes (Nogo-A, mAb 11C7, kindly provided by M. E. Schwab, Brain Research Institute, Department of Neuromorphology, University and ETH Zurich). Avidin-biotin technique with 3,3-diaminobenzidine was used for the visualization of bound primary antibodies. The density of activated macrophages/microglia, T-cells, glial cells and APP^+ axons within lumbar white matter was determined per mm^2. For the analysis of the immune cell infiltration after combined ROS and RNS scavenger therapy, the total number of $MAC3^+$ macrophages or $CD3^+$ T cells was determined using a counting grid and related to the lesion area (determined as the demyelinated area by LFB/PAS staining) for each individual spinal cord cross-section. The average for all analyzed cross-sections was calculated per animal and expressed as cells per mm^2 lesion area.

Histopathological analysis of multiple sclerosis tissue was performed on PFA-fixed sections from human brain biopsies of individuals with multiple sclerosis. All tissue blocks were first classified with regard to lesion activity[5]. Only early active lesions were considered for further analysis. For general lesion assessment LFB/PAS (myelin) and Bielschowsky silver impregnation (axons) stainings were performed. The frequency (% of total axons) of

different stages of axonal damage were separately quantified in demyelinated areas and within normal appearing white matter on Bielschowsky silver impregnated sections (thickness, 4 μm). Avidin-biotin developed immunohistochemical stainings were performed to assess infiltrates of activated macrophages/microglia (KiM1P[6], kindly provided by Prof. H.J. Radzun, Göttingen) and T-cells (CD3, Clone CD3-12, AbDSerotec). For fluorescence immunohistochemistry, multiple sclerosis biopsies were consecutively incubated with antibodies recognizing antigens of myelin (MBP, rabbit-anti-human polyclonal serum, Dako Cytomation), axons (NF 200, mouse IgG_1, Clone N52, SigmaImmunoChemicals) and mitochondria (Porin, mouse IgG_{2b}, Clone 31HL, Invitrogen). Bound antibodies were visualized with species and immunoglobulin subtype specific secondary antibodies (Alexa647 anti-mouse IgG_{2b}, Alexa555 anti-mouse IgG_1; both antibodies from Invitrogen, and Cy2 anti-rabbit IgG, Jackson Immunoresearch). Counterstaining of cells was performed with fluorescent Nissl-like nucleic acid stain (NeuroTrace 435, Invitrogen).

In situ automated evaluation of axonal densities

Cross-sections of spinal cords were stained by Bielschowsky silver impregnation and the axon densities were quantified automatically applying a custom-programmed script in *Cognition Network Language* based on the Definiens Cognition Network Technology® platform (Definiens Developer XD software). Briefly, the programmed script first discriminates between tissue and background (no tissue) by spectral difference detection. Subsequently, the area of detected tissue (region of interest, ROI) is calculated and "axonal structures" within this ROI are detected based on their dark black color. To discriminate between nucleoli of inflammatory cells and axons (both structures are stained black in Bielschowsky silver impregnation) only black structures without a faint brown-stained circumference (nucleus) were classified as "axonal structures". In a next step, multiple axons in direct contact with each other were further split into the corresponding individual axons, if

the splitting improved the elliptic shape of an axon. Finally, all axons were grouped into different size-classes based on their largest diameter.

The robustness of this script was verified on high magnification images of randomly chosen EAE lesions and normal appearing white matter (n = 24 areas, total analyzed area = 2.2 x 10^5 μm^2). The difference in calculated axonal densities between manual counting and automated image evaluation was 2.6 ± 1.9% (mean ± s.d.) and obtained densities were not significantly different (P = 0.40, paired t-test). To adapt for the variation of axonal densities within different affected anatomical tracts of the spinal cord, the numbers of axons were quantified within a lesion as well as in the normal appearing perilesional white matter (NAWM). Numbers of axons within a given lesion were subsequently expressed in % of corresponding NAWM (set as 100%). To correct for tissue swelling (assuming a similar degree of swelling in the x- and y-dimensions), we used EAE sections with unilateral lesions from different disease time points (n = 5–6 sections per time point). Next, we measured the white matter extent (from the grey matter border to the tissue surface) on the lesion side and in the same anatomical location on the contralateral, unaffected side. The relative swelling of inflamed white matter was then calculated by normalizing to the unaffected side to obtain a "correction factor" for each disease time point. To obtain edema-corrected lesion areas at a specific disease time point, the total lesion area was divided by the corresponding squared correction factor. This corrected lesion area was then used for density calculations.

In vivo imaging

To image cellular interactions in the lumbar spinal cord, we surgically exposed the dorsal spinal cord as previously described[7,8]. Briefly, mice were anaesthetized by an i.p. injection of ketamine-xylazine (ketamine 87 mg kg^{-1}, xylazine 13 mg kg^{-1}). Ketamine-xylazine was reapplied every 60–90 min. To access the dorsal lumbar spinal cord, a laminectomy was performed, which was superfused with pre-warmed physiological saline or mouse artificial

cerebrospinal fluid (aCSF). To minimize movement during high-resolution imaging, the vertebral column was immobilized using a spinal adapter for a stereotaxic frame[9] (Narishige STS-A). *In vivo* time-lapse imaging was performed on two types of imaging setups: To visualize axons over longer distances (covering several hundred μm) we used a wide-field set-up based on an Olympus BX51 microscope equipped with x4/0.13 dry, x10/0.3 and x20/0.5 dipping cone water-immersion objectives and a cooled Sensicam QE CCD camera (pco/ Visitron) controlled by MetaMorph software (Universal Imaging) as previously described[7,8]. Image streams of 25–50 images were acquired for each field and time point. To visualize cellular interactions and axonal changes with a higher resolution, we either used a custom-build multi-photon imaging setup based on an Olympus FV300 scanner[10] or a commercially available Olympus FV1000 MPE both equipped with a femto-second pulsed Ti:Sapphire laser (Mai Tai HP, Newport/Spectra-Physics). We tuned the laser wavelength to 910-920 nm in order to excite both Y/GFP and CFP, and collected fluorescence using emission barrier filters for Y/GFP (535/30 or 510 IF) and CFP (480/40 or 470/24). Laser power was attenuated using a polarization-based beam splitter (Newport) or acousto-optical modulators. We acquired high-resolution images stacks (spaced at 1 μm) of lumbar spinal lesion areas with x25/1.05 or x60/0.9 dipping cone water-immersion objective.

Two *in vivo* imaging protocols were used: continuous imaging and repetitive imaging. For continuous imaging, we followed individual axons after a single surgical access for several hours by acquiring an image stack every 10 mins. Further we followed a larger population of axons using "overview" *in vivo* time-lapse imaging. For this purpose, an area containing a lesion was chosen and, using the Olympus Fluoview Ver2.1b Time Controller application, 8 scan stacks of zoom 3 were taken every 30 min. Thereby we could image ~20– 40 axons in a spinal volume of approximately 600 μm x 300 μm x 100 μm for up to 6 h. For repetitive imaging, we documented the same axons on multiple consecutive days with the animal recovering between recording sessions. In this case, after surgical closure of the laminectomy,

animals were transferred to a warmed recovery chamber and injected with physiological saline to prevent dehydration.

To control for phototoxicity we used the same imaging approaches in healthy mice. To control for phototoxicity on our wide-field microscope, we followed individual fluorescently labeled axons in *Thy1-GFP-S* mice for 3–6 h (n = 5 experiments). For multi-photon microscopy, we followed fluorescently labeled axons and mitochondria in *Thy1-YFP-16* x *Thy1-MitoCFP-P* mice for 3–6 h (n = 3, see **Supplementary Video 2** online). In none of the experiments did we see axonal or mitochondrial changes reminiscent of FAD. The absence of significant phototoxicity in our experiments is further supported by the following observations: First, all stages of the FAD process can also be detected in fixed tissue that has never been imaged *in vivo* (see e.g. **Fig. 1a,b**). Second, the FAD progression events that are observed *in vivo* occur evenly distributed over time and do not increase in frequency with prolonged exposure to fluorescence illumination over time (*data not shown*). Finally, axonal recovery, which is unlikely to occur in the presence of phototoxicity, is observed *in vivo* with the same imaging protocols (see **Fig. 1f** and **Supplementary Video 4** online).

To assess the myelination status of axons *in vivo*, Cell Trace BODIPY TR methyl ester dye (Invitrogen) was used as a lipophilic stain at a concentration of 100 mM diluted in aCSF. The solution was incubated on the exposed spinal cord of *Thy1-YFP-16* x *Thy1-MitoCFP-P* mice for 30 min in the dark, and then washed thoroughly for 5 min with aCSF. Myelin and axons could then be imaged simultaneously at a wavelength of 740 nm with a G/R filter set (BA495–540, BA570–625). Nodes of Ranvier were identified as sites of local reduction in axon caliber, with flanking enlargements and commonly emerging collateral branches. Sites identified as nodes by these criteria using *in vivo* imaging, showed ultrastructure typical of nodes in correlated EM reconstructions (**Fig. 2** and **Supplementary Fig. 2**), as well as characteristic “myelin gaps” after BODIPY application.

To measure the electrochemical potential of mitochondria *in vivo*, the potential-sensitive dye tetramethylrhodamine, methyl ester, perchlorate (TMRM, Invitrogen) was applied to the surgically exposed superficial spinal cord of *Thy1-YFP-16* x *Thy1-MitoCFP-P* mice (after removal of the dura) at a concentration of 1.25 μM (25mM DMSO stock) diluted in aCSF and incubated for 30 min in the dark. We then simultaneously imaged YFP, CFP and TMRM fluorescence on an Olympus FV1000 MPE, with the laser tuned to a wavelength of 840 nm (Filters: BA 460–500, BA 520–560, BA 575–630). To evaluate the mitochondrial potential, we determined the TMRM signal in mitochondria from healthy mice (n = 185 mitochondria, 3 mice) and EAE mice 2 days after the onset of EAE (n = 235 mitochondria, 4 mice). To account for differences in the mitochondrial volume we normalized the TMRM fluorescence to the CFP fluorescence in a given mitochondrion. To account for differences in staining intensity in different scans, we normalized the CFP-corrected TMRM signals to the average TMRM signal in normally shaped mitochondria in a given scan. Mitochondrial potential in EAE mitochondria was considered low if the normalized TMRM signal was lower than the mean minus 2 s.d. of control mitochondria.

ROS and RNS Imaging

To measure tissue levels of hydrogen peroxide (H_2O_2) *in vivo* we exposed the superficial lumbar spinal cord of anaesthetized mice by laminectomy. Amplex Ultra Red was diluted in saline to a concentration of 200 μM (stock solution: 20 mM in DMSO), then applied directly to the spinal cord and incubated for 30 min in the dark. After a 2 min wash with aCSF, the spinal cord was continuously superfused with aCSF solution. Amplex Ultra Red fluorescence was imaged over time by acquiring image streams of 25–50 images with a x 4/0.13 dry objective on a wide-field microscope (Olympus BX51) equipped with an appropriate red filter cube (AHF, TxRed HC filter set, F36-504). Imaging was performed before the application of Amplex Ultra Red (3 time points spaced apart by 10 min each) to determine the background

fluorescence and every 10 min after the application of Amplex Ultra Red (starting after a 2 min wash in aCSF). We then measured the average fluorescence intensity of the spinal cord surface (excluding blood vessels) using MetaMorph or ImageJ/Fiji software and subtracted the average background fluorescence to determine the Amplex Ultra Red signal. The Amplex Ultra Red signal measured 20 min after application was used for further analysis. To calibrate the Amplex Ultra red signal, we first incubated the spinal cord with Amplex Ultra Red as described above and then added 0, 10 and 100 mM of exogenous H_2O_2 diluted in saline to the spinal cord of healthy C57BL/6 mice (n = 3 mice per group). After 2 min of incubation, we removed the Amplex Ultra Red solution before measuring and analyzing the fluorescent signal. Amplex fluorescence levels measured in acute EAE lesions were in a similar range as those measured after the application of 100 mM H_2O_2 (*data not shown*).

To measure tissue levels of nitric oxide (NO) *in vivo,* we exposed the superficial lumbar spinal cord of C57BL/6 mice to 200 μM of the NO sensor DAF-FM diacetate (4-amino-5-methylamino-2′,7′-difluorofluorescein diacetate, Invitrogen; in saline). Before DAF-FM application, the dura was opened. After 30 min incubation in the dark, the DAF-FM diacetate solution was removed and the spinal cord was incubated with 200 μM of isolectin GS-IB_4 conjugated with Alexa 647 (Invitrogen) for an additional 30 min. We then acquired image streams of 25–50 images with a x4/0.13 dry and x20/0.5 dipping cone water-immersion objectives on a wide-field microscope (Olympus BX51) equipped with appropriate filter cubes (GFP for DAF, and Cy5 for Alexa 647). After *in vivo* imaging animals were perfused transcardially with 4% PFA and vibratome sections were cut for confocal documentation. We then counted the number of DAF-FM diactetate positive cells at the spinal cord surface (excluding blood vessels) in EAE and control animals in image streams that were acquired by *in vivo* imaging. By overlaying the DAF-FM acetate channel and the isolectin GS-IB_4 channel using ImageJ/Fiji software, we determined how many of the DAF-FM actetate positive cells were also isolectin GS-IB_4 positive.

Correlated serial EM reconstruction

To obtain correlated electron micrographs of specific axons, we first identified swollen (stage 1) axons *in vivo* in EAE animals (or control axons in healthy animals) using multi-photon imaging of fluorescently labeled axons in *Thy1-GFP-S* (x *Thy1-MitoCFP-P*) mice. After *in vivo* documentation, animals were perfused transcardially with 2.5% EM-grade glutaraldehyde and 2% paraformaldehyde in 0.1 M PBS (Electron Microscopy Sciences). After post-fixation for 24 h, the spinal cords were isolated and the previously imaged axons were identified in thick (100–150 μm) vibratome sections using a confocal microscope. The axon and surrounding fiduciary marks were documented to allow subsequent re-identification. Vibratome sections were then processed for electron microscopy using standard protocols. Next, crystals of 1, 1'-dioctadecyl-3,3,3',3'-tetramethylindodicarbo-cyanine-5,5'-disulfonic acid (Dil, Invitrogen) were applied to the surface of the spinal cord slice next to the axon of interest. To render the Dil crystal electron dense, we photo-oxidized for ~20 min with an achroplan x40/0.80 water immersion objective (Zeiss) until the fluorescence was replaced with a dark brown DAB precipitate. Vibratome sections were then stained with 1% osmium tetroxide reduced in 1.5% potassium ferrocyanide, washed in 4 changes of 0.1 M sodium cacodylate buffer, and dehydrated in an ascending ethanol series. After dehydration, tissue blocks were placed in 2 changes of 100% propylene oxide, infiltrated with Araldite 502/ EMbed812 resin (Electron Microscopy Sciences), and polymerized at 60 °C for 48 h. Ultrathin sections were cut and documented according to standard protocols.

ROS and RNS application and imaging

To investigate the effects of ROS application on axonal and mitochondrial morphology *in vivo* we anaesthetized healthy *Thy1-YFP-16* x *Thy1-MitoCFP-P* mice and exposed the lumbar dorsal spinal cord as described above. We then documented the morphology of a group of

axons and their mitochondria by acquiring an image stack on the multi-photon microscope. Then H_2O_2 (10–330mM diluted in aCSF or saline) was applied directly to the exposed lumbar spinal cord and incubated for 30 min in the dark. The same group of axons was then imaged repetitively by multi-photon microscopy every 10 min for 150–300 min. The H_2O_2 solution was removed each time prior to image acquisition and re-applied thereafter. Image stacks were analyzed with MetaMorph or ImageJ/Fiji software. Axons were staged according to the presence of local swellings (stage 1) or fragmentation (stage 2). In addition, in selected axons we measured the shape factors of individual mitochondria and calculated the mean mitochondrial shape factor for the imaged stretches of the axon. Axonal and mitochondrial changes reminiscent of FAD were consistently observed starting from a dose of 10 mM H_2O_2 (as previously used in cell culture[11,12]) and became more frequent with increasing doses of H_2O_2 (100–330 mM).

We investigated the effects of RNS application on axonal and mitochondrial morphology *in vivo* using a similar approach. In this case, the NO donor Spermine NONOate (Alexis Biochemicals) was diluted to a final concentration of 10 mM in aCSF and applied to the exposed spinal cord (after laminectomy and removal of the dura) of *Thy1-YFP-16* x *Thy1-MitoCFP-P* mice. As described above, we then imaged axonal morphology by *in vivo* multi-photon microscopy for a total of 4–5 h. Image stacks were analyzed with ImageJ/Fiji software and axons were staged according to the presence of local swellings (stage 1) or fragmentation (stage 2).

CCCP application and imaging

To investigate the role of mitochondrial damage in the progression of FAD, we applied a mitochondrial protonophore, CCCP (carbonyl cyanide 3-chlorophenylhydrazone, Sigma) to the exposed spinal cords of healthy *Thy1-YFP-16* x *Thy1-MitoCFP-P* mice. A concentration of 100 μM diluted in aCSF was used, and CCCP remained on the spinal cord for the duration

of the experiment. Images were collected immediately after application, every 10 min for the first 30 min (in order to visualize mitochondrial changes before the onset of axon morphology changes) and every 20 min thereafter for 4–5 h. A total of 30 axons from three animals were evaluated for mitochondrial shape factor and axonal morphology changes using ImageJ/Fiji software. To determine the myelination status of axons exposed to CCCP, we repeated the experiments in healthy *Thy1-YFP-16* x *Thy1-MitoCFP-P* mice that were labeled with the lipophilic BODIPY TR methyl ester dye (as described above) before treatment with 100 μM CCCP. A total of 30 axons from 4 mice were evaluated for axonal changes and myelination up to 4 h while incubated in CCCP.

Therapy with ROS and RNS scavengers

To evaluate the effect of ROS and RNS scavengers on FAD we performed two sets of experiments. First, we induced EAE in C57BL/6 mice by immunization with MOG as described above. At weight loss (typically one day before disease onset) mice were treated either with vehicle or a ROS and RNS scavenger cocktail containing the following components: FeTPPS (5,10,15,20-Tetrakis(4-sulfonatophenyl)porphyrinato Iron (III), Chloride, Calbiochem), a peroxynitrate scavenger[13]; PBN (N-tert-Butyl-α-phenylnitrone, Sigma), a spin trap that reacts with superoxide and hydroxyl radicals[14]; and EUK134 (Cayman Chemicals), a catalase and superoxide dismutase analogue[15]. ROS and RNS scavengers (single dose: FeTPPS 20 mg kg^{-1}, PBN 50 mg kg^{-1} and EUK134 15 mg kg^{-1}) or vehicle solution (physiological saline containing 3% of DMSO) were injected i.p. every 12 h. At 2 d after onset animals were perfused transcardially with 4% PFA, the spinal cords were dissected and histopathology was analyzed by a blinded observer as detailed above. While this treatment reduced the total size of the demyelinated area, the number of oligodendrocytes and astrocytes in the lesion area was not significantly altered (*data not shown*). To evaluate whether ROS and RNS scavengers can reverse early stages of axon damage, we induced EAE

in *Thy1-GFP-S* mice (x *Thy1-MitoCFP-S*) as described above. Two days after onset animals with a clinical score of at least 2 were randomized to a ROS and RNS scavenger and a vehicle group. Mice were then anaesthetized and the dorsal spinal cord was exposed as described above. Axons with localized swellings (stage 1 axons) were identified *in vivo* and documented by acquiring image streams (20-50 images) with an *in vivo* wide-field microscope equipped with a x4/0.13 dry and x20/0.5 water immersion objective as described above. After imaging the animals were treated i.p. either with vehicle or a ROS/RNS scavenger cocktail (see above). After 48 h of treatment animals were re-imaged *in vivo* and the previously identified axons were documented again using x4 and x20objectives as described above. Animals were then either perfused directly or after 48 h of additional treatment. For evaluation of axon stages *in vivo* image streams of the same axons before and after treatment were staged by two observers.

Image processing

Image streams obtained with wide-field microscopy were aligned using Autoquant (MediaCybernetics), in-focus frames were selected and averaged using Metamorph or the free-ware ImageJ/Fiji (http://rsbweb.nih.gov/ij)[16]. Image stacks obtained with multi-photon or confocal microscopy were processed using Metamorph and ImageJ/Fiji software to generate maximum intensity projections. To obtain final visualizations, these maximum intensity projections were further processed in Photoshop (Adobe) using gamma adjustments to enhance visibility of intermediate gray values and 'despeckle' or median filtering to suppress detector noise, where necessary. Gamma adjustment was not used on panels that illustrate intensity variations (e.g. **Fig. 3e**). To avoid overlap artifacts in maximum intensity projections, e.g. due to dural second harmonics signals, or to avoid z-movement-induced duplications of structures, image stacks were split and overlapping partial projections were generated and re-merged in Photoshop. Such partial projections, as well as large-scale

reconstructions, were generated by fusing multiple projections taking advantage of the 'mask' function of Adobe to smoothen seams between partial projections or stitched fields of view[17].

Electron micrographs were individually scanned with an Epson Perfection V700 Photo scanner, montaged with Panvue Image Assembler (PanaVue Inc.), and imported into Reconstruct[18]. A calibration grid was used to determine pixel size in x- and y-dimension, while section thickness was estimated using the cylindrical diameters method[19]. Sections were aligned, and surface contours of objects of interest (axons, mitochondria, etc.) were manually traced in Reconstruct. Contours were then tessellated into three dimensional Boissonnant surface models and rendered using 3ds Max (Autodesk).

Quantitative analysis

For quantification of axon damage stages in fixed tissue, *Thy1-MitoCFP-S* x *Thy1-YFP-16* or *Thy1-MitoCFP-P* x *Thy1-YFP-16* double transgenic mice were perfused transcardially at the first day of weight loss, as well as at the first day of clinical symptoms and 2, 8 and 30 d thereafter. Longitudinal sections of the lumbar spinal cord were cut and imaged on an Olympus FV1000 confocal microscope equipped with standard filter sets and a x60/1.42 oil objective. High resolution image stacks were obtained from inflammatory lesions defined by the presence of a cellular infiltrate (Iba-1 staining or Neurotrace labeling). The axon stages were quantified in the entire lesion area including the lesion border by evaluating the volume of the stack in Metamorph. Axons were staged using the following criteria: stage 0 – unaltered axon, stage 1 – axonal swelling, stage 2 – axon fragments.

For quantification of APP immunoreactivity in EAE, we analyzed the lumbar spinal cord of mice perfused 2 d after onset of EAE and fixed in 4% PFA for 12–24 h using two protocols. First, cross-sections and longitudinal section were cut after paraffin- embedding. After microwave processing, sections were immunostained in consecutive steps with a

monoclonal anti-APP antibody (clone 22C11, Millipore) and a monoclonal anti-Neurofilament 200 antibody (clone N52, Sigma). Second, cross-sections and longitudinal sections from *Thy1-CFP-23* mice were cut on a cryostat. After microwave processing sections were counterstained with a rabbit polyclonal anti-APP antibody (Invitrogen). For sections stained with both protocols we then counted the number of APP^+ structures in cross-sections and related it to the lesion area in mm^2.

For quantification of the myelination status of EAE axons we analyzed the lumbar spinal cord of *Thy1-MitoCFP-S* x *Thy1-YFP-16* or *Thy1-MitoCFP-P* x *Thy1-YFP-16* double-transgenic mice perfused either at the weight loss stage of EAE (n = 3 animals) or 2 d after the onset of clinical symptoms (n = 3 animals). Longitudinal sections were cryosectioned and counterstained with FluoroMyelin red fluorescent myelin stain (Invitrogen) and NeuroTrace 640/660 (Invitrogen). The lesion area was identified by the dense cell infiltration and image stacks were taken either at the lesion border or in the lesion center using a confocal microscope (see above). After image processing, we followed axons and their myelin sheaths through the image stacks and graded their myelination status according to the following categories: intact myelination, axons are wrapped by a continuous myelin sheath with consistent thickness; partial demyelination, axons are wrapped by abnormal myelin sheaths that show either local gaps or local thinning; complete demyelination, axons are not wrapped by discernable myelin sheaths. The same criteria were used to determine the myelination status of axons in multiple sclerosis lesions based on anti-MBP immunohistochemistry (see above).

Mitochondrial damage was assessed by optical imaging and electron microscopy as follows: In electron micrographs, mitochondria were identified by their characteristic ultrastructural features, including the presence of cristae and double membranes in serial sections of the organelle[20]. Alterations in mitochondrial ultrastructure were then evaluated based on two previously described criteria[20,21]: First, disorganized cristae and internal

membranes and, second, electron lucidity of the matrix. Mitochondria were considered damaged if both criteria were met. To measure shape factors (length/ width) in electron micrographs, we identified mitochondria oriented parallel to the axis of sectioning and measured their lengths and widths in sections where these values reached a maximum. Compared to measurements of entire mitochondria in 3D, this method slightly underestimates mitochondrial length (**Fig. 2g** cf. **Supplementary Fig. 2e**). In image stacks acquired by confocal or multi-photon microscopy from *Thy1-MitoCFP-S* or *Thy1-MitoCFP-P* mice, we measured mitochondrial length and width by following mitochondria through consecutive sections, and recording the cumulated length and the maximal width.

For quantification of cell infiltration around axons in different stages of FAD, we analyzed the lumbar spinal cord of healthy or EAE-induced *Thy1-MitoCFP-P* x *Thy1-YFP-16* double-transgenic mice. Longitudinal section were cut on a cryostat and counterstained with Neurotrace 640/660 (Molecular Probes) to detect cell bodies. The lesion area was identified by dense cell infiltration and image stacks were taken from the lesion area using a confocal microscope (see above). After image processing, we determined the cell density around axons in different stages of FAD by first dividing the axons in 25 µm segments. In the image stack, we then counted all nuclei within a distance of 5 µm on both sides of the axon segment over a z-distance of about 2 µm (6 consecutives image planes spaced apart by 0.33 µm). We used a similar approach to quantify cell densities around axons in *Thy1-GFP-S* mice that we had previously imaged *in vivo*. For this purpose we re-identified the imaged axons in longitudinal vibratome sections of the spinal cord that were counterstained with Neurotrace 640/660 (Molecular Probes). We then reconstructed the axon and the surrounding nuclei over a length of 500 µm around the imaged site by high resolution confocal microscopy and determined the cell density per axon segment as described above.

SUPPLEMENTARY REFERENCES

1. Feng, G. *et al.* Imaging neuronal subsets in transgenic mice expressing multiple spectral variants of GFP. *Neuron* **28**, 41-51 (2000).

2. Misgeld, T., Kerschensteiner, M., Bareyre, F.M., Burgess, R.W. & Lichtman, J.W. Imaging axonal transport of mitochondria in vivo. *Nat. Methods* **4**, 559-61 (2007).

3. Singbartl, K. *et al.* A CD2-green fluorescence protein-transgenic mouse reveals very late antigen-4-dependent CD8+ lymphocyte rolling in inflamed venules. *J. Immunol.* **166**, 7520-6 (2001).

4. Jung, S. *et al.* Analysis of fractalkine receptor CX(3)CR1 function by targeted deletion and green fluorescent protein reporter gene insertion. *Mol. Cell. Biol*. **20**, 4106-14 (2000).

5. Brück, W. *et al.* Monocyte/macrophage differentiation in early multiple sclerosis lesions. *Ann. Neurol*. **38**, 788–96 (1995).

6. Radzun, H.J. *et al.* Detection of monocyte/macrophage differentiation antigen in routinely processed paraffin-embedded tissues by monoclonal antibody Ki-M1P. *Lab. Invest.* **65**, 306-15 (1991).

7. Kerschensteiner, M., Schwab, M.E., Lichtman J.W. & Misgeld, T. In vivo imaging of axonal degeneration and regeneration in the injured spinal cord. *Nat. Med*. **11**, 572-7 (2005).

8. Misgeld, T., Nikic, I. & Kerschensteiner, M. In vivo imaging of single axons in the mouse spinal cord. *Nat. Protoc.* **2**, 263-8 (2007).

9. Davalos, D. *et al*. Stable in vivo imaging of densely populated glia, axons and blood vessels in the mouse spinal cord using two-photon microscopy. *J. Neurosci. Methods* **169**, 1-7 (2008).

10. Majewska, A., Yiu, G. & Yuste, R. A custom-made two-photon microscope and deconvolution system. *Pflugers Arch*. **441**, 398-408 (2000).

11. Hoyt, K.R., Gallagher, A.J., Hastings, T.G. & Reynolds, I.R. Characterization of hydrogen peroxide toxicity in cultured rat forebrain neurons. *Neurochem. Res.* **22**, 333-40 (1997).

12. Lim, C.-S., Lee, J.-C., Kim, S.D., Chang, D.-J. & Kaang, B.-K. Hydrogen peroxide-induced cell death in cultured Aplysia sensory neurons. *Brain Res.* **941**, 137-45 (2002).

13. Bolton, C., Scott, G.S., Smith, T. & Flower RJ. The acute and chronic phases of chronic relapsing experimental autoimmune encephalomyelitis (CR EAE) are ameliorated by the peroxynitrite decomposition catalyst, 5,10,15,20-tetrakis(4-sulfonatophenyl)porphyrinatoiron (III) chloride, (FeTPPS). *Eur. J. Pharmacol.* **601**, 88-93 (2008).

14. Fan, L.W. *et al.* Alpha-Phenyl-n-tert-butyl-nitrone attenuates lipopolysaccharide-induced brain injury and improves neurological reflexes and early sensorimotor behavioral performance in juvenile rats. *J Neurosci Res.* **86**, 3536-47 (2008).

15. Peng, J., Stevenson, F.F., Doctrow, S.R. & Andersen J.K. Superoxide dismutase/catalase mimetics are neuroprotective against selective paraquat-mediated dopaminergic neuron death in the substantial nigra, implications for Parkinson disease. *J. Biol. Chem*. **280**, 29194-8 (2005).

16. Kerschensteiner, M., Reuter, M.S., Lichtman, J.W. & Misgeld, T. Ex vivo imaging of motor axon dynamics in murine triangularis sterni explants. *Nat. Protoc.* **3**, 1645-53 (2008).

17. Beck, J.C., Murray, J.A., Willows, A.O. & Cooper, M.S. Computer-assisted visualizations of neural networks: expanding the field of view using seamless confocal montaging. *J. Neurosci. Methods* **98**, 155-63 (2000).

18. Fiala, J.C. Reconstruct: a free editor for serial section microscopy. *J. Microsc.* **218**, 52-61 (2005).

19. Fiala, J.C. & Harris, K.M. Cylindrical diameters method for calibrating section thickness in serial electron microscopy. *J. Microsc.* **202**, 468-72 (2001).

20. Perkins G., Bossy-Wetzel E. & Ellisman M.H. New insights into mitochondrial structure during cell death. *Exp. Neurol.* **218**, 183-92 (2009).

21. Sun, M.G. *et al.* Correlated three-dimensional light and electron microscopy reveals transformation of mitochondria during apoptosis. *Nature Cell. Biol.* **9**, 1057-65 (2007).

Cellular, subcellular and functional *in vivo* labeling of the spinal cord using vital dyes

Elisa Romanelli[1,6], Catherine D Sorbara[1,2,6], Ivana Nikić[1,6], Athanasios Dagkalis[1], Thomas Misgeld[2–5] & Martin Kerschensteiner[1,5]

[1]Institute of Clinical Neuroimmunology, Ludwig-Maximilians Universität München, Munich, Germany. [2]Biomolecular Sensors, Center for Integrated Protein Sciences (Munich) at the Institute of Neuroscience, Technische Universität München, Munich, Germany. [3]Institute of Advanced Study, Technische Universität München, Munich, Germany. [4]German Center for Neurodegenerative Diseases (DZNE), Munich, Germany. [5]Munich Cluster for Systems Neurology (SyNergy), Munich, Germany. [6]These authors contributed equally to this work. Correspondence should be addressed to M.K. (martin.kerschensteiner@med.uni-muenchen.de).

Published online 7 February 2013; doi:10.1038/nprot.2013.022

Here we provide a protocol for rapidly labeling different cell types, distinct subcellular compartments and key injury mediators in the spinal cord of living mice. This method is based on the application of synthetic vital dyes to the surgically exposed spinal cord. Suitable vital dyes applied in appropriate concentrations lead to reliable *in vivo* labeling, which can be combined with genetic tags and in many cases preserved for postfixation analysis. In combination with *in vivo* imaging, this approach allows the direct observation of central nervous system physiology and pathophysiology at the cellular, subcellular and functional level. Surgical exposure and preparation of the spinal cord can be achieved in less than 1 h, and then dyes need to be applied for 30–60 min before the labeled spinal cord can be imaged for several hours.

INTRODUCTION

In vivo microscopy is a powerful technique for visualizing cellular behavior in the healthy and diseased nervous system[1,2]. In the spinal cord, for example, *in vivo* microscopy has revealed the degeneration and regeneration of axons after injury[3–5], as well as the cellular interactions and targets of injury in neuroinflammation[6–8]. In this protocol, we describe a vital dye–based approach for rapidly labeling cells, subcellular compartments and molecular effectors in the spinal cord of living mice.

Although the development of new microscopy techniques, in particular the advent of multiphoton imaging[9,10], has driven the rapid expansion of this field, recent progress has also crucially depended on the development of suitable labels for cellular, subcellular and molecular imaging[11–14]. This has primarily been achieved by the generation of new transgenic mouse lines that express genetically encoded fluorescent proteins or sensors. However, the genetic approach has its limitations: for example, the generation of new transgenic mouse lines consumes substantial time and resources. Further, when labels have to be combined or used in genetic disease models, complex breeding schemes ensue. This delays experimental progress and often precludes the combination of three or more labels and alleles. Moreover, the limited spectral range and broad two-photon absorption of fluorescent proteins make them suboptimal fluorescent probes. Therefore, synthetic vital dyes remain an important complement. Such dyes are often available across the detectable wavelength spectrum, exist in a broad range of functionalized forms and can easily be combined with established transgenic labeling. Thus, these dyes in principle provide an ideal shortcut around the obstacles of all-genetic labeling. However, although vital dyes have been extensively used in cell culture, only a few of them have so far been used *in vivo,* in particular in the nervous system. The few notable exceptions, including 'multicell bolus loading' of calcium indicator dyes[15–17] and local application of receptor-binding toxins (e.g., bungarotoxin)[18,19] or of organelle- or cell type–specific fluorescent dyes such as 4-Di-2-ASP[20,21] or sulforhodamine 101 (refs. 22,23), show that such approaches can be highly successful and—when properly documented—widely used.

As part of our work on the *in vivo* pathogenesis of immune-mediated axon damage[7], we recently found that vital dye–based labeling techniques can also be successfully used to visualize cellular behavior, the functional status of intracellular organelles and the release of toxic mediators in the spinal cord of living mice[7]. While establishing these labeling approaches we have identified several important determinants for the successful use of vital dyes *in vivo*. These include the following:

- *Choice of the best vital dye of a given class for the desired application.* Even structurally related dyes can vastly differ in their ability to label *in vivo*.
- *Determination of the correct dye concentration.* Depending on the concentration, the same dye can label different structures.
- *Choice of optimal fixation conditions.* This enables postfixation analysis of imaged structures with some dyes.

In summary, we provide a protocol that enables researchers to label different cell types (such as oligodendrocytes or macrophages/microglia), subcellular compartments (such as myelin), organelles (such as mitochondria) or the release of soluble mediators (such as reactive oxygen species). These labeling strategies provide a fast and reliable complement to genetic techniques, and they can be visualized in the mouse spinal cord by *in vivo* multiphoton or wide-field imaging and thus provide dynamic insights into the cellular, subcellular and molecular pathogenesis of neuroinflammatory, traumatic or neurodegenerative disease processes.

Experimental design

Surgical and imaging approach for vital dye labeling. Vital dye–based imaging requires surgical access to the spinal cord, the stabilization and controlled movement of the mouse in *x–y* and *z*, and imaging modalities that allow combined and long-term visualization with little bleaching or phototoxicity. These challenges have been successfully tackled in recent years, and techniques required for spinal *in vivo* imaging are described

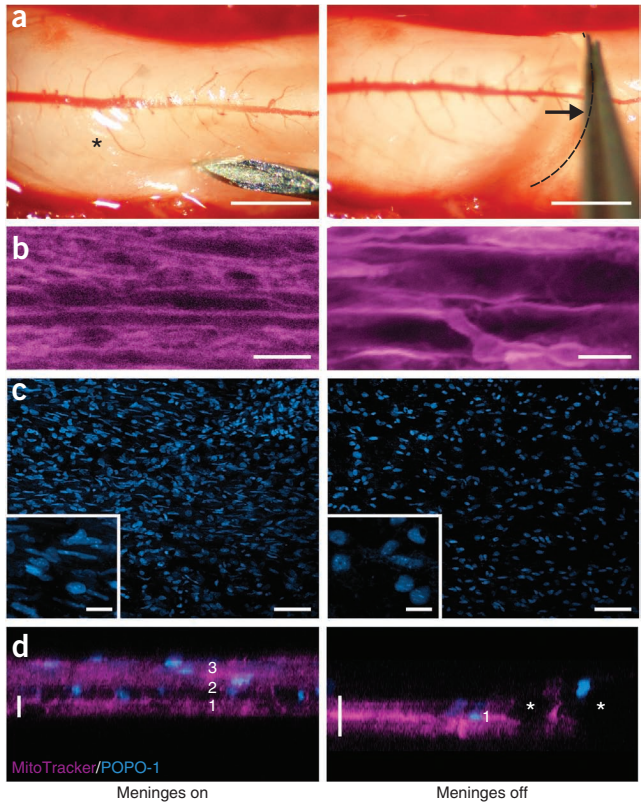

Figure 1 | Removal of the meninges. (**a**) After laminectomy, the meninges are first punctured with the tip of a hypodermic needle to allow access with surgical tools. The reflective surface, labeled with an asterisk (*), is indicative of an intact dura and is absent in the right image, in which the meninges (dura and arachnoidea) have been peeled off using fine forceps. The direction in which the meninges have been pulled is indicated by the arrow. The free margin of the meninges is outlined by a dashed line. (**b**) Removal of the meninges substantially improves the quality of labeling, e.g., by MitoTracker Red (magenta images equalized to full dynamic range; thus, note the higher noise level in the left image). (**c**) Removal of the meninges improves nuclear labeling with POPO-1 iodide (cyan), which will primarily stain cells in the meningeal layers if the meninges are left on (left), as opposed to when the meninges are removed (right). (**d**) *x–z* projection of an image stack with (left) or without (right) the dura and arachnoidea in place shows that penetration into the spinal cord is doubled when the meninges are removed; (1) dorsal spinal cord; (2) subarachnoideal space; (3) dura mater and arachnoidea. All animal experiments conformed to institutional guidelines and were approved by the Animal Study Committee of the Regierung von Oberbayern. Scale bars, (**a**) 1 mm; (**b**) 10 µm; (**c**) 50 µm; (**c**) 10 µm (inset); (**d**) 8 µm (left) and 16 µm (right).

in detail in a number of recent publications[3,16,24–26]. For example, the dorsal spinal cord can be readily accessed after a multilevel laminectomy[3,26], the exposed spinal cord can then be secured using a spinal clamping device that minimizes movement and breathing artifacts[24,25] and fluorescent signals can be recorded *in vivo* using adapted wide-field[3,26] or multiphoton[16,24,25] imaging systems. The reader is referred to the cited references for setting up a stable *in vivo* imaging system for the spinal cord.

For vital dye–based imaging, the following modifications are critical. First, the meninges (dura mater and arachnoidea) must be removed using a hypodermic needle and fine forceps (**Fig. 1a**). Removal of the meninges substantially improves labeling and image quality, as the intact meninges limit dye penetration and vital dyes may also label structures within the dura and arachnoidea (e.g., nuclei), thus obscuring spinal labeling (**Fig. 1b–d**). Therefore, the need to remove the meninges makes vital dye–based labeling primarily suitable for acute imaging experiments, and at least currently limits its application in conjunction with recently developed approaches for chronic spinal *in vivo* imaging[27,28]. Second, for controlled dye exposure, the liquid level on the exposed spinal cord needs to be stabilized. This can best be achieved by forming an agarose 'well' around the laminectomy opening. The care with which this well is formed crucially determines the extent of fluid loss, as well as the stability of the meniscus that keeps the long working distance objectives submerged in the superfusion solution that doubles as immersion medium.

Vital dye labeling. By using this protocol, we have assessed the ability of vital dyes, which have so far primarily been used for *in vitro* studies, to label the spinal cord *in vivo*. We have applied a range of commercially available vital dyes that can be categorized as 'structural' ('cell type–specific' or targeted to a specific 'subcellular compartment') or 'functional' (**Table 1**). In **Table 1**, we provide key information for each dye about its application, visualization and fixation conditions. For each group, we highlight in bold font the dye that, in our hands, is best suited for *in vivo* imaging on the basis of its reliability, brightness, longevity during imaging and ability to be fixed after imaging.

A number of points need to be considered once the appropriate dye is chosen. First, it is important to determine a suitable dye concentration for the intended application. This is particularly crucial, as the same dye might label different structures depending on its dilution. At low concentration, for example, MitoTracker Red labels mitochondria (**Fig. 2a**). A moderate increase in concentration will label both mitochondria and myelin (**Fig. 2b**), whereas at an even higher concentration the strong myelin signal completely obscures mitochondrial labeling (**Fig. 2c**). Second, the expected penetration depth of the dye into the spinal cord needs to be taken into account. After dura removal, most dyes penetrate between 15 and 30 µm into the spinal cord (the penetration depths of individual dyes are shown in **Table 1**), indicating that mostly superficial structures can be imaged. However, it should be noted that the depth that can be imaged in the heavily myelinated spinal cord even with two-photon microscopy (about 40 µm with similar imaging settings) is much more limited than, e.g., in the cortex. Yet given the homogenous organization of the spinal dorsal white matter, it can be argued that dye penetration issues are not as limiting in the dorsal spinal cord as they would be in a tissue with a more complex architecture that requires deep imaging. Third, for many applications, it is helpful to determine the labeling efficiency of a given dye, i.e., to establish which percentage of a cellular or subcellular target population in the penetration volume can be expected to be labeled *in vivo*. We have therefore determined the labeling efficiency for all recommended dyes by comparing them with established transgenic or immunohistochemical markers (**Table 1**). Labeling efficiency is particularly high for nuclear dyes, which label nearly 100% of the nuclei (as determined by DAPI staining after fixation), as well as for MitoTracker Red (for myelin) and *Griffonia simplicifolia* B4 isolectin (GSA-B4; for activated macrophages/microglia). All vital dyes tested label at least 40% of their target population.

For applications that require dyes to be re-applied over time, it is further important to know how reliably the same cells or organelles can be relabeled and thereby followed over extended periods of

TABLE 1 | Vital dyes for cellular, subcellular and functional imaging.

Dye	Company, cat. no.	Labeled structure	Dilution/ concentration	Incubation time	Optimal excitation (nm)	Persistence of label	Penetration depth, comparison to genetic label[a]	Labeling efficiency[b]	Fixation (in 4% PFA)
Structural dyes									
Cell type–specific dyes									
Isolectin GS-IB4 from *Griffonia simplicifolia*, Alexa Fluor 647 conjugate	Invitrogen, I32450	Activated microglial cells (macrophages)	200 µM	1 h	840 (2P)	>2 h	14 ± 2 µm, 35 ± 2 %	87 ± 5%[c]	Yes
Vybrant CFDA SE Cell Tracer Kit	Invitrogen, V12883	Oligodendrocytes	25 µM	30 min	800 (2P)	>2 h	18 ± 4 µm, 45 ± 4 %	54 ± 7%[d]	Yes
Subcellular compartment dyes									
NeuroTrace 435/455 blue fluorescent Nissl stain	Invitrogen, N-21479	Nuclei	1:250	30 min	850 (2P)	>2 h			Yes
NeuroTrace 640/660 deep-red fluorescent Nissl stain	Invitrogen, N-21483	Nuclei	1:250	30 min	740 (2P)	>2 h			Yes
Nuclear-ID Red DNA stain	Enzo Life Sciences, ENZ-52406	Nuclei	1:250	45 min	740 (2P)	>2 h	20 ± 1 µm, 50 ± 1%	96 ± 4%[e]	Yes
POPO-1 iodide (434/456)	Invitrogen, P3580	Nuclei	1 µM	30 min	850 (2P)	>2 h	16 ± 3 µm, 40 ± 3%	100%[f]	Yes
SYTO 64 red fluorescent nucleic acid stain	Invitrogen, S11346	Nuclei	2.5 µM	45 min	700 (2P)	>2 h			Yes
Cell Trace BODIPY TR methyl ester	Invitrogen, C34556	Myelin	100 µM	40 min	780 (2P)	Re-apply after 2 h			Yes, but weak signal
DiOC6(3) (3,3′-Dihexyloxacarbocyanine iodide)	Invitrogen, D273	Myelin	5 µM	45 min	910 (2P)	>2 h			Yes, but weak signal
FluoroMyelin red fluorescent myelin stain	Invitrogen, F34652	Myelin	1:50	30 min	940 (2P)	>2 h			Yes, but weak signal
FluoroMyelin green fluorescent myelin stain	Invitrogen, F34651	Myelin	1:50	30 min	910 (2P)	>2 h			Yes, but weak signal
MitoTracker Red CMXRos	Invitrogen, M7512	Myelin and mitochondria	0.5 µM	30 min	740 (2P)	>2 h	14 ± 1 µm, 35 ± 1%	43 ± 6%[g]	No
MitoTracker Red CMXRos	Invitrogen, M7512	Myelin	8 µM	30 min	740 (2P)	>2 h	18 ± 2 µm, 45 ± 2%	95 ± 2%[h]	No
Functional dyes									
Amplex UltraRed reagent	Invitrogen, A36006	Hydrogen peroxide sensor (extracellular)	200 µM	30 min	RFP excitation (1P) 740 (2P)	~20 min	31 ± 4 µm, 78 ± 4 %		Not applicable
TMRM	Invitrogen, T-668	Mitochondrial potential	0.6 µM	30 min	910 (2P)	>2 h	20 ± 2 µm, 50 ± 2%	60 ± 10%[i]	Not applicable

[a]Percentage based on comparison with the imaging depth of a transgenic mouse line (average of three mice per dye ± s.e.m.).
[b]Labeling efficiency calculated as percentage of a well-established immunohistochemical or transgenic marker double-labeled with a given vital dye (average of three mice per dye ± s.e.m.).
[c]Percentage of anti-Iba1 (rabbit antibody, WAKO)-positive cells double-positive for isolectin.
[d]Percentage of anti-APC (mouse monoclonal antibody clone CC-1, Calbiochem)-positive cells double-positive for CFDA.
[e]Percentage of DAPI-positive cells double-positive for Nuclear-ID.
[f]Percentage of NT530/615 (NeuroTrace red fluorescent Nissl stain, Invitrogen)-positive cells double-positive for POPO-1 iodide.
[g]Percentage of mitochondria in a *Thy1*-MitoS, double-positive for MitoTracker Red.
[h]Percentage of FLM (FluoroMyelin green fluorescent myelin stain, Invitrogen)-positive axons double-positive for MitoTracker Red.
[i]Percentage of mitochondria in a *Thy1*-MitoS, double-positive for TMRM.
Note: for each group, we highlight in **bold** font the dye that, in our hands, is best suited for *in vivo* imaging on the basis of its reliability, brightness, longevity during imaging and ability to be fixed after imaging.

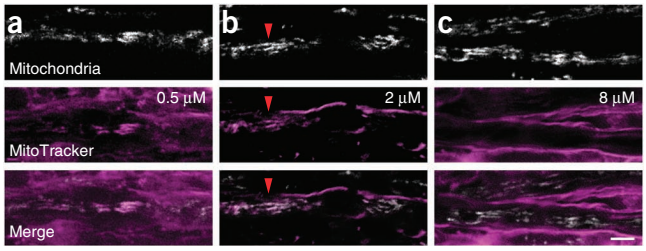

Figure 2 | Concentration dependence of vital dye labeling. The vital dye, MitoTracker Red, can be used to label different structures depending on the concentration. (**a**) Sparse mitochondrial labeling is achieved after application of 0.5 µM MitoTracker Red (magenta), which colocalizes with genetically labeled mitochondria in MitoMice[39] (merge). (**b**) Increasing the dye concentration to 2 µM reveals myelin, whereas only a few mitochondria remain visible (arrowheads). (**c**) After further increasing the dye concentration to 8 µM, only myelin is visible, probably because the intensity of myelin labeling increases compared with the mitochondrial labeling. All animal experiments conformed to institutional guidelines and were approved by the Animal Study Committee of the Regierung von Oberbayern. Scale bar, 5 µm.

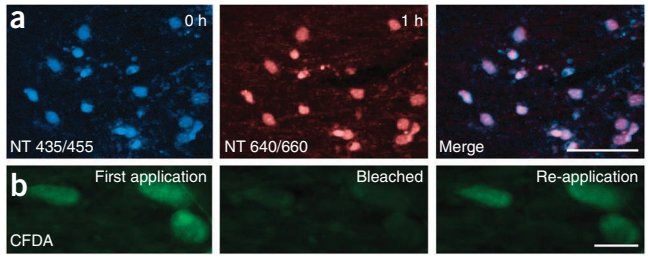

Figure 3 | Reliability of relabeling using vital dyes. (**a**) Consecutive labeling of the same dorsal spinal cord at two time points (0 and 1 h) with two spectrally distinct versions of a nuclear dye, NeuroTrace (NT) 435/455 (blue, left) and NeuroTrace 640/660 (red, middle), reveal a near identical labeling pattern (merge, right). (**b**) CFDA was applied to a healthy spinal cord (left) and bleached with a two-photon laser (middle). After re-application of the vital dye, the same cells were labeled (right). All animal experiments conformed to institutional guidelines and were approved by the Animal Study Committee of the Regierung von Oberbayern. Scale bars, (**a**) 50 µm; (**b**) 10 µm.

time. Both the time-delayed application of two spectral versions of a similar dye (e.g., NeuroTrace 435/455 and NeuroTrace 640/660; **Fig. 3a**) and the re-application of the same dye after photobleaching (e.g., carboxyfluorescein diacetate (CFDA); **Fig. 3b**) indicate that vital dyes lead to a highly reproducible labeling pattern even when repetitively applied (94 ± 5% of nuclei were relabeled with NeuroTrace 640/660 and 97 ± 2% of bleached cells were relabeled with CFDA, $n = 3$ experiments). This high labeling fidelity not only facilitates imaging over longer periods of time but also can be used to detect changes in the cellular or subcellular composition (e.g., cell infiltration can be visualized by applying spectrally distinct versions of nuclear dyes at defined time intervals).

To obtain valid results, it is crucial to control for toxic or confounding effects caused by the dye application (see TROUBLESHOOTING). To exclude toxicity of the dye, different concentrations of the dye should be tested and the highest working dilution should be used. Further, characteristic changes observed after dye application *in vivo* should also be detected in fixed tissue that has neither been imaged nor labeled with a vital dye. In this case, immunohistochemistry or genetic labeling techniques can be used to reveal the structures of interest. These types of experiments are particularly important, as they control not only for dye toxicity but also for phototoxicity and potential damage caused by the surgical preparation.

MATERIALS

REAGENTS

- Mice, 2–12 months old (C57BL/6 mice or transgenic mice, e.g., *Thy1-XFP* (ref. 29)) **! CAUTION** Experiments involving live rodents must conform to all relevant governmental and institutional regulations.
- Ketamine (dose: 87 µg per g body weight, administered intraperitoneally)
- Xylazine (dose: 13 µg per g body weight, administered intraperitoneally)
- Bepanthen oral and nasal gel
- Mouse artificial cerebrospinal fluid (aCSF), available commercially (Harvard Apparatus, Harvard Apparatus, cat. no. 597316) or prepared according to the method provided by Alzet (http://www.alzet.com/products/guide_to_use/cfs_preparation.html)
- DMSO (Sigma-Aldrich, cat. no. D8418)
- PBS, 0.01 M (1× PBS, e.g., Sigma-Aldrich, cat. no. P3813-10PAK)
- Agarose, 2% (wt/vol) (Sigma-Aldrich, cat. no. A9539) in PBS
- Vital dye(s) of choice (see **Table 1** for suitable dyes)
- **Optional reagents**
- Paraformaldehyde, 4% (wt/vol) (PFA) (Sigma-Aldrich, cat. no. P6148) in 0.1 M phosphate buffer (PB) **! CAUTION** PFA is a toxic reagent. Avoid inhalation or contact with skin and eyes. Use proper gloves and a mask to handle PFA **! CAUTION** Follow the relevant institutional rules for using chemicals and discarding waste material.
- Anti-fading medium for fluorescence microscopy (e.g., Vectashield, Vector Laboratories, cat. no. H-1000) or Gel Mount aqueous mounting medium with anti-fading agents (Sigma-Aldrich, cat. no. G0918).

EQUIPMENT

- Magnets with rubber bands to stabilize the mouse during surgery
- Disposable scalpel blade (Feather, blade no. 20)
- Noyes spring scissors, 14-mm blade (Fine Science Tools, cat. no. 15012-12)
- Vannas spring scissors, 4-mm blade (Fine Science Tools, cat. no. 15018-10)
- Dumont no. 3 and no. 5 forceps (Fine Science Tools, cat. no. 11231-30 and 11252-20)
- Sterile triangles (Fine Science Tools, cat. no. 18105-03)
- Gel foam (Ethicon, cat. no. MS0003)
- Silk sutures (Ethicon, cat. no. 667H)
- Betadine swabs or ethanol
- Hypodermic needle (BD, cat. no. 304000)
- Stereomicroscope with 'cold' light illumination through light guide (Olympus)
- Small animal ventilator (Harvard Apparatus, cat. no. 733590)
- Custom-built magnet-mounted retractors
- Intratracheal cannula (1.0 mm OD, 13 mm length; Harvard Apparatus, cat. no. 732731)
- Spinal clamping device (spinal adaptor for a stereotaxic frame; Narishige STS-A)
- Gravity superfusion system containing in-line heater (Warner Instruments)
- Custom-built vacuum system with suction tube
- Plastic pipettes
- Stage customized for attachment of spinal clamping device (e.g., based on Luigs & Neumann SM 5-9 stage and controller unit)

- Multiphoton microscope e.g., Olympus FV1000MPE equipped with femtosecond-pulsed Ti:Sapphire laser (Mai Tai HP, Newport/Spectra Physics) and opto-electrical intensity regulation
- BX51W1 upright microscope (Olympus) equipped with neutral density and infrared filters in light path, fast shutter and filter wheel (Sutter) and a cooled charge-coupled device (CCD) camera (e.g., Sensicam, Cooke). This setup was used for the imaging of Amplex UltraRed.
- Objectives: ×25/1.05 numerical aperture (NA), ×60/0.9 NA, ×20/0.5 NA water-immersion dipping cone objectives (infrared-corrected), ×4/0.13 air objective (for the wide-field setup)
- Dichroic mirrors and emission barrier filters based on the spectra of the vital dyes used
- Image-processing software (e.g., Fiji, Adobe Photoshop) on appropriate computer

EQUIPMENT SETUP

Multiphoton imaging system. We use a multiphoton microscope (Olympus FV1000MPE) with a customized stage to obtain high-resolution images of the superficial dorsal spinal cord. A low-power, high-NA objective (×25/1.05 NA) allows us to acquire large low-resolution overview images and zoomed-in high-resolution detail. The microscope is also equipped with a four-channel nondescanned detector unit that allows imaging of up to three colors simultaneously (and potentially a fourth structural channel, such as second harmonics). The customized stage permits the use of a stereotactic spinal clamping device[24,25] and provides space to place the necessary superfusion, suction and heating lines around the mouse without disrupting the setup.

Stage and stabilization. As described in detail in refs. 24,25, the mouse spinal clamping device must firmly support the lumbar spinal cord, thereby reducing breathing artifacts. For spinal imaging, it is important to angle the clamps in a way that allows the insertion of the objective between them, while leaving room to move laterally along the laminectomy (at an angle of ~45°, depending on the size of the objective tip). A steel plate that holds the clamping device can then be screwed directly onto the stage, allowing translation in the *x*–*y* position, whereas the *z*-position of the mouse can be changed using a lifting mechanism that is part of the spinal clamping device.

Life support. A critical parameter for *in vivo* imaging is maintaining the health of the mouse. To minimize breathing artifacts, especially when imaging subcellular structures, it is helpful to intubate the mouse. In this case, extra care must be taken to ensure that the ventilator tubing is not displaced or kinked. Monitoring of ventilation and anesthesia is essential at all times, as is ensuring that the mouse's body temperature and the temperature in the laminectomy opening are maintained within the physiological range. To achieve the latter, it is necessary to superfuse the laminectomy with a physiological solution, such as mouse aCSF prewarmed to 35–37 °C. An in-line heater, which is feedback-controlled via a thermistor probe, is optimal. Shining an infrared lamp at the mouse during surgery and/or dye incubation may also be used to avoid hypothermia.

PROCEDURE

Surgical exposure of the lumbar spinal cord ● TIMING 15–30 min

1| Surgically expose the lumbar spinal cord as described previously[24–26].

Preparation for vital dye–based imaging ● TIMING 15–30 min

2| Remove the meninges (dura mater and arachnoidea) using the tip of a hypodermic needle to poke a hole, and then carefully peel off the dura with either fine forceps or a bent hypodermic needle (**Fig. 1a**).
▲ CRITICAL STEP Avoid touching the spinal cord or the blood vessels in order to prevent injury.

3| Fill the laminectomy opening with physiological solution (e.g., aCSF) and keep the spinal cord covered with fluid during the subsequent steps of the procedure.

4| Use a spinal clamping device to suspend the mouse and fix the position of the spinal cord. Open the grips of the device and place them in close proximity of the spinal opening, angled at roughly 45 degrees.

5| Clamp the vertebra rostral to the opening. Separate the muscles to make room for the clamp.

6| Clamp the vertebra caudal to the opening, closer to the sacral area, and adjust the angle if needed, keeping in mind the diameter and opening angle of the objective. To achieve optimal stability, we recommend suspending the tail of the mouse as well.

7| Adjust the height of the mouse in order to ensure that it is freely hanging within reach of the objective while the ventilation tubing is resting undisturbed.
▲ CRITICAL STEP Move the clamps horizontally and vertically in order to get the spinal cord into a horizontal orientation (keep the spinal cord as flat as possible) for better image quality and larger fields of view.

8| Heat 2% (wt/vol) agarose in a microwave and use a plastic pipette to make an agarose well around the laminectomy opening, along the muscles and skin. Allow the agarose to set.
▲ CRITICAL STEP This step is temperature sensitive: if agarose is too hot, it will run directly onto the spinal cord, causing damage.

9| Fill the well with physiological solution.
▲ CRITICAL STEP The agarose well must create a seal with the skin and muscles to avoid leakage.

Dye application ● TIMING 30 min–1 h

10| Dilute the dye in physiological solution (the final DMSO concentration must not exceed 3% vol/vol).

11| Replace the physiological solution with dye-containing solution and incubate it in the dark.
▲ CRITICAL STEP Suitable dyes, dye concentrations and incubation times are listed in **Table 1**.

***In vivo* time-lapse imaging ● TIMING 10 min–2 h**
12| Wash the laminectomy opening carefully and repeatedly with physiological solution.
▲ CRITICAL STEP Dye debris on the spinal cord can affect the quality of the images.
? TROUBLESHOOTING

13| Fill the agarose well with physiological solution.

14| Transfer the mouse to the imaging stage. (If an image is needed before dye application, the animal should be transferred after Step 9.)

15| Install the perfusion system to superfuse the spinal cord with prewarmed physiological solution (35–37 °C; flow rate ~1 ml min^{-1}).

16| Use a water-immersion objective and fluorescence excitation to get an overview of the laminectomy opening in order to find the areas of interest.

17| Perform time-lapse imaging and acquire image stacks.

Tissue fixation for immunostaining and confocal microscopy ● TIMING 20 min (plus postfixation time)
18| Transfer the mouse from the imaging stage.

19| Open the clamps and release the mouse from the device.

20| Carefully remove the intra-tracheal cannula.

21| Perfuse the mouse transcardially (with 1× PBS followed by 4% (wt/vol) PFA) after ensuring deep sedation.

22| Isolate and postfix the vertebral column with the spinal cord in 4% (wt/vol) PFA for 12–24 h.

23| Dissect the spinal cord and process for postfixation immunohistochemistry and analysis.

? TROUBLESHOOTING
Problems arising from the surgical opening and spinal imaging in general have been discussed in detail in our previous protocol[26]. Troubleshooting advice on vital dye–based imaging can be found in **Table 2**.

TABLE 2 | Troubleshooting table.

Problem	Possible reason	Solution
Images appear unstable upon acquisition	Loose attachment of the mouse to the positioning system or to the stage	Ensure that the mouse positioning system is securely fastened to the stage and tightened around the vertebrae of the mouse
	Mouse respiration is unstable	Check if intubation cannula has been dislodged from trachea; if so, re-insert Check parameters of ventilator to ensure appropriate ventilation volume and frequency Shut off ventilation briefly during image acquisition; follow by hyperventilation of the mouse
	Body of the mouse is touching the stage (resulting in vibrations)	Adjust the height of the mouse to ensure that it is freely suspended
	Superfusion is disturbing image acquisition	Place the superfusion tubing such that it is resting against the objective and that the solution runs smoothly into and out of the laminectomy

(continued)

TABLE 2 | Troubleshooting table (continued).

Problem	Possible reason	Solution
Signal too dim or not present	Bleeding during imaging	Stop the bleeding and clean the spinal cord
	Bleeding during incubation (might have reduced the effective concentration)	Stop the bleeding, clean the spinal cord and re-incubate the dye
	Agarose well is leaking (resulting in shorter incubation times than expected)	Remake the agarose; re-incubate
	Dye is expired; stock is too old	Prepare fresh stock solution
	Meninges are not completely removed	Remove the meninges
	Concentration is too low or incubation time is too short	Try different concentration/incubation times (**Table 1**)
Dye deposits on the spinal cord	Solution is too cold	Warm solution to 37 °C before incubation
	Solution was not properly dissolved	Make less concentrated stocks (add more DMSO), but in the final dilution, keep the DMSO below 3% (vol/vol)
	Aggregation is an intrinsic dye property	Try incubating the dye with meninges on and removing the meninges before imaging
	Stock solution formed precipitates	Filter the stock solution or briefly centrifuge it at 23,000*g* before making dilution
Dye seems to be toxic	Dye is too concentrated	Repeat the experiment to exclude tissue damage due to surgical access or removal of the meninges Try lower concentrations or shorter incubation times
Nonspecific labeling	Dye is too concentrated	Try lower concentrations or shorter incubation times

Problems arising from the surgical opening and spinal imaging in general have been discussed in detail in our previous protocol[26].

● **TIMING**

Step 1, surgical exposure of the lumbar spinal cord: 15–30 min
Steps 2–9, preparation for spinal imaging: 15–30 min
Steps 10 and 11, dye application: 30 min–1 h
Steps 12–17, *in vivo* time-lapse imaging: 10 min–2 h
Steps 18–23, tissue preparation for immunostaining: 20 min (plus 12–24 h for postfixation)

ANTICIPATED RESULTS

By using this protocol, it is possible to label structural and functional components of the nervous system in conjunction with genetic labeling. To give examples of the types of results that can be expected, in the following paragraphs we summarize the labeling patterns that we observed with the different groups of dyes.

Cell type–specific dyes

Notably, some cellular dyes intended for general cell labeling can have surprising cell-type specificity, as previously shown for sulforhodamine 101 (refs. 22,23) and tomato lectin[30]. In our hands, the Vybrant CFDA SE Cell Tracer mostly labels oligodendrocytes and their processes in the spinal cord (**Fig. 4a–c**). The labeling pattern is similar to the pattern observed in transgenic mice, in which the *PLP* promoter directs the expression of fluorescent proteins to oligodendrocytes[31] (**Fig. 4a** and **Table 1**). In fixed sections of the superficial spinal cord that had been previously exposed to CFDA *in vivo*, about half of the oligodendrocytes (identified by immunostaining for APC[32], **Fig. 4b** and **Table 1**) are brightly labeled, whereas only a small proportion of astrocytes (identified by immunostaining for S100 (ref. 33)) and few, if any, microglia cells (identified by immunostaining for Iba1 (ref. 7)) showed comparable labeling.

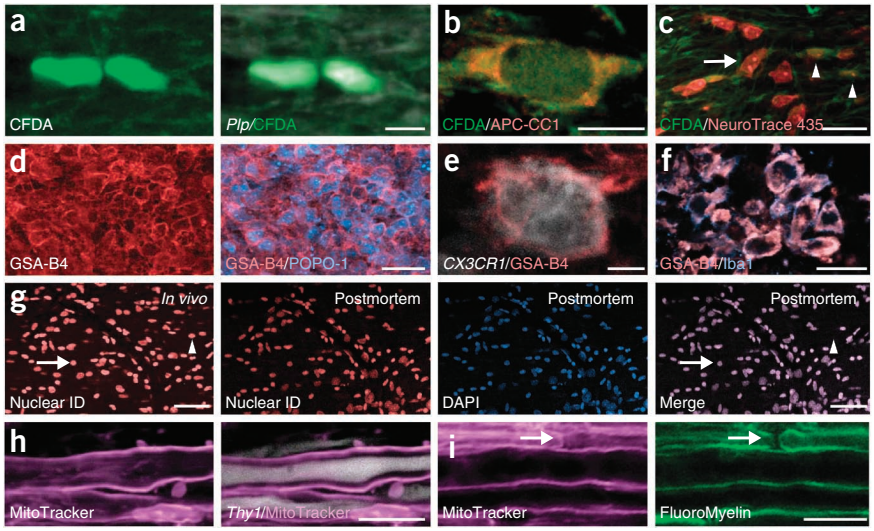

Figure 4 | Structural dyes. (**a**) *In vivo* multiphoton image that illustrates that the dye CFDA (green) colocalizes with somata and processes of transgenically labeled oligodendrocytes in a tamoxifen-injected *Plp*-CreERT2 × TdTomato mouse (TdTomato, white). (**b**) Confocal image of an oligodendrocyte in a mouse spinal cord that was labeled *in vivo* with CFDA (green) and stained postfixation with an APC-specific (CC-1) antibody (red) to label mature oligodendrocytes. (**c**) Lower-magnification image of a spinal cord stained *in vivo* with CFDA (green) and subsequently with the nuclear dye NeuroTrace 435/455 (red) after fixation, illustrating that although some nuclei are CFDA positive (arrowheads) others are not co-labeled (arrow). (**d**) *In vivo* multiphoton image of activated microglia/macrophages labeled with GSA-B4 (red) and counterstained with the nuclear dye, POPO-1 iodide (cyan) in a C57BL/6 mouse, 2 d after onset of EAE. (**e**) *In vivo* image of an activated macrophage/micoglial cell after labeling with GSA-B4 (red) in a *CX3CR1*$^{GFP/+}$ mouse in which macrophages/microglial cells are labeled with GFP (white; ref. 40). (**f**) Confocal image of the spinal cord of an EAE mouse that was stained *in vivo* with GSA-B4 and postfixed with an Iba1-specific antibody (cyan) that labels macrophages and microglia cells. (**g**) *In vivo* multiphoton image of a healthy spinal cord after application of NuclearID Red to visualize nuclei (red). The same spinal cord was fixed after imaging and imaged by confocal microscopy to reveal nearly identical staining (arrow identifies an example of an identical cell *in vivo* and postmortem; arrowhead indicates differences in the labeling pattern, probably as a result of minor changes in the way the spinal cord is angled). Counterstaining the fixed spinal cord with DAPI (cyan) postmortem confirms specific nuclear localization of the *in vivo* NuclearID label (merge). (**h**) *In vivo* multiphoton image of a healthy axon, transgenically labeled in a *Thy1-YFP-16* mouse[29] (YFP, white), and its myelin sheath, labeled with MitoTracker Red (magenta). (**i**) *In vivo* co-labeling of myelin with MitoTracker Red (magenta, left panel) and FluoroMyelin (green, right panel). The arrow identifies a node of Ranvier. All animal experiments conformed to institutional guidelines and were approved by the Animal Study Committee of the Regierung von Oberbayern. Scale bars, (**a**) 10 μm; (**b**) 10 μm; (**c**) 20 μm; (**d**) 50 μm; (**e**) 20 μm; (**f**) 25 μm; (**g**) 50 μm; (**h**) 10 μm; (**i**) 10 μm.

GSA-B4, a lectin that binds to a galactose-containing, membrane-associated glycoconjugate expressed by activated microglia[34], is another example of a cell type–specific label. It has been used previously to detect microglia in fixed tissue[35] and living tissue slices[36]. Fluorescently conjugated GSA-B4 can also be directly applied *in vivo* to label activated macrophages/microglia in a mouse model of multiple sclerosis, experimental autoimmune encephalomyelitis (EAE) (**Fig. 4d–f**)[7]. Although the penetration of the lectin is limited to the most superficial parts of the spinal cord (**Table 1**), postmortem analysis showed that in these areas more than 80% of activated macrophages and microglia cells (identified by immunostaining for Iba1 (ref. 7)) can be brightly labeled by GSA-B4 (**Fig. 4f** and **Table 1**). Although activated macrophages/microglial cells are thus efficiently labeled, it should be noted that GSA-B4 does not stain resting microglial cells in the spinal cord.

Subcellular compartment dyes

In some cases, several dyes and spectral variants are available for a given application. Nuclei, for example, can be consistently labeled *in vivo* with all the nuclear dyes that we have tested. Incubation time and penetration depth do not differ greatly between the dyes tested, which are available in many spectral variants. Further, labeling efficiency approaches 100% as determined by comparing *in vivo* dye labeling with postmortem staining using the well-established nuclear dye DAPI (illustrated for NuclearID Red in **Fig. 4g**). POPO-1 iodide and NuclearID Red were, in our hands, the most suitable nuclear *in vivo* dyes because of their bright staining pattern at a relatively low concentration and because, in contrast to dyes from the NeuroTrace family, they do not show additional labeling of the neuropil.

In other cases, fewer suitable dyes are available. Reliable myelin labeling *in vivo*, for example, can be best accomplished using MitoTracker Red (**Fig. 4h** and **Table 1**). One limitation of MitoTracker Red is, however, that this labeling pattern is not maintained after fixation. If postmortem analysis is planned, the use of FluoroMyelin, which has been previously used to selectively label myelin[37,38], is a good alternative (although the labeling intensity does decrease after fixation). The *in vivo* labeling patterns of FluoroMyelin and MitoTracker Red are nearly identical (**Fig. 4i**). However, a higher concentration of FluoroMyelin is generally required to obtain a bright labeling. In addition, in our hands, the consistency of the labeling pattern and intensity between different experiments was higher with MitoTracker Red. In general, it should be noted that myelin dyes are extremely sensitive to the cleanliness of the spinal preparation, as off-target staining of blood clots or meninges is common. Notably, myelin dyes appear to only label the outermost layers of myelin as indicated by the gap that is visible between the myelin stain and cytoplasmic labeling of the axon (**Fig. 4h**). As the name suggests, MitoTracker Red

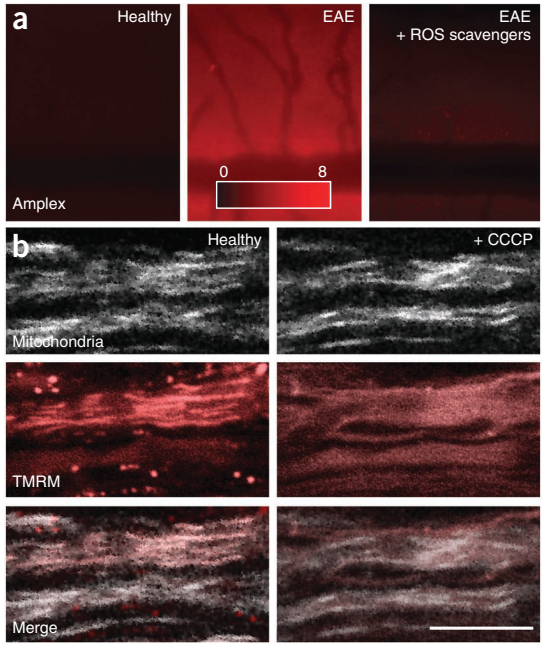

Figure 5 | Functional dyes. (**a**) Measurement of extracellular H_2O_2 concentration detected with Amplex UltraRed in the dorsal spinal cord of healthy mouse (left), a mouse 2 d after onset of EAE (middle) and a mouse at a similar stage of EAE treated intraperitoneally with a cocktail of ROS/RNS scavengers (right). (**b**) Mitochondrial potential was assessed by bath application of TMRM (red, left images). Mitochondrial labeling disappears immediately after application of 100 µM CCCP (right images). All animal experiments conformed to institutional guidelines and were approved by the Animal Study Committee of the Regierung von Oberbayern. Scale bars, (**a**) 250 µm (calibration bar); (**b**) 10 µm. Panel **a** was modified with permission from ref. 7.

can also be used to label mitochondria when applied at very low concentrations (**Fig. 2**). However, this labeling is sparse (only about 40% of the genetically labeled mitochondria are detected with MitoTracker Red), shows limited penetration and, in our hands, does not replace the use of genetically labeled 'MitoMice'[39] (**Table 1**).

Functional dyes

Another use of vital dyes is the detection of toxic mediator release. In the EAE model of multiple sclerosis, for example, it is possible to detect the presence of extracellular hydrogen peroxide using Amplex UltraRed (**Fig. 5a**)[7]. Although only background staining is observed in the spinal cord of control animals (**Fig. 5a**, left), the staining intensity is markedly increased in mice with acute inflammatory lesions in the spinal cord (**Fig. 5a**, middle). If EAE mice are treated with reactive oxygen species/reactive nitrogen species (ROS/RNS) scavengers, Amplex fluorescence diminishes as expected (**Fig. 5a**, right). The lifetime of Amplex is relatively short (~20 min), and thus for prolonged *in vivo* experiments re-application is needed. Amplex can also spuriously label axons and axonal fragments in inflammatory lesions. In addition to detecting the release of reactive molecular species, vital dyes can also be used to assess organelle function. Tetramethylrhodamine (TMRM), for example, can be used to assess the mitochondrial potential in spinal axons *in vivo*[7]. As in the case of MitoTracker, care must be taken to use low concentrations of TMRM to ensure mitochondrial labeling as opposed to myelin staining. Moreover, only a subset of axonal mitochondria will be labeled within the penetration depth when compared with transgenic MitoMice, apparently because the dye can only access a subset of axons (**Fig. 5b**, left and **Table 1**). In those mitochondria that are labeled, however, the dye retention depends on the mitochondrial membrane potential, as application of 100 µM carbonyl cyanide m-chlorophenyl hydrazone (CCCP), a protonophore, will immediately release TMRM from the mitochondria (**Fig. 5b**, right).

Combination with transgenic labels

To further increase the versatility of spinal *in vivo* imaging experiments, dyes can be combined with transgenic labeling. Such combinations can then be used to assess disease models of the spinal cord (**Fig. 6**). We have used the application of myelin dyes in a *Thy1-XFP* transgenic mouse line to study the relationship between demyelination and axon injury after oxidative damage[7]. Taken together, the approach laid out in this protocol greatly increases the number of questions that can be answered in a single *in vivo* imaging experiment without a major investment of time or money by the investigator.

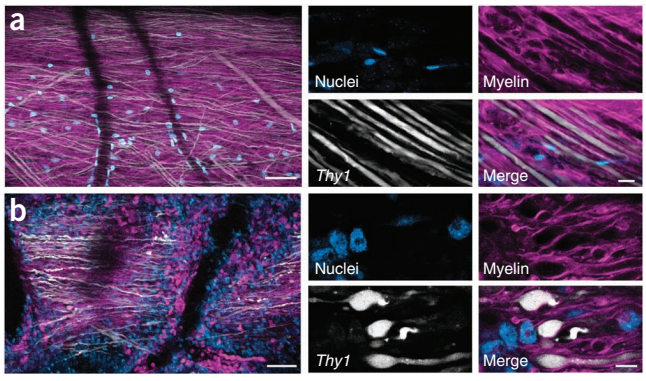

Figure 6 | Typical results from the *Thy1-YFP-16* mouse. (**a**) *In vivo* multiphoton image of the spinal cord of a healthy *Thy1-YFP-16* mouse after application of Mitotracker Red (magenta) and POPO-1 iodide (cyan) to stain myelin and nuclei, respectively. (**b**) Overview of a *Thy1-YFP-16* mouse labeled with the same dye combination at 2 d after onset of EAE. Here, infiltrating nuclei, myelin and axonal damage are indicative of an inflammatory lesion. Note that some inflammatory cells also label with the MitoTracker Red dye. Higher-magnification images of nuclei, myelin and axons are shown on the right. All animal experiments conformed to institutional guidelines and were approved by the Animal Study Committee of the Regierung von Oberbayern. Scale bars, left images, 50 µm; middle and right images, 10 µm.

ACKNOWLEDGMENTS We thank G. Heitmann for excellent technical assistance and D. Matzek for animal husbandry. Work in M.K.'s laboratory is financed through grants from the European Research Council (ERC Starting Grant), and the Deutsche Forschungsgemeinschaft (DFG; Sonderforschungsbereiche (SFB) 571, SFB 870 and SFB-Tr 128), the German Federal Ministry of Research and Education (Competence Network Multiple Sclerosis) and the 'Verein Therapieforschung für MS-Kranke e.V.' T.M. is supported by the Institute of Advanced Studies (Technische Universität München), the Alexander von Humboldt Foundation, the Center for Integrated Protein Science (Munich), the DFG (SFB 596) and the German Center for Neurodegenerative Disease (DZNE Munich). Work on this project was further supported by the national funding agency ('Bundesministerium für Bildung und Forschung') in the frame of ERA-Net '2-photon imaging' (T.M.) and a grant from the DANA foundation to M.K. and T.M. C.D.S. was supported by the Graduate School of Technische Universität München (TUM-GS).

AUTHOR CONTRIBUTIONS M.K., T.M., E.R., C.D.S. and I.N. conceived the experiments. E.R., C.D.S., I.N. and A.D. performed imaging experiments and image analysis. M.K., T.M., E.R., C.D.S. and I.N. wrote the protocol.

COMPETING FINANCIAL INTERESTS The authors declare no competing financial interests.

Published online at http://www.nature.com/doifinder/10.1038/nprot.2013.022. Reprints and permissions information is available online at http://www.nature.com/reprints/index.html.

1. Lichtman, J.W. & Fraser, S.E. The neuronal naturalist: watching neurons in their native habitat. *Nat. Neurosci.* **4** (suppl.) 1215–1220 (2001).
2. Misgeld, T. & Kerschensteiner, M. *In vivo* imaging of the diseased nervous system. *Nat. Rev. Neurosci.* **7**, 449–463 (2006).
3. Kerschensteiner, M. *et al.* *In vivo* imaging of axonal degeneration and regeneration in the injured spinal cord. *Nat. Med.* **11**, 572–577 (2005).
4. Ertürk, A. *et al.* Disorganized microtubules underlie the formation of retraction bulbs and the failure of axonal regeneration. *J. Neurosci.* **27**, 9169–9180 (2007).
5. Debarbieux, F. *et al.* Quantitative analysis by *in vivo* imaging of the dynamics of vascular and axonal networks in injured mouse spinal cord. *Proc. Natl. Acad. Sci. USA* **106**, 9459–9464 (2009).
6. Bartholomäus, I. *et al.* Effector T cell interactions with meningeal vascular structures in nascent autoimmune CNS lesions. *Nature* **462**, 94–98 (2009).
7. Nikic, I. *et al.* A reversible form of axon damage in experimental autoimmune encephalomyelitis and multiple sclerosis. *Nat. Med.* **17**, 495–499 (2011).
8. Siffrin, V. *et al.* *In vivo* imaging of partially reversible T_H17 cell-induced neuronal dysfunction in the course of encephalomyelitis. *Immunity* **33**, 424–436 (2010).
9. Denk, W. *et al.* Two-photon laser scanning fluorescence microscopy. *Science* **248**, 73–76 (1990).
10. Helmchen, F. & Denk, W. Deep tissue two-photon microscopy. *Nat. Methods* **12**, 932–940 (2005).
11. Shu, X. *et al.* Mammalian expression of infrared fluorescent proteins engineered from a bacterial phytochrome. *Science* **324**, 804–807 (2009).
12. Shaner, N.C., Steinbach, P.A. & Tsien, R.Y. A guide to choosing fluorescent proteins. *Nat. Methods* **2**, 905–909 (2005).
13. Livet, J. *et al.* Transgenic strategies for combinatorial expression of fluorescent proteins in the nervous system. *Nature* **450**, 56–62 (2007).
14. Zhao, Y. *et al.* An expanded palette of genetically encoded Ca(2) indicators. *Science* **333**, 1888–1891 (2011).
15. Stosiek, C. *et al.* *In vivo* two-photon calcium imaging of neuronal networks. *Proc. Natl. Acad. Sci. USA* **100**, 7319–7324 (2003).
16. Johannssen, H.C. & Helmchen, F. *In vivo* Ca^{2+} imaging of dorsal horn neuronal populations in mouse spinal cord. *J. Physiol.* **588**, 3397–3402 (2010).
17. Grienberger, C. & Konnerth, A. Imaging calcium in neurons. *Neuron* **73**, 862–865 (2012).
18. Balice-Gordon, R.J. & Lichtman, J.W. *In vivo* visualization of the growth of pre- and postsynaptic elements of neuromuscular junctions in the mouse. *J. Neurosci.* **10**, 894–908 (1990).
19. Akaaboune, M. *et al.* Rapid and reversible effects of activity on acetylcholine receptor density at the neuromuscular junction *in vivo*. *Science* **286**, 503–507 (1999).
20. Magrassi, L., Purves, D. & Lichtman, J.W. Fluorescent probes that stain living nerve terminals. *J. Neurosci.* **7**, 1207–1214 (1987).
21. Lichtman, J.W., Magrassi, L. & Purves, D. Visualization of neuromuscular junctions over periods of several months in living mice. *J. Neurosci.* **7**, 1215–1222 (1987).
22. Nimmerjahn, A., Kirchhoff, F., Kerr, J.N. & Helmchen, F. Sulforhodamine 101 as a specific marker of astroglia in the neocortex *in vivo*. *Nat. Methods* **1**, 31–37 (2004).
23. Nimmerjahn, A., Mukamel, E.A. & Schnitzer, M.J. Motor behaviour activates Bergmann glial networks. *Neuron* **62**, 400–412 (2009).
24. Davalos, D. *et al.* Stable *in vivo* imaging of densely populated glia, axons and blood vessels in the mouse spinal cord using two-photon microscopy. *J. Neurosci. Methods* **169**, 1–7 (2008).
25. Davalos, D. & Akassoglou, K. *In vivo* imaging of the mouse spinal cord using two-photon microscopy. *J. Vis. Exp.* **59**, e2760 (2012).
26. Misgeld, T., Nikic, I. & Kerschensteiner, M. *In vivo* imaging of single axons in the mouse spinal cord. *Nat. Protoc.* **2**, 263–268 (2007).
27. Farrar, M.J. *et al.* Chronic *in vivo* imaging in the mouse spinal cord using an implanted chamber. *Nat. Methods* **9**, 297–302 (2012).
28. Fenrich, K.K. *et al.* Long-term *in vivo* imaging of normal and pathological mouse spinal cord with subcellular resolution using implanted glass windows. *J. Physiol.* **590**, 3665–3675 (2012).
29. Feng, G. *et al.* Imaging neuronal subsets intransgenic mice expressing multiple spectral variants of GFP. *Neuron* **28**, 41–51 (2000).
30. Schwendele, B., Brawek, B., Hermes, M. & Garaschuk, O. High-resolution *in vivo* imaging of microglia using a versatile nongenetically encoded marker. *Eur. J. Immunol.* **42**, 2193–2196 (2012).
31. Leone, D. *et al.* Tamoxifen-inducible glia-specific Cre mice for somatic mutagenesis in oligodendrocytes and Schwann cells. *Mol. Cell. Neurosci.* **22**, 430–440 (2003).
32. Fancy, S.P. *et al.* Axin2 as regulatory and therapeutic target in newborn brain injury and remyelination. *Nat. Neurosci.* **14**, 1009–1016 (2011).
33. Ogata, K. & Kosaka, T. Structural and quantitative analysis of astrocytes in the mouse hippocampus. *Neuroscience* **113**, 221–233 (2002).
34. Streit, W.J. & Kreutzberg, G.W. Lectin binding by resting and reactive microglia. *J Neurocytol.* **16**, 249–260 (1987).
35. Moreira, T.J. *et al.* Enhanced cerebral expression of MCT1 and MCT2 in a rat ischemia model occurs in activated microglial cells. *J. Cereb. Blood Flow Metab.* **29**, 1273–1283 (2009).
36. Dailey, M.E. & Waite, M. Confocal imaging of microglial cell dynamics in hippocampal slice cultures. *Methods* **18**, 222–230 (1999).
37. Watkins, T.A. *et al.* Distinct stages of myelination regulated by gamma-secretase and astrocytes in a rapidly myelinating CNS coculture system. *Neuron* **60**, 555–569 (2008).
38. Monsma, P.C. & Brown, A. FluoroMyelin Red is a bright, photostable and non-toxic fluorescent stain for live imaging of myelin. *J. Neurosci. Methods* **209**, 344–50 (2012).
39. Misgeld, T. *et al.* Imaging axonal transport of mitochondria *in vivo*. *Nat. Methods* **7**, 559–561 (2007).
40. Jung, S. *et al.* Analysis of fractalkine receptor CX(3)CR1 function by targeted deletion and green fluorescent protein reporter gene insertion. *Mol. Cell. Biol.* **20**, 4106–4114 (2000).

Pervasive axonal transport deficits in multiple sclerosis models

Catherine D. Sorbara[1,2], Naomi E. Wagner[1], Anne Ladwig[1], Ivana Nikić[1], Doron Merkler[3,4], Tatjana Kleele[2], Petar Marinković[2], Ronald Naumann[5], Leanne Godinho[2], Florence M. Bareyre[1,6], Derron Bishop[7], Thomas Misgeld[2,6,8*] and Martin Kerschensteiner[1,6*]

[1] Institute of Clinical Neuroimmunology, Ludwig-Maximilians University Munich, Munich, Germany

[2] Institute of Neuronal Cell Biology, Technical University Munich, Munich, Germany

[3] Department of Pathology and Immunology, University of Geneva, Geneva, Switzerland

[4] Division of Clinical Pathology, Geneva University Hospital, Geneva, Switzerland

[5] Transgenic Core Facility, Max-Planck-Institute of Molecular Cell Biology and Genetics, Dresden, Germany

[6] Munich Cluster of Systems Neurology (SyNergy), Munich, Germany

[7] Department of Physiology, Indiana University School of Medicine-Muncie, Muncie, Indiana, USA

[8] German Center for Neurodegenerative Diseases (DZNE), Munich, Germany

* These authors contributed equally to this work.

Correspondence should be addressed to

T.M. (thomas.misgeld@lrz.tu-muenchen.de) or

M.K. (martin.kerschensteiner@med.uni-muenchen.de)

Keywords: multiple sclerosis, axonal transport, mitochondria, microtubules, *in vivo* microscopy

Words: 1042 *Figures:* 3 (+ 8 Suppl. Figures and 5 Suppl. Videos) *References:* 20

Impairments of axonal transport can lead to axon loss. Here we used *in vivo* two-photon imaging to directly measure organelle transport and microtubule dynamics in mouse models of multiple sclerosis, a common inflammatory disease of the central nervous system. We found widespread and persistent transport deficits, which preceded structural alterations of axons, cargos or microtubules, and which could be reversed by acute anti-inflammatory interventions or redox scavenging.

Axon degeneration is a hallmark of the neuroinflammatory disease multiple sclerosis (MS) and causes permanent neurological disability in advanced stages[1,2]. As neurons are highly polarized and extended cells, they critically depend on shuttling organelles along microtubule tracks to and from their soma. Indeed, impairments of axonal transport contribute to axon loss in many neurodegenerative disorders[3,4]. However, if and when axonal transport deficits occur in neuroinflammatory lesions, how they relate to structural axon damage and which inflammatory mediators induce them, is not fully understood.

To address these questions we used an acute experimental autoimmune encephalomyelitis (EAE) model of MS, in which neuroinflammatory lesions with axon damage evolve in the spinal cord of mice (**Fig. 1a,b**). We then established a spinal *in vivo* two-photon imaging approach[5,6] that allowed us to follow the dynamics of individual fluorescently-labelled organelle cargos, such as mitochondria (in *Thy1-MitoCFP* mice[7]) or peroxisomes (in newly generated *Thy1-PeroxiYFP* mice, **Supplementary Fig. 1**), in individual spinal axons (see **Online Methods** and **Supplementary Videos 1** and **2**). Our *in vivo* recordings show that anterograde and retrograde transport of mitochondria and peroxisomes were markedly reduced in spinal axons that pass through neuroinflammatory lesions (**Fig. 1c-f** and **Supplementary Videos 3**). Strikingly, transport was not only reduced in axons that were swollen and hence had entered the degeneration process[6], but also in the majority of normal-appearing axons in the lesion area. Moreover, transport deficits were not only observed in acute lesions, but persisted for several weeks in a progressive MS model (**Supplementary Fig. 2**). Transport deficits resulted in a long-lasting reduction of net organelle delivery from the soma to the synapses, as anterograde deficits were more profound than retrograde ones. In the case of mitochondria, for example, parts of axons that are distal to inflamed sites lack several hundred mitochondria per day (**Supplementary Fig. 3**). As

continued supply of mitochondria and other cargos is essential for neuronal health[3,4], these results suggest that impaired distal organelle supply can contribute to the progressive axonal dystrophy observed in advanced stages of MS[8,9].

To better understand why organelle transport is impaired, we tracked the movements of individual mitochondria through acute neuroinflammatory lesions. Our results show that while parameters, such as moving speed and stop frequency, were only moderately altered, the duration of mitochondrial stops was dramatically increased in neuroinflammatory lesions and often persistent arrests of organelles can be observed (**Supplementary Fig. 4**). Such persistent stops likely explain the accumulation of axonal organelles in neuroinflammatory lesions (**Supplementary Fig. 5**) that have been previously documented in MS tissue[10-12].

We next asked whether focal structural alterations could explain why organelles accumulate in neuroinflammatory lesions. Demyelination, for instance, has been previously shown to associate with organelle arrest in axons[13-15]. To address the role of demyelination *in vivo*, we labelled myelin using a vital dye[16] and measured organelle transport in acute neuroinflammatory lesions. Interestingly, transport deficits were already present in myelinated axons (**Supplementary Fig. 6**). This suggests that – while local demyelination might perpetuate transport deficits[17] – loss of myelin is not necessary to induce such deficits. Another possibility would be that damage to the organelle cargo itself, as described for mitochondria in neuroinflammatory lesions[6,9,11], might lead to transport disruption. However, when we measured mitochondrial transport rates in intact-appearing axons with either normally-shaped or altered mitochondria, we found that transport deficits preceded structural changes to organelles (**Supplementary Fig. 7**). Finally we asked whether alterations of the microtubule tracks, along which organelles travel, interfere with transport. To assess the state of microtubule tracks in individual axons at different stages of neuroinflammatory damage,

we analysed the orientation and tyrosination status of microtubules by electron microscopy and immunohistochemistry, respectively. In parallel, we assayed the density and orientation of dynamic microtubules by *in vivo* two-photon imaging of *Thy1-EB3-YFP* mice[18], which express a fluorescently-tagged version of the plus end-binding protein EB3 in neurons. Together these analyses show that transport deficits occur in axons before marked alterations of the microtubule cytoskeleton. Furthermore, the occurrence of disorganized, tyrosinated and destabilized microtubules in a subset of swollen axons indicates that alterations to the microtubule cytoskeleton might mark the transition to more permanent structural axon damage and predispose affected axons to subsequent degeneration (**Fig. 2**, **Supplementary Fig. 8** and **Supplementary Video 4**).

Our results show that transport deficits are initiated in morphologically normal axons with intact myelin, normal-appearing cargos and unaltered microtubule tracks. Hence, transport deficits appear to represent an early state of inflammation-induced axonal "dysfunction" rather than a later sequel of structural alterations. This suggests that transport deficits could reverse once the underlying inflammatory driving force subsides. Indeed, transport deficits started to recover within a few days after the peak of disease in the acute EAE model. This recovery could be accelerated by treating mice at the peak of their symptoms with a single dose of corticosteroids, an intervention that is commonly used to curb disease exacerbation in MS patients[19] (**Fig. 3a**). Next we asked, which inflammatory mediators could cause such reversible axonal dysfunction. Reactive oxygen species (ROS) and reactive nitrogen species (RNS) were previously shown to induce transport deficits in *vitro*[20] and to initiate structural axon damage *in vivo*[6]. Indeed, when we applied the NO donor, Spermine NONOate, to the exposed spinal cord of healthy *Thy1-MitoCFP* mice, organelle transport came to a complete halt within 90 min, but could be re-started by application of the

NO scavenger cPTIO (**Fig. 3b** and **Supplementary Video 5**). Notably, transport deficits could be induced by NO donor doses that were substantially lower than those required for the induction of structural damage[6]. This suggests that an inflammatory lesion might have a center, in which high doses of reactive species induce structural axon damage, surrounded by a larger "penumbra", in which lower doses of such mediators cause axonal dysfunction. In line with this concept, treatment of EAE mice with ROS/RNS scavengers not only limits structural axon damage, as we have previously shown[6], but also ameliorates axonal transport deficits (**Fig. 3c**).

In summary, our study shows that neuroinflammation induces a pervasive state of reversible subcellular dysfunction of axons, which likely represents a major substrate of acute disease symptoms and that – if perpetuated – could contribute to progressive axon loss in advanced MS. Anti-inflammatory interventions as well as redox scavenging can reverse this transport-based axonal dysfunction and thereby help to counteract emerging axonal dystrophy.

ACKNOWLEDGMENTS

We would like to thank A. Schmalz, M. Adrian, Y. Hufnagel and K. Wullimann for excellent technical assistance, D. Matzek, M. Budak, N. Budak and L. Marinković for animal husbandry. We thank D. Crane (Griffith University, Brisbane) for the gift of anti-PEX14 antibody and R. Hohlfeld for critical reading of the manuscript. We thank E. Ruthazer (McGill University, Montreal) for pointing out the CANDLE denoising algorithm. Work in M.K.'s laboratory is financed through grants from the Deutsche Forschungsgemeinschaft (DFG; Transregio 128), the German Federal Ministry of Research and Education (BMBF; Competence Network Multiple Sclerosis), the European Research Council under the European Union's Seventh Framework Program (FP/2007-2013; ERC Grant Agreement n. 310932), the Hertie-Foundation and the "Verein Therapieforschung für MS-Kranke e.V.". T.M. is supported by the Center for Integrated Protein Science (Munich, EXC 114), the European Research Council under the European Union's Seventh Framework Program (FP/2007-2013; ERC Grant Agreement n. 616791) and the German Center for Neurodegenerative Disease (DZNE Munich). F.M.B. is supported by an independent group leader award of the BMBF. F.M.B., M.K. and T.M. are supported by the Munich Center for Systems Neurology (SyNergy; EXC 1010). M.K. and T.M. are supported by the DFG Priority Program 1710. F.M.B., L.G., and T.M. are supported by the DFG-funded collaborative research center 870. C.S., T.K. and P.M. were supported by the Graduate School of Technische Universität München (TUM-GS)

AUTHORS CONTRIBUTIONS

M.K., T.M. and C.S. conceived the experiments. C.S., M.K. and T.M. performed imaging experiments and image analysis. C.S., N.E.W., A.L., I.N., D.M. and F.M.B. contributed to histological analysis. T.K., R.N., L.G., and P.M. generated and characterized transgenic mouse lines. D.B. and C.S. performed electron microscopy analysis. T.M., M.K. and C.S. wrote the paper.

The authors declare no competing financial interests.

REFERENCES

1. Trapp, B.D. *et al.* Axonal transection in the lesions of multiple sclerosis. *N. Engl. J. Med.* **33**, 278-285 (1998).

2. Trapp, B.D. & Nave, K.A. Multiple sclerosis: an immune or neurodegenerative disorder? *Ann. Rev. Neurosci.* **31**, 247-269 (2008).

3. Coleman, M. Axon degeneration mechanisms: commonality amid diversity. *Nat. Rev. Neurosci.* **6**, 889-898 (2005).

4. Millecamps, S. & Julien J.P. Axonal transport deficits and neurodegenerative diseases. *Nat. Rev. Neurosci.* **14**, 161-176 (2013).

5. Davalos, D. *et al*. Stable in vivo imaging of densely populated glia, axons and blood vessels in the mouse spinal cord using two-photon microscopy. *J. Neurosci. Methods* **169**, 1-7 (2008).

6. Nikić, I., *et al*. A reversible form of axon damage in experimental autoimmune encephalomyelitis and multiple sclerosis. *Nat. Med.* **17**, 495–499 (2011).

7. Misgeld, T., Kerschensteiner, M., Bareyre, F. M., Burgess, R. M. & Lichtman J. W. Imaging axonal transport of mitochondria in vivo. *Nat. Methods* **4**, 559-561 (2007).

8. Schirmer, L., Antel, J.P., Brück, W. & Stadelmann, C. Axonal loss and neurofilament phosphorylation changes accompany lesion development and clinical progression in multiple sclerosis. *Brain. Pathol.* **21**, 428-440 (2011).

9. Witte, M. E., Mahad, D.J., Lassmann, H. & van Horssen, J. Mitochondrial dysfunction contributes to neurodegeneration in multiple sclerosis. *Trends. Mol. Med.* **20**, 179-187 (2014).

10. Ferguson, B., Matyszak, M.K., Esiri, M.M. & Perry, V.H. Axonal damage in acute multiple sclerosis lesions. *Brain* **120**, 393-399 (1997).

11. Mahad, D.J. *et al*. Mitochondrial changes within axons in multiple sclerosis. *Brain* **132**, 1161-1174 (2009).

12. Vergo, S. *et al*. Acid-sensing ion channel 1 is involved in both axonal injury and demyelination in multiple sclerosis and its animal model. *Brain* **134**, 571-584 (2011).

13. Edgar, J.M. *et al*. Oligodendroglial modulation of fast axonal transport in a mouse model of hereditary spastic paraplegia. *J. Cell Biol.* **166**, 121-131 (2004).

14. Kiryu-Seo, S., Ohno, N., Kidd, G.J., Komuro, H. & Trapp, B.D. Demyelination increases axonal stationary mitochondria size and the speed of axonal mitochondrial transport. *J. Neurosci.* **30**, 6658-6666 (2010).

15. Kim, J. Y. *et al*. HDAC1 nuclear export induced by pathological conditions is essential for the onset of axonal damage. *Nat. Neurosci.* **13**, 180-189 (2010).

16. Romanelli, E. *et al.* Cellular, subcellular and functional in vivo labelling of the spinal cord using vital dyes. *Nat. Protoc.* **8**, 481-490 (2013).

17. Nave, K.A. Myelination and support of axon integrity by glia. *Nature* **468**, 244-252 (2010).

18. Kleele, T. *et al.* Microtubule dynamics in developing and diseased neurons. Program No. 467.01/EE2 2013 Neuroscience Meeting Planner. San Diego, CA: Society for Neuroscience (2013).

19. Sellebjerg, F. *et al.* EFNS guideline on treatment of multiple sclerosis relapses: report of an EFNS task force on treatment of multiple sclerosis relapses. *Eur. J. Neurol.* **12**, 939-946 (2005).

20. Stagi, M. *et al.* Breakdown of axonal synaptic vesicle precursor transport by microglial nitric oxide. *J. Neurosci.* **25**, 352-362 (2005).

FIGURE LEGENDS

Figure 1 | *In vivo* imaging of organelle transport in neuroinflammatory lesions. (**a**) *In vivo* two-photon image of the spinal cord of a control *Thy1-YFP-16* x *Thy1-MitoCFP-P* mouse (top) and a *Thy1-YFP-16* x *Thy1-MitoCFP-P* mouse 2 d after onset of EAE (bottom; axons, white; nuclei labeled by *in vivo* application of Nuclear-ID Red, red; mitochondrial channel not shown). (**b**) Magnified views of axons from neuroinflammatory lesions illustrating different stages of axon morphology (N, axon from a control mouse; stage 0, normal appearing axon within an inflammatory lesion; stage 1, swollen axon within an inflammatory lesion; corresponding symbols as used throughout the figures shown on the right). (**c**,**d**) *In vivo* two-photon time-lapse images of control axons (upper panels) and stage 0 axons imaged 2 d after onset of EAE (lower panels) with moving mitochondria (**c**, in *Thy1-YFP-16 x Thy1-MitoCFP-P* mice) and peroxisomes (**d**, in *Thy1-OFP-3 x Thy1-PeroxiYFP-376* mice*)* represented as pseudo-colored overlays (lines represent tracks during the indicated time period). (**e**,**f**) Quantification of anterograde (upper panels) and retrograde (lower panels) mean flux rate in control axons and EAE axons (imaged at 2d after onset) for mitochondria (**e**, n = 9-187 axons from 8-18 *Thy1-YFP-16 x Thy1-MitoCFP-P* mice per group; flux compared to control axons by Kruskal-Wallis test followed by Dunn's Multiple Comparison test) and peroxisomes (**f**, n = 153-157 axons from 6 *Thy1-XFP x Thy1-PeroxiYFP* mice per group; flux compared to control axons by Mann-Whitney test). Pie charts represent the percentage of axons at each stage where no transport was seen (black slice, percentage indicated above). Scale bars are 50 μm in (**a**), 10 μm in (**b**) and 5 μm in (**c**) and (**d**). All graphs show mean + s.e.m.; ** $P < 0.01$; *** $P < 0.001$.

Figure 2 | Transport deficits occur before marked alterations of microtubule tracks. (**a-c**) Ultrastructural analysis of axons in the lumbar spinal cord of a control mouse (**a**) and a mouse perfused 2 d after onset of EAE (**b**, stage 0 axon; **c**, stage 1 axon). Upper panels show overview transmission electron micrographs of the axons, lower panels are larger magnifications (boxed on top) illustrating microtubule morphology (arrows). Polar plots to the right indicate the angle of deviation of microtubules from the corresponding axon axis (n = 22-65 axons from 3 mice per group). (**d**) *In vivo* two-photon assay of dynamic microtubule ends ("comets") in control and EAE (2d after onset) *Thy1-EB3-YFP* mice. Upper panels show *in vivo* time-lapse images of axons from control and EAE (2d after onset) *Thy1-EB3-YFP* mice (YFP, white). Comets and their directionality are highlighted by arrows (green, anterograde; pink, retrograde). Lower panels are polar plots that indicate the angle of deviation of comets from the corresponding axon axis and their directionality. Percentages of anterograde *vs.* retrograde comets are indicated above each polar plot. Significantly fewer comets show an anterograde orientation in stage 1 EAE axons (78 ± 5%) compared to stage 0 EAE axons (94 ± 1%) and control axons (96 ± 1%; $P < 0.001$ for stage 1 compared to stage 0 or control; Kruskal-Wallis test followed by Dunn's Multiple Comparison test). (**e**) Quantification of comet density in control and EAE axons (n = 12-49 axons per group from 4 control and 6 EAE mice; densities in EAE axons compared to control axons by Kruskal-Wallis test followed by Dunn's Multiple Comparison test). Scale bars are 1 μm in **c**, upper panel (also for panels in **a**, **b**); 100 nm in blow-up in **c** (also for magnified details in **a**, **b**) and 5 μm in **d**, right panel (also for middle and left panel). Graph shows mean + s.e.m.; * $P < 0.05$.

Figure 3 | Transport deficits can be reversed by glucocorticoid treatment and redox scavenging

(**a**) Schematic diagram (top) of the treatment of *Thy1-YFP-16 x Thy1-MitoCFP-P* mice with a single dose (20 mg/kg) of methylprednisolone at 2 d after onset of EAE followed by *in vivo* imaging the following day. Lower panels show quantification of anterograde and retrograde mitochondrial flux in EAE mice treated with vehicle ("Vehicle") or methylprednisolone ("Treated") compared to untreated EAE mice imaged at 5 d after onset (n = 33-79 stage 0 axons with normally-shaped mitochondria from 3-5 mice per group; flux in methylprednisolone-treated mice compared to flux in vehicle-treated mice with Mann-Whitney test; "nt", not tested). Pie charts represent the percentage of axons where no transport was seen (black slice, percentage indicated above). As a comparison, dashed gray line and gray pie chart represent average flux and percentage of axons with no transport measured in healthy mice as shown in **Fig. 1**. (**b**) Schematic diagram (top) of the sequential bath application of low-dose nitric oxide donor (Spermine NONOate, 8 mM; "NO") and the NO scavenger cPTIO (500 μM; "+cPTIO") to the exposed lumbar spinal cord of control *Thy1-YFP-16 x Thy1-MitoCFP-P* mice. Lower panels show quantification of anterograde and retrograde flux of mitochondria at different timepoints (n = 22 axons from 5 mice; flux compared to initial timepoint, "0 min", by Kruskal-Wallis test followed by Dunn's Multiple Comparison test). Pie charts represent the percentage of axons where no transport was seen (black slice, percentage indicated above). (**c**) Schematic diagram (top) of the treatment of *Thy1-YFP-16 x Thy1-MitoCFP-P* mice with i.p. injections of vehicle ("Vehicle") or a ROS/RNS scavenger cocktail ("Treated") beginning at weight loss ("-1"), and continued every 12 hours, until 2 days after onset of disease. Lower panels show quantification of mitochondrial flux measured at 2 d after onset with accompanying pie charts of the

percentage of axons without transport (n = 156-158 stage 0 axons with normally-shaped mitochondria from 8 mice per group; flux compared to flux in vehicle-treated mice with Mann-Whitney test). As a comparison, dashed gray line and gray pie chart represent average flux and percentage of axons with no transport measured in healthy mice as shown in **Fig. 1**. All graphs show mean + s.e.m.; * $P < 0.05$; *** $P < 0.001$.

ONLINE METHODS

Animals: In *Thy1-YFP-16* (Jackson Laboratory strain designation: *Tg(Thy1-YFP)16Jrs/J*) and *Thy1-CFP-5* mice a large proportion of axons is labeled, while the *Thy1-GFP-S* line labels only a small subset[21]. In *Thy1-MitoCFP-P* and *Thy1-MitoCFP-S* (Jackson Laboratory strain designation: *Tg(Thy1-CFP/COX8A)S2Lich/J*) mice a mitochondrial import sequence directs CFP expression selectively to neuronal mitochondria[7]. To study mitochondria transport rates in the acute EAE model we used double-transgenic *Thy1-YFP-16* x *Thy1-MitoCFP-P* mice. To study mitochondrial transport in chronic EAE, BiozziABH mice were obtained from Harlan Laboratories (strain designation BiozziABH/RijHsd) and crossed with *Thy1-MitoCFP-P* or *Thy1-MitoCFP-S* mice. F1 mice were used for analysis. *Thy1-YFP-EB3-J045* mice, which express a YFP-tagged version of the plus-end binding protein EB3 selectively in neurons[18], were used for *in vivo* microtubule "comet" analysis and crossed with *Thy1-OFP-3* mice[22] to visualize axons. All animal procedures were performed according to institutional guide-lines and approved by the Regierung von Oberbayern.

Generation of mice with fluorescently labelled peroxisomes: The *Thy1-PeroxiYFP* construct was generated by conventional cloning procedures as previously described[23]. The peroxisomal targeting signal 1 encoding the tripeptide SKL was fused in-frame to the C-terminal end of YFP and cloned downstream of the Thy1 promoter[24]. Transgenic *Thy1-PeroxiYFP* mice were generated by standard pronuclear injection. Several founder lines were screened for neuronal expression and the transgenic mouse strains *Thy1-PeroxiYFP-339* and *Thy1-PeroxiYFP-376* were used in this study. To study transport, these mice were crossed with *Thy1-OFP-3* or *Thy1-CFP-5* mice to visualize axons. Transgenic peroxisome labeling

was validated by immunostaining of endogenous peroxisomes using a rabbit polyclonal antibody specific for the peroxisomal marker, PEX14, a gift from Denis Crane (Griffith University, Brisbane)[25].

Induction of experimental autoimmune encephalomyelitis: Monophasic EAE was induced in adult mice between the ages of 6-12 weeks as previously described[26]. Briefly, mice were immunized with 250 µl of an emulsion comprised of 200-350 µg of purified recombinant myelin oligodendrocyte glycoprotein (MOG, N1-125, expressed in *E. coli*) in complete Freund's adjuvant (Sigma) with 5 mg/ml mycobacterium tuberculosis H37 Ra (Difco). On day 0 and day 2 following immunization, 250-400 ng of pertussis toxin (Sigma) was administered intraperitoneally. Mice were weighed daily and a score was assigned according to the severity of neurological deficits as has been standardized for EAE: 0, no detectable clinical signs; 0.5, partial tail weakness; 1, tail paralysis; 1.5, gait instability or impaired righting ability; 2, hind limb paresis; 2.5, hind limb paresis with partial dragging; 3, hind limb paralysis; 3.5, hind limb paralysis and forelimb paresis; 4, hind limb and forelimb paralysis; 5, death.

A progressive EAE model was induced in BiozziABH x *Thy1-MitoCFP-P* or BiozziABH x *Thy1-MitoCFP-S* adult mice between the ages of 6-12 weeks. For this purpose mice were immunized twice, one week apart, with an emulsion containing purified recombinant MOG (50-150 µg). On day 0 and day 1 following immunizations, pertussis toxin (50-150 ng) was administered intraperitoneally. This protocol resulted in chronic EAE symptoms (**Supplementary Fig. 2**) as described previously in BiozziABH mice[27].

***In vivo* microscopy:** For *in vivo* imaging, the dorsal lumbar spinal cord was surgically exposed as previously described[6,28]. Animals were first anaesthetized with ketamine-xylazine (ketamine 87 mg/kg, xylazine 13 mg/kg) intraperitoneally, and anaesthesia was maintained during imaging sessions by regular injections (every 60 minutes). Mice were first tracheotomised and attached to a small animal ventilator (Harvard apparatus) to ensure a stable breathing rate throughout the imaging session. A laminectomy was then performed to expose the lumbar spinal cord and, when exposed, the spinal cord was continually superfused with artificial cerebral spinal fluid (aCSF). The vertebral column was fixed using a spinal adaptor for a stereotaxic frame (Narishige STS-A)[5], and a well surrounding the spinal opening was built using 4% agarose to hold aCSF throughout the imaging session as previously described[16]. *In vivo* imaging was performed using two-photon microscopes, either a custom-built setup based on the Olympus FV300 scanner or on commercially available Olympus FV1000 MPE and FVMPE-RS systems. All microscopes are equipped with femto-second pulsed Ti:Sapphire lasers (Mai Tai HP or Insight, Spectra-Physics) and laser power was attenuated by a polarization-based beam splitter (Spectra Physics) or acousto-optical modulators.

To image transport of mitochondria, the laser was tuned to 910 nm to simultaneously excite both CFP (mitochondria) and YFP (axons) and fluorescence was collected using emission barrier filters 480/40 for CFP and 535/30 for YFP. To image transport of peroxisomes, the laser was tuned either to 850 nm to excite YFP (peroxisomes) alone, to 910 nm to simultaneously excite CFP (axons) and YFP (peroxisomes) or to 750 nm to excite both YFP (peroxisomes) and OFP (axons), depending on the genotype. In the latter case, fluorescence was collected using a G/R filter set (BA495-540, BA570-625). Time-lapse images were acquired with an x25/1.05 or x60/0.9 dipping cone water-immersion objective at

640x640-pixel resolution. Image stacks were acquired at a rate of less than 3 sec per stack for a total of 5-15 minutes. To assess axonal transport rates in EAE, axons were chosen that were in the area of an inflammatory lesion, which was identified by the presence of damaged axons. To confirm the identification of inflammatory lesions we labelled the exposed spinal cords with Nuclear-ID Red DNA Stain (Enzo Life Sciences, ENZ-52406, 1:250) in some animals as previously described[16]. Following dye incubation, the spinal cord was washed thoroughly with aCSF, and mitochondria, axons and nuclei could be imaged simultaneously with confocal laser lines 458, 515 and 559 (excitation DM405-488/515/559/635) or with a two-photon microscope at a wavelength of 740 nm and a G/R filer set (BA495-540, BA570-625).

To assess the myelination status of axons *in vivo*, MitoTracker Red CMXRos (Invitrogen, M7512; this dye labels myelin at higher concentrations, even though it is primarily described as a mitochondrial dye[16]) was applied to the spinal cord at a concentration of 8 μM for 30 min in the dark prior to imaging followed by an aCSF wash as previously described[16]. Axons were imaged using C/Y/R filer set (BA420-460 for mitochondria, BA520-560 for axons, and BA575-630 for myelin) with the laser tuned to 850 nm.

To image microtubule dynamics *in vivo* a commercially available Olympus FVMPE-RS multi-photon imaging system was used. Here the laser was tuned to 930 nm and fluorescence was collected using emission barrier filters 535/30 for YFP. Time-lapse images were acquired with an x25/1.05, zoom 6.5, dipping cone water-immersion objective at 640x640-pixel resolution. Images were averaged over 5 frames and taken at 2 second intervals (100 images were acquired for each time-lapse). In EAE animals, Nuclear-ID Red DNA Stain (as above) was applied as described above to identify inflammatory lesions.

Image processing and analysis: To determine transport flux, i.e. the number of mitochondria or peroxisomes travelling in the anterograde or retrograde direction per minute, we counted the number of fluorescent organelles, which passed a vertical line drawn through the center of the video. In the figures, bar graphs show the mean flux (+ s.e.m.) of all axons analysed; the pie chart below shows the percentage of all axons with and without transport over the observation period that we observed. For single particle analysis, the movement of the organelle was traced using the "Manual Tracking" plugin available in the open-source software ImageJ/Fiji (http://fiji.sc). An organelle was considered motile if its displacement exceeded 5 μm over the length of the movie. A stop was counted when a previously motile organelle moved less than 2 pixels per second while a persistent stop was defined as a previously motile organelle, which did not move again for the remaining observation period (and paused at least for 100 sec). The average speed was calculated as the total distance travelled divided by the observation time while average moving speed excluded time spent stopping.

Axon damage in neuroinflammatory lesions was staged as described previously[6]. Briefly, stage 0 axons were morphologically unaltered, stage 1 axons contained focal swellings and stage 2 axons were fragmented or end-bulbs. Stage 0 axons were further differentiated in axons with normal-appearing and altered mitochondria using the mitochondrial shape factor also described previously[6]. The shape factor is calculated for each mitochondrion by dividing its length by its width. These measurements were taken using the "freehand line" tool in Image J/Fiji. In a given field of view all mitochondria within an axon were measured and then averaged. An axon which had an average mitochondrial shape factor two standard deviations below the average shape factor measured in control axons from healthy mice was deemed to have altered mitochondria.

To assess microtubule dynamics we measured the density of EB3-YFP comets using the "MTrackJ" plugin available in Image J/Fiji. The number of times a comet was seen traveling in either the anterograde or retrograde direction was summed and divided by the observed area of the axon (taken as an average from three measurements at three different time points). For illustration, a sub-stack of 20 frames was projected and comets were drawn as arrows after visual confirmation.

Time-lapse movies were filtered and denoised using the CANDLE (Collaborative Approach for eNhanced Denoising under Low-light Excitation) algorithm[29] for presentation as Supplementary Videos, as well as for the evaluation of comet density and orientation. Organelle transport was evaluated using unprocessed time-lapse files. Supplementary Videos were also registered using the Fiji plugin "StackReg" to reduce breathing artefacts.

For figure representation, different channels of confocal or two-photon image series were combined in pseudocolor using the "screen" function in Adobe Photoshop. Gamma was adjusted nonlinearly to enhance low-intensity objects, and *in vivo* images were denoised using the aforementioned CANDLE algorithm. In **Supplementary Fig. 1a**, multiple images were stitched together to create a large montage and masking was used to obscure borders between individual images. In **Supplementary Fig. 4a**, kymographs were created using the 'reslice' tool in ImageJ/Fiji.

***In vivo* analysis of pharmacological interventions:** To assess the effect of glucocorticoids on alleviating the axonal transport deficit in EAE, we induced an acute EAE model in *Thy1-YFP-16* x *Thy1-MitoCFP-P* mice as described above. Two days following the onset of disease mice were treated intraperitoneally with vehicle (saline) or 20 mg/kg of methylprednisolone-

21-hydrogensuccinat (Urbason soluble, Sanofi Aventis). The following day, mice with a score of at least 2.5 were anaesthetized, placed on breathing support and spinal cords exposed for imaging as described above. A minimum of 10 axons were followed per animal found within or adjacent to a lesion area to assess axonal transport levels. The experimenter was blind to the treatment during scoring, imaging and analysis.

In order to assess the effects of exogenous RNS on axonal transport we exposed the dorsal lumbar spinal cord of anaesthetized healthy *Thy1-YFP-16* x *Thy1-MitoCFP-P* mice and applied the NO Donor, Spermine NONOate ((Z)-1-[N-[3-aminopropyl]-N-[4-(3-aminopropylammonio)butyl]-amino]diazen-1-ium-1,2-diolate, Cayman Chemicals) at a concentration of 8 mM (diluted in aCSF from a stock solution of 100 mM in 10 mM NaOH, pH 9). The same axons were imaged before application and every 30 min following application of the donor and transport rates were measured. At each imaging timepoint, the NO donor was replenished. Ninety minutes after NO donor application, when the majority of transport had ceased, aCSF containing 500 μM cPTIO (2-(4-carboxyphenyl)-4,4,5,5-tetramethylimidazoline-1-oxyl-3-oxide, Invitrogen), an NO scavenger[30], was added to the spinal cord. After 30 minutes incubation axonal transport rates were re-assessed. As a control, transport rates in axons from healthy *Thy1-YFP-16* x *Thy1-MitoCFP-P* mice were repetitively imaged every 30 minutes for 90 minutes in the presence of NO Donor vehicle and showed stable transport rates.

To evaluate whether ROS and RNS scavengers could ameliorate axonal transport deficits in EAE mice, we induced an acute EAE model in *Thy1-YFP-16 x Thy1-MitoCFP-P* mice as described above. Beginning at weight loss, mice were treated intraperitoneally with either vehicle (3% DMSO) or a ROS/RNS scavenger cocktail of the following components: 20 mg/kg FeTPPS (5,10,15,20-tetrakis(4-sulfonatophenyl)porphyrinate iron (III) chloride,

Calbiochem), 50 mg/kg PBN (N-tert-butyl-α-phenylnitrone, Sigma), 15 mg/kg EUK143 (Caymen Chemicals) and 1 mg/kg of cPTIO per dose. FeTPPS is a peroxynitrate scavenger[31], PBN is a scavenger of superoxide and hydroxyl radicals[32], while EUK134 is a catalase and superoxide dismutase analogue[33]. ROS/RNS scavengers were injected every 12 hours until 2 days after onset of disease (7 injections in total) as we previously established[6]. At this time, imaging and evaluation was performed as described above for the glucocorticoid therapy by an experimenter who was blind to the treatment during scoring, imaging and analysis.

Electron microscopy analysis of microtubules: To evaluate microtubule organization in axons by electron microscopy, healthy and EAE (2 days after onset) *Thy1-GFP-S* x *Thy1-MitoCFP-P* mice were perfused intracardially with 0.9% NaCl, containing Heparin-EDTA solution until exsanguinated (approximately 3-5 minutes) followed by approximately 80 ml of 2.5% glyceraldehyde and 2% paraformaldehyde in 0.1M PBS (Electron Microscopy Sciences). Lumbar spinal cord tissue was immediately dissected and post-fixed for 2 hours at 4°C in the same fixative used during perfusion. The tissue was then rinsed thoroughly in 0.1 M PBS and embedded in a 4% agarose block. Dorsal sections (100 μm thick) were cut using a vibratome in 0.1 M PBS. Sections were then washed in 3 changes of 0.1 M sodium-cacodylate buffer, stained with 1% osmium-tetroxide in sodium cacodylate (0.1 M) at 4°C for 1 hour, washed again in 3 changes of 0.1 M sodium-cacodylate buffer and then dehydrated in increasing ethanol concentrations. The dried sections were then incubated in propylene oxide, embedded in Araldite502/Embed812 resin (Electron Microscopy Sciences) and polymerized at 60°C for 2 days. Serial ultrathin sections were cut, collected onto pioloform-coated slot grids, and counterstained with aqueous uranyl acetate and Reynold's lead citrate (30 min each). Electron micrographs were obtained at 120KV using a JEOL JEM-1400 equipped with

a Gatan Ultrascan 1000XP camera. Evaluation was performed by measuring the angle of deviation of the microtubule from the axonal axis as described previously[34] using Image J /Fiji.

In situ **analysis of mitochondria and microtubules:** To assess mitochondrial density in fixed tissue, we perfused *Thy1-YFP-16* x *Thy1-MitoCFP-S* double transgenic mice transcardially with PBS followed by 4% PFA at 2d after onset of EAE. Following overnight incubation in PFA and 2-5 day incubation in 30 % sucrose, thirty micron longitudinal sections of the lumbar spinal cord were cryosectioned and stained with NeuroTrace® 640/660 (Invitrogen, N-21483, 1:500) or a rabbit anti-Iba-1 polyclonal antibody (Wako, 019-19741, 1:200) to identify inflammatory lesions. High resolution images were obtained with an Olympus FV1000 confocal microscope equipped with standard filter sets and an x60/1.42 oil objective. Axons adjacent to the lesion were staged and divided into 20 micron segments, in which mitochondrial shape factor and density were quantified using Image J/Fiji.

To quantify the proportion of tyrosinated tubulin by immunohistochemistry, we perfused mice transcardially with comparably slow rate of 5 ml/min (in all other instances, this rate was 20 ml/min) for 2-3 minutes in PBS and 15 minutes in 4% PFA. The tissue was then microdissected immediately and post-fixed for an additional 30 minutes in 4% PFA. After post fixation, the tissue was transferred into 0.2 M PB overnight at 4°C. The following day the tissue was transferred into a 15% sucrose solution in PBS for half a day at room temperature and then into a 30% sucrose solution overnight at 4°C. Tissue was then embedded in OCT, cryosectioned and 20 µm thick sections were collected into cell-culture 8-well plates for free-floating staining. After methanol incubation and blocking of non-specific staining with 10% goat serum, sections were counterstained for total tubulin with rabbit

polyclonal anti-β3 tubulin antibody (Covance, PRB-4335P, 1:500) and for destabilized tubulin with a rat polyclonal anti-tyrosinated tubulin (Abcam, Ab6160, 1:500) antibody. After completion of staining and washing, slides were mounted with Vectashield® mounting medium, allowed to dry for at least 30 minutes and then immediately imaged with the Olympus FV100 confocal microscope as the antibody signal began to decay after 24 hours. Imaging parameters were kept identical between control and EAE tissue so that ratiometric measurements of tyrosinated versus total tubulin expressed by their respective mean gray values could be calculated. Only those axons which appeared positive for β3 tubulin were included in the evaluation.

Statistics: All data sets were tested for normal distribution with the D'Agostino-Pearson normality test using GraphPad Prism software. If the data sets failed said test, a non-parametric test was chosen to compare the significance of means between groups (Mann-Whitney test for two samples, Kruskal-Wallis test followed by Dunn's Multiple Comparison test for more than two samples). The chosen statistical test is indicated in each accompanying figure legend along with its corresponding *P*-value if applicable.

REFERENCES (ONLINE METHODS)

21. Feng, G.*, et al.* Imaging neuronal subsets in transgenic mice expressing multiple spectral variants of GFP. *Neuron* **28**, 41-51 (2000).

22. Brill, M. S., Lichtman, J.W., Thompson, W., Zuo, Y. & Misgeld, T. Spatial constraints dictate glial territories at murine neuromuscular junctions. *J. Cell. Biol.* **195**, 293-305 (2011).

23. Marinkovic, P., Godinho, L. & Misgeld, T. Generation and screening of mice with transgenic neuronal labeling controlled by Thy1 regulatory elements. in *Imaging in Neuroscience: A Laboratory Manual* (ed. Helmchen, F., Konnerth, A., & Yuste, R) 207-213 (Cold Springs Harbor Lab Press, Plainview, NY, 2011).

24. Caroni, P. Overexpression of growth-associated proteins in the neurons of adult transgenic mice. *J. Neurosci. Methods* **71**, 3-9 (1997).

25. Nguyen, T., Bjorkman, J., Paton, B.C. & Crane, D.I. Failure of microtubule-mediated peroxisome division and trafficking in disorders with reduced peroxisome abundance. *J. Cell Sci.* **119**, 636-645 (2006).

26. Abdul-Majid, K.B.*, et al.* Screening of several H-2 congenic mouse strains identified H-2(q) mice as highly susceptible to MOG-induced EAE with minimal adjuvant requirement. *J. Neuroimmunol.* **111**, 23-33 (2000).

27. Baker, D.*, et al.* Induction of chronic relapsing experimental allergic encephalomyelitis in Biozzi mice. *J. Neuroimmunol.* **28**, 261-270 (1990).

28. Misgeld, T., Nikic, I. & Kerschensteiner, M. In vivo imaging of single axons in the mouse spinal cord. *Nat. Protoc.* **2**, 263-268 (2007).

29. Coupe, P., Munz, M., Manjon, J.V., Ruthazer, E.S. & Collins, D.L. A CANDLE for a deeper in vivo insight. *Med. Image Analysis* **16**, 849-864 (2012).

30. Yune, T.Y.*, et al.* Increased production of tumor necrosis factor-alpha induces apoptosis after traumatic spinal cord injury in rats. *J. Neurotrauma* **20**, 207-219 (2003).

31. Bolton, C., Scott, G.S., Smith, T. & Flower, R.J. The acute and chronic phases of chronic relapsing experimental autoimmune encephalomyelitis (CR EAE) are ameliorated by the peroxynitrite decomposition catalyst, 5,10,15,20-tetrakis(4-sulfonatophenyl)porphyrinatoiron (III) chloride, (FeTPPS). *Eur. J. Pharmacol.* **601**, 88-93 (2008).

32. Fan, L.W.*, et al.* alpha-Phenyl-n-tert-butyl-nitrone attenuates lipopolysaccharide-induced brain injury and improves neurological reflexes and early sensorimotor behavioral performance in juvenile rats. *J. Neurosci. Res.* **86**, 3536-3547 (2008).

33. Baker, K.*, et al.* Synthetic combined superoxide dismutase/catalase mimetics are protective as a delayed treatment in a rat stroke model: a key role for reactive oxygen species in ischemic brain injury. *J. Pharmacol. Exp. Ther.* **284**, 215-221 (1998).

34. Erturk, A., Hellal, F., Enes, J. & Bradke, F. Disorganized microtubules underlie the formation of retraction bulbs and the failure of axonal regeneration. *J. Neurosci.* **27**, 9169-9180 (2007).

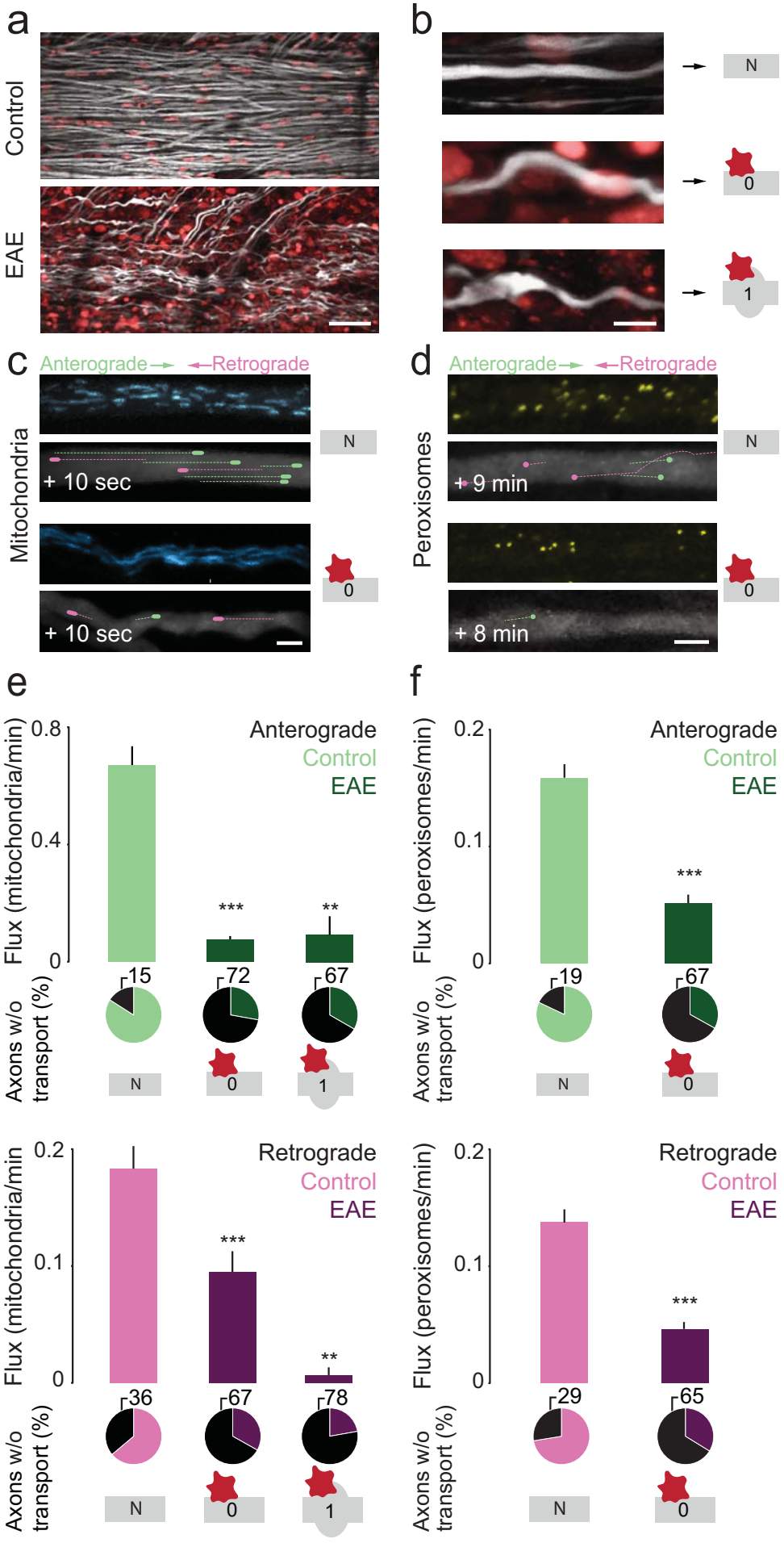

Sorbara et al., Figure 1

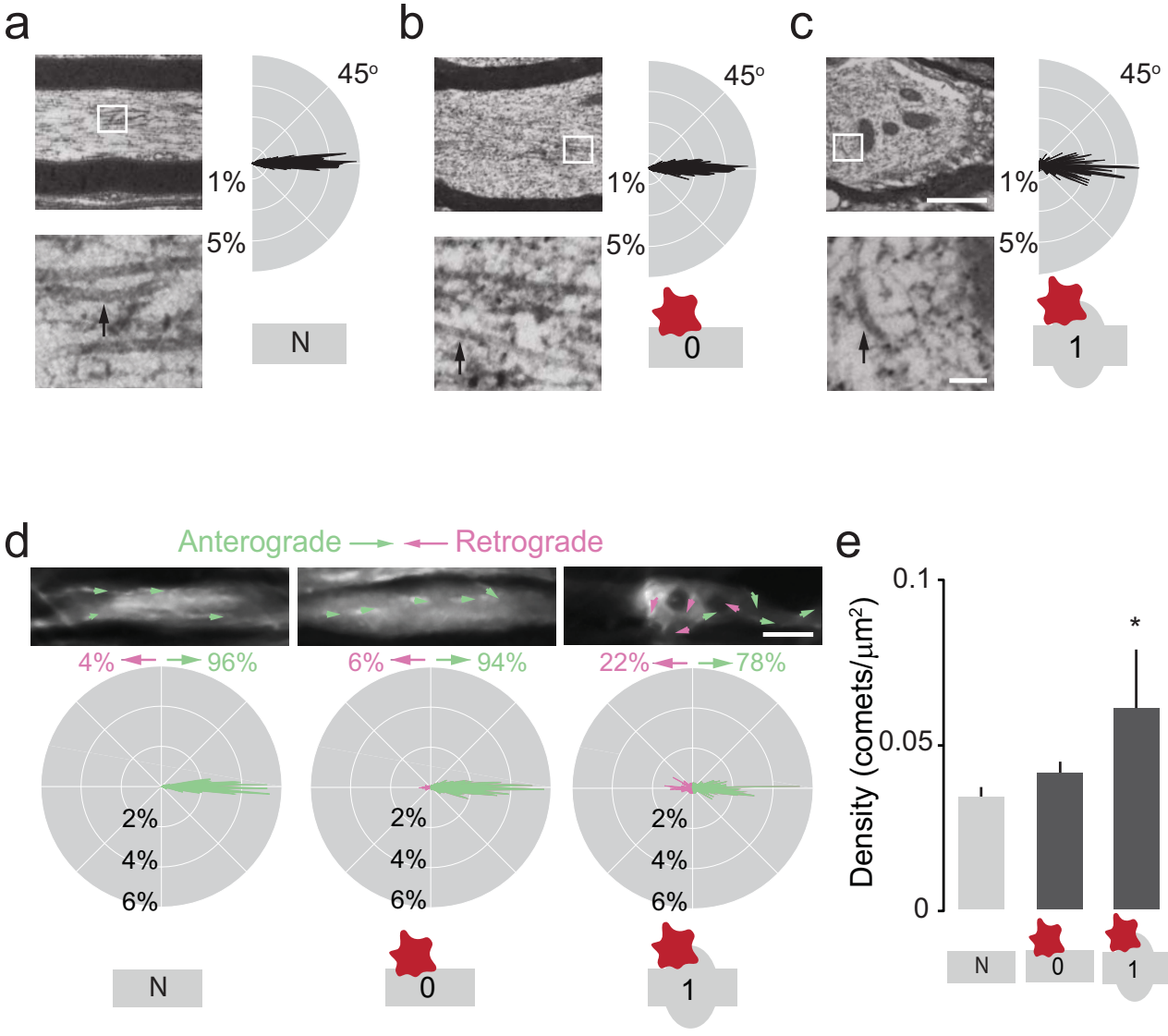

Sorbara et al., Figure 2

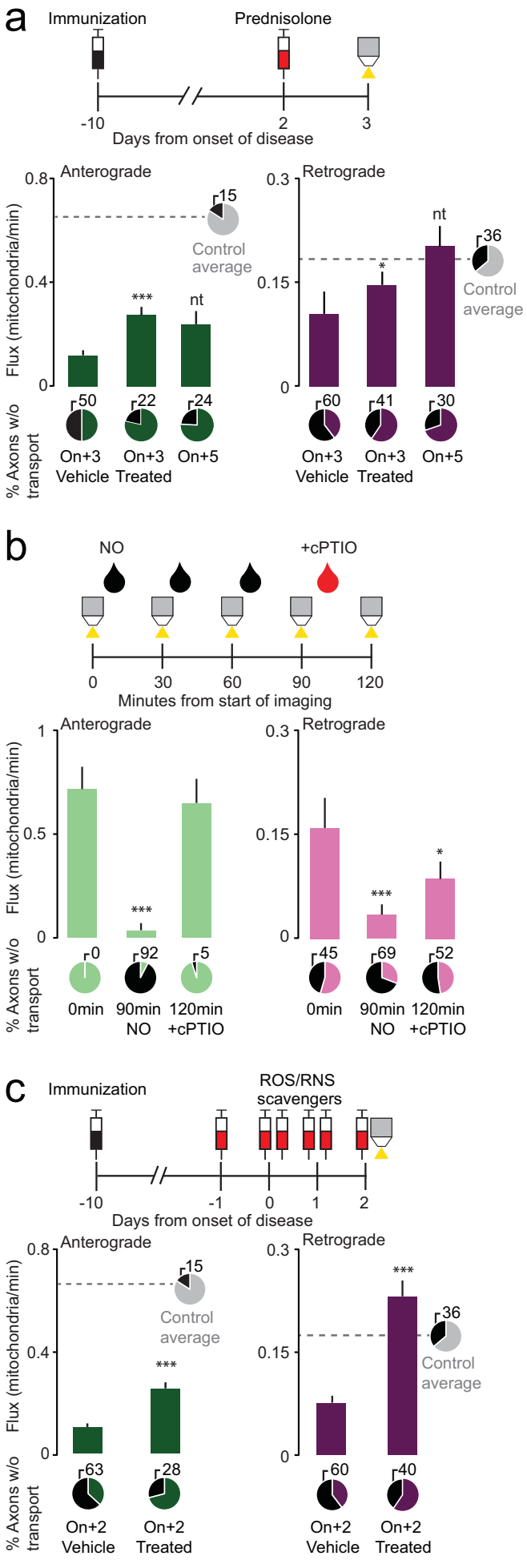

Sorbara et al., Figure 3

Pervasive axonal transport deficits in multiple sclerosis models

– Supplementary Information –

Catherine D. Sorbara[1,2], Naomi E. Wagner[1], Anne Ladwig[1], Ivana Nikić[1], Doron Merkler[3,4], Tatjana Kleele[2], Petar Marinković[2], Ronald Naumann[5], Leanne Godinho[2], Florence M. Bareyre[1,6], Derron Bishop[7], Thomas Misgeld[2,6,8*] and Martin Kerschensteiner[1,6*]

[1] Institute of Clinical Neuroimmunology, Ludwig-Maximilians University Munich, Munich, Germany

[2] Institute of Neuronal Cell Biology, Technical University Munich, Munich, Germany

[3] Department of Pathology and Immunology, University of Geneva, Geneva, Switzerland

[4] Division of Clinical Pathology, Geneva University Hospital, Geneva, Switzerland

[5] Transgenic Core Facility, Max-Planck-Institute of Molecular Cell Biology and Genetics, Dresden, Germany

[6] Munich Cluster of Systems Neurology (SyNergy), Munich, Germany

[7] Department of Physiology, Indiana University School of Medicine-Muncie, Muncie, Indiana, USA

[8] German Center for Neurodegenerative Diseases (DZNE), Munich, Germany

* These authors contributed equally to this work.

Correspondence should be addressed to

T.M. (thomas.misgeld@lrz.tu-muenchen.de) or

M.K. (martin.kerschensteiner@med.uni-muenchen.de)

Keywords: multiple sclerosis, axonal transport, mitochondria, microtubules, *in vivo* microscopy

SUPPLEMENTARY FIGURE LEGENDS

Supplementary Figure 1 | Characterization of *Thy1-PeroxiYFP* mice. (**a**) Overview of the lumbar spinal cord from a *Thy1-PeroxiYFP* mouse (line POY339) counterstained with NeuroTrace to label nuclei (cyan). (**b**) Dorsal root ganglion (DRG; top) and motor neuron (bottom) of the same mouse line shows overlay of transgenically-labeled peroxisomes with immuno-labeling of peroxisomes using PEX-14 antibody. Scale bar in **a**, 500 μm; in **b**, 10 μm.

Supplementary Figure 2 | Transport deficits persist in progressive EAE. (**a**) Clinical course of BiozziABH x *Thy1-MitoCFP-P* mice (n = 17 mice) indicating acute (On+2) and chronic (On+60) timepoints. (**b**) Quantification of mitochondrial flux in control and EAE (On+2 and On+60) EAE BiozziABH x *Thy1-MitoCFP-P* mice plotted as mean flux rate + s.e.m (n = 68-170 axons from 4-9 mice per group; flux compared to control axons by Kruskal-Wallis test followed by Dunn's Multiple Comparison test). Pie charts represent the percentage of axons at each stage where no transport was seen (black slice, percentage indicated above). * $P < 0.05$; *** $P < 0.001$.

Supplementary Figure 3 | Net transport of mitochondria is significantly decreased in both acute and progressive EAE models. Quantification of mitochondrial transport in *Thy1-YFP-16* x *Thy1-MitoCFP-P* control axons and stage 0 axons 2 d after onset of EAE shows a significant decrease in net transport towards the axon periphery (n = 158-187 axons from 8-18 mice per group; compared to control axons by Mann-Whitney test). Similarly, in progressive EAE using BiozziABH x *Thy1-MitoCFP-P* mice net transport is significantly decreased both at acute and chronic timepoints compared to controls (n = 68-170 axons from 4-9 mice per

group; Kruskal-Wallis test followed by Dunn's Multiple Comparison test). Bars represents mean + s.e.m.; *** $P < 0.001$.

Supplementary Figure 4 | Increased stop duration in EAE stage 0 axons. (**a**) Kymograph of a control axon (*left*) and a stage 0 axon, 2 d after onset of EAE (*right*) in *Thy1-YFP-16* x *Thy1-MitoCFP-P* mice, illustrating single mitochondrial transport characteristics such as average speed, moving speed and stopping. (**b**) Quantification of single mitochondrial transport characteristics (n = 81-454 mitochondria, n = 118-134 stage 0 axons with normally shaped mitochondria from 8-18 mice per group; compared to control axons by Mann-Whitney test). (**c**) Line diagram of mitochondrial stop durations taken from 250 randomly chosen stops organized from shortest (1) to longest (250). Inset shows percentage of all tracked mitochondria with persistent stops. Values expressed as mean + s.e.m. *** $P < 0.001$.

Supplementary Figure 5 | Organelle accumulations are observed in EAE axons *in situ*. (**a**) Analysis of mitochondrial density in different stages of axon damage in fixed tissue derived from *Thy1-YFP-16* x *Thy1-MitoCFP-S* control mice and mice 2 d after onset of EAE, measured per 20 μm axon segment. Density significantly increased compared to control axons beginning in stage 0 axons with normal-appearing mitochondria (symbolized by single cyan elliptic mitochondrion symbol; n = 47-205 segments from 10-35 axons, n = 3-4 mice per group; Kruskal-Wallis test followed by Dunn's Multiple Comparison test). Values > $1/\mu m^2$ were not resolvable and set to $1/\mu m^2$ for calculations. (**b**) Representative confocal images of *Thy1-YFP-16* x *Thy1-MitoCFP-S* axons from each axon stage with a 20 μm segment highlighted in cyan. Black lines in **a** indicate mean ± s.e.m.; *** $P < 0.001$.

Supplementary Figure 6 | Axonal transport deficits are present in myelinated axons. (**a**) *In vivo* two-photon image of a control axon (*left*) and a stage 0 axon, 2 days after onset of EAE (*right*). Axons (gray) and mitochondria (cyan) are transgenically labelled in a *Thy1-YFP-16* x *Thy1-MitoCFP-P* mouse and myelin sheaths (orange) are labeled with a vital dye, MitoTracker Red. (**b**) Quantification of mitochondrial flux in myelinated control and myelinated EAE axons (n = 31-40 axons from 3-4 mice per group; flux compared to control axons by Mann-Whitney test). Pie charts represent the percentage of axons where no transport was seen (black slice, percentage indicated above). Scale bar in **a**, 10 μm. Bars represent mean + s.e.m.; ** $P < 0.01$; *** $P < 0.001$.

Supplementary Figure 7 | Axon transport deficits precede alterations in mitochondrial morphology. Comparison of stage 0 axons (EAE, 2 days after onset) with normal-appearing mitochondria (symbolized by single cyan elliptic mitochondrion symbol) and those with altered mitochondrial shape (multiple cyan spherical mitochondria symbols) indicate that mitochondrial flux is significantly decreased before morphological damage becomes apparent (n = 53-134 axons from 8-18 mice per group; flux compared to control axons by Kruskal-Wallis test followed by Dunn's Multiple Comparison test). Control values are replotted from **Fig. 1e**. Pie charts represent the percentage of axons at each stage where no transport was seen (black slice, percentage indicated above). Bars represent mean + s.e.m.; ** $P < 0.01$; *** $P < 0.001$.

Supplementary Figure 8 | *In situ* analysis of post-translational microtubule alterations. (**a**) Confocal images of *Thy1-YFP-16* x *Thy1-MitoCFP-P* mice (shown is YFP channel) immuno-labeled with anti-tyrosinated tubulin antibody to visualize tyrosinated (and hence

likely destabilized; "Tyr") microtubules in control mice and EAE mice at 2 days after onset. (**b**) Quantification of levels of tyrosinated tubulin immunoreactivity in axons, expressed as a ratio of tyrosinated tubulin over total tubulin (immuno-labeled with anti-βIII tubulin antibody; n = 212, 244 and 5 axons for control, stage 0 and stage1, respectively, from 4-5 mice per group; ratio compared to control axons by Kruskal-Wallis test followed by Dunn's Multiple Comparison test). Scale bar in **a**, 10 μm. Values expressed as mean + s.e.m; ** $P < 0.01$; *** $P < 0.001$.

SUPPLEMTARY VIDEO LEGENDS

Supplementary Video 1│ *In vivo* two-photon time-lapse showing mitochondrial transport in a spinal axon of a healthy *Thy1-YFP-16* x *Thy1-MitoCFP-P* mouse.

Supplementary Video 2│ *In vivo* two-photon time-lapse showing peroxisome transport in a spinal axon of a healthy *Thy1-OFP-3 x Thy1-YFP-PeroxiYFP-376* mouse.

Supplementary Video 3│ *In vivo* two-photon time-lapse showing mitochondrial transport in an axon of a *Thy1-YFP-16* x *Thy1-MitoCFP-P* mouse, 2 days after onset of EAE. This video shows the marked reduction of transport in a stage 0 axon with normal-appearing mitochondria.

Supplementary Video 4│ *In vivo* two-photon time-lapse showing microtubule dynamics in stage 0 and stage 1 axons of a *Thy1-EB3-YFP* mouse 2 d after onset of EAE. This video shows normal comet behaviour in stage 0 axons, while there are obvious changes in comet directionality within the swollen axon.

Supplementary Video 5│ *In vivo* two-photon time-lapse showing mitochondrial transport following application of a nitric oxide donor ("NO") in a spinal axon of a healthy *Thy1-YFP-16* x *Thy1-MitoCFP-P* mouse. Normal transport of mitochondria is halted after application of 8 mM Spermine NONOate without affecting axon or mitochondrial morphology. Transport is re-started following application of an NO scavenger, cPTIO ("+cPTIO").

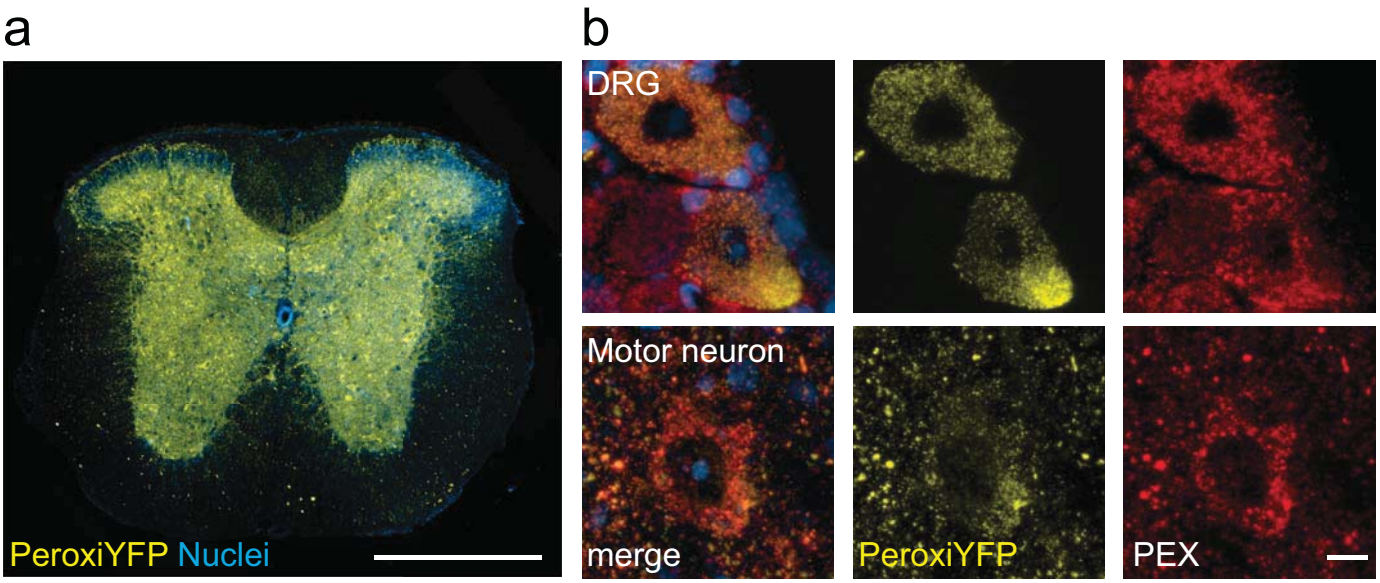

Sorbara et al., SFigure1

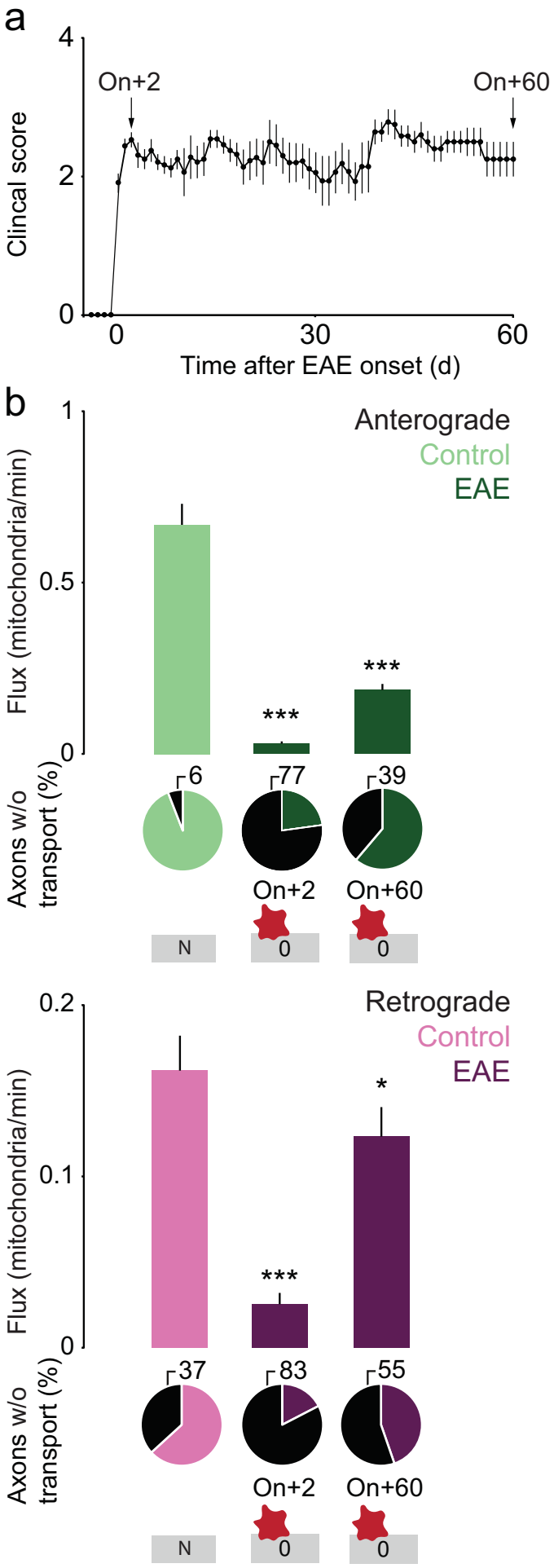

Sorbara et al., SFigure2

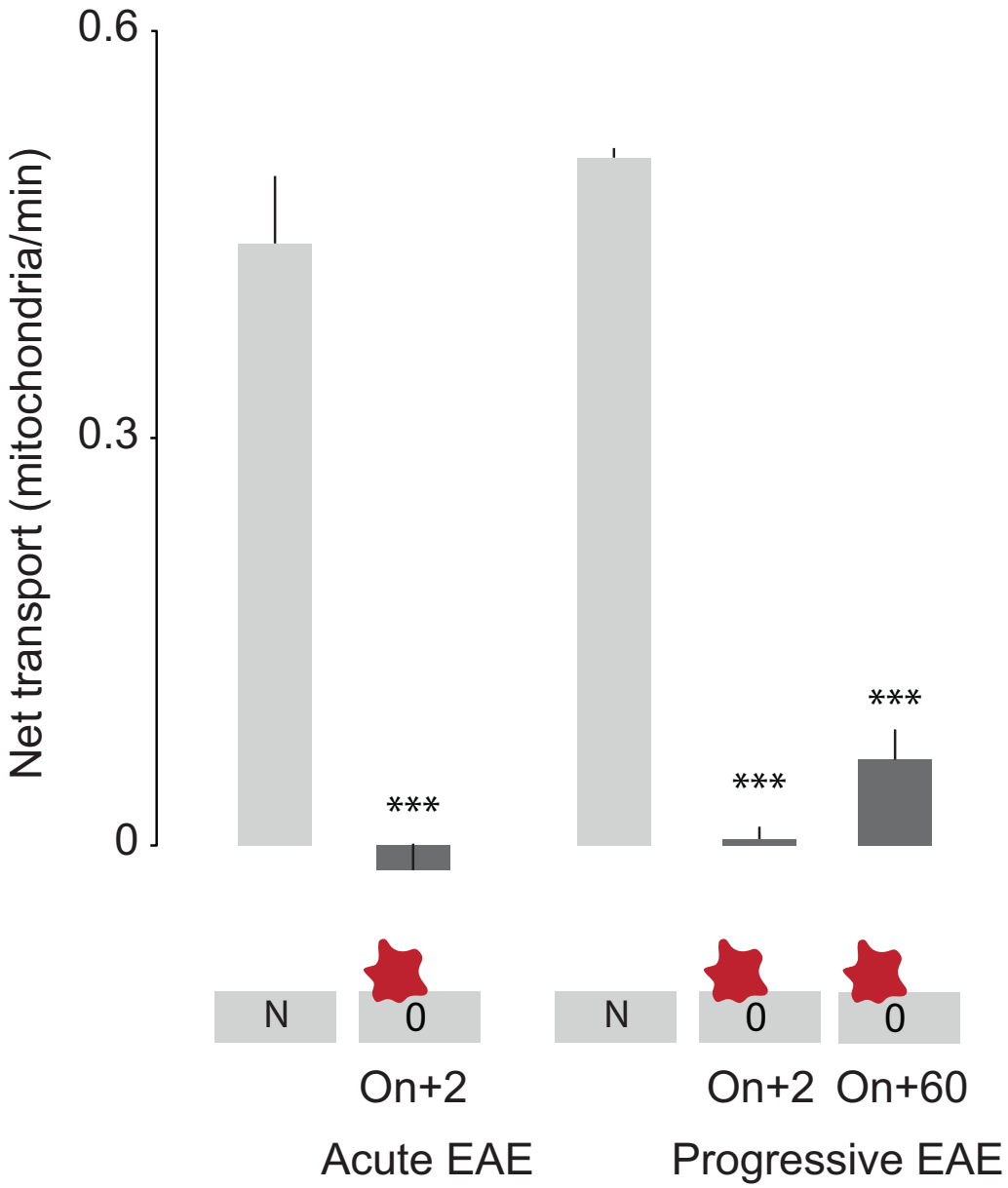

Sorbara et al., SFigure3

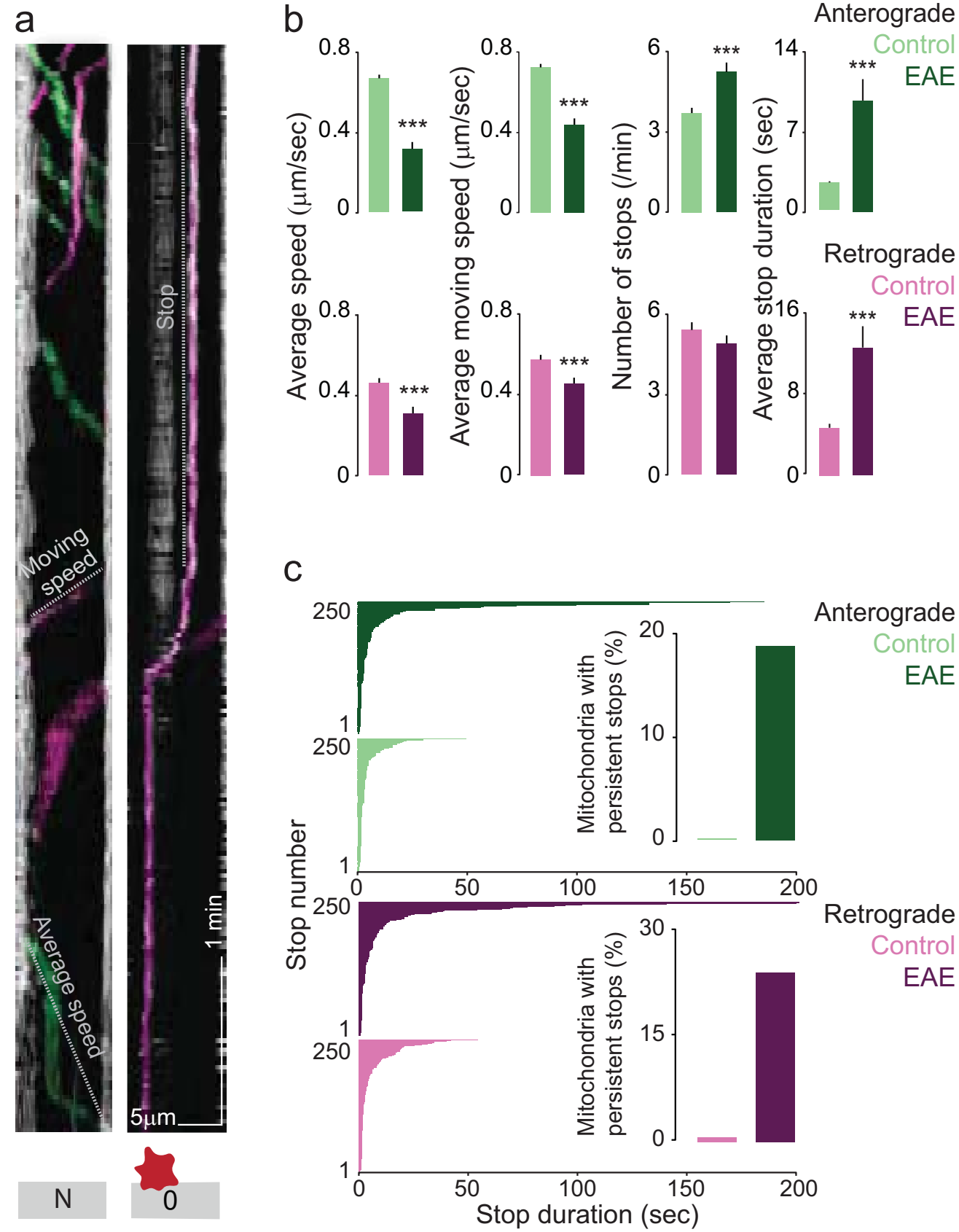

Sorbara et al., SFigure4

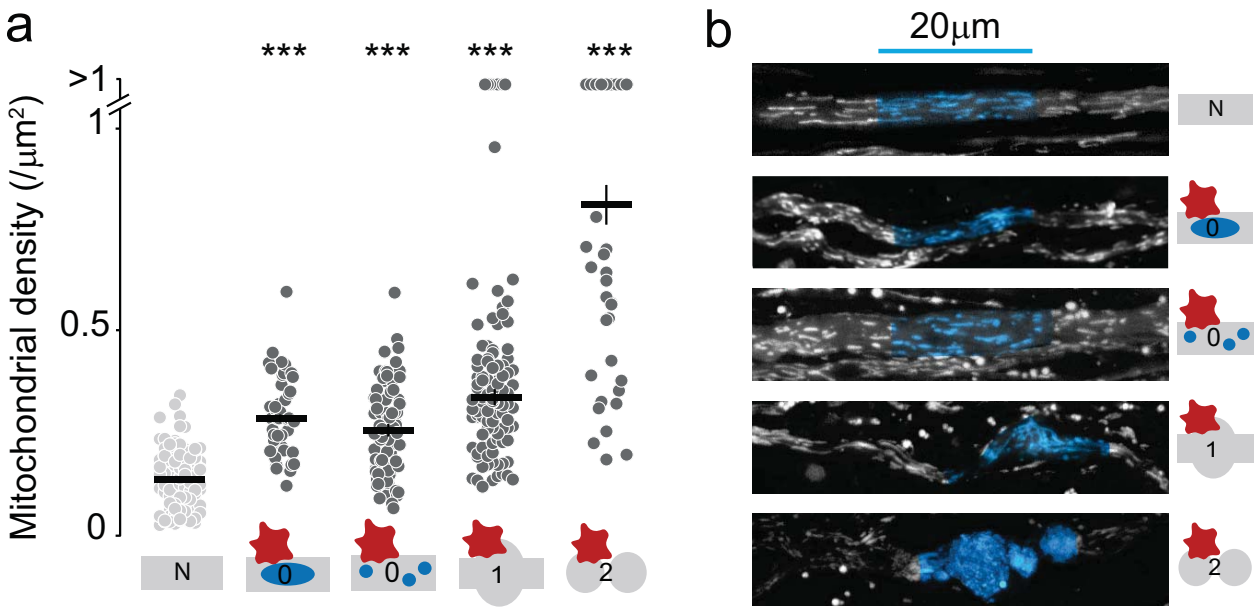

Sorbara et al., SFigure5

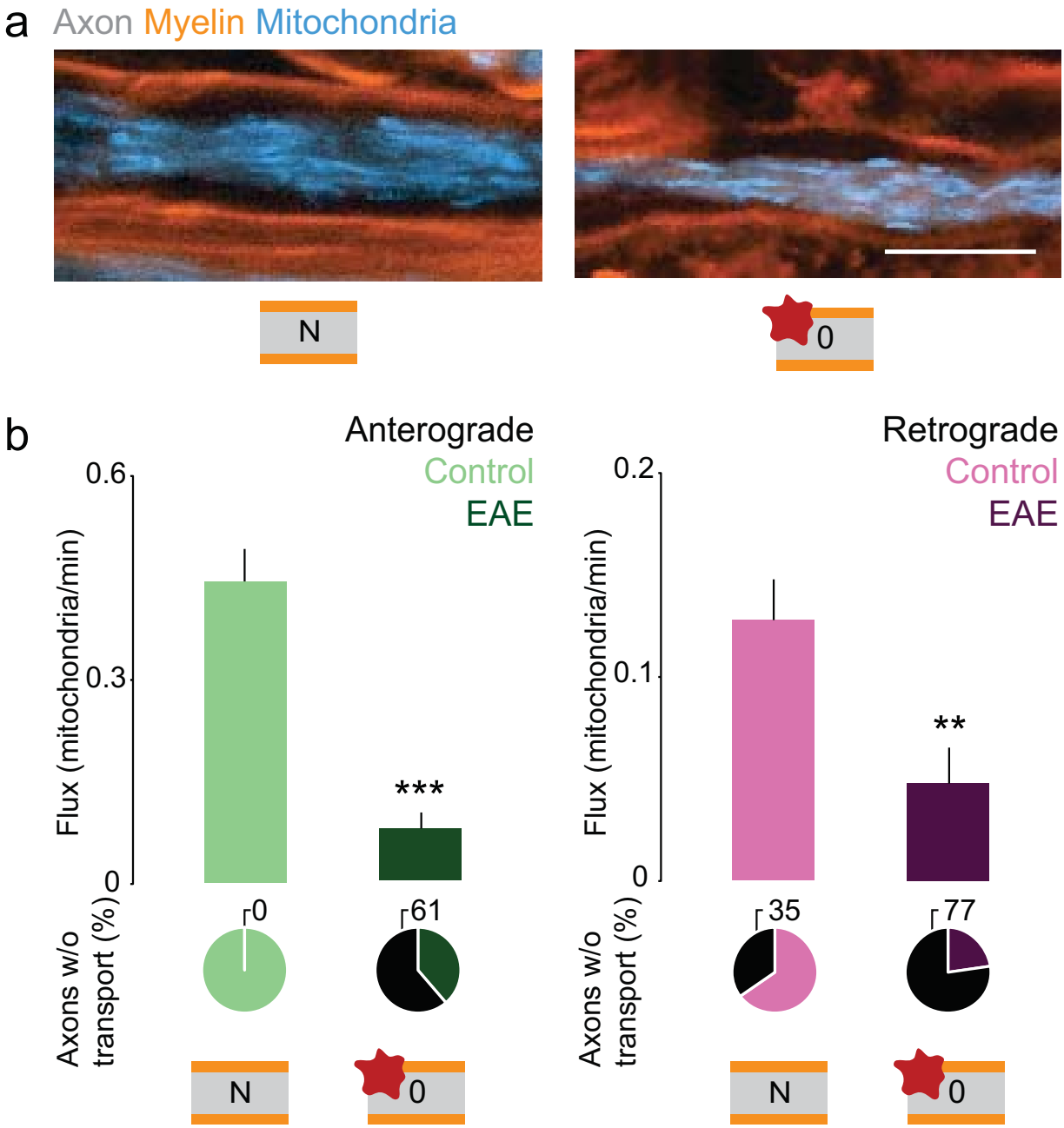

Sorbara et al., SFigure6

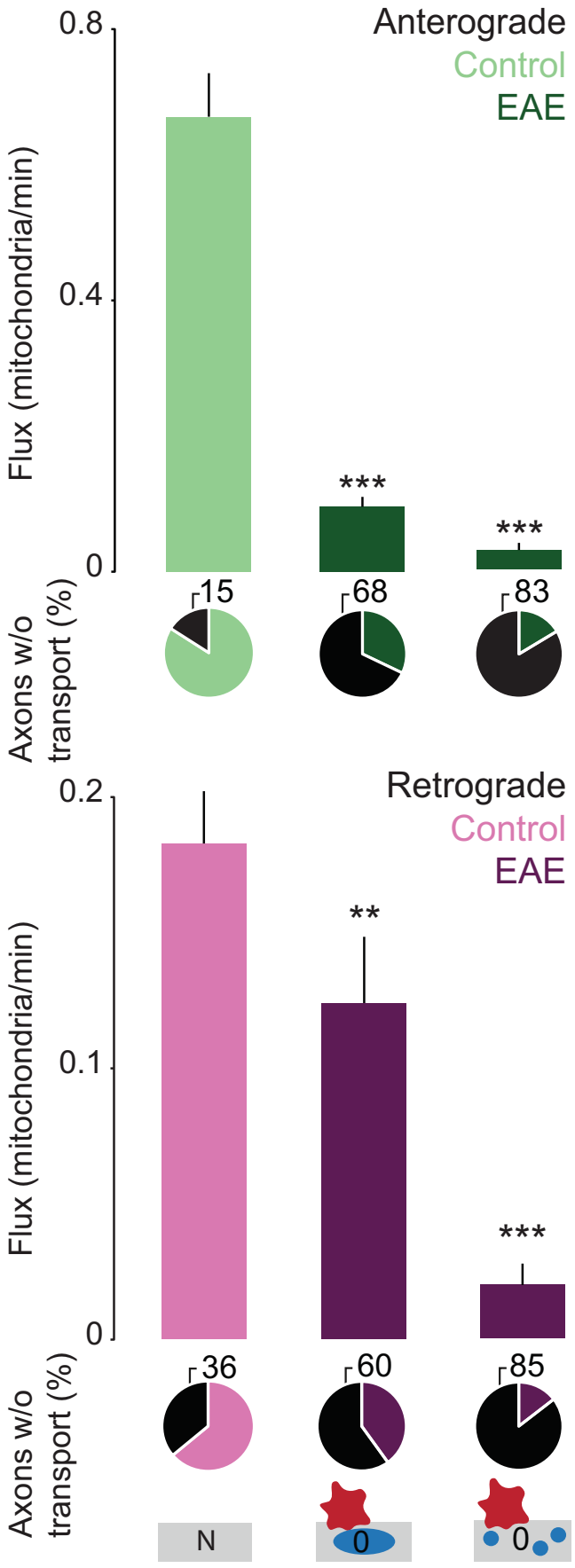

Sorbara et al., SFigure7

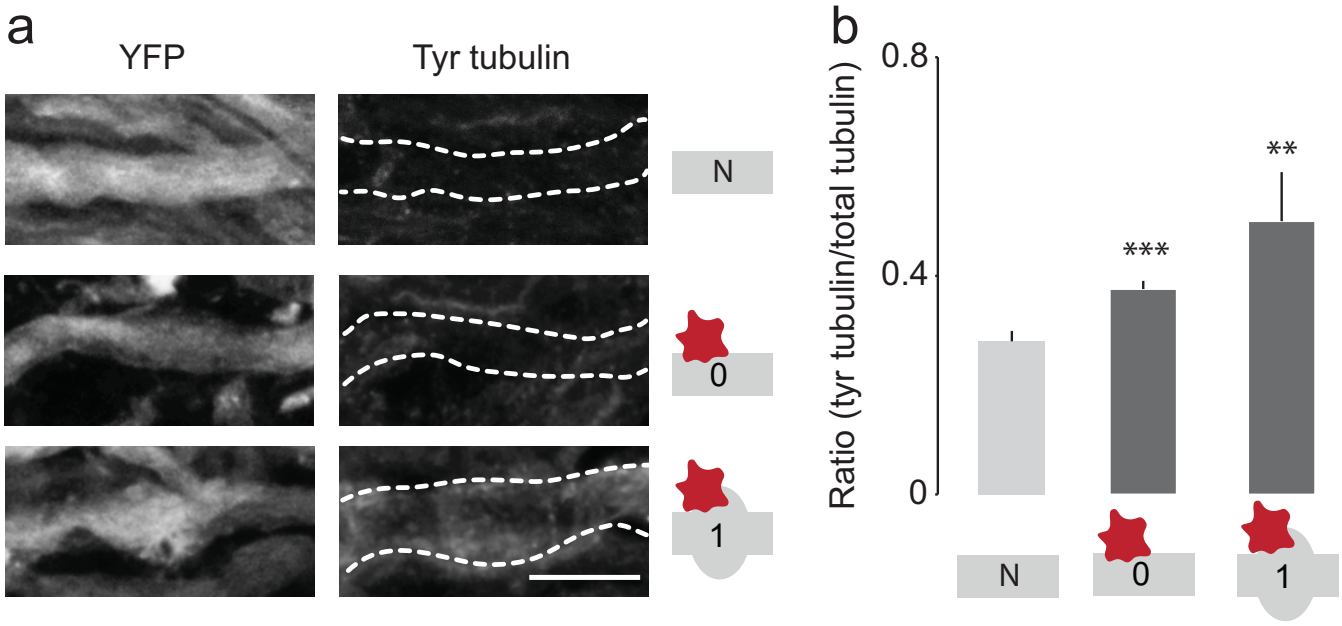

Sorbara et al., SFigure8

In Vivo Imaging of the Diseased Nervous System: An Update

Catherine Sorbara[1], Thomas Misgeld[2,3] and Martin Kerschensteiner[1,*]

[1]*Research Unit Therapy Development, Institute of Clinical Neuroimmunology, Ludwig-Maximilians Universität München, Munich, Germany;* [2]*Chair for Biomolecular Sensors, Center for Integrated Protein Science Munich at the Institute of Neuroscience, Technische Universität München, Munich, Germany;* [3]*Institute for Advanced Study, Technische Universität München, Munich, Germany*

Abstract: Cellular *in vivo* imaging can reveal the induction, progression and resolution of nervous system pathology in real-time. In this review, we summarize recent research in the field to illustrate how *in vivo* imaging has enhanced our understanding of a variety of neurological conditions caused by trauma, degeneration, ischemia or inflammation. Finally, we look ahead and discuss how novel biosensors might help us to follow not only the cellular but also the molecular pathogenesis of neurological diseases *in vivo*.

Keywords: *In vivo* imaging, multi-photon microscopy, neurodegeneration, neurotrauma, ischemia, neuroinflammation.

INTRODUCTION

Over the last decade, advances in microscopy and labeling techniques have made it possible to use dynamic imaging to study the pathogenesis of neurological conditions *in vivo* [1-3]. We have previously reviewed these technological advances and described first studies that used *in vivo* imaging to study neurological diseases [3]. In this brief review, we will provide a short introduction to *in vivo* imaging and an updated overview of the field by summarizing a number of recent studies that provide new insights into the *in vivo* pathogenesis of neurological diseases caused by degeneration, trauma, ischemia or inflammation (for overview see Table **1**).

TECHNICAL BASIS FOR *IN VIVO* IMAGING

Optical microscopy has been adapted for *in vivo* imaging by improving resolution and decreasing phototoxicity while allowing for longer working distances. Early *in vivo* imaging studies often employed wide-field microscopy in which the image produced represents illumination of the entire field of view. Of course, all specimens are naturally thick. To see thick images clearly without physically cutting the object required the development of optical sectioning techniques like confocal microscopy that exclude signals from out of focus planes and generate a clearer image in the plane of focus (reviewed in [4]). However, probably the most important step forward for *in vivo* imaging was the development of multi-photon microscopy (for an in depth technological explanation, see [1, 2]). This type of microscopy is based on two photon-excitation that occurs when two photons of about equal energy interact with a molecule producing an excitation equivalent to the absorption of a single photon possessing twice the energy. The wavelength of light required for this type of excitation must be twice that required for single photon excitation as energy is inversely proportional to wavelength. The advantages of two-photon microscopy are thus three-fold. The use of long wavelengths for excitation allows for penetration deeper into tissue, which can reach 1000 μm with special instrumentation [5]. The long wavelength also reduces the sensitivity to scattering associated with excitation confinement. Finally, two-photon excitation minimizes photobleaching and phototoxicity outside the focal region. In 1997 Svoboda *et al* were among the first to show how this technology could be used for *in vivo* imaging when they measured sensory-stimulus-induced dendritic calcium dynamics in pyramidal neurons in intact rat brain [6].

*Address correspondence to this author at the Institute of Clinical Neuroimmunology, Klinikum der Universität München, Marchioninistr. 17, 81377 Munich; Tel: ++49 89 2180 78282; Fax: ++49 89 2180 78285;
E-mail: martin.kerschensteiner@med.uni-muenchen.de

NEURODEGENERATIVE DISEASE

In vivo imaging has been used to study a number of neurodegenerative diseases, most prominently Alzheimer's disease (AD), a progressive neurodegenerative form of dementia. Murine models of AD lend themselves for *in vivo* imaging, as a major part of the pathological changes takes place in superficial cerebral cortex, which is accessible for high-resolution optical studies. Multi-photon imaging, using a craniotomy or a thinned skull area, has been used to characterize the growth of amyloid plaques [7, 8], the concomitant production of reactive oxygen species [9] and the emergence of neurite damage [10, 11]. More recently, De Calignon and colleagues monitored the formation of neurofibrillary tangles in living tau transgenic mice. By concomitantly assaying the activation of pro-apoptotic caspases, these authors proposed that caspase activation mediates cleavage of tau. Cleaved tau then recruits normal tau protein, inducing its misfolding and tangle formation. This proposition reverses the previously held notion that tangle formation leads to caspase activation and cell death. In fact, time-lapse imaging could directly show that neurons containing tangles survive for extended periods of time, indicating that neuronal cell death is unlikely to be a direct consequence of tangle formation [12]. Combining two-photon *in vivo* microscopy with elegant transgenic mouse models has also allowed studying the potential neurotoxic role of microglia in AD. In this study, transgenic mice carrying five transgenes were used: a triple transgenic AD mouse model combined with neuron-specific yellow fluorescent protein (YFP) and microglia-specific green fluorescent protein (GFP) expression. *In vivo* imaging revealed that microglial cells play a key role in the elimination of neurons, by showing that hindering the interaction between microglia and neurons can ameliorate neuronal loss [13]. Finally, calcium imaging has been used to assay the activity patterns of neurons and astrocytes near amyloid plaques. For example, calcium indicator dyes were used to localize calcium overload to neurites adjacent to plaques, which preceded subsequent neuronal degeneration [14]. Another recent imaging study identified a population of neurons near amyloid plaques that displayed hyperactivity, measured as an increase in spontaneous calcium transients. This was surprising given the prevailing hypothesis that neuronal dysfunction in AD is due to a progressive decrease in neuronal activity. These new data point toward an alternative view, where altered network activity creates silent, as well as hyperactive neurons that results in cognitive dysfunction [15]. Hyperactivity in AD does not seem to be restricted to neurons as shown in a study using fluorescent lifetime imaging microscopy (FLIM) to measure astrocytic calcium levels. This approach revealed that hyperactivity of astrocytes was distinct from that of neurons, namely synchronous across

1873-4286/12 $58.00+.00

Table 1. Summary of *In vivo* Imaging Studies of the Diseased Nervous System

Neurological Models	Imaging Approach	Labeling Approaches	Experimental Aim(s)	References
Alzheimer's Disease	Multiphoton imaging of cerebral cortex	neurofibrillary tangles: thioflavin S	characterization of neurofibrillary tangles	[7]
		amyloid plaques: methoxy-X04	characterization of amyloid plaques	[8]
		reactive oxygen species: AmplexRed reagent; amyloid plaques: thioflavin S	association of ROS production with amyloid plaques	[9]
		neurons: Thy1-XFP, amyloid plaques: methoxy-X04	dendritic spine alterations in association with amyloid plaques	[10, 11]
		neurofibrillary tangles: thioflavin S; caspases: FLICA – fluorescent inhibitor of caspase reagent	temporal sequence of caspase activation	[12]
		microglia: $Cx_3Cr1GFP+/-$; neurons: Thy1-XFP	neurotoxic role of microglia	[13]
		amyloid plaques: methoxy-X04; calcium indicator: calcium indicator YC3.6 or oregan green bapta-AM	activity patterns of neurons and astrocytes near lesion sites	[14, 15]
Ischemia (Stroke)	Multiphoton imaging of cerebral cortex	neurons: Thy1-YFP; blood flow: fluorescein isothiocyanate (FITC)-labeled dextran or Texas Red dextran	acute and chronic observation of post-ischemia vasculature and neuronal reorganization	[26-28]
			induction of ischemia with high spatial and temporal accuracy for targeted observation of microvessels and arterioles	[29-31]
			measurement of partial oxygen pressure in cerebral vasculature and tissue	[32]
Neurotrauma	Multiphoton and widefield epiflourescent microscopy of peripheral nerves and/or spinal cord	neurons: Thy1-XFP	mechanism and characteristics of axon degeneration	[17, 18]
		neurons: AAV-mediated expression of dsRed; calcium indicator: Oregon green 488 bapta-1;		[19, 20]
		neurons: Thy1-XFP	relationship between microtubule disorganization and the potential for axonal regeneration	[21]
		neurons: Thy1-XFP; blood vessels: Rhodamin B isothiocyanate-Dextran	role of vasculature in axon guidance	[22]
	Multiphoton imaging of cerebral cortex	microglia: $Cx_3Cr1GFP+/$; neurons: Thy1-XFP	activation and role of microglia cells after injury	[40-42]
Multiple sclerosis	Multiphoton imaging of spinal cord, brainstem	CD4+ T cells retrovirally engineered to express EGFP	recruitment and effector function of T cells	[36]
		calcium monitoring using flourescent resonance energy transfer (FRET) in Thy1-CerTNL15 mice; neurons Thy1-EGFP; T cells -XFP		[37, 38]
		neurons: Thy1-YFP16; mitochondria: Thy1-MitoCFP; T cells: CD2-GFP; Microglia: $Cx_3Cr1GFP+/-$; reactive oxygen/nitrogen species indicators: eg. AmplexRed dye	mechanism of immune-mediated axonal loss	[49]
Acute viral meningitis	Multiphoton imaging of cerebral cortex	meningeal vasculature: Qtracker 655nm non-targeted quantum dots; neutrophils/monocytes: LysM gfp/+; T cell receptor: GFP+ transgenic mice express GFP under β-actin promoter and express TCR that recognizes the LCMV glycoprotein (amino acids 33-41) present in $H\text{-}2D^b$	pathogenesis of viral mediated inflammation and vascular damage	[51]

long distances and independent of the position of amyloid plaques [16]. *In vivo* imaging studies have thus challenged long-standing theories regarding the pathogenesis of AD, and help us to better understand the mechanisms leading to neuronal dysfunction and ultimately neuronal cell death.

NEUROTRAUMA

Axonal transection is another common form of neuronal damage that is accessible to *in vivo* imaging due to the superficial location of axonal tracts in peripheral nerves and the spinal cord. A number of studies have used transgenic mice with subsets of fluorescently labeled neurons ("subset" *Thy1*-XFP mice) to follow the fate of transected axons. In the peripheral nervous system, Nguyen and collaborators examined the re-innervation pattern of peripheral motor axons after crush and cut lesion. Interestingly, they could show that when distal Schwann cell tubes remained intact following nerve crush, axons were able to re-establish their original pathways and synaptic contacts with high precision, suggesting a guidance role of peripheral glial cells [17]. Later a similar imaging approach for central axons was established that allowed tracking individual fluorescently labeled sensory axons in the dorsal column of the mouse spinal cord [18]. Using this approach, transected axons could be followed continuously over several hours, as well as repetitively over several days with mice recovering between recording sessions. This led to the identification of acute axonal degeneration, a novel mechanism of axon loss that is activated within 30 min after axon transection and underlies axonal die-back after trauma [18]. Knoferle and colleagues demonstrated that acute axonal degeneration is also induced after a lesion of the optic nerve [19]. Further mechanistic analysis revealed the involvement of autophagy as well as intra-axonal calcium rises, as blocking either process lead to a decrease in acute axonal degeneration [19, 20]. Acute axonal degeneration is often followed by a period of axon retraction that leads to the formation of retraction bulbs. Studying cytoskeletal components during this process has revealed a crucial role of microtubule disorganization in axonal bulb formation [21]. Imaging has not only been used to follow post-traumatic axon loss but also to reveal mechanisms that contribute to the failure of axon regeneration in the CNS. Initial studies showed that at least some spinal axons mount an early growth response; however, these axons grow in random patterns and thus likely lack directional cues [18]. More recently, Dray and colleagues co-visualized axonal and vascular changes after spinal cord injury [22]. This work showed that during the first two weeks following spinal cord injury axonal growth along blood vessels can increase speed but does not provide directed axon guidance. In the future, novel microsurgical approaches that use femto-second pulsed lasers to transect single axons without substantial damage to the local environment [23] might help to understand better the behavior of axons after injury. In particular, such approaches might contribute to unraveling intrinsic and extrinsic mechanisms that contribute to the failure of CNS axon regeneration.

NEUROVASCULAR CONDITIONS

Cerebral ischemia can be induced and assessed in animals in a defined way that is well suited to *in vivo* imaging techniques. In fact, the perfusion properties of the superficial microvasculature of the brain were already visualized more than 15 years ago following injection of fluorescent dextran-conjugates [24]. Subsequently, the development of multi-photon imaging allowed assessment of blood flow in deeper cortical layers [25]. In recent years, *in vivo* imaging has been used to reveal the neuronal consequences of ischemia. Time-lapse two-photon microscopy over several hours after ischemia induction showed that YFP-labeled dendrites within layer 5 of the somatosensory cortex are resistant to moderate ischemia. Severe ischemia, on the other hand, caused rapid spine and dendrite loss, which could be almost fully rescued if reperfusion occurred within 60 minutes [26]. Mapping of cortical function after acute ischemia showed that preserved blood flow 80 microns away was sufficient to maintain synapses. Tissue surrounding the infarct remained functional within the first hours following ischemia, and provided a rim of functional tissue, which can be recruited to aid in recovery [27]. Likewise, after transient global ischemia the structural damage of dendrites can recover if reperfusion occurs within 10 minutes [28].

In vivo microscopy can not only be used to visualize the cellular consequences of ischemia, but also to induce local ischemia with high temporal and spatial precision. Nishimura and colleagues described a transcranial method to induce three types of cerebral vascular injury using a femto-second pulsed laser, namely, hemorrhage, extravasation, or occlusion. In conjunction with labeling of the blood plasma with fluorescein-dextran, two-photon imaging allows mapping CNS vasculature and measuring blood flow rates based on tracks of individual erythrocytes [29]. Follow-up studies based on such photochemically-induced focal thromboses examined occlusions to the penetrating arteriole that connects the surface of the cortex with underlying vascular beds, as well as occlusions to individual microvessels on the pial surface. Interestingly, individual micro-vessels downstream of the occlusion were able to redistribute blood flow, potentially mitigating ischemic damage [30]. Following occlusion of a single penetrating artery, however, the blood flow was irreversibly decreased within a 350 μm radius, suggesting that distinct cortical regions exist that are supplied by a single penetrating arteriole [31]. In addition to following blood flow *per se*, a recently developed approach based on a phosphorescent nano-probe allows to use multi-photon imaging to directly measure partial oxygen pressure in cerebral vasculature and tissue [32]. Further, while most studies so far have investigated the acute consequences of cerebral ischemia, new advances in craniotomy techniques now allow for thinned skull preparations to be stabilized for months, furthering the potential for chronic observation of post-ischemic vascular and neuronal reorganization [33].

NEUROINFLAMMATORY DISEASE

The neurovascular unit plays an important role in forming the blood brain barrier, a protective shield of CNS parenchyma against cells and macromolecular components traveling in the bloodstream. In neuroinflammatory conditions like multiple sclerosis and its animal model, experimental autoimmune encephalomyelitis (EAE), large numbers of activated T-lymphocytes cross the blood brain barrier and initiate the formation of inflammatory lesions by recruiting additional immune cells, including macrophages and B cells. An important early study used *in vivo* wide-field microscopy in combination with a spinal cord window to directly visualize white matter microcirculation and assess the recruitment, adhesion and migration of autoaggressive T cells across vessel walls [34]. More recent imaging studies used two-photon microscopy to follow the migration of myelin basic protein-specific CD4+ effector T cells that had been engineered to express GFP in spinal cord slices [35]. This study revealed that T cells can move rapidly in CNS parenchyma. Some T cells occasionally reduce their mobility to form putative immune synapses and likely recognize their antigen [35]. Recently, direct *in vivo* observation revealed the migration path of CD4+ effector T cells during the formation of neuroinflammatory lesions. CNS-antigen specific T cells could be followed as they travel through the leptomeninges, contact antigen-presenting cells and ultimately enter underlying CNS tissue prior to clinical onset of disease [36]. Direct *in vivo* visualization of immune cells within the brainstem of mice with active EAE supports the idea that T cells can move rapidly along vessel walls and reveals that this movement is dependent on expression of the chemokine, CXCL12, and its receptor, CXCR4 [37]. This may facilitate efficient and rapid monitoring of perivascular antigen presenting cells and thus be an important preparatory step for initiation of CNS inflammation. When CD4+ T cells enter the CNS, they not only encounter their antigen but also directly contribute to tissue damage. Siffrin and colleagues recently described direct contacts of a specific subset of T cells,

Th17 lymphocytes, with neuronal cell bodies and axons in acute EAE lesions that were associated with increased intra-axonal calcium levels [38]. Notably these neuro-immune contacts seem to be antigen-independent, as non-CNS antigen specific Th17 cells could form similar long lasting contacts with neurons.

Another major contributor to neuroinflammation are microglial cells, which are activated upon injury. Studying microglia cells *in vivo* has been facilitated through engineering of transgenic mice, in which the CX_3CR1 gene is replaced with a gene encoding GFP [39]. Using two-photon microscopy, microglial cells have been observed in the cortex and turned out to be remarkably dynamic. Even in their supposed "resting" state, these cells constantly survey their environment with highly dynamic processes. Upon injury, microglial processes extend immediately towards the injury, a reaction that is known to be ATP-dependent [40, 41]. More recently, double transgenic mice with fluorescently labeled microglia and neurons were studied to better understand neuron-microglia interactions *in vivo* [42]. Wake and colleagues observed that microglia processes made transient but direct contacts with neuronal synapses, perhaps to monitor their functional status. These contacts are increased following injury and synapse loss, suggesting that microglia might be involved in synaptic turnover and remodeling.

Immune cells also contact neuronal processes in neuroinflammatory conditions. In diseases like multiple sclerosis the resulting axon damage contributes to permanent disability [43]. Our understanding of the mechanisms that induce immune-mediated axon damage is limited and was so far mainly based on *in vitro* and post mortem analysis [44-48]. Recently, we have used an *in vivo* imaging approach to identify Focal Axonal Degeneration (FAD) a new axon loss process that contributes to axon damage in experimental and human neuroinflammatory lesions ([49] and (Fig. **1**)). FAD is characterized by the presence of intermediate stages of damage that can persist for several days *in vivo* and are spontaneously reversible.

In addition to autoimmune reactions, viral infections also have the ability to induce inflammatory responses in the nervous system (reviewed in [50]). Here, McGavern and colleagues used *in vivo* imaging to elucidate the immune mechanisms involved in protecting or harming the nervous system following an acute viral infection. In the lymphocytic choriomenigitis virus infection (LCMV) model they were, for example, able to reveal the recruitment of monocytes and neutrophils following LCMV specific cytotoxic T cell invasion [51]. This cell influx is required for induction of vascular pathology, cell death and seizure activity.

PERSPECTIVES

Future progress in *in vivo* imaging will have to aim to extend analysis from the cellular to the molecular domain. This will depend on two complimentary approaches: first, the advancement of optical approaches to increase resolution (reviewed in [52]) and second, the development of fluorescent biosensors that monitor molecular changes. Classical examples of such biosensors are calcium indicator dyes, which as they chelate calcium change their fluorescence intensity or spectrum. Such small-molecular calcium indicators have been commonly used to monitor neuronal activity, but can also be used to visualize calcium changes related to neuronal damage. Initially, microelectrodes were used to load calcium-sensitive fluorophores into a small population of neurons [6, 53]. *In vivo* application to larger ensembles of CNS neurons became possible with the so called multi-cell bolus loading technique [54]. Further progress is to be expected from genetically encoded calcium sensors that monitor changes in calcium concentration using fluorescent resonance energy transfer (FRET). In these FRET sensors a calcium-induced conformational change, e.g. of a calcium-binding linker peptide such as Troponin C or Calmodulin [55, 56], leads to change in proximity of a donor and acceptor fluorophore. This alters the energy transfer between fluorophores and hence the FRET efficiency. Optimized sensors such as the TN-XXL protein have been used to gauge calcium levels chronically *in vivo* in mice and flies [57] and to monitor intra-axonal calcium changes associated with neuroinflammatory disease [37]. Another recent development with great potential for studying neurological disease concerns sensors of oxidative stress [37]. For example, transgenic mice expressing a mitochondrially targeted redox-sensitive green fluorescent protein in the substantia nigra were used to directly visualize

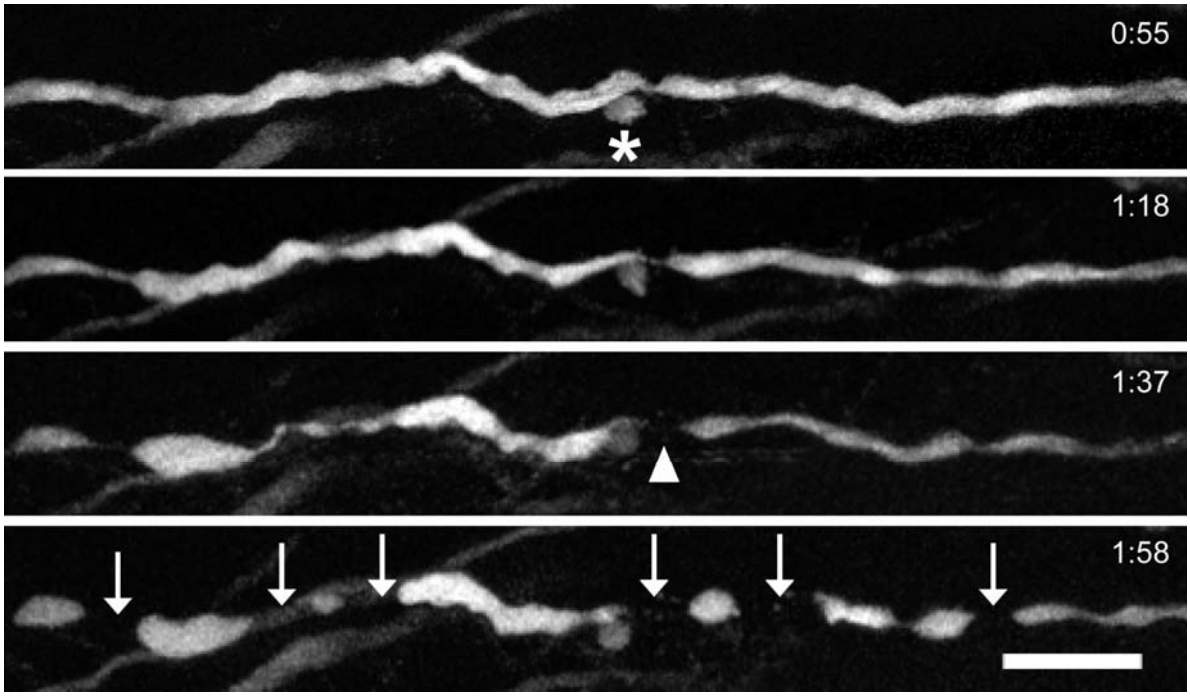

Fig. (1). *In vivo* imaging of FAD. Multi-photon time-lapse images of a stage 1 axon (white) in EAE. Time is shown as h:min. The axon first breaks (arrowhead) near a small swelling (asterix) at a putative node of Ranvier before fragmenting (arrows). Scale bar: 25 μm (adapted, with permission, from [49]).

mitochondrial oxidative stress evoked by pace-making in dopaminergic neurons, a crucial cell population lost in Parkinson`s disease [58].

Advances as those mentioned above should allow expanding *in vivo* imaging approaches from the cellular to the molecular domain. This will provide the basis for a dynamic appraisal of the cellular and molecular interactions that govern the emergence and resolution of neurological conditions.

CONFLICT OF INTEREST

The authors confirm that this article content has no conflicts of interest.

ACKNOWLEDGEMENTS

This work is an update of our previous review [3]. Work in M.K.'s laboratory is financed through grants from the DFG (Emmy-Noether Program, SFB 571 and SFB 870), the Federal Ministry of Education and Research ("Understand MS") and the "Verein Therapieforschung für MS-Kranke e.V.". T.M. is supported by the Institute of Advanced Studies (Technische Universität München), by the Deutsche Forschungsgemeinschaft (DFG; Sonderforschungsbereich SFB 596), by the Alexander-von-Humboldt-Foundation, and the Center for Integrated Protein Science (Munich).

REFERENCES

[1] Denk W, Svoboda K. Photon upmanship: why multiphoton imaging is more than a gimmick. Neuron 1997; 18: 351-7.

[2] Helmchen F, Denk W. Deep tissue two-photon microscopy. Nat Methods 2005; 2: 932-40.

[3] Misgeld T, Kerschensteiner M. *In vivo* imaging of the diseased nervous system. Nat Rev Neurosci 2006; 7: 449-63.

[4] Conchello JA, Lichtman JW. Optical sectioning microscopy. Nat Methods 2005; 2: 920-31.

[5] Theer P, Hasan MT, Denk W. Two-photon imaging to a depth of 1000 microm in living brains by use of a Ti:Al2O3 regenerative amplifier. Opt Lett 2003; 28: 1022-4.

[6] Svoboda K, Denk W, Kleinfeld D, Tank DW. *In vivo* dendritic calcium dynamics in neocortical pyramidal neurons. Nature 1997; 385: 161-5.

[7] Christie RH, Bacskai BJ, Zipfel WR, *et al.* Growth arrest of individual senile plaques in a model of Alzheimer's disease observed by *in vivo* multiphoton microscopy. J Neurosci 2001; 21: 858-64.

[8] Yan P, Bero AW, Cirrito JR, *et al.* Characterizing the appearance and growth of amyloid plaques in APP/PS1 mice. J Neurosci 2009; 29: 10706-14.

[9] McLellan ME, Kajdasz ST, Hyman BT, Bacskai BJ. *In vivo* imaging of reactive oxygen species specifically associated with thioflavine S-positive amyloid plaques by multiphoton microscopy. J Neurosci 2003; 23: 2212-7.

[10] Spires TL, Meyer-Luehmann M, Stern EA, *et al.* Dendritic spine abnormalities in amyloid precursor protein transgenic mice demonstrated by gene transfer and intravital multiphoton microscopy. J Neurosci 2005; 25: 7278-87.

[11] Tsai J, Grutzendler J, Duff K, Gan WB. Fibrillar amyloid deposition leads to local synaptic abnormalities and breakage of neuronal branches. Nat Neurosci 2004; 7: 1181-3.

[12] de Calignon A, Fox LM, Pitstick R, *et al.* Caspase activation precedes and leads to tangles. Nature 2010; 4647292: 1201-4.

[13] Fuhrmann M, Bittner T, Jung CK, *et al.* Microglial Cx3cr1 knockout prevents neuron loss in a mouse model of Alzheimer's disease. Nat Neurosci 2010; 13: 411-3.

[14] Kuchibhotla KV, Goldman ST, Lattarulo CR, *et al.* Abeta plaques lead to aberrant regulation of calcium homeostasis *in vivo* resulting in structural and functional disruption of neuronal networks. Neuron 2008; 59: 214-25.

[15] Busche MA, Eichhoff G, Adelsberger H, *et al.* Clusters of hyperactive neurons near amyloid plaques in a mouse model of Alzheimer's disease. Science 2008; 321: 1686-9.

[16] Kuchibhotla KV, Lattarulo CR, Hyman BT, Bacskai BJ. Synchronous hyperactivity and intercellular calcium waves in astrocytes in Alzheimer mice. Science 2009; 323: 1211-5.

[17] Nguyen QT, Sanes JR, Lichtman JW. Pre-existing pathways promote precise projection patterns. Nat Neurosci 2002; 5: 861-7.

[18] Kerschensteiner M, Schwab ME, Lichtman JW, Misgeld T. *In vivo* imaging of axonal degeneration and regeneration in the injured spinal cord. Nat Med 2005; 11: 572-7.

[19] Knoferle J, Koch JC, Ostendorf T, *et al.* Mechanisms of acute axonal degeneration in the optic nerve *in vivo*. Proc Natl Acad Sci USA 2010; 107: 6064-9.

[20] Koch JC, Knoferle J, Tonges L, *et al.* Acute axonal degeneration *in vivo* is attenuated by inhibition of autophagy in a calcium-dependent manner. Autophagy 2010; 6: 658-9.

[21] Erturk A, Hellal F, Enes J, Bradke F. Disorganized microtubules underlie the formation of retraction bulbs and the failure of axonal regeneration. J Neurosci 2007; 27: 9169-80.

[22] Dray C, Rougon G, Debarbieux F. Quantitative analysis by *in vivo* imaging of the dynamics of vascular and axonal networks in injured mouse spinal cord. Proc Natl Acad Sci USA 2009; 106: 9459-64.

[23] Steinmeyer JD, Gilleland CL, Pardo-Martin C, *et al.* Construction of a femtosecond laser microsurgery system. Nat Protoc 2010; 5: 395-407.

[24] Villringer A, Them A, Lindauer U, Einhaupl K, Dirnagl U. Capillary perfusion of the rat brain cortex. An *in vivo* confocal microscopy study. Circ Res 1994; 75: 55-62.

[25] Kleinfeld D, Mitra PP, Helmchen F, Denk W. Fluctuations and stimulus-induced changes in blood flow observed in individual capillaries in layers 2 through 4 of rat neocortex. Proc Natl Acad Sci USA 1998; 95: 15741-6.

[26] Zhang S, Boyd J, Delaney K, Murphy TH. Rapid reversible changes in dendritic spine structure *in vivo* gated by the degree of ischemia. J Neurosci 2005; 25: 5333-8.

[27] Zhang S, Murphy TH. Imaging the impact of cortical microcirculation on synaptic structure and sensory-evoked hemodynamic responses *in vivo*. PLoS Biol 2007; 55: e119.

[28] Murphy TH, Li P, Betts K, Liu R. Two-photon imaging of stroke onset *in vivo* reveals that NMDA-receptor independent ischemic depolarization is the major cause of rapid reversible damage to dendrites and spines. J Neurosci 2008; 28: 1756-72.

[29] Nishimura N, Schaffer CB, Friedman B, *et al.* Targeted insult to subsurface cortical blood vessels using ultrashort laser pulses: three models of stroke. Nat Methods 2006; 3: 99-108.

[30] Schaffer CB, Friedman B, Nishimura N, *et al.* Two-photon imaging of cortical surface microvessels reveals a robust redistribution in blood flow after vascular occlusion. PLoS Biol 2006; 4: e22.

[31] Nishimura N, Schaffer CB, Friedman B, Lyden PD, Kleinfeld D. Penetrating arterioles are a bottleneck in the perfusion of neocortex. Proc Natl Acad Sci USA 2007; 104: 365-70.

[32] Sakadzic S, Roussakis E, Yaseen MA, *et al.* Two-photon high-resolution measurement of partial pressure of oxygen in cerebral vasculature and tissue. Nat Methods. 2010; 79: 755-9.

[33] Drew PJ, Shih AY, Driscoll JD, *et al.* Chronic optical access through a polished and reinforced thinned skull. Nat Methods 2010; 7: 981-984.

[34] Vajkoczy P, Laschinger M, Engelhardt B. Alpha4-integrin-VCAM-1 binding mediates G protein-independent capture of encephalitogenic T cell blasts to CNS white matter microvessels. J Clin Invest 2001; 108: 557-65.

[35] Kawakami N, Nagerl UV, Odoardi F, *et al.* Live imaging of effector cell trafficking and autoantigen recognition within the unfolding autoimmune encephalomyelitis lesion. J Exp Med 2005; 201: 1805-14.

[36] Bartholomaus I, Kawakami N, Odoardi F, *et al.* Effector T cell interactions with meningeal vascular structures in nascent autoimmune CNS lesions. Nature 2009; 462: 94-8.

[37] Siffrin V, Brandt AU, Radbruch H, *et al.* Differential immune cell dynamics in the CNS cause CD4+ T cell compartmentalization. Brain 2009; 132 5: 1247-58.

[38] Siffrin V, Radbruch H, Glumm R, *et al. In vivo* imaging of partially reversible th17 cell-induced neuronal dysfunction in the course of encephalomyelitis. Immunity 2010; 33: 424-36.

[39] Jung S, Aliberti J, Graemmel P, *et al.* Analysis of fractalkine receptor CX(3)CR1 function by targeted deletion and green

fluorescent protein reporter gene insertion. Mol Cell Biol 2000; 20: 4106-14.

[40] Davalos D, Grutzendler J, Yang G*, et al.* ATP mediates rapid microglial response to local brain injury *in vivo*. Nat Neurosci 2005; 8: 752-8.

[41] Nimmerjahn A, Kirchhoff F, Helmchen F. Resting microglial cells are highly dynamic surveillants of brain parenchyma *in vivo*. Science 2005; 308: 1314-8.

[42] Wake H, Moorhouse AJ, Jinno S, Kohsaka S, Nabekura J. Resting microglia directly monitor the functional state of synapses *in vivo* and determine the fate of ischemic terminals. J Neurosci 2009; 29: 3974-80.

[43] Bjartmar C, Kidd G, Mork S, Rudick R, Trapp BD. Neurological disability correlates with spinal cord axonal loss and reduced N-acetyl aspartate in chronic multiple sclerosis patients. Ann Neurol 2000; 48: 893-901.

[44] Peterson JW, Bo L, Mork S, Chang A, Trapp BD. Transected neurites, apoptotic neurons, and reduced inflammation in cortical multiple sclerosis lesions. Ann Neurol 2001; 50: 389-400.

[45] Fu L, Matthews PM, De Stefano N*, et al.* Imaging axonal damage of normal-appearing white matter in multiple sclerosis. Brain 1998; 121: 103-13.

[46] Evangelou N, Esiri MM, Smith S, Palace J, Matthews PM. Quantitative pathological evidence for axonal loss in normal appearing white matter in multiple sclerosis. Ann Neurol 2000; 47: 391-5.

[47] Bjartmar C, Kinkel RP, Kidd G, Rudick RA, Trapp BD. Axonal loss in normal-appearing white matter in a patient with acute MS. Neurology 2001; 57: 1248-52.

[48] Bjartmar C, Trapp BD. Axonal and neuronal degeneration in multiple sclerosis: mechanisms and functional consequences. Curr Opin Neurol 2001; 14: 271-8.

[49] Nikic I, Merkler D, Sorbara C*, et al.* A reversible form of axon damage in experimental autoimmune encephalomyelitis and multiple sclerosis. Nat Med 2011; 17: 495-9.

[50] McGavern DB, Kang SS. Illuminating viral infections in the nervous system. Nat Rev Immunol 2011; 11: 318-29.

[51] Kim JV, Kang SS, Dustin ML, McGavern DB. Myelomonocytic cell recruitment causes fatal CNS vascular injury during acute viral meningitis. Nature 2009; 457: 191-5.

[52] Toomre D, Bewersdorf J. A new wave of cellular imaging. Annu Rev Cell Dev Biol 2010; 26: 285-314.

[53] Svoboda K, Helmchen F, Denk W, Tank DW. Spread of dendritic excitation in layer 2/3 pyramidal neurons in rat barrel cortex *in vivo*. Nat Neurosci 1999; 2: 65-73.

[54] Stosiek C, Garaschuk O, Holthoff K, Konnerth A. *In vivo* two-photon calcium imaging of neuronal networks. Proc Natl Acad Sci USA 2003; 100: 7319-24.

[55] Heim N, Griesbeck O. Genetically encoded indicators of cellular calcium dynamics based on troponin C and green fluorescent protein. J Biol Chem 2004; 279: 14280-6.

[56] Miyawaki A, Llopis J, Heim R*, et al.* Fluorescent indicators for Ca2+ based on green fluorescent proteins and calmodulin. Nature 1997; 388: 882-7.

[57] Mank M, Santos AF, Direnberger S*, et al.* A genetically encoded calcium indicator for chronic *in vivo* two-photon imaging. Nat Methods 2008; 5: 805-11.

[58] Guzman JN, Sanchez-Padilla J, Wokosin D*, et al.* Oxidant stress evoked by pacemaking in dopaminergic neurons is attenuated by DJ-1. Nature 2010; 468: 696-700.

Received: March 6, 2012 **Accepted: March 26, 2012**